SPATIAL AND TEMPORAL VARIABILITY IN THE WATER BALANCE OF OIL SANDS MINE RECLAMATION COVERS

A thesis submitted to the College of

Graduate and Postdoctoral Studies

In Partial Fulfillment of the Requirements

for the Degree of Doctor of Philosophy

In the Department of Civil, Geological

and Environmental Engineering

University of Saskatchewan

Saskatoon

Canada

By

MD. SHAHABUL ALAM

© Md. Shahabul Alam, June 2020. All rights reserved.

PERMISSION TO USE AND DISCLAIMER

In presenting this thesis in partial fulfillment of the requirements for a Postgraduate degree from the University of Saskatchewan, I agree that the Libraries of this University may make it freely available for inspection. I further agree that permission for copying of this thesis/dissertation in any manner, in whole or in part, for scholarly purposes may be granted by the professor or professors who supervised my thesis work or, in their absence, by the Head of the Department or the Dean of the College Graduate and Postdoctoral Research. It is understood that any copying or publication or use of this thesis or parts thereof for financial gain shall not be allowed without my written permission. It is also understood that due recognition shall be given to me and to the University of Saskatchewan in any scholarly use which may be made of any material in my thesis.

Reference in this thesis to any specific commercial products, process, or service by trade name, trademark, manufacturer, or otherwise, does not constitute or imply its endorsement, recommendation, or favoring by the University of Saskatchewan. The views and opinions of the author expressed herein do not state or reflect those of the University of Saskatchewan, and shall not be used for advertising or product endorsement purposes.

Requests should be addressed to:

Head of the Department of Civil, Geological and Environmental Engineering

57 Campus Drive

University of Saskatchewan

Saskatoon, Saskatchewan S7N 5A9 Canada

OR

Dean

College of Graduate and Postdoctoral Studies

University of Saskatchewan

116 Thorvaldson Building, 110 Science Place

Saskatoon, Saskatchewan S7N 5C9 Canada

ABSTRACT

The oil sands industry in Canada routinely uses soil-vegetation-atmosphere-transfer (SVAT) models, calibrated against short-term (<~10 years) field monitoring data to generate a single set of optimized soil hydraulic parameters. These calibrated SVAT models are then used to evaluate long-term reclamation cover performance based on long-term (~60 years) historical climate data. This approach attempts to characterize variability in the long-term water balance of these covers using historical climate variability but does not incorporate the potential variability associated with soil hydraulic parameters. In addition, little attention has been given to date on the variability that might be associated with future climate change.

The focus of this research was on the long-term water balance of reclamation covers used in the oil sands industry. The objectives of this research were to: (1) quantify parameter variability in the modelling of water balance; (2) characterize the impact that future projected climate change will have on the water balance; and (3) evaluate methods of downscaling global climate change projections to regional (local) scales to evaluate changes in future water balances.

Parameter variability was characterized through Inverse Modelling (IM) of soil hydraulic parameters for 12 soil cover designs, replicated in triplicate, at Syncrude Canada Ltd's Aurora North mine site. Global scale climate change projections were downscaled (using LARS-WG) from Coupled Model Intercomparison Project Phase 5 (CMIP5) for the baseline and future periods at Fort McMurray Airport Station, while regional scale climate projections were generated for the 4km grid covering the Fort McMurray Airport station using the Weather Research and Forecasting (WRF) model.

The key findings include the following: (1) variability in the simulated actual evapotranspiration (AET) is controlled primarily by climate variability, while variability in the simulated net percolation (NP) is controlled equally by parameter and climate variability; (2) future AET and NP will increase relative to the historical baseline period regardless of the climate change projection, time period, or cover soil profile; and (3) relative increases in the future AET and NP from WRF are not significantly different from LARS-WG.

Overall, the findings highlight that the relative increase in future NP is significantly higher than that for AET, particularly for the reclamation covers. Increases in the NP rates are likely to

result in accelerated flushing of constituents contained within the mine waste but will also create larger water yields to surface waterbodies and downstream receptors. Here the water yield represents the total release of water from the covers that includes NP and runoff. These changes should be taken into account in the design of reclamation covers at oil sands mine sites.

ACKNOWLEDGEMENTS

I express my heartfelt gratitude to….

First and foremost, the Almighty Allah, the most merciful and most beneficent. He has been in total control in guiding me to the career path that I always dreamt of.

Dr. Lee Barbour, my supervisor, for continuously guiding and motivating me with the highest level of tolerance to accomplish more than I ever imagined. He always exaggerated all the small achievements in my research that kept me motivated to dream bigger. My personal and professional development would not be possible without his humility, wisdom, and unparalleled teaching skills.

Dr. Mingbin Huang, my co-supervisor, for his guidance, patience, and support throughout my Ph.D. program.

My advisory committee Dr. Amin Elshorbagy, Dr. Bing Cheng Si, Dr. Andrew Ireson, and committee chair Dr. David Elwood, for their valuable suggestions and feedback throughout the program.

Syncrude Canada Ltd., NSERC, and Department of Civil, Geological and Environmental Engineering, University of Saskatchewan, for the financial supports to undertake this research.

Dallas Heisler and Marty Yarmuch of Syncrude Canada Ltd. for their constant support and feedback on my research. Amy Heidman and Larisa Doucette of O'Kane Consultants Inc. for supporting with the access to Syncrude Watershed Research data, reports, and drawings. Dr. Yanping Li and Dr. Zhenhua Li of Global Institute for Water Security (GIWS) for sharing Weather Research and Forecasting (WRF) model outputs, and Dr. Willemijn Appels, Dr. Amin Haghnegahdar, and Dr. Shervan Gharari of GIWS for their help with the MATLAB coding.

My research colleagues, particularly my lab mates, for providing technical advice, and general and mental support throughout my program.

Last but not the least; my family and friends, who stayed by my side at the time of difficulty to take me this far -especially my deceased mother and my father, my wife, my sisters, my nephews and nieces, my in-laws, and all my relatives. My father and my wife made the biggest

sacrifices, one being very far from me and one being with me leaving a career behind that anyone would dream of.

DEDICATION

This is dedicated to my beloved parents

In loving memory of my wonderful mother

PERMISSION TO REPRODUCE

The third chapter of this thesis has been published as an article by the Copernicus Publications in the Hydrology and Earth System Sciences Journal (Alam et al. 2020). The authors retain the copyright under the Creative Commons Attribution 4.0 License since June 6, 2017, so there is no need to seek the publisher's permission to allow reproduction.

The fourth chapter of this thesis is reprinted from the Journal of Hydrometeorology, 19, M. S. Alam, S. L. Barbour, A. Elshorbagy, and M. Huang, The impact of climate change on the water balance of oil sands reclamation covers and natural soil profiles, 1731-1752. © American Meteorological Society. Used with permission.

The fifth chapter of this thesis has been published by Springer Nature in the Journal of Mine Water and the Environment (Alam et al. 2020). The authors retain the copyright to use the final published article in other publications such as dissertations, so there is no need to seek the publisher's permission to allow reproduction.

TABLE OF CONTENTS

LIST OF TABLES

LIST OF FIGURES

LIST OF SYMBOLS AND ABBREVIATIONS

AE	Actual evaporation
AET	Actual Evapotranspiration
AMALGAM	A MultiAlgorithm Genetically Adaptive Method
ANPP	Annual net primary production
ASCS	Aurora Soil Capping Study
AP	Air permeameter
AR5	IPCC Fifth Assessment Report
AT	Actual transpiration
AWHC	Available water holding capacity
CanESM2	The second generation Canadian earth system model
CDF	Cumulative density function
CF	Change factor
CFD	Cumulative frequency distribution
CGCM3	The third-generation Canadian coupled general circulation model
CI	Confidence interval
CMIP5	Coupled Model Intercomparison Project Phase 5
CMIP6	Coupled Model Intercomparison Project Phase 6
CTL	Control period

CV	Coefficient of variation
DDS	Dynamically Dimensioned Search
DS	Soil moisture deficit
ECCC	Environment and Climate Change Canada
GCM	General Circulation Model
GLUE	Generalized Likelihood Uncertainty Estimation
GP	Guelph permeameter
HGS	HydroGeoSphere
IM	Inverse Modelling
IQR	Inter-quartile range
IPCC	Intergovernmental Panel on Climate Change
LAI	Leaf Area Index
LARS-WG	Long Ashton Research Station Weather Generator
LHS	Latin Hypercube Sampling
LOS	Lean oil sands
Ks	Saturated hydraulic conductivity
MC	Monte Carlo
MCMC	Monte Carlo Markov Chain
MOSCEM-UA	Multiobjective Shuffled Complex Evolution Metropolis-University of Arizona

NP	Net percolation
NSERC	Natural Sciences and Engineering Research Council
NSGA	Nondominated Sorting Genetic Algorithm
OB	Overburden
OKC	O'Kane Consultants Inc.
OSTRICH	Optimization Software Toolkit for Research Involving Computational Heuristics
PDF	Probability density function
PEST	Parameter Estimation Tool
PET	Potential evapotranspiration
PE	Potential evaporation
PGW	Pseudo-global warming
PLHS	Progressive Latin Hypercube Sampling
PPT	Precipitation
PSD	Particle size distribution
PT	Potential transpiration
RCF	Relative change factor
RCM	Regional Climate Model
RCP	Representative Concentration Pathway
RMSE	Root mean square error

SBH	South Bison Hill
SCL	Syncrude Canada Ltd.
SCE	Shuffled Complex Evolution
SD	Standard deviation
SRES	Special report on emission scenarios
SSQ	Sum of squares
SV	Soil vegetation
SVAT	Soil-vegetation-atmosphere-transfer
SWAT	Soil Water Assessment Tool
SWE	Snow water equivalent
SWSS	Southwest sand tailings storage
TRT	Treatment
VG	van Genuchten
VWC	Volumetric water content
WRC	Water retention curve
WRF	Weather research and forecasting

CHAPTER 1 - **INTRODUCTION**

1.1 Background

Soil-vegetation-atmosphere-transfer (SVAT) models are routinely used in the mining industry to characterize the water balance for reclamation soil covers placed over mine waste. Conventional practice in the oil sands industry has been to calibrate SVAT models against short-term (e.g. 5-10 years) reclamation cover monitoring data and then to use these models to simulate expected cover performance over long-term (e.g. 60 years) historical climate cycles (Huang et al. 2015a). In this manner, optimal reclamation cover designs can be developed for various types of oil sands mine waste and targeted end land use.

Conventional practice has been to develop an optimized parameter set based on one or two soil cover monitoring locations for each landform or alternative cover design prototype. Generally, this approach involves obtaining a single set of parameters that best simulates all the years monitored. However, the development of only a single 'best' set of calibrated (optimized) parameters has limitations and possibly missed opportunities to more fully understand the controls and sources of uncertainty in cover performance. First, in most methods of calibration to date, the uncertainty associated with the calibrated material (hydraulic) parameters is not quantified. Without this quantification, it is difficult to evaluate how this uncertainty will be expressed when predicting long-term cover performance. This uncertainty is likely to be accentuated by other uncertainties, especially those associated with climate variability as well as future climate change. Both parameter and climate variability lead to uncertainty in the predictions of water balance components.

The changes in the climate are currently characterized by General Circulation Models (GCM) and Representative Concentration Pathways (RCP) as well as downscaled (local/regional) projections for application to site-specific simulations.

Another constraint of the conventional optimization approach is the model's inability to differentiate and quantify variability associated with heterogeneity (i.e. spatial variability) versus temporal variability in cover properties. This constraint could be addressed if parameter variability was quantified for multiple monitoring sites over several years, enabling researchers to interpret and characterize sources of this variability. For example, pinpointing parameter differences between sites could help in the assessment of spatial variability, while doing the same for differences over time could help in the assessment of temporal variability.

Temporal variability has been measured for oil sands reclamation covers using field testing; however, spatial variability is also expected to occur as a result of material heterogeneity, cover construction/placement conditions, topography, or vegetation development. For example, the evolution of a key soil property (saturated hydraulic conductivity, Ks) was observed on the reclamation covers at South Bison Hill (SBH) of Mildred Lake Mine in northern Alberta, Canada (Meiers et al., 2011; Huang et al., 2016). This temporal variability was thought to be due to changes in density and pore-size distribution (e.g. formation of macropores) as a result of freeze/thaw or wet/dry cycles and vegetation establishment. Longer-term temporal variability may also occur due to climate change (i.e. changes in average annual precipitation and evaporation) (Huntington, 2006), which could potentially affect the long-term performance of oil sands reclamation covers.

The central issue in long-term reclamation cover performance, then, is that spatial and temporal variability (i.e. variability in model parameters) has not been routinely quantified in the calibration of the SVAT models or applied in the evaluation of long-term cover

performance. Before being used, SVAT models should be calibrated using the best possible optimization technique. One such technique used over the years is inverse modelling (IM). Optimization is a method of searching for model parameters that minimize the discrepancy between the observed and estimated data. IM is a mathematical approach that estimates the causes (e.g. model parameters) iteratively using a system's measured effects (e.g. water content or pressure head) during a historical period (Hopmans et al. 2002). Although several IM methods have been developed in recent years, they have not been applied to the SVAT models in oil sands mine industry.

1.2 Problem statement

The various sources of spatial and temporal variability make it challenging to calibrate a SVAT model using monitoring data sets, which are of limited spatial and temporal extent. It is particularly difficult to calibrate models for newly constructed oil sands reclamation covers, which are still rapidly evolving due to weathering (e.g. freeze/thaw, wet/dry cycling) and in which vegetation is still becoming established. Spatial variability is unavoidable due to differences in material placement conditions (compaction, texture, and cover thickness) and material heterogeneity (texture or constituent content). Where possible, it is of value to quantify this variability and incorporate this variability in SVAT modelling.

The potential impacts of climate change make the evaluation of long-term cover performance more challenging as the future water balance components are expected to changes relative to those that might occur within the baseline (historical) time period. The simulation of future water balance components is associated with uncertainties due to the choice of climate models, emission scenarios, time periods, and downscaling methods. Without the quantification of these uncertainties, a reliable evaluation of long-term future water balance components is not attainable.

1.3 Research objectives

The overall goal of this research was to develop methods for evaluating spatial and temporal variability in hydraulic parameters affecting the hydrologic performance of oil sands reclamation covers and to incorporate variability in SVAT models to evaluate performance of these covers over the long-term.

The specific objectives were.

(1) To quantify parameter variability in the modelling of water balance for oil sands reclamation covers by obtaining optimized parameter sets for the cover materials based on independent soil monitoring locations (spatial variability) and for different time series (temporal variability), using the combination of the SVAT modelling packages and inverse modelling techniques;

(2) To characterize the impact that future projected climate change will have on the water balance of oil sands reclamation covers; and

(3) To evaluate methods of downscaling global climate change projections to regional (local) scales to evaluate changes in future water balances.

1.4 Thesis structure

Chapter 2 presents a literature review that develops the literature context and theoretical background necessary for understanding the research presented in this thesis.

The next three chapter contain unaltered copies of three manuscripts that have been published or submitted for publication. A preface to each of these chapters helps to connect the specific focus of the paper to the overall thesis objective and also defines the contribution of the PhD candidate to the paper development. All three papers have been published and

only minor modifications have been made to these papers for the editorial purposes as suggested by the examining committee.

The first manuscript, “Characterizing uncertainty in the hydraulic parameters of oil sands mine reclamation covers and its influence on water balance predictions”, has been published in the *Hydrology and Earth System Sciences* (Alam et al., 2020). This study demonstrates how to use inverse modelling to obtain optimized soil hydraulic parameters for 155 water balance models, while a set of 155 optimized parameters was used to provide the statistical distributions for spatial and temporal variability of the soil hydraulic parameters. Since temporal variability was insignificant, a Latin hypercube sampling technique was used to fully characterize the spatial variability of soil hydraulic parameters.

The second manuscript, “The impact of climate change on the water balance of oil sands reclamation covers and natural soil profiles”, has been published in the *Journal of Hydrometeorology* (Alam et al., 2018). This study demonstrated how to couple GCM outputs and a physically-based water balance model (HYDRUS-1D) through the downscaling methods to evaluate the long-term performances of oil sands mine reclamation covers under climate change as compared to the performances of pre-mining forest sites.

The final manuscript, “The application of statistical and dynamical downscaling to assess climate change impacts on mine reclamation cover water balances”, has been published in *the Journal of Mine Water and the Environment.* This chapter extends the analyses presented in the second manuscript to explore the impacts of climate change projections obtained from a high-resolution regional climate model (RCM), with an aim to compare the relative impacts between the statistical and dynamical downscaling methods in characterizing future water balance components of the reclamation covers.

Chapter 6 provides a summary of the overall results of the research and recommendations for future research at Syncrude Canada Ltd's mining sites.

CHAPTER 2 - LITERATURE REVIEW

This section reviews and synthesizes the key literature associated with the following topics: SVAT modelling of mine reclamation covers; the use of inverse modelling to characterize the hydraulic parameters associated with SVAT models including the impact that parameter variability has on modelling outcomes; and the methods currently used to characterize future changes in the global climate and to downscale these predictions to a regional scale.

2.1 Soil-vegetation-atmosphere-transfer (SVAT) models

Soil-Vegetation-Atmosphere Transfer (SVAT) models are used to represent the effects of physiological properties of vegetation in terms of leaf area index (LAI) and stomatal conductance on water and energy balance (Arora 2002) in the soil-vegetation-atmosphere continuum. The main purpose of using SVAT models is to quantify the components of the water balance (Demarty et al. 2004; Olioso et al. 2005). According to the level of complexity, SVAT models can be classified into three categories: (a) single-layer, (b) two-layer, and (c) multi-layer models. The simple single-layer model explicitly describes the overall exchange between the soil-vegetation system and the atmosphere, such as evapotranspiration, without incorporating processes that occur inside the canopy (Courault et al. 1996; Soer 1980). A two-layer model with intermediate complexity simulates the transpiration from the vegetation layer and evaporation from the soil surface separately, whereas complex multi-layer models describe the microclimate inside the canopy and/or soil profiles (Braud et al. 1995; Bruckler and Witono 1989; Meyers and Paw U 1987).

SVAT models can also be categorized according to whether they are standalone (i.e. when decoupled from an atmospheric model) or coupled (i.e. when coupled with an

atmospheric model). Some of these standalone or coupled models are used to simulate the surface-energy balance and the soil water balance in the unsaturated zone. Many of these SVAT models (e.g. sowatet, HYDRUS, unsat2, leachcm, swat, micro-weather, cupid, enwatbal, unsat2e, isba, isba-ags, stics, rzwqm) used for the unsaturated zone are listed in Bastiaanssen et al. (2007). Among these SVAT models the physically-based SVAT models (e.g. HYDRUS) can describe highly non-linear processes and interactions in the unsaturated soil, which were considered in this research.

The standalone SVAT models simulate the main hydrological processes in the soil profile (Facchi et al. 2004), they are unable to represent the interactions of the water fluxes with the vegetation growth and atmospheric changes although these interactions can be extremely important (Casanova and Judge 2008). Standalone SVAT are sometimes used to study evapotranspiration, but coupled models are also common, especially a SVAT model coupled with an atmospheric model (e.g. Boegh et al. 2004). These SVAT models are also coupled with root water uptake models (Feddes et al. 1974; Simunek et al. 2013) to represent interaction between the water fluxes in the soil and vegetation.

Two commonly used commercial models that are based on Richard's equation are the SVAT models SEEP/W (GEO-SLOPE 2020) and HYDRUS-1D (Simunek et al. 2013). HYDRUS-1D has been widely used to simulate water balance in the unsaturated soil profiles and, particularly, to determine the key water balance components (including evapotranspiration and net percolation) of cover system designs (Huang et al. 2011b, 2015a). The application of SEEP/W has been evaluated using the work of Huang et al. (2015a). HYDRUS-1D was chosen for use in this research because of its capability to undertake inverse modelling to estimate key hydraulic parameters and for its previous utilization at a number of the study sites. For example, Huang et al. (2011b, 2015a) used HYDRUS-1D to

obtain soil hydraulic parameters from inverse modelling of 5-10 years of soil monitoring data after which the calibrated HYDRUS-1D model was used to estimate the long-term (~60 years) water balance.

SVAT models based on the solution of Richard's equation can also incorporate vapour diffusion using Fick's Law. The calculation of vapour diffusion requires an understanding of the temperature profile across the soil profile; however, if the dominant water transfer mechanism is assumed to be liquid water flow and transpiration, then simpler isothermal models are often used.

Most SVAT models require potential evapotranspiration (PET) as an input to the model in order for it to be partitioned to potential transpiration (PT) or potential evaporation (PE). The PET can be calculated from a wide variety of methods linked to site specific climatic data such as air temperature, relative humidity, and windspeed. The partitioning to PT and PE is based on a description of the vegetation cover using the Leaf Area Index (LAI). The actual evaporation (AE) from the ground surface is calculated from the PE and some limiting water stress (i.e. suction) at the top of the soil profile. Actual transpiration (AT) is calculated by distributing PT over a prescribed rooting zone where root uptake is limited by water stress, as calculated by a root water uptake model (Kool et al. 2014; Simunek et al. 2013; Soylu et al. 2014; Pereira et al. 2015; Feddes et al. 1974).

2.2 Methods for estimating soil hydraulic properties

Representative soil hydraulic properties are often determined using laboratory tests or field experiments. However, both these methods have limitations. Laboratory measurements often inadequately represent field scale soil hydraulic properties because of sample disturbances and scaling effects (Hopmans et al. 2002). Field methods are more reliable, but

measurements are more time consuming and complicated due to the use of classical steady-state methods than the transient methods (Simunek et al. 2012), hence it is not feasible for the soil profiles with variable initial and boundary conditions.

2.2.1 Model optimization using inverse modelling

Researchers have attempted to overcome the limitations of laboratory and field experiments by developing better methods for measuring soil hydraulic properties. These improved methods involve optimizing model parameters through a search for the best parameter set that minimizes the discrepancy between the simulated and observed data.

A widely-used optimization method referred to as "inverse modelling (IM)" is a mathematical approach that estimates unknown causes (i.e. model parameters) iteratively using the observed effects (e.g. water content or pressure head) of a system during a historical period (Hopmans et al. 2002). The IM estimates soil hydraulic functions, $\theta(\psi)$ and $K(\psi)$ through simulation of easily monitored parameters (e.g. water content or pressure heads). Since IM estimates the soil hydraulic properties from iterative solutions of the governing equation, this method has heavy computational demands. However, IM has the advantage over laboratory testing in that essentially all of the field monitoring data becomes a full-scale field test that best captures in situ conditions.

IM is based on the repeated numerical solutions of the governing equation (e.g. Richard's equation) (Simunek et al. 2013):

$$\frac{\partial \theta}{\partial t} = \frac{\partial}{\partial z}\left[K(h)\frac{\partial h}{\partial z} + K(h)\right] - S, \tag{2.1}$$

where θ denotes volumetric water content [L^3 L^{-3}], t is time [T], z is the vertical spatial coordinate [L] taken as positive upward, h is the water pressure head [L], K is the unsaturated hydraulic conductivity [LT^{-1}], and S is the sink term representing processes such as plant

water uptake [$L^3 L^{-3} T^{-1}$]. Closed form equations are used to describe the hydraulic functions for hydraulic conductivity and volumetric water content as a function of suction such as the commonly-used model proposed by van Genuchten (1980) as follows:

$$\theta(h) = \begin{cases} \theta_r + \frac{\theta_s - \theta_r}{[1+|\alpha h|^n]^m} & h < 0 \\ \theta_s & h \geq 0 \end{cases}, \tag{2.2}$$

$$K(h) = \begin{cases} K_s S_e^{1/2} \left[1 - \left(1 - S_e^{1/m}\right)^m\right]^2 & h < 0 \\ K_s & h \geq 0 \end{cases}, \tag{2.3}$$

$$S_e = \frac{\theta - \theta_r}{\theta_s - \theta_r}, \tag{2.4}$$

where Se is the effective saturation; h is the pressure head [L]; θ is the volumetric water content [L^3/L^{-3}]; subscripts r and s refer to residual and saturated volumetric water contents, respectively; α [L^{-1}], n, and m are VG equation parameters where m=1-1/n; and Ks is the saturated hydraulic conductivity [LT^{-1}].

How well the individual model parameters (i.e. θr, θs, α, n, Ks) are estimated determines the overall accuracy of the estimation of soil hydraulic properties. To estimate these parameters, model calibration is typically employed. The parameters are iteratively adjusted (known as optimization) so that model simulations can reproduce the observed (historical) response of a system (e.g. soil water content) as closely as possible (Hopmans et al. 2002), where the discrepancy between the observed values and the simulated system response is expressed by a suitable objective function. IM has been widely used as an optimization tool, where the initial estimates of the model parameters are iteratively improved by minimizing the objective function until a desired level of precision is achieved (Simunek et al. 2013).

2.2.2 Minimizing the objective function

The judgement criteria (i.e. objective function) for obtaining the best optimized parameter set typically uses the minimum sum of squares (SSQ) so that, when the change in SSQ is no longer noticeable, the difference between the observed and the simulated values is minimal. Most methods require users to specify initial estimates as well as bounding values of the unknown parameters to be optimized to constrain the solutions. The objective function is evaluated in the neighborhood of the initial estimate and the subsequent direction of the solution is chosen in the response surface (the objective function presented graphically in the parameter space). In this way, the values of the unknown parameters are updated until the best optimized parameter set is obtained.

2.2.3 Gradient-based methods

Methods based on this minimization approach are known as gradient-based methods (e.g. steepest descent, Newton's method, Marquardt's method, and Gauss method), which are all different from each other based on their choice of step size and step direction (Bard 1974). Among these methods, the Marquardt-Levenberg method (Marquardt 1963) is the most efficient. This method combines the Newton method with the steepest descent method, making it a standard in nonlinear least-square fitting that is appropriate for both hydrologists and soil scientists (Kool et al. 1985, 1987).

Generally, the Marquardt-Levenberg method performs best when a limited number of parameters are to be optimized (Simunek et al. 2012). However, the initial values of the optimized parameters also affect the minimization methods (e.g. the Marquardt-Levenberg method). When the objective function is topographically complex, with several possible local minima in the parameter space, an initial estimate can lead the final solution to a local

minimum instead of the global minimum. This problem with the gradient-based optimization techniques may be overcome by using different initial estimates of the optimized parameters and by selecting those parameter values for which the objective function is minimized.

2.2.4 Gradient-free methods

In the last few decades, the limitations of the gradient-based local optimization methods have encouraged scientists and engineers to develop gradient-free global optimization methods. However, their use in the field of unsaturated soils (vadose zone) is sparse (Simunek and Hopmans 2002; Simunek et al. 2012). Recent research has focused on the development of automatic and more effective and efficient optimization methods (Madsen 2003). Most of the research on automatic optimization methods has been based on the single-objective function; however, even with the careful selection of a single-objective function, an automatic optimization method cannot fully characterize the observed data (Vrugt et al. 2003b). Instead of single-objective function methods, multi-objective optimization methods can characterize different aspects of the system's behavior and identify a set of non-dominated, efficient, or pareto optimal solutions (Gupta et al. 1998; Yapo et al. 1998; Boyle et al. 2000). The multi-objective optimization method (e.g. Multiobjective Shuffled Complex Evolution Metropolis (MOSCEM-UA), Vrugt et al. 2003a) yields the pareto solution set rather than a single parameter set.

As we have seen, while many optimization methods identify a single "optimal" parameter set, some methods, such as MOSCEM-UA mentioned above, identify several "plausible" parameter sets (i.e. probability distribution of the optimal parameters). To quantify parameter uncertainty, the model independent calibration tools, such as UCODE (Poeter and Hill 1998), PEST (Doherty 2005), and OSTRICH (Matott 2005), are also used. However, UCODE and PEST include only one or two optimization algorithms for parameter estimation, whereas

OSTRICH includes several different optimization algorithms. These algorithms include local search (e.g. Marquardt-Levenberg), global search (e.g. Dynamically Dimensioned Search (DDS), Shuffled Complex Evolution (SCE), single-objective (e.g. Shuffled Complex Evolution (SCE), multi-objective (e.g. Pareto Archived DDS), and uncertainty-based (e.g. GLUE) optimization on the same platform. Thus, OSTRICH seems superior to UCODE and PEST. In addition, some of the optimization methods embedded in OSTRICH can estimate the uncertainty in the optimized parameters; however, their use has not been as common with the SVAT models as with other hydrological/rainfall-runoff models. Not only does the multi-objective optimization method (available in OSTRICH) enable the calibration of the models along with the estimation of parameter uncertainty, but also it determines the best optimization method from a number of embedded methods. However, these methods would be computationally too expensive.

2.3 Applications of IM to SVAT modelling

2.3.1 Applications of SVAT models

As mentioned earlier, the simulation of water balance in unsaturated soils (vadose zone) has commonly been performed using SVAT models based on Richard's equation. Several of the SVAT models are physically-based water balance models which require the hydraulic properties defined by the water retention curve and the hydraulic conductivity function. HYDRUS-1D has been extensively used over the years to estimate these hydraulic properties (e.g. Simunek et al. 1998; Butters and Duchateau 2002; Bitterlich et al. 2004; Schindler et al. 2010; Scharnagl et al. 2011; Bordoni et al. 2017).

HYDRUS-1D has also been used to investigate the impact of soil properties and meteorological conditions on water dynamics and water balance (e.g. Moricz et al. 2012;

Nasta and Gates 2013; Huang et al. 2015a; Altdorff et al. 2017; Shelia et al. 2018) or to characterize spatially- and/or temporally-distributed properties of the unsaturated zone (e.g. Thomasson and Wierenga 2003; Vrugt et al. 2004; Wissmeier and Barry 2008; Harman et al. 2011; Jirku et al. 2013; Chen et al. 2014; Qu et al. 2014).

In the specific case of reclamation covers for oil sands mines, HYDRUS-1D has been used to study long-term water balances, soil moisture dynamics, and alternative reclamation cover designs (e.g. Huang et al. 2011 a,b,c, 2015 a,b; Zettl et al. 2011; Sigouin et al. 2016). HYDRUS-1D seem to be promising physically-based water balance SVAT model for such research due to their ability to estimate soil hydraulic properties and the long-term water balance of the cover systems.

2.3.1.1 Applications of IM

Early estimations of soil hydraulic properties using IM started in the laboratory. The first application of IM was undertaken by Gardner (1956) to interpret the results from a pressure plate outflow experiment for an initially saturated soil core. In this test, the drainage outflow was measured with time for a series of step-wise increasing applications of suction. Following Gardner's (1956) study, other research (Doering, 1965; Passioura, 1976), contributed to a simplified and timesaving outflow interpretation method. These studies described the water retention and unsaturated hydraulic conductivity relationships based on the Brooks and Corey (1966) model of soil hydraulic properties.

In the 1980s, studies of IM moved beyond the laboratory. Dane and Hruska (1983) were among the first to apply an IM approach to field conditions, using transient drainage data to estimate soil physical parameters. Since then, researchers have utilized IM to estimate soil hydraulic properties across spatial scales, given that the parameters conceptually and

effectively represent the spatial and temporal heterogeneity of the watershed properties at the scale of interest (Vrugt et al. 2008).

Recent studies (Madsen 2003; Vrugt et al. 2004; Huang et al. 2011c) have applied IM to spatially-distributed data with physically-based water flow models and simulated the long-term water balance of soil covers using long-term soil monitoring data with a physically-based SVAT model. Since its first application, the suitability of IM to estimate soil hydraulic parameters has been widely studied (Vrugt et al., 2008). Many authors have quantified the uncertainty of the parameters estimated by IM (Kool and Parker 1988; Hollenbeck and Jensen 1998; Vrugt and Bouten 2002; Vrugt et al. 2003b 2004). Several authors have developed and applied search methods to locate the optimal parameters in rough and multimodal response surfaces (Abbaspour et al. 1997, 2001; Lambot et al. 2002; Vrugt and Bouten 2002; Mertens et al. 2006).

2.3.1.2 Application of model independent calibration tools

The model independent calibration tools, combined with HYDRUS-1D, have been used to simultaneously optimize soil hydraulic parameters and/or simulate water balance components. UCODE software combined with HYDRUS-1D was found to simultaneously optimize soil hydraulic parameters and simulate potential evaporation (Dahiya et al. 2007), as well as to simultaneously optimize soil hydraulic and solute transport parameters and estimate solute transport constants and concentration profiles (Jacques et al. 2012).

In several studies, PEST has been applied to calibrate HYDRUS-1D. For example, PEST combined with HYDRUS-1D was used to evaluate soil hydraulic parameters using field measured data at different levels of soil water salinity in the Tranquillity site, San Joaquin Valley, California, (Singh et al. 2010; Singh and Wallender, 2011). The same combination

was used to analyze the infiltration and drainage processes in multi-layered coarse soils in several sites north of Fort McMurray, Alberta, Canada (Huang et al. 2011a).

2.3.1.3 Recent applications of IM

The soil hydraulic parameters of HYDRUS-1D can be optimized using recently developed global optimization algorithms. Vrugt et al. (2008) used the evolutionary search-based approach, a MultiAlgorithm Genetically Adaptive Method (AMALGAM), to estimate 15 van Genuchten-Mualem (VG) parameters using HYDRUS-1D, with the pressure head data recorded at five different depths, replicated three times, by 15 tensiometer probes. Similarly, Vrugt and Robinson (2007) and Wohling et al. (2008), in comparing the performance of the global optimization algorithms AMALGAM, the Nondominated Sorting Genetic Algorithm (NSGA-II, Deb et al. 2002), and MOSCEM-UA (Vrugt et al. 2003a), found that AMALGAM was significantly better in finding solutions. AMALGAM was able to find the pareto optimal parameter sets faster than two other methods, while MOSCEM-UA was the second fastest of the three. These studies reflect the suitability of global multi-objective optimization algorithms in finding multiple sets of soil hydraulic parameters using HYDRUS-1D with the advent of high-performance computing resources.

2.3.1.4 Applications of IM in uncertainty estimation

The main challenge of IM is finding a unique set of parameters that characterizes the soil hydraulic processes. Since different sets of the estimated parameters may lead to identical values of the objective function, uncertainty in the estimated parameters is an integral part of IM (Boyle et al. 2000). This phenomenon of obtaining identical objective functions is known as equifinality, which denotes uncertainty (Beven, 1993); however, more reliable models can be obtained by quantifying parameter uncertainty (Cooley 1993).

Material heterogeneity is unavoidable in the construction of reclamation covers, which are subject to temporal variation because cover materials evolve with time (Meiers et al. 2011). Huang et al. (2016) characterized spatial variability due to material heterogeneity by using various methods (e.g. air permeability) to measure the values of saturated hydraulic conductivity (Ks) and geostatistical analysis. However, measuring parameters (e.g. Ks) at the scale of interest (space and time) is a difficult task and a single objective function might be unable to represent the multidimensional inherent characteristics of the measured data from the complex oil sands mine sites.

The computationally efficient IM of HYDRUS-1D provides an efficient means of characterizing the spatial and temporal (a) variability in the estimated parameters and (b) uncertainty in the long-term water balance components of alternate reclamation cover designs. When these distributions of best parameter sets are utilized in SVAT models with variable climate inputs, the uncertainty in the future water balance components can be evaluated.

2.4 Impact of parameter uncertainty on the water balance components

Uncertainties in the model results may be categorized as model structure uncertainties, model parameter uncertainties, model input variable uncertainties, and measurement uncertainties (Radwan et al. 2004). Different sources of uncertainties in the model outputs (e.g. water balance components, runoff, and streamflow) have been frequently characterized using probability distributions (Elshorbagy and Barbour 2007; Bastidas et al. 2003). The relative probability distributions of model outputs for various sources of uncertainties are compared to show the relative contributions of various uncertainties to the total uncertainty. The uncertainty in the soil hydraulic parameters of oil sands mine reclamation covers was characterized by probability distributions in previous studies using both direct testing (Meiers

et al. 2011) and IM (Huang et al. 2015, 2016). Meiers et al. (2011) characterized temporal variability in the measured hydraulic conductivity (Ks) in the reclamations covers at SCL's Mildred Lake mine, while Huang et al. (2015) showed similar temporal variability in Ks using IM. Huang et al. (2016) characterized spatial variability in Ks obtained by conducting air-permeability test on the reclamation covers.

2.5 Impact of climate change on the water balance components

Several studies have utilized physically-based SVAT models (e.g. SWAT and HGS) to assess the potential impacts of climate change on catchment water balance or streamflow (Githui et al. 2009; Leta et al. 2016; Mango et al. 2011) and water flow and availability in Canada's Boreal Plains (Thompson et al. 2017). A few studies (e.g. Keshta et al. 2012) based on system dynamics water balance models have evaluated the performance of alternate cover designs in northern Alberta under previously available future climate scenarios from CMIP3.

2.5.1 Downscaling methods

Climate change research community has adopted the GCMs as the primary tool for future climate change projections (Meehl et al. 2007). The GCMs providing outputs at coarse resolutions (typically 100-300 km) hinder their ability to represent local (point scale) and regional (typically 25-50 km) scales climate change attributes due to their inability to incorporate convective cloud processes adequately (Joubert and Hewitson, 1997). To overcome this issue of inconsistent resolution between the GCMs and climate change impact study, several downscaling methods have been used. Broadly, these downscaling methods are of two categories: statistical and dynamical downscaling (Fowler et al. 2007; Wilby and Wigley, 1997). The selection of the downscaling methods depends on the application area as well as their relative advantages and disadvantages over each other. For instance, the

statistical downscaling is easy to implement and computationally cheap, whereas the computationally expensive dynamical downscaling is able to incorporate physical processes in simulating high resolution climate projections (Fowler et al. 2007; Wilby and Dawson, 2004).

2.5.1.1 Statistical downscaling

Statistical downscaling relies on the statistical relationships between the observed climate variables (the predictands) at local scale and the atmospheric climate variables (the predictors) at global scale to generate point-scale climate change projections (Wilby et al. 1998). Over the past two-three decades both simple (e.g. delta change) and highly sophisticated (e.g. regression models, weather typing schemes, and stochastic weather generators) methods have been developed (Wilby and Wigley, 1997). To evaluate the performance of oil sands mine reclamation covers, Keshta et al. (2012) used Statistical DownScaling Model (SDSM, Wlby and Dawson 2007), a regression-based downscaling method, to downscale climate change projections from the global scale to the point. However, they did not incorporate the uncertainty estimation in their future water balance simulations.

2.5.1.2 Dynamical downscaling

Dynamical downscaling is based on the regional climate models (RCMs) driven by the outputs of GCMs as the horizontal boundary conditions (Fowler at el. 2007; Sharma et al. 2011; Wilby and Dawson, 2004; Xue at al. 2014). Since the RCMs are parameterized using the physical atmospheric processes, the improvement of climate change projection from GCMs is achieved by incorporating underlying surface and local circulation patterns to represent small-scale properties and atmospheric processes (Castro et al. 2005; Gao et al. 2012; May, 2008).

2.6 Research gaps

The parameters obtained from inverse modelling are inadequate for complete characterization of the variability in the soil hydraulic parameters. However, they can be analyzed for the uncertainty estimation using an appropriate sampling algorithm. Most popular sampling algorithms include the Monte Carlo approach (Metropolis and Ulam, 1949), which was found to be computationally more expensive than an efficient sampling algorithm known as Progressive Latin Hypercube Sampling (PLHS, Sheikholeslami and Razavi, 2017). PLHS was developed from the Latin Hypercube Sampling (LHS, Mckay et al. 1979). There has not been any work related to undertaking IM for multiple monitoring sets (multiple monitoring sites over multiple years) to characterize spatial and temporal variability of the soil hydraulic parameters. The characterization of these IM-based parameter distributions can be extended based on the PLHS sampling approach to predict the uncertainty in the expected performance of the reclamation covers over a long period when coupled with SVAT modelling.

Previous studies have not attempted to estimate uncertainty in the long-term future water balance of oil sands mine reclamation covers due to climate projections from the updated GCM outputs. In particular, the physically-based water balance SVAT models, namely HYDRUS-1D, has not been employed for this purpose. With the advent of updated climate projections from GCMs under Coupled Model Intercomparison Project (CMIP5) with the associated RCPs, the future performance of the cover designs demands to be revisited. The performance of the covers needs to be evaluated based on two key water balance components (AET and NP), while the previous studies did not evaluate potential changes in NP.

Since previous studies only used statistical downscaling methods (e.g. SDSM), high-resolution dynamical downscaling methods (e.g. WRF) may be explored for the evaluation of

performances of mine reclamation covers. No previous study evaluated the relative impacts on the future water balance components when climate change projections are downscaled using statistical and dynamical downscaling methods.

References

Abbaspour, K. C., M. T. van Genuchten, R. Schulin, and E. Schläppi, 1997: A sequential uncertainty domain inverse procedure for estimating subsurface flow and transport parameters. *Water Resour. Res.*, **33**, 1879–1892, doi:10.1029/97WR01230.

Abbaspour, K. C., R. Schulin, and M. T. van Genuchten, 2001: Estimating unsaturated soil hydraulic parameters using ant colony optimization. *Adv. Water Resour.*, **24**, 827–841, doi:10.1016/S0309-1708(01)00018-5.

Alam, M. S., and A. Elshorbagy, 2015: Quantification of the climate change-induced variations in Intensity-Duration-Frequency curves in the Canadian Prairies. *J. Hydrol.*, **527**, 990–1005, doi:10.1016/j.jhydrol.2015.05.059.

Alam, M. S., S. L. Barbour, A. Elshorbagy, and M. Huang, 2017: The Impact of Climate Change on the Performance of Oil Sands Reclamation Covers: A Comparison of Multiple General Circulation Models and Representative Concentration Pathways. *Proceedings of 70th Canadian Geotechnical Society Conference, GeoOttawa 2017, Ottawa, Ontario, October 2-4.*

Altdorff, D., L. Galagedara, and A. Unc, 2017: Impact of projected land conversion on water balance of boreal soils in western Newfoundland. *J. Water Clim. Chang.*, **8**, 613–626, doi:10.2166/wcc.2017.016.

Arora, V., 2002. Modeling vegetation as a dynamic component in soil-vegetation-atmosphere transfer schemes and hydrological models. *Rev. Geophys.,* 40(2), 1006, doi:10.1029/2001RG000103.

Barbour, S. L., and Coauthors, 2004: Tracking the evolution of reclaimed landscapes through the use of instrumented watersheds—A brief history of the Syncrude Southwest 30

Overburden Reclamation Research Program. *Proceedings of International Instrumented Watershed Symposium, Edmonton, Canada, 22-25 June 2004.*

Bard, Y., 1974: *Nonlinear Parameter Estimation*. New York, Academic Press, 341 pp.

Bastiaanssen, W. G. M., R. G. Allen, P. Droogers, G. D'Urso, and P. Steduto, 2007: Twenty-five years modeling irrigated and drained soils: State of the art. *Agric. Water Manag.*, **92**, 111–125, doi:10.1016/j.agwat.2007.05.013.

Bastidas, L. A., H. V., Gupta, K., Hsu, and S., Sorooshian, 2003: Parameter, structure, and model performance evaluation for land–surface schemes. Calibration of watershed models, Q. Duan, H. V. Gupta, S. Sorooshian, A. N. Rousseau, and R. Turcotte, eds., American Geo-physical Union, Washington, D.C.

(2) (PDF) Probabilistic Approach for Design and Hydrologic Performance Assessment of Reconstructed Watersheds. Available from: https://www.researchgate.net/publication/228669741_Probabilistic_Approach_for_Design_and_Hydrologic_Performance_Assessment_of_Reconstructed_Watersheds [accessed Feb 14 2020].

Beven, K., and A. Binley, 1992: The future of distributed models: Model calibration and uncertainty prediction. *Hydrol. Process.*, **6**, 279–298, doi:10.1002/hyp.3360060305.

Beven, K., 1993: Prophecy, reality and uncertainty in distributed hydrological modelling. *Adv. Water Resour.*, **16**, 41–51, doi:10.1016/0309-1708(93)90028-E.

Bitterlich, S., W. Durner, S. C. Iden, and P. Knabner, 2004: Inverse Estimation of the Unsaturated Soil Hydraulic Properties from Column Outflow Experiments Using Free-Form Parameterizations. *Vadose Zo. J.*, **3**, 971–981, doi:10.2113/3.3.971.

Boegh, E., and Coauthors, 2004: Incorporating remote sensing data in physically based distributed agro-hydrological modelling. *J. Hydrol.*, **287**, 279–299, doi:10.1016/j.jhydrol.2003.10.018.

Bordoni, M., M. Bittelli, R. Valentino, S. Chersich, and C. Meisina, 2017: Improving the estimation of complete field soil water characteristic curves through field monitoring data. *J. Hydrol.*, **552**, 283–305, doi:10.1016/j.jhydrol.2017.07.004.

Boyle, D. P., H. V. Gupta, and S. Sorooshian, 2000: Toward improved calibration of hydrologic models: Combining the strengths of manual and automatic methods. *Water Resour. Res.*, **36**, 3663–3674, doi:10.1029/2000WR900207.

Braud, I., A. C. Dantas-Antonino, M. Vauclin, J. L. Thony, and P. Ruelle, 1995: A simple soil-plant-atmosphere transfer model (SiSPAT) development and field verification. *J. Hydrol.*, **166**, 213–250, doi:10.1016/0022-1694(94)05085-C.

Brooks, R. H., and A. T. Corey, 1966: Properties of porous media affecting fluid flow. J. Irrig. Drain. Div., **IR2**, 61–88.

Bruckler, L., and H. Witono, 1989: Use of remotely sensed soil moisture content as boundary conditions in soil-atmosphere water transport modeling: 2. Estimating soil water balance. *Water Resour. Res.*, **25**, 2437–2447, doi:10.1029/WR025i012p02437.

Butters, G. L., and P. Duchateau, 2002: Continuous Flow Method for Rapid Measurement of Soil Hydraulic Properties: I. Experimental Considerations. *Vadose Zo. J*, **1**, 239–251, doi:10.2113/1.2.239.

Cameron, D., K. Beven, and P., Naden, 2000: Flood frequency estimation by continuous simulation under climate change (with uncertainty). *Hydrol. Earth Syst. Sci.*, **4**, 393–405.

Casanova, J. J., and J. Judge, 2008: Estimation of energy and moisture fluxes for dynamic vegetation using coupled SVAT and crop-growth models. *Water Resources Research*, 44, W07415, 1-20, doi:10.1029/2007WR006503.

Chen, J., F. P. Brissette, and R. Leconte, 2011: Uncertainty of downscaling method in quantifying the impact of climate change on hydrology. *J. Hydrol.*, **401**, 190–202, doi:10.1016/j.jhydrol.2011.02.020.

Chen, M., G. R. Willgoose, and P. M. Saco, 2014: Spatial prediction of temporal soil moisture dynamics using HYDRUS-1D. *Hydrol. Process.*, **28**, 171–185, doi:10.1002/hyp.9518.

Cooley, R. L., 1993: Exact Scheffé-type confidence intervals for output from groundwater flow models: 2. Combined use of hydrogeologic information and calibration data. *Water Resour. Res.*, **29**, 35–50, doi:10.1029/92WR01864.

Courault, D., J. P. Lagouarde, and B. Aloui, 1996: Evaporation for maritime catchment combining a meteorological model with vegetation information and airborne surface temperatures. *Agric. For. Meteorol.*, **82**, 93–117, doi:10.1016/0168-1923(96)02338-6.

Dahiya, R., J. Ingwersen, and T. Streck, 2007: The effect of mulching and tillage on the water and temperature regimes of a loess soil: Experimental findings and modeling. *Soil Tillage Res.*, **96**, 52–63, doi:10.1016/j.still.2007.02.004.

Dane, J. H., and S. Hruska, 1983: In-Situ Determination of Soil Hydraulic Properties during Drainage1. *Soil Sci. Soc. Am. J.*, **47**, 619, doi:10.2136/sssaj1983.03615995004700040001x.

Deb, K., A. Pratap, S. Agarwal, and T. Meyarivan, 2002: A fast and elitist multiobjective genetic algorithm: NSGA-II. *IEEE Trans. Evol. Comput.*, **6**, 182–197, doi:10.1109/4235.996017.

Demarty, J., C. Ottlé, I. Braud, A. Olioso, J. Frangi, L. Bastidas, and H. Gupta, 2004: Using a multiobjective approach to retrieve information on surface properties used in a SVAT model. *J. Hydrol.*, **287**, 214–236, doi:10.1016/j.jhydrol.2003.10.003.

Doering, E. J., 1965: Soil water diffusivity by the one-step method. *Soil Sci.*, **99**, 322–326.

Doherty, J., 2016: PEST: Model-Independent Parameter Estimation. User Manual. 366 pp.

Elshorbagy, A., and S. L. Barbour, 2007: Probabilistic approach for design and hydrologic performance assessment of reconstructed watersheds. *J. Geotech. Geoenvironmental Eng.*, **133(9)**, 1110–1118, doi:10.1061/(ASCE)1090-0241(2007)133:9(1110).

Facchi, A., B., Ortuani, D., Maggi, C., Gandolfi, 2004: Coupled SVAT–groundwater model for water resources simulation in irrigated alluvial plains. *Environ Model Softw.*. 19, 1053–1063, doi: 10.1016/j.envsoft.2003.11.008.

Feddes, R. A., E. Bresler, and S. P. Neuman, 1974: Field test of a modified numerical model for water uptake by root systems. *Water Resour. Res.*, **10**, 1199–1206.

Flato, G and Coauthors, 2013: Evaluation of climate models. Evaluation of Climate Models. In: Climate Change 2013: The Physical Science Basis. Cambridge University Press, Cambridge, United Kingdom and New York, NY, USA.

Franczyk, J., and H. Chang, 2009: The effects of climate change and urbanization on the runoff of the Rock Creek basin in the Portland metropolitan area, Oregon, USA. *Hydrol. Process.*, **23(6)**, 805–815, doi:10.1002/hyp.7176.

Gardner, W. R., 1956: Calculation of Capillary Conductivity from Pressure Plate Outflow Data1. *Soil Sci. Soc. Am. J.*, **20**, 317, doi:10.2136/sssaj1956.03615995002000030006x.

GEO-SLOPE, 2007: Seepage modeling with SEEP/W: An engineering methodology, GEOSLOPE International Ltd., Calgary, Canada.

GEO-SLOPE, 2016: Land-climate interaction hydraulic modeling of a soil cover system located in northern Canada. GEOSLOPE International Ltd., Calgary, Canada.

Githui, F., W. Gitau, F. Mutua, and W. Bauwens, 2009: Climate change impact on SWAT simulated streamflow in western Kenya. *Int. J. Climatol.*, **29**, 1823–1834, doi:10.1002/joc.1828.

Gupta, H. V., S. Sorooshian, and P. O. Yapo, 1998: Toward improved calibration of hydrologic models: Multiple and noncommensurable measures of information. *Water Resour. Res.*, **34**, 751–763, doi:10.1029/97WR03495.

Hagemann, S., C. Chen, J. O. Haerter, J. Heinke, D. Gerten, and C. Piani, 2011: Impact of a Statistical Bias Correction on the Projected Hydrological Changes Obtained from Three GCMs and Two Hydrology Models. *J. Hydrometeorol.*, **12**, 556–578, doi:10.1175/2011JHM1336.1.

Hannula, H.-R., J. Lemmetyinen, A. Kontu, C. Derksen, and J. Pulliainen, 2016: Spatial and temporal variation of bulk snow properties in northern boreal and tundra environments based on extensive field measurements. *Geosci. Instrumentation, Methods Data Syst.*, **5**, 347–363, doi:10.5194/gi-5-347-2016.

Harman, C. J., P. S. C. Rao, N. B. Basu, G. S. McGrath, P. Kumar, and M. Sivapalan, 2011: Climate, soil, and vegetation controls on the temporal variability of vadose zone transport. *Water Resour. Res.*, **47**, doi:10.1029/2010WR010194.

Hashmi, M. Z., A. Y. Shamseldin, and B. W. Melville, 2011: Comparison of SDSM and LARS-WG for simulation and downscaling of extreme precipitation events in a watershed. *Stoch. Environ. Res. Risk Assess.*, **25(4)**, 475–484, doi:10.1007/s00477-010-0416-x.

Hollenbeck, K. J., and K. H. Jensen, 1998: Maximum-likelihood estimation of unsaturated hydraulic parameters. *J. Hydrol.*, **210**, 192–205, doi:10.1016/S0022-1694(98)00185-1.

Hopmans, J. W., J. Simunek, N. Romano, and W. Durner, 2002: Chapter 3.6.2: Inverse Methods. In *J.H. Dane G.C. Topp Methods Soil Anal. Part 4. Phys. methods. SSSA B. Ser. 5. SSSA, Madison, WI.*

Huang, M., S. L. Barbour, A. Elshorbagy, J. D. Zettl, and B. Cheng Si, 2011a: Infiltration and drainage processes in multi-layered coarse soils. *Can. J. Soil Sci.*, **91**, 169–183, doi:10.4141/cjss09118.

Huang, M., S. L. Barbour, A. Elshorbagy, J. Zettl, and B. Cheng Si, 2011b: Water availability and forest growth in coarse-textured soils. *Can. J. Soil Sci.*, **91**, 199–210, doi:10.4141/cjss10012.

Huang, M., Zettl, J., and Barbour, L., 2011c: Preliminary soil-water-atmospheric modeling of the proposed Aurora capping treatments. Report prepared for Syncrude Canada Limited.

Huang, M., Barbour, L., and Carey, S., 2012: Numerical modelling of the long-term water dynamics and the impact of soil cover depth on transpiration from reclamation soil covers over shale overburden. Report prepared for Syncrude Canada Limited.

Huang, M., S. L. Barbour, and S. K. Carey, 2015a: The impact of reclamation cover depth on the performance of reclaimed shale overburden at an oil sands mine in Northern Alberta, Canada. *Hydrol. Process.*, **29(12)**, 2840–2854, doi:10.1002/hyp.10229.

Huang, M., J. N. Hilderman, and L. Barbour, 2015b: Transport of stable isotopes of water and sulphate within reclaimed oil sands saline-sodic mine overburden. *J. Hydrol.*, **529**, 1550–1561, doi:10.1016/j.jhydrol.2015.08.028.

Huang, M., J. D. Zettl, S. L. Barbour, and D. Pratt, 2016: Characterizing the spatial variability of the hydraulic conductivity of reclamation soils using air permeability. *Geoderma*, **262**, 285–293, doi:10.1016/j.geoderma.2015.08.014.

Huntington, T. G., 2006: Evidence for intensification of the global water cycle: Review and synthesis. *J. Hydrol.*, **319(1-4)**, 83–95, doi:10.1016/j.jhydrol.2005.07.003.

Jacques, D., C. Smith, J. Šimůnek, and D. Smiles, 2012: Inverse optimization of hydraulic, solute transport, and cation exchange parameters using HP1 and UCODE to simulate cation exchange. *J. Contam. Hydrol.*, **142**–**143**, 109–125, doi:10.1016/j.jconhyd.2012.03.008.

Jirků, V., R. Kodešová, A. Nikodem, M. Mühlhanselová, and A. Žigová, 2013: Temporal variability of structure and hydraulic properties of topsoil of three soil types. *Geoderma*, **204**–**205**, 43–58, doi:10.1016/j.geoderma.2013.03.024.

Karavanova, E. I., and M. S. Malinina, 2007: Spatial and temporal variation in the elemental composition of soil solution from gleyic peaty-podzolic soils. *Eurasian Soil Sci.*, **40**, 830–838, doi:10.1134/S1064229307080042.

Kelln, C., S. L. Barbour, and C. Qualizza, 2008: Controls on the spatial distribution of soil moisture and solute transport in a sloping reclamation cover. *Can. Geotech. J.*, **45**, 351–366, doi:10.1139/T07-099.

Keshta, N., A. Elshorbagy, and S. Carey, 2012: Impacts of climate change on soil moisture and evapotranspiration in reconstructed watersheds in northern Alberta, Canada. *Hydrol. Process.*, **26(9)**, 1321–1331, doi:10.1002/hyp.8215.

Kool, J. B., J. C. Parker, and M. T. van Genuchten, 1985: *ONESTEP: A nonlinear parameter estimation program for evaluating soil hydraulic properties from one-step outflow experiments*. Bull. 85- 3. Virginia Agric. Exp. Stn., Blacksburg, VA.

Kool, J. B., J. C. Parker, and M. T. van Genuchten, 1987: Parameter estimation for unsaturated flow and transport models - A review. *J. Hydrol.*, **91**, 255–293, doi:10.1016/0022-1694(87)90207-1.

Kool, J. B., and J. C. Parker, 1988: Analysis of the inverse problem for transient unsaturated flow. *Water Resour. Res.*, **24**, 817–830, doi:10.1029/WR024i006p00817.

Kool, D., N. Agam, N. Lazarovitch, J. L. Heitman, T. J. Sauer, and A. Ben-Gal, 2014: A review of approaches for evapotranspiration partitioning. *Agric. For. Meteorol.*, **184**, 56–70, doi:10.1016/j.agrformet.2013.09.003.

Lambot, S., M. Javaux, F. Hupet, and M. Vanclooster, 2002: A global multilevel coordinate search procedure for estimating the unsaturated soil hydraulic properties. *Water Resour. Res.*, **38**, 6-1-6–15, doi:10.1029/2001WR001224.

Leta, O. T., A. I. El-Kadi, H. Dulai, and K. A. Ghazal, 2016: Assessment of climate change impacts on water balance components of Heeia watershed in Hawaii. *J. Hydrol. Reg. Stud.*, **8**, 182–197, doi:10.1016/j.ejrh.2016.09.006.

Madsen, H., 2003: Parameter estimation in distributed hydrological catchment modelling using automatic calibration with multiple objectives. *Adv. Water Resour.*, **26**, 205–216, doi:10.1016/S0309-1708(02)00092-1.

Mango, L. M., A. M. Melesse, M. E. McClain, D. Gann, and S. G. Setegn, 2011: Land use and climate change impacts on the hydrology of the upper Mara River Basin, Kenya: results of a modeling study to support better resource management. *Hydrol. Earth Syst. Sci.*, **15**, 2245–2258, doi:10.5194/hess-15-2245-2011.

Marquardt, D. W., 1963: An Algorithm for Least-Squares Estimation of Nonlinear Parameters. *J. Soc. Ind. Appl. Math.*, **11**, 431–441, doi:10.1137/0111030.

Matott, L. S., 2005: OSTRICH – An Optimization Software Toolkit for Research Involving Computational Heuristics Documentation and User's Guide.

May, W., 2008: Potential future changes in the characteristics of daily precipitation in Europe simulated by the HIRHAM regional climate model. *Clim. Dyn.*, **30**, 581–603, doi:10.1007/s00382-007-0309-y.

Meiers, G. P., S. L. Barbour, C. V. Qualizza, and B. S. Dobchuk, 2011: Evolution of the Hydraulic Conductivity of Reclamation Covers over Sodic/Saline Mining Overburden. *J. Geotech. Geoenvironmental Eng.*, **137**, 968–976, doi:10.1061/(ASCE)GT.1943-5606.0000523.

Mertens, J., R. Stenger, and G. F. Barkle, 2006: Multiobjective Inverse Modeling for Soil Parameter Estimation and Model Verification. *Vadose Zo. J.*, **5**, 917, doi:10.2136/vzj2005.0117.

Metropolis, N., and S. Ulam, 1949: The Monte Carlo Method. *Journal of the American Statistical Association*, **44(247)**, 335–341.

Meyers, T. P., and K. T. Paw U, 1987: Modelling the plant canopy micrometeorology with higher-order closure principles. *Agric. For. Meteorol.*, **41**, 143–163, doi:10.1016/0168-1923(87)90075-X.

Móricz, N., C. Mátyás, I. Berki, E. Rasztovits, Z. Vekerdy, and Z. Gribovszki, 2012: Comparative water balance study of forest and fallow plots. *iForest - Biogeosciences For.*, **5**, 188–196, doi:10.3832/ifor0624-005.

Najafi, M. R., H. Moradkhani, and I. W. Jung, 2011: Assessing the uncertainties of hydrologic model selection in climate change impact studies. *Hydrol. Process.*, **25**, 2814–2826, doi:10.1002/hyp.8043.

Nasta, P., and J. B. Gates, 2013: Plot-scale modeling of soil water dynamics and impacts of drought conditions beneath rainfed maize in Eastern Nebraska. *Agric. Water Manag.*, **128**, 120–130, doi:10.1016/j.agwat.2013.06.021.

O'Kane Consultants Inc. (OKC), 2001: *Southwest Sands Storage and 30-Dump automated water balance monitoring systems at Syncrude Canada Ltd*. OKC Report No. 653--2 pp.

O'Kane Consultants Inc. (OKC), 2016: *Instrumented watershed monitoring program at the Southwest Sands Storage facility: Performance monitoring report for the period January 2015 to December 2015*. OKC Report No. 690/01--72 pp.

O'Kane Consultants Inc. (OKC), 2017: Aurora Soil Capping Study Five Year Performance Monitoring Report November 2012 to September 2017. 690/141--001.

Olioso, A., and Coauthors, 2005: Future directions for advanced evapotranspiration modeling: Assimilation of remote sensing data into crop simulation models and SVAT models. *Irrig. Drain. Syst.*, **19**, 377–412, doi:10.1007/s10795-005-8143-z.

Passioura, J., 1976: Determining soil water diffusivities from one-step outflow experiments. *Austr. J. Soil Res.*, **15**, 1–8.

Pereira, L. S., R. G. Allen, M. Smith, and D. Raes, 2015: Crop evapotranspiration estimation with FAO56: Past and future. *Agric. Water Manag.*, **147**, 4–20, doi:10.1016/j.agwat.2014.07.031.

Poeter, E. P., and M. C. Hill, 1998: Documentation of UCODE: a computer code for universal inverse modeling. US Geological Survey, Water-Resources Investigations Report 98-4080, 121 pp.

Qu, W., H. R. Bogena, J. A. Huisman, G. Martinez, Y. A. Pachepsky, and H. Vereecken, 2014: Effects of Soil Hydraulic Properties on the Spatial Variability of Soil Water Content: Evidence from Sensor Network Data and Inverse Modeling. *Vadose Zo. J.*, **13**, doi:10.2136/vzj2014.07.0099.

Racsko, P., L. Szeidl, and M. Semenov, 1991: A serial approach to local stochastic weather models. *Ecol. Modell.*, **57**, 27–41, doi:10.1016/0304-3800(91)90053-4.

Scharnagl, B., J. A. Vrugt, H. Vereecken, and M. Herbst, 2011: Inverse modelling of in situ soil water dynamics: investigating the effect of different prior distributions of the soil hydraulic parameters. *Hydrol. Earth Syst. Sci.*, **15**, 3043–3059, doi:10.5194/hess-15-3043-2011.

Schindler, U., W. Durner, G. von Unold, and L. Müller, 2010: Evaporation Method for Measuring Unsaturated Hydraulic Properties of Soils: Extending the Measurement Range. *Soil Sci. Soc. Am. J.*, **74**, 1071, doi:10.2136/sssaj2008.0358.

Schoups, G., J. W. Hopmans, C. A. Young, J. A. Vrugt, and W. W. Wallender, 2005: Multi-criteria optimization of a regional spatially-distributed subsurface water flow model. *J. Hydrol.*, **311**, 20–48, doi:10.1016/j.jhydrol.2005.01.001.

Semenov, M. A., and E. M. Barrow, 1997: Use of a stochastic weather generator in the development of climate change scenarios. 397–414.

Shelia, V., J. Šimůnek, K. Boote, and G. Hoogenbooom, 2018: Coupling DSSAT and HYDRUS-1D for simulations of soil water dynamics in the soil-plant-atmosphere system. *J. Hydrol. Hydromechanics*, **66**, doi:10.1515/johh-2017-0055.

Sigouin, M. J. P., M. Dyck, B. C. Si, and W. Hu, 2016: Monitoring soil water content at a heterogeneous oil sand reclamation site using a cosmic-ray soil moisture probe. *J. Hydrol.*, **543**, 510–522, doi:10.1016/j.jhydrol.2016.10.026.

Šimůnek, J., M. T. van Genuchten, and O. Wendroth, 1998: Parameter Estimation Analysis of the Evaporation Method for Determining Soil Hydraulic Properties. *Soil Sci. Soc. Am. J.*, **62**, 894, doi:10.2136/sssaj1998.03615995006200040007x.

Simunek, J., and J. Hopmans, 2002: Parameter optimization and nonlinear fitting. In: Dane, J.H., Topp, G.C. (Eds.), Methods of Soil Analysis. Part 4: Physical Methods, vol. 5. Soil Science Society of America Book, Madison, WI. 139–157.

Simunek, J., J. M. Kohne, R. Kodesova, and M. Sejna, 2008: Simulating Nonequilibrium Movement of Water, Solutes and Particles Using HYDRUS – A Review of Recent Applications. *Soil Water Res.*, **3**, S42--S51.

Simunek, J., M. T. van Genuchten, and M. Sejna, 2012: HYDRUS: Model use, calibration, and validation. *Am. Soc. Agric. Biol. Eng.*, **55**, 1261–1274.

Simunek, J., Šejna, M., Saito, H., Sakai, M., and van Genuchten, M. T., 2013: The HYDRUS-1D Software Package for Simulating the One-Dimensional Movement of Water, Heat, and Multiple Solutes in Variably-Saturated Media. University of California, Riverside, CA.

Singh, P. N., W. W. Wallender, M. P. Maneta, S. L. L., and B. A. Olsen, 2010: Sustainable Root Zone Salinity and Shallow Water Table in the Context of Land Retirement. *J. Irrig. Drain. Eng.*, **136**, 289–299, doi:10.1061/(ASCE)IR.1943-4774.0000065.

Singh, P. N., and W. W. Wallender, 2011: Effects of Soil Water Salinity on Field Soil Hydraulic Functions. *J. Irrig. Drain. Eng.*, **137**, 295–303, doi:10.1061/(ASCE)IR.1943-4774.0000290.

Soer, G. J. R., 1980: Estimation of regional evapotranspiration and soil moisture conditions using remotely sensed crop surface temperatures. *Remote Sens. Environ.*, **9**, 27–45, doi:10.1016/0034-4257(80)90045-0.

Soylu, M. E., C. J. Kucharik, and S. P. Loheide, 2014: Influence of groundwater on plant water use and productivity: Development of an integrated ecosystem – Variably saturated soil water flow model. *Agric. For. Meteorol.*, **189**–**190**, 198–210, doi:10.1016/j.agrformet.2014.01.019.

Taylor, K. E., 2001: Summarizing multiple aspects of model performance in a single diagram. Journal of Geophysical Research: Atmospheres, **106(D7)**, 7183–7192, doi:10.1029/2000JD900719.

Taylor, K. E., R. J. Stouffer, and G. A. Meehl, 2012: An overview of CMIP5 and the experiment design. *Bull. Am. Meteorol. Soc.*, **93**, 485–498, doi:10.1175/BAMS-D-11-00094.1.

Thomasson, M. J., and P. J. Wierenga, 2003: Spatial variability of the effective retardation factor in an unsaturated field soil. *J. Hydrol.*, **272**, 213–225, doi:10.1016/S0022-1694(02)00266-4.

Thompson, C., C. A. Mendoza, and K. J. Devito, 2017: Potential influence of climate change on ecosystems within the Boreal Plains of Alberta. *Hydrol. Process.*, **31(11)**, 2110–2124, doi:10.1002/hyp.11183.

Therrien, R., R. G. Mclaren, E. A. Sudicky, and S. M. Panday, 2010: HydroGeoSphere: A Three-dimensional Numerical Model Describing Fully-integrated Subsurface and Surface Flow and Solute Transport, report, Groundwater Simul. Group, Univ. of Waterloo, Ontario, Waterloo.

van Genuchten, M. T., 1980: A closed-form equation for predicting the hydraulic conductivity of unmatured soils. *Soil Sci. Soc. Am. J.*, **44(5)**, 892–898.

Vrugt, J., and W. Bouten, 2002: Validity of First-Order Approximations to Describe Parameter Uncertainty in Soil Hydrologic Models. *Soil Sci. Soc. Am. J.*, **66**, 1740–1751, doi:10.2136/sssaj2002.1740.

Vrugt, J. A., H. V Gupta, L. A. Bastidas, W. Bouten, and S. Sorooshian, 2003a: Effective and efficient algorithm for multiobjective optimization of hydrologic models. *Water Resour. Res.*, **39**, 19, doi:10.1029/2002WR001746.

Vrugt, J. A., W. Bouten, H. V. Gupta, and J. W. Hopmans, 2003b: Toward Improved Identifiability of Soil Hydraulic Parameters: On the Selection of a Suitable Parametric Model. *Vadose Zo. J.*, **2**, 98–113, doi:10.2113/2.1.98.

Vrugt, J. A., G. Schoups, J. W. Hopmans, C. Young, W. W. Wallender, T. Harter, and W. Bouten, 2004: Inverse modeling of large-scale spatially distributed vadose zone properties using global optimization. *Water Resour. Res.*, **40**, doi:10.1029/2003WR002706.

Vrugt, J. A., and B. A. Robinson, 2007: Improved evolutionary optimization from genetically adaptive multimethod search. *Proc. Natl. Acad. Sci.*, **104**, 708–711, doi:10.1073/pnas.0610471104.

Vrugt, J. A., P. H. Stauffer, T. Wöhling, B. A. Robinson, and V. V. Vesselinov, 2008: Inverse Modeling of Subsurface Flow and Transport Properties: A Review with New Developments. *Vadose Zo. J.*, **7**, 843, doi:10.2136/vzj2007.0078.

Whisler, F. D., and K. K. Watson, 1968: One-dimensional gravity drainage of uniform columns of porous materials. *J. Hydrol.*, **6**, 277–296, doi:10.1016/0022-1694(68)90104-2.

Wilby, R. L., and I. Harris, 2006: A framework for assessing uncertainties in climate change impacts: Low-flow scenarios for the River Thames, UK. *Water Resour. Res.*, **42**, doi:10.1029/2005WR004065.

Wilby, R. L., and C. W. Dawson, 2007: SDSM 4.2 – A decision support tool for the assessment of regional climate change impacts. Version 4.2 User Manual.

Wissmeier, L., and D. A. Barry, 2008: Reactive transport in unsaturated soil: Comprehensive modelling of the dynamic spatial and temporal mass balance of water and chemical components. *Adv. Water Resour.*, **31**, 858–875, doi:10.1016/j.advwatres.2008.02.003.

Wöhling, T., J. A. Vrugt, and G. F. Barkle, 2008: Comparison of Three Multiobjective Optimization Algorithms for Inverse Modeling of Vadose Zone Hydraulic Properties. *Soil Sci. Soc. Am. J.*, **72**, 305, doi:10.2136/sssaj2007.0176.

Yapo, P. O., H. V. Gupta, and S. Sorooshian, 1998: Multi-objective global optimization for hydrologic models. *J. Hydrol.*, **204**, 83–97, doi:10.1016/S0022-1694(97)00107-8.

Zettl, J., S. L. Barbour, M. Huang, B. Si, and L. A. Leskiw, 2011: Influence of textural layering on field capacity of coarse soils. *Can. J. Soil Sci.*, **91(2)**, 133–147, doi:10.4141/cjss09117.

Zettl, J., M. Huang, S. L. Barbour, and L. Barber, 2012: Field air permeability testing to characterize the hydraulic conductivity of coarse textured reclamation covers over uranium mine waste. *GeoManitoba, Winnipeg, Manitoba, Paper 320*, 7–25.

CHAPTER 3 - CHARACTERIZING UNCERTAINTY IN THE HYDRAULIC PARAMETERS OF OIL SANDS MINE RECLAMATION COVERS AND ITS INFLUENCE ON WATER BALANCE PREDICTIONS (ALAM ET AL. 2020)

Preface

The first objective of this research was: "To quantify parameter uncertainty in the modelling of water balance for oil sands reclamation covers by obtaining optimized parameter sets for the cover materials based on independent soil monitoring locations (spatial variability) and for different time series (temporal variability), using the combination of the SVAT modelling packages and inverse modelling techniques".

The first published paper presented in this chapter quantifies parameter variability through inverse modelling and then evaluates the long-term performances of oil sands mine reclamation covers incorporating both variability in hydraulic parameters as well as temporally variable parameters such as climate and vegetation. This study demonstrated how to use inverse modelling to obtain optimized soil hydraulic parameters for 155 water balance models, while a set of 155 optimized parameters was used to provide the statistical distributions for spatial and temporal variability of the soil hydraulic parameters. Since temporal variability was insignificant, a Latin hypercube sampling technique was used to fully characterize the spatial variability of soil hydraulic parameters. This is the first known application of parameter variability to evaluate the long-term performance of oil sands reclamation covers. The published paper in this chapter is presented with minor changes as suggested by the examining committee.

I, Md. Shahabul Alam, developed, calibrated and validated (using an indirect approach) all the physically-based water balance models (HYDRUS-1D), reviewed the literature, conducted numerical simulations, analyzed and discussed the results, and wrote the manuscript. As supervisor, Dr. S. L. Barbour and as co-supervisor, Dr. M. Huang supervised all parts of the work, critically reviewed and edited the manuscript, and provided feedbacks on different aspects of the study. This chapter has been published with the following citation:

Alam, M. S., Barbour, S. L., and Huang, M. (2020). Characterizing uncertainty in the hydraulic parameters of oil sands mine reclamation covers and its influence on water balance predictions, *Hydrol. Earth Syst. Sci.*, 24, 735–759, https://doi.org/10.5194/hess-24-735-2020.

Abstract

One technique to evaluate the performance of oil sands reclamation covers is through the simulation of long-term water balance using calibrated soil–vegetation–atmosphere transfer models. Conventional practice has been to derive a single set of optimized hydraulic parameters through inverse modelling (IM) based on short-term (< 5– 10 years) monitoring datasets. This approach is unable to characterize the impact of variability in the cover properties. This study utilizes IM to optimize the hydraulic properties for 12 soil cover designs, replicated in triplicate, at Syncrude's Aurora North mine site. The hydraulic parameters for three soil types (peat cover soil, coarse-textured subsoil, and lean oil sand substrate) were optimized at each monitoring site from 2013 to 2016. The resulting 155 optimized parameter values were used to define distributions for each parameter/soil type, while the progressive Latin hypercube sampling (PLHS) method was used to sample parameter values randomly from the optimized parameter distributions. Water balance models with the sampled parameter sets were used to evaluate variations in the maximum sustainable leaf area index (LAI) for five illustrative covers and quantify uncertainty

associated with long-term water balance components and LAI values. Overall, the PLHS method was able to better capture broader uncertainty in the water balance components than a discrete interval sampling method. The results also highlight that climate variability dominates the simulated uncertainty in actual evapotranspiration and that climate and parameter variability have a similar influence on the uncertainty in net percolation.

3.1 Introduction

The hydraulic parameters of reclamation soil covers on oil sands mine waste have most commonly been characterized by calibrating water dynamics models against a single profile of field-monitored water content and suction. In many cases, this has been undertaken by deriving a single set of optimized parameter values from inverse modelling (IM) of short-term (5–10 years) monitoring data (Alam et al., 2017; Boese, 2003; Huang et al., 2015, 2011a, b, c; Keshta et al., 2009; Price et al., 2010; Qualizza et al., 2004). Devito et al. (2012) recommend that model calibration be focused on seasonal and inter-annual climate variability (e.g., wet or dry) and also take into account spatial variations in water movement within a spatially heterogeneous landscape. The current modelling approach that attempts to determine a single set of "best fit" properties based on IM of a single monitoring station is unable to characterize the spatial or temporal variability within the hydraulic properties of the cover soil and underlying mine waste. Quantifying spatial and temporal variability would be of value when assessing the expected long-term performance of reclaimed oil sands closure landscapes. However, spatial and temporal variability in model parameters is not conventionally quantified or incorporated into the soil–vegetation–atmosphere transfer (SVAT) models used to simulate long-term cover performance.

The focus of this study is characterization of the variability in the hydraulic parameters of reclamation soil covers over oil sands mining waste and the impact of this variability on

predictions of the long-term water balance for these sites. The two key measures of success for oil sands mine reclamation are the water balance components of actual evapotranspiration (AET) and net percolation (NP). AET quantifies the ability of the cover to support re-vegetation, while NP quantifies recharge into the underlying mine waste and the concomitant impact on water and contaminant release to downgradient surface water bodies.

The temporal variability of hydraulic parameters for these cover soils has been characterized by both direct testing and IM. Temporal variability in hydraulic conductivity (K_s) was measured in reclamation covers over saline–sodic overburden at Syncrude's Mildred Lake mine by Meiers et al. (2011), and a similar evolution in K_s was also obtained through IM by Huang et al. (2015). Such observed temporal variability was assumed to be the result of changes in density and pore-size distribution of reclamation soils as a result of freeze–thaw or wet–dry cycles and vegetation establishment. Spatial variability would be expected to occur in reclamation covers because of variations in soil texture, cover construction/placement conditions, topography, or vegetation establishment. For example, Huang et al. (2016) characterized the spatial variability of K_s using air-permeability testing of covers.

More recently, IM has been undertaken on multiple monitoring sets collected over multiple years to evaluate the impact of parameter variability on the predicted long-term performance of reclamation covers (Alam et al., 2017; Huang et al., 2017; OKC, 2017). Recently, Alam et al. (2017) and Alam et al. (2018b) undertook a preliminary evaluation of the impact of variability in the hydraulic properties of reclamation covers on the long-term water balance of oil sands reclamation covers. In that study, IM using HYDRUS-1D was undertaken for four different reclamation covers (replicated in triplicate) over 3 monitoring years to characterize the water retention and hydraulic conductivity of the covers. The

calibrated (optimized) parameters showed that parameter variability could be linked to both spatial and temporal variability, but was dominated by spatial variability. A key limitation of this previous study was that the variability in the hydraulic properties was represented only by discrete values (i.e., the mean value of the parameter as well as upper and lower bounding values) without a full statistically based characterization of the parameter variability. The value of a full statistical description of variability in characterizing the uncertainty in the predicted water balance of the covers under a prescribed, future, climate variability was unknown.

The use of soil hydraulic parameters with spatial and/or temporal variability instead of a single parameter set can provide more information about prediction uncertainty associated with watershed response to climate variability (Benke et al., 2008). Various Monte Carlo (MC)-based approaches (e.g., generalized likelihood uncertainty estimation (GLUE; Beven and Binley, 1992), the Metropolis algorithm, and Monte Carlo Markov chain (MCMC; Metropolis et al., 1953)) can be used to sample parameters randomly from the posterior distributions of the optimized parameters. Given that MC-based sampling strategies can be computationally expensive and sometimes unaffordable for computationally demanding models, other sampling strategies have been developed and improved over the last several decades. Of these, Latin hypercube sampling (LHS; McKay et al., 1979) has been most commonly used for uncertainty and sensitivity analysis in the field of water and environmental modelling (Hossain et al., 2006; Gong et al., 2015; Higdon et al., 2013; Sheikholeslami and Razavi, 2017). The LHS approach offers a sampling strategy that can significantly reduce the sample size without compromising the accuracy of uncertainty estimation compared to the MC sampling approach (Iman and Conover, 1980; Iman and Helton, 1988; McKay et al., 1979). However, a major drawback of traditional LHS- and MC-based sampling strategies is that the entire sample set is generated together and,

unfortunately, an appropriate sample size is not known a priori. An appropriate sample size here refers to a sufficiently large number of sampled parameters so as to achieve convergence towards a common mean and standard deviation (SD) of the parameters, as well as the mean and SD of major components of the water balance (e.g., AET and NP).

The appropriate sample size for each parameter can be determined using a convergence criterion in the case of LHS; however, the whole sample size is discarded if the convergence criteria fail, and a new set of simulations must be conducted with a larger sample size to achieve convergence. To overcome this computationally demanding approach, a new, efficient, and sequential sampling strategy called progressive Latin hypercube sampling (PLHS; Sheikholeslami and Razavi, 2017) can be used. In PLHS, the sample size is divided into a series of smaller subsets (in place of the single sample set used for LHS), and each subset is added progressively to sequentially grow the sample size. This can be summarized as follows: (i) each smaller subset forms a Latin hypercube, (ii) the progressively added subsets form a Latin hypercube, and (iii) the entire sampled parameter set (consists of all smaller subsets) also forms a Latin hypercube. The details on LHS and PLHS are provided in Appendix A.

The two key advantages of the PLHS method over other sampling methods (e.g., MC) are as follows: (i) it achieves given convergence criterion with a smaller number of samples (i.e., smaller sample size) and (ii) it allows for sequential sampling without having to discard the whole sample size when convergence criteria are not attained.

The key research question of this study is as follows: what is the influence of soil hydraulic parameter variability on the long-term cover performance of the reclamation covers in northern Alberta, Canada? This question led us to the following study objectives: (i) identify the most efficient way to characterize distributions of the optimized hydraulic

parameters from a physically based water balance model for an oil sands reclamation cover in northern Alberta, Canada, and (ii) quantify relative uncertainty from various sources associated with the long-term water balance of the reclamation covers.

These objectives will be met by undertaking IM of multiple monitoring sets (multiple monitoring sites in multiple years) to develop a statistical distribution of parameter variability. While IM will be used to characterize only parameter variability, this parameter variability combined with climate variability will be incorporated to characterize uncertainty in water balance elements due to each source of variability. These distributions will be primarily utilized within a PLHS-based sampling approach to predict uncertainty in the expected performance of the covers over the long term based on SVAT modelling. Comparisons will determine how these predictions differ if either a discrete or continuous distribution function is used to characterize material variability. To the best of our knowledge, this more rigorous approach to evaluating the long-term performance of soil covers has not been conducted in general or specifically applied to the evaluation of oil sands reclamation covers.

3.2 Materials and methods

3.2.1 Study sites and reclamation covers

This study used soil monitoring data and meteorological data collected from the Aurora Soil Capping Study (ASCS), located at the Aurora North Mine of Syncrude Canada Ltd. (SCL) in Alberta, Canada (Fig. 3-1a). The ASCS is comprised of a series of 12 alternate, 1 ha covers, replicated in triplicate, and placed over a lean oil sands (LOS) overburden dump. The primary purpose of the different cover designs was to compare the performance of alternate materials and cover thicknesses in supporting vegetation and net percolation (OKC, 2017).

The layouts of the 12 covers (replicated) are shown in Fig. 3-1b and are designated by a treatment number (i.e., TRT no.), with each treatment having 3 replicate cells for a total of 36 cells in the ASCS that were randomly placed across the watershed.

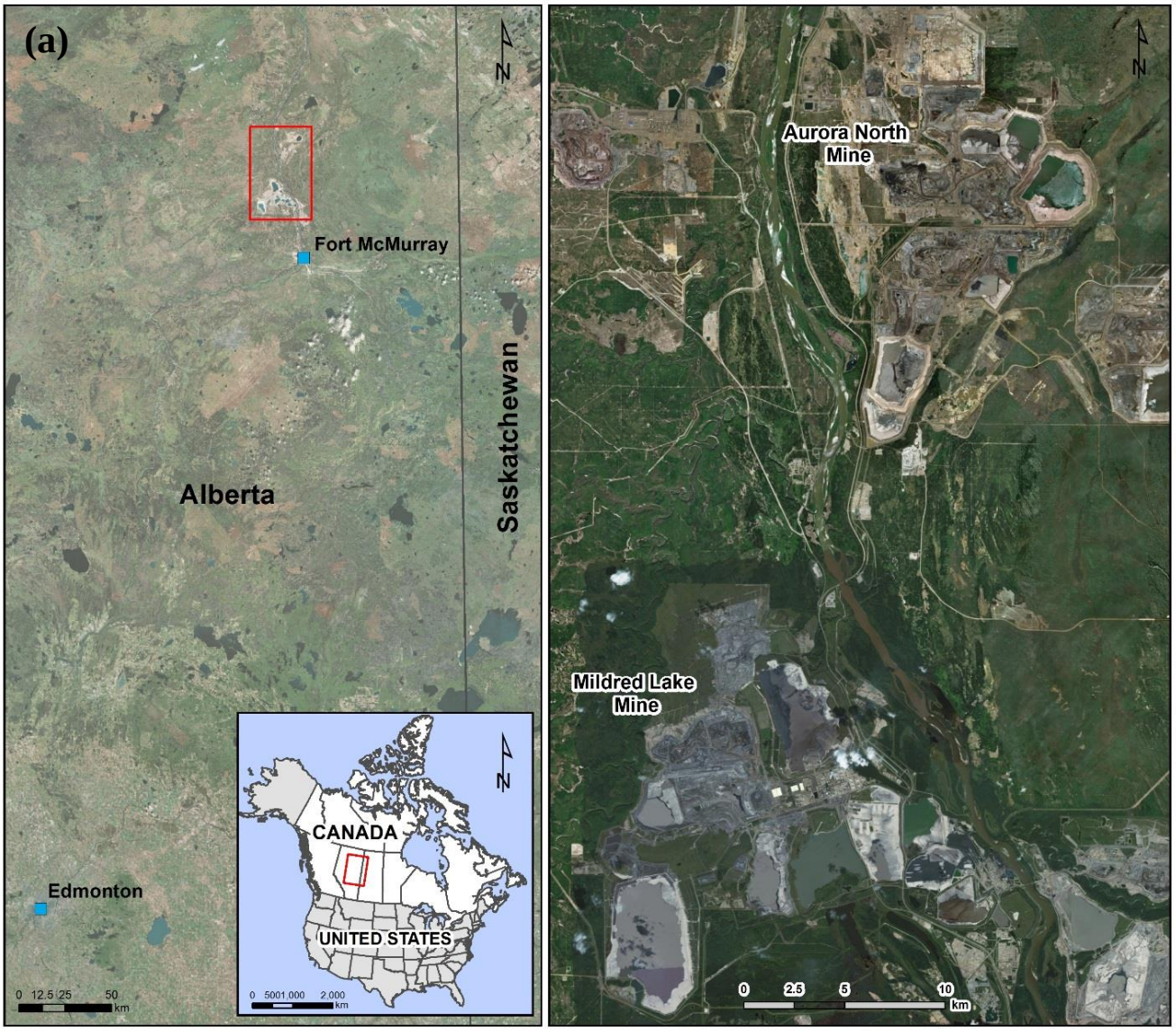

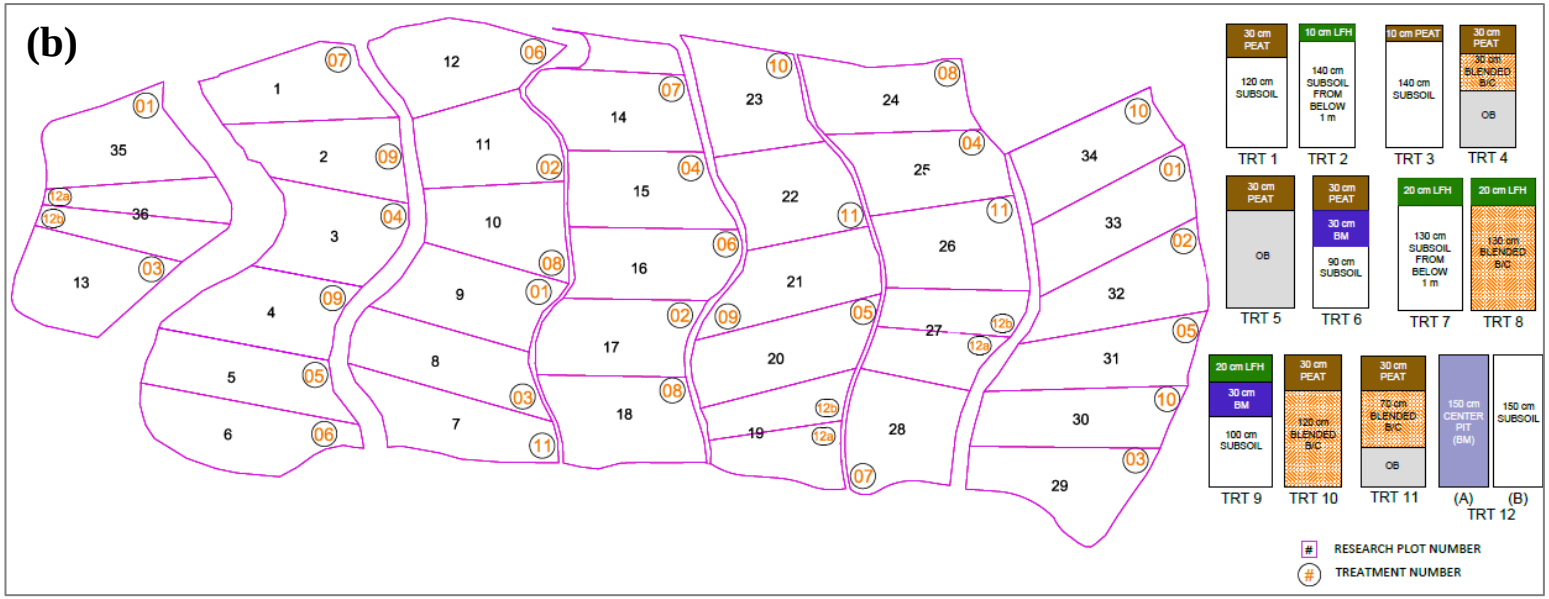

Figure 3-1: (a) Location map of Aurora North Mine of Syncrude Canada Ltd. (map sources: Esri, DigitalGlobe, GeoEye, Earthstar, Geographics, CNES/Airbus DS, USDA, USGS, Aerogrid, IGN, and the GIS User Community) and (b) soil cover design treatments (TRT) at ASCS (adapted from OKC, 2017). LOS overburden (OB) underlies all treatments, even though treatments with less than 150 cm total soil cap thickness only show OB.

All the treatment covers within the ASCS were constructed in 2012 using three distinct soil layers, including cover soil, subsoil, and LOS. The cover soil utilized in the treatment covers was either salvaged peat or LFH material. The Soil Classification Working Group (1998) in Canada defined LFH as "organic soil horizons (L, F, H) developed primarily from the accumulation of leaves, twigs and woody materials, with or without a minor component of mosses, that are normally associated with upland forest soils with imperfect drainage or drier". The L, F, and H horizons are characterized by the accumulation of original organic matter, partially decomposed organic matter, and decomposed organic matter, respectively. The peat was predominantly organic material with a total organic carbon of about 17 % (by weight), while the general texture of the mineral component of LFH was sand (about 92 % by mass). The cover soil was underlain by different selected coarse-textured subsoils salvaged from different locations (i.e., depositional environments) and depths within the mine site (Soil Classification Working Group, 1998). In general, the subsoil texture is sand (92 %–95 % by mass). The bottom layer was constructed using LOS overburden materials that were overlain by cover soil and subsoil layers. The LOS materials consist of loamy sand to sandy loam with an oil content of 0.1 % to 7.7 % (NorthWind Land Resources Inc., 2013). Overall, the LOS comprises a range of different oil contents and particle sizes compared to the cover soil and subsoil materials. All of the 13 treatment covers (which include two sub-categories of TRT 12) were included in this study.

Particle size distribution (PSD) analyses of the cover soil (LFH and peat), subsoil, and LOS were performed by a commercial laboratory (OKC, 2009) in November of 2009 based on ASTM standard testing method D422 (ASTM, 1998). The ASTM D422 method is based on the assumption that the particles are spherical in shape, so the PSD for peat may not be representative. The PSDs for the LFH and peat cover soils, coarse-textured subsoil, and LOS are presented in Fig. 3-2. The PSDs for the subsoils are the most variable, being salvaged

from different depths and depositional environments located on the Aurora North mine site. For the purposes of the IM, the peat and LFH cover soils were ultimately combined into a single group, as were different salvaged subsoils and LOS overburden materials. Combining the soil layers in this manner produces additional variability within each grouping; however, it ensures the maximum number of observations are utilized to capture the variability associated with each layer of the soil reclamation covers. According to Syncrude Canada Ltd., in the final cover design, the top layer might be either peat/LFH or a combination of the two, and the distributions of parameters for these two materials together seem reasonable for use in the illustrative covers for long-term simulation of water balance components. Therefore, the PLHS method was used to randomly sample from the distributions of the two materials grouped together.

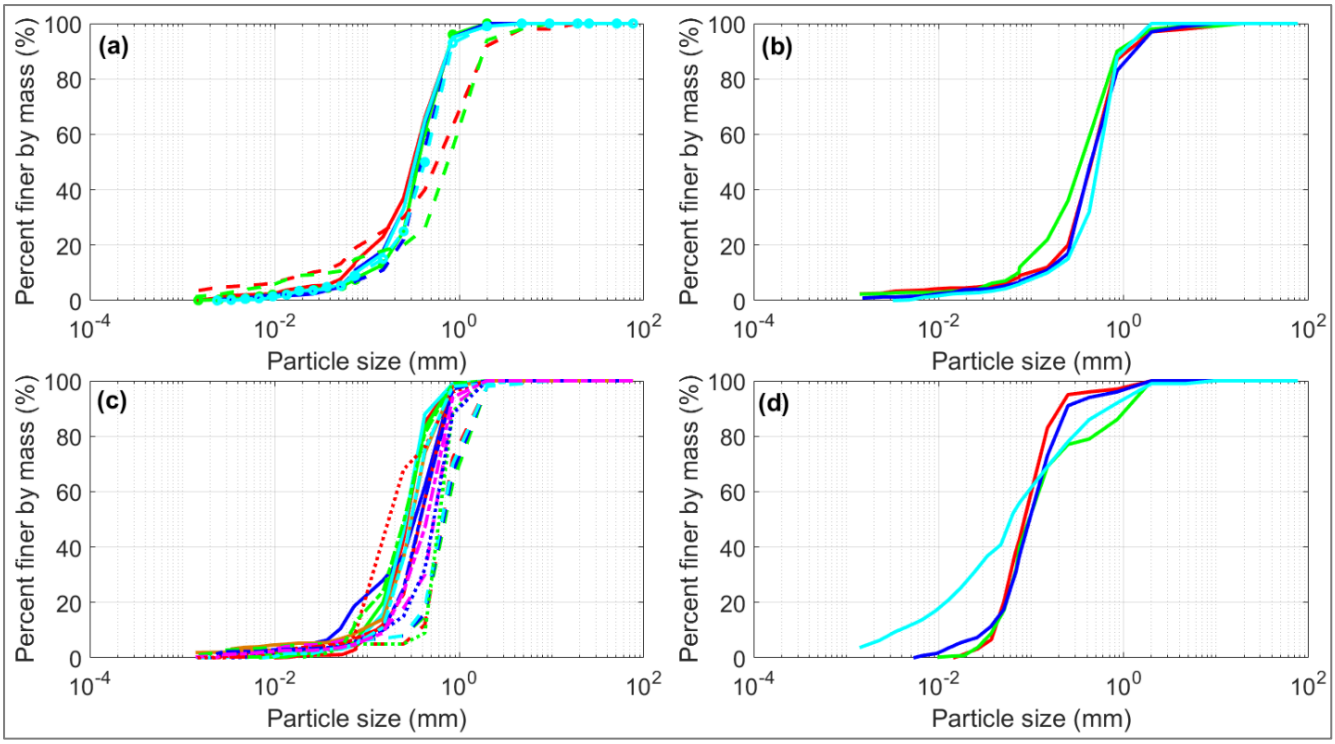

Figure 3-2: Particle size distribution (PSD) for (a) LFH, (b) peat, (c) subsoil, and (d) LOS materials for the treatment covers (OKC, 2009). The lines in the subplots show PSDs for different samples collected from the LFH, peat, subsoil, and LOS layers, respectively.

3.2.2 Field monitoring data

A climate monitoring station (Aurora Met) was established in 2012 to measure precipitation, air temperature, wind speed, net radiation, and relative humidity at the study site. The precipitation (rainfall and snow depth), air temperature, relative humidity, wind speed, and net radiation were measured daily and/or hourly using automated methods of measurement. The measurement instruments included a Texas Electronics TE525 tipping bucket (rain) and SR50 sonic ranging sensor (snow depth) for precipitation, a CS HMP45C sensor for air temperature and relative humidity, a RM Young 05103AP anemometer for

wind speed, and a KIPP & Zonen NRLife net radiometer (OKC, 2017). Each treatment cell also had a soil monitoring location where volumetric water content, temperature, and suction were measured at multiple depths (typically every 10 cm) within the treatment covers and the underlying LOS. The volumetric water content was measured using Campbell Scientific CS616 time domain reflectometers (TDRs), and the soil temperature and suction were measured using CS229 suction sensors (OKC, 2017). The monitoring data utilized in this study were collected from 2013 to 2016.

3.2.3 Parameter estimation using inverse modelling

The meteorological and soil monitoring data were used to calibrate a physically based SVAT model for each treatment cell based on IM. This provided a set of optimized soil hydraulic parameter values for the cover soil (LFH or peat), the subsoil, and the LOS. These parameters were interpreted to define spatial (cell to cell variation) and temporal (year-to-year variation) variability in the saturated hydraulic conductivity (K_s) and water retention curves (WRCs). The Mualem tortuosity parameter was set to 0.5 and was not optimized as the goal was to only optimize a limited set of key parameters. This is denoted by l in HYDRUS-1D and defined as the pore-connectivity parameter in the hydraulic conductivity function as estimated by Mualem (1976) to be approximately 0.5 as an average for many soils.

IM is a mathematical approach that estimates unknown causes (e.g., model parameters) using observed variables (e.g., water content and/or pressure heads) during a historical period by iteratively solving the governing equation (Hopmans et al., 2002). The governing equation (i.e., Richard's equation) for water flow in unsaturated soil was solved using HYDRUS-1D (Simunek et al., 2013). In HYDRUS-1D, potential evapotranspiration (PET) is calculated from climatic conditions using the Penman–Monteith equation (Brutsaert, 1982). It is then

apportioned into potential evaporation (PE) and potential transpiration (PT) based on a prescribed leaf area index (LAI) value. The actual evaporation (AE) from the ground surface is calculated from the pressure head gradient between the top two nodes and hydraulic conductivity with two limiting conditions: (1) AE must be less than PE and (2) the calculated water pressure at the top node must be in the range from 0 kPa to a maximum suction equivalent to the atmospheric water vapor pressure. Actual transpiration (AT) is calculated by distributing PT over a prescribed rooting zone where root water uptake is limited by water stress, as calculated by a root water uptake model (Feddes et al., 1974). The root water uptake parameters were obtained from previous studies on the oil sands mine reclamation covers by Huang et al. (2011a, 2015, 2017). The Feddes model parameters were set as P0 = 0 kPa; P2H = -5000 kPa; P2L = -8000 kPa; P3 = -19000 kPa; r2H = 0.5 cmd^{-1}; and r2L = 0.1 cmd^{-1} for all models as obtained from the preliminary study on the same sites by Huang et al. (2017).

HYDRUS-1D embeds an IM method into the numerical solution of Richard's equation. The IM method uses the Marquardt–Levenberg gradient-based approach (Simunek et al., 2013) in which values of the five individual model parameters (i.e., θ_r, θ_s, α, n, K_s) are varied for each material until a combination of the parameters is found that provides an optimal fit to the observed variation in a specific observation (i.e., volumetric water content) (Hopmans et al., 2002). The first four parameters (θ_r, θ_s, α, n) are known as van Genuchten (VG) parameters (van Genuchten, 1980) and are used to describe the volumetric water content function (i.e., water content vs. suction). *Ks* is the saturated hydraulic conductivity of the soil. A closed form solution then estimates the hydraulic conductivity function (i.e., *K* vs. suction) from the VG parameters and *Ks*. How well these individual parameters are estimated determines the overall accuracy of parameter estimation. Details of IM used in HYDRUS-1D can be found in Simunek et al. (2013).

In this study, the embedded IM method in HYDRUS-1D was used to simulate volumetric water content by optimizing the soil hydraulic parameters until the simulated water content matched the measured values at various depths and times. To optimize the parameters, an initial value as well as a search range defined by an upper and lower limit of each parameter were specified. The initial parameter values with their lower and upper limits for TRT 10 (cell no. 23 in year 2013) are shown in Table 3-1 for the peat and subsoil reclamation materials as well as for the LOS substrate. To conduct IM in this study, the ranges of initial parameter values were estimated from the measured particle size distributions (PSDs) and bulk density using the Arya–Paris model (Arya et al., 1999). The WRCs for each PSD from peat/LFH, subsoil, and LOS were estimated using the equations presented in the Arya–Paris model, and the RETC least-square optimization program (van Genuchten et al., 1991) was used to fit the VG–Mualem equation to the estimated WRC from the Arya–Paris model to estimate the VG parameters (θ_r, θ_s, α, n). The Kozeny–Carman equation (Kozeny 1927; Carman 1938, 1956) was used to estimate *Ks* values from the PSDs, as it is one of the most widely used and accepted methods (Huang et al., 2011a; Mathan et al., 1995). The estimation of parameters using these methods helps to constrain the initial parameter ranges in the inverse modelling. In addition to the Ayra–Paris model, the initial range of θ_s can also be approximated from the measured water content data for the covers, where the maximum water content values are observed at the depths of 5–10 cm. After setting up the initial range of parameter values based on the above methods, the inverse modelling is repeated with different initial values. Once there is no significant change in the θ_r and θ_s parameters and the objective function (i.e., sum of least squares), these parameters are assumed to be optimized and kept fixed in the subsequent IM for the remaining parameters. Step by step the least sensitive parameters are kept fixed, thereby reducing the number of parameters to be optimized by IM. Reducing the number of parameters, constraining the range of initial

parameter values, and repeating the IM with initial parameter values were done as recommended by Hopmans et al. (2002). However, details of all these steps are not included in this paper, only referenced to Hopmans et al. (2002), for the brevity of the paper. It is important to note that the purpose of this manuscript was not to focus on IM techniques, but rather to highlight how reasonably optimized parameter sets can resemble the distribution of the measured key parameter (i.e., *Ks*) and represent the parameter variability. This comparison between the optimized and measured key parameter values was assumed to be an indirect validation of the inverse modelling approach used in this study, which can be used for further sampling based on PLHS with a certain level of confidence.

3.2.4 Discretization of the model domain

The simulated model domain used in HYDRUS-1D had a maximum height of 2.50 m with a minimum of 1.00 m of LOS overlain by the various soil profiles (Fig. 3-1b). The various soil cover designs (TRT) are summarized in Fig. 3-1b. Note the following cover construction: Treatments 2 and 7–9 used LFH as the cover soil layer; Treatments 4, 8, and 10–11 were constructed using blended B/C horizons as the subsoil; and Treatments 6, 9, and 12a were constructed using a Bm as the subsoil layer. Figure 3-1b also demonstrates the choice of two depths (0.10 and 0.30 m) for the peat, two depths (0.10 and 0.20 m) for the LFH, and various depths for the subsoil reclamation materials. The spatial discretization used for all of the model domains was 1 cm and the time step was 86.4 s.

3.2.5 Initial and boundary conditions

Only the days in which the treatment covers were unfrozen were simulated in the IM. Snowmelt infiltration and drainage following ground thaw were assumed to be complete prior to the start of the simulation. As a consequence, any snowmelt-induced change in the soil water storage was already incorporated into the water content profiles from the first unfrozen

day (i.e., soil temperature > 0 ^{o}C). The measured volumetric water content profile of the first unfrozen day was set as the initial condition, while a unit gradient (i.e., gravity gradient) was set as the lower boundary condition of the model domain. The SVAT parameters (e.g., climate and vegetation characteristics) were used as the upper boundary condition.

3.2.6 Vegetation and root distribution

Maximum LAI values for each treatment cover were estimated from measurements by Bockstette (2017) and photographs taken on site by OKC (2017). The estimated LAI values varied from 0.2 at TRT 5 to 1.5 at TRT 2, TRT 7, and TRT 8. Huang et al. (2017) found that the temporal variation obtained with IM for similar sites was relatively minor compared to the spatial variability in the cover properties. Examining the photographs revealed that the sites were initially bare and developed a vegetative cover over the first few years. Although the covers were planted with one of three tree species (i.e., trembling aspen, jack pine, white spruce) or a mix thereof, the dominant early establishment vegetation during the study period (2013–2016) was understory vegetation species (not trees). The understory development (i.e., density and species) was variable, depending on the treatment cover soil materials (i.e., peat or LFH; Jones, 2016). Due to the early dominance of understory species, the LAI was assumed to be relatively constant over the study period (i.e., 4 years). The seasonal distribution of LAI adopted for the simulations was the same as that used by Huang et al. (2015): (a) a linear rise in the spring from zero to a maximum value, (b) maximum in the summer, and (c) a linear decrease from the maximum value to zero in the fall.

In 2014, the maximum root depths used in the IM were 0.3 m at TRT 5; 0.5 m at TRT 1–4, TRT 6–8, TRT 10–11, TRT 12a, and TRT 12b; and 1.0 m at TRT 9 based on the measurements by Bockstette (2017). The roots were assumed to be distributed within the cover soils using an exponential function of root mass with depth, with the maximum root

mass at the surface decreasing to zero at the maximum root depth. In the long-term simulations (discussed below), the root depths were assumed to have extended to the full depth of the covers.

Table 3-1: Initial value and lower and upper limits of the five soil hydraulic parameters for TRT 10 (Cell no. 23 in 2013) used in the inverse modelling to optimize parameters for peat, subsoil, and LOS

	Parameter value				
	$*\theta_r$ (m^3/m^{-3})	θ_s (m^3m^{-3})	α (m^{-1})	$*n$ [-]	$\log(K_s)$ (ms^{-1})
PEAT					
Initial value	0.0160	0.610	4.50	1.50	-4.53
Lower limit	0	0.461	2.50	1.20	0
Upper limit	0.0900	0.700	6.80	2.30	-3.64
SUBSOIL					
Initial value	-2.22	0.361	2.50	0.310	-4.62
Lower limit	0	0.261	2.50	0.310	0
Upper limit	-1.05	0.500	4.80	0.360	-3.64
LOS					
Initial value	0.0900	0.368	4.50	1.74	-6.14
Lower limit	0	0.328	3.00	1.55	0
Upper limit	0.0900	0.450	6.50	1.83	-4.94

*The logarithmic (log10) values are shown for θ_r and n parameters of the subsoil layer; however, lower limits (0 values) were not log-transformed for subsoil θ_r and Ks of all soil types

3.2.7 Probability distributions of the optimized parameters

IM was undertaken using the monitored water content profiles at each of the treatment cells along with the site-specific meteorological data for each individual monitoring year. Because one cell of TRT 5 was missing data in 2013, a total of 155 HYDRUS-1D models (13 treatments, three replicated cells, and 4 years of data) were calibrated by optimizing five soil hydraulic parameters for each soil type. The 155 sets of optimized parameters (both VG parameters and saturated hydraulic conductivity) were then used to populate a continuous probability distribution that represents the variability in each individual parameter. A cumulative density function (CDF) for each of the optimized parameters was plotted for all soil types to investigate whether peat and LFH cover soil and all subsoil variations could be grouped together for the simplification of long-term water balance simulations.

The Kolmogorov–Smirnov (K–S) test was used to verify the distribution types of the five model parameters as obtained from the IM for all cells and all years. The K–S test checks the null hypothesis that a distribution belongs to a standard normal distribution (mean = 0, standard deviation = 1) if the resulting p value is greater than the level of significance (e.g., 1 %). The parameter values were centered and scaled using the corresponding mean and SD values prior to application of the K–S test. The distributions of the parameters that fail the normality check as stated above were log transformed, centered, and scaled before the K–S test. In addition, probability density functions were plotted for the parameters of each soil type to visually inspect the types of distributions.

3.2.8 Simulation of long-term water balance with parameter variability

3.2.8.1 Sampling of parameters

Alam et al. (2017) and Huang et al. (2017) used a limited number of alternate parameter sets to define variability to limit simulation times. The optimized soil properties (WRC and *Ks*) were grouped into discrete intervals representing the 10th, 25th, 50th, 75th, and 90th percentiles of the parameter distributions obtained from optimized parameter sets. The range of possible water balance outcomes (e.g., AT and NP) over a 60-year climate cycle was then simulated using the discrete percentiles' parameter sets. However, these discrete (not randomly selected rather fixed) percentiles (i.e., 10th, 25th, 50th, 75th, and 90th percentiles) of parameter distributions are not representative of the whole range of parameter distributions.

A more efficient and sequential LHS-based sampling process – PLHS, as described above – was adopted in this study. According to Sheikholeslami and Razavi (2017), PLHS is an extension of conventional LHS, where PLHS consists of several sub-samples (called slices) in such a way that the union of these slices also retains the properties of the LHS. The PLHS sampling technique was implemented in this study using the MATLAB-based PLHS Toolbox developed by Sheikholeslami and Razavi (2017) to generate an appropriate sample size of n data points in a d-dimensional hypercube [0;1] formed by the union of t small Latin hypercubes with $m = n/t$ sample points. For example, an appropriate sample size is determined by generating a sample size of n parameter sets, where the maximum value of n was 2000 in a 5-D (where 5 refers to the total number of parameters) hypercube formed by the union of 100 small Latin hypercubes. So, 20 sample sizes (equally sized slices) were obtained (i.e., m = 2000/20) to determine an appropriate sample size. Each of the 100 parameter sets was sequentially added to the next 100 parameter sets to generate PLHS-based

parameter sets starting from 100 to 2000. While HYDRUS-1D can be used to optimize parameters with reasonable computational cost, our goal was simply to use HYDRUS-1D to optimize a set of parameters for each cover with each year's monitoring data. Thus, we obtained 155 sets of parameters which include 13 treatment covers, replicated in triplicate and monitored in 4 consecutive years. Since these parameters form a distribution of parameters representative of the measured parameter distributions (at least for K_s), we decided to use a standard sampling technique (e.g., PLHS) to do the rest with regards to generating multiple sets of parameters. Comparison between the multiple sampling from HYDRUS-1D and from PLHS could be an extension of the current study in terms of both performance and computational cost.

Once the distributions of both the optimized and PLHS-based sampled parameters were verified to be similar, the appropriate number of randomly sampled parameter sets was used to simulate realizations of AET and NP over 60 years of climate variability using HYDRUS-1D. The realizations of AET and NP were expected to encompass a wider range of uncertainty in the water balance of the reclamation covers due to parameter variability than using discrete percentiles of the optimized parameters. The classical MC sampling method was also used to verify its limitations relative to the PLHS and discrete sampling approaches.

3.2.8.2 Illustrative covers

The long-term cover performance was evaluated by simulating long-term climate records represented by 62 years (1952–2013) of climate data from Fort McMurray Airport Weather Station. The first 2 years (1952–1953) were used to spin up the model and establish the initial conditions. Uncertainty in the long-term cover performance was incorporated by simulating five illustrative covers of 0.20 m peat and 1 m LOS overburden with five different depths of subsoil (A50 (0.50 m), A75 (0.75 m), A100 (1.00 m), A125 (1.25 m), and A150 (1.50 m))

with the PLHS-based sampled soil properties. Similar illustrative cover designs were used in Alam et al. (2017) and Huang et al. (2017) with minor modifications in the model domain, where the order of the soil profile was peat/subsoil/LOS.

The modelling approach (model domain, spatial/temporal discretization, etc.) was the same as for the IM, but with several key differences. First, the accumulated snowpack from winter precipitation was added to the cover in the early spring of each year. While runoff from the watershed would largely depend on the slope of the watershed, the amount of runoff would vary between the reclamation cover systems. Huang et al. (2015) showed an average runoff of 34 mm each year from a sloping cover (~ 5H : 1V), while other reclamation covers were flat-lying and assumed to have negligible runoff in previous studies (Alam et al., 2018a; Huang et al., 2015, 2017). So, the runoff from the flat-lying reclamation cover was not simulated in this study, but rather incorporated into the NP rates. Therefore, the simulated NP rates represent the total water yield from the covers that may eventually reach the downgradient surface water bodies. Besides, there was no measurement to confirm which one between runoff and infiltration dominates in the reclamation cover sites. The melt volume was calculated using the degree-day method (Carrera-Hernández et al., 2011) when the mean daily temperature was greater than 0 ^{o}C and was then added to any precipitation occurring during the winter period and to any stored water in the soil profile in the early spring of each year. This method of calculating melt volume uses a constant that accounts for all the factors affecting the snowmelt amount and varies with time. The method did not consider sublimation as intercepted snow results in the highest rates of sublimation; however, interception of snow is quite low in the case of a deciduous tree (e.g., aspen). Consequently, snowmelt calculation without considering sublimation might overestimate the snowmelt into liquid water in some areas which need further investigation. Second, the roots were assumed to have an exponential root distribution that fully penetrates the covers without penetrating

into the LOS layer. It is possible that the roots would eventually penetrate into the LOS substrate over the long-term period; however, this more conservative assumption restricts root water uptake to the reclamation materials. The maximum root depth assumed in this study seems reasonable compared to the root depths of tree species, between 3 and 57 years of age, in boreal forests (range 0.3 to 2m; Strong and La Roi, 1983). Third, the method proposed by Huang et al. (2011b, 2017) was used to constrain the LAI values used in the simulation based on the predicted range of AET values. The maximum sustainable LAI (LAI_max) values were evaluated to ensure the predicted values of AET were sufficient to support the prescribed LAI used in the simulations. The maximum sustainable LAI is defined as an optimal vegetation coverage that can balance soil water recharge and consumption as well as maintain sustainable plant growth. In this study, it was represented by the intersection point between the simulated and required AET when several LAI values are plotted against the simulate AET and a literature-based line representing the annual AET required to support a particular LAI. In the IM, the measured LAI values were used to obtain the optimized model parameters, and no significant evolution in the LAI values was observed or simulated. However, the long-term simulation of water balance requires a specified pattern of seasonal variations in LAI to determine the LAI_max for each illustrative cover. The seasonal variations in LAI were represented in a similar way to Huang et al. (2015) using six seasonal patterns of LAI (i.e., LAI of 1, 2, 3, 4, 5, and 6) for each illustrative cover. Huang et al. (2011b, 2015) and Alam et al. (2018a) used literature-based relationships between above-ground net primary production (ANPP), LAI, and actual evapotranspiration (AET) to constrain LAI_max values in the long-term simulations. Because parameter variability is expected to influence the long-term water balance (AET and NP) of the treatment covers, the ANPP–LAI–AET relationships are also expected to be influenced by the parameter variability. Consequently, the variability in LAI_max has an influence on the long-term cover

performance in combination with the parameter variability. For details of this approach, interested readers are referred to Alam et al. (2018b).

3.2.9 Statistical methods

The K–S test was used to verify the distribution of the optimized parameter values. The mean and SD were used as the convergence criteria while selecting an appropriate sample size. The PLHS method was used to sample from the distributions of the VG parameters and *Ks* using various sample sizes between 15 and 2000. When the mean and SD of the sampled parameters converge to the mean and SD of the optimized parameters and remain unchanged, the sample size was considered "appropriate". The uniformly distributed sample points in the PLHS approach were transformed to a normal distribution using the inverse cumulative distribution function (i.e., ICDF as a transfer function). The parameters showing log-normal distribution were transferred to a normal distribution using log transformation prior to using the ICDF.

3.3 Results and discussion

3.3.1 Performance of inverse modelling for the treatment covers

The performance of the inverse modelling technique of the HYDRUS-1D model was first evaluated by comparing the measured and simulated water contents at various depths within each of 13 treatment covers. The coefficient of determination (R^2) and root-mean-square errors (RMSEs) between the measured and simulated water contents are shown in Table 3-2, while the comparison between the measured and simulated water contents at various depths within each of 13 treatment covers in a typical year during 2013–2016 is shown in Fig. 3-3. For the treatment covers, the R^2 values are mostly above 0.8, and RMSE values are mostly less than 0.10 cm^3cm^{-3}, except for a few treatment covers. The performance criteria as well as

the graphical comparison between the measured and simulated water contents at various depths within the treatment covers show that the models perform reasonably well given diverse soil conditions, number of treatment covers, and number of parameters to be optimized.

Table 3-2: Performance statistics (R^2 and RMSE) of inverse modelling for each of 13 treatment covers at the Aurora North Mine site

Treatment cover #	R^2	RMSE (cm^3cm^{-3})
1	0.89	0.07
2	0.82	0.06
3	0.73	0.04
4	0.81	0.08
5	0.62	0.10
6	0.86	0.11
7	0.79	0.03
8	0.82	0.04
9	0.51	0.11
10	0.84	0.07
11	0.84	0.07
12a	0.81	0.03
12b	0.90	0.03

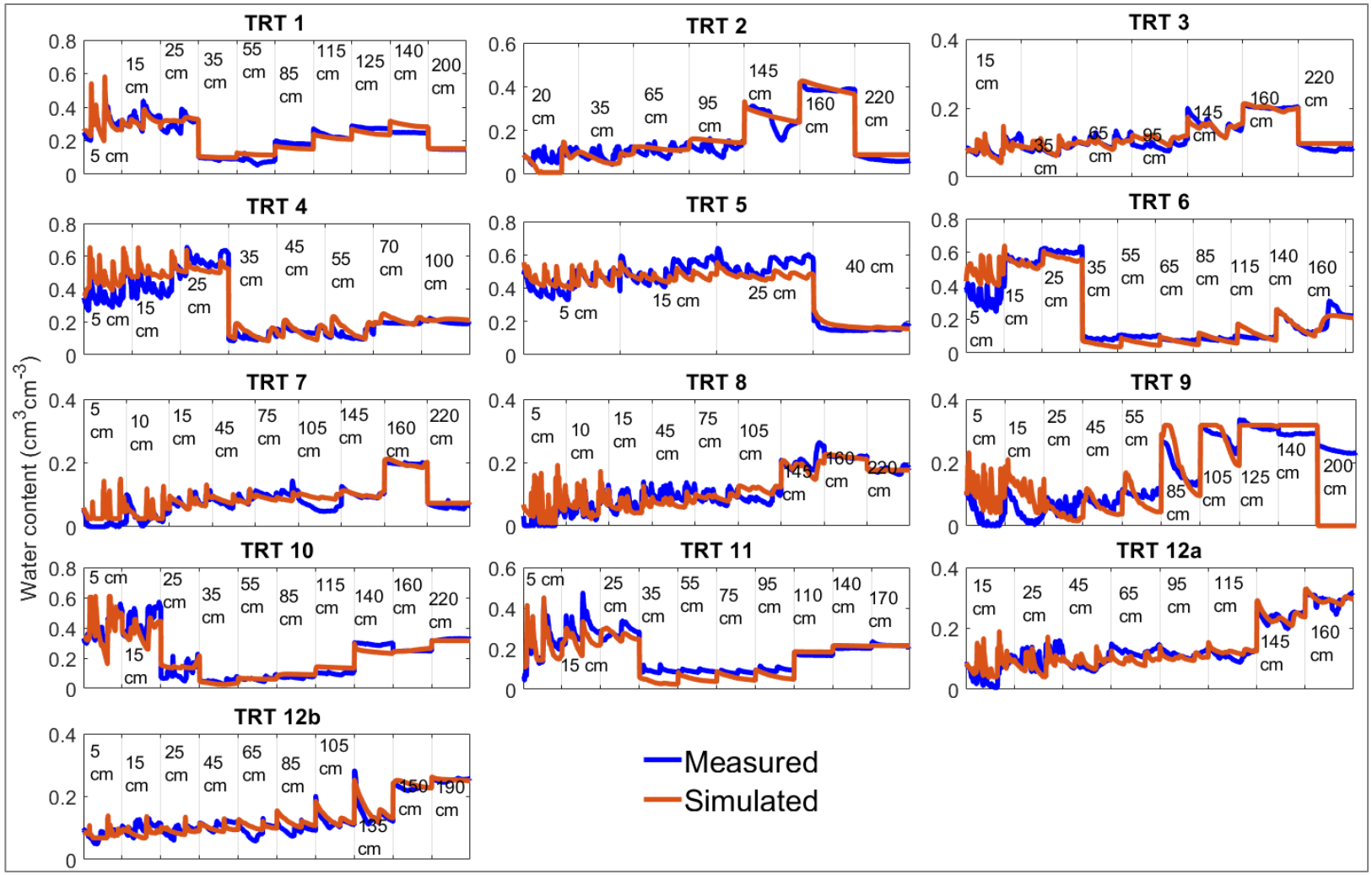

Figure 3-3: Comparison between the measured and simulated water contents at different depths within each of 13 treatment covers for the days when temperature is greater than 0 ^{o}C. Typical depths at which the water content measurements are recorded vary from 5 to 200 cm within the treatment covers.

3.3.2 Probability distributions of the optimized and sampled parameters

The K–S test was used to verify the distributions for each of the five parameters from IM of all cells and all years. K–S test results indicate that the VG parameters of soil types (except θ_r and n of subsoil) were normally distributed at the 1 % significance level. The θ_r and n parameters of subsoil were log-normally distributed at the 0.001 and 0.1 % significance levels, respectively. K_s was log-normally distributed (Fig. 3-4) at the 1 % significance level for all three soil types. K_s values are commonly found to be log-normally distributed (Huang et al., 2017; Kosugi, 1996).

Despite differences in the CDF (see Fig. A-1) of the optimized parameters for the peat or LFH cover soil as well as differences between various salvaged subsoils and different LOS overburden materials, the treatment cover materials were grouped as peat, subsoil, and LOS. This grouping was adopted for the purpose of this study because it maximizes the number of IM parameter sets and helps illustrate the impacts of parameter uncertainty on expected performance. According to Syncrude Canada Ltd., in the final cover design the top layer might be either peat/LFH or a combination of the two. The distributions of parameters for these two materials together seem reasonable to be used in the illustrative covers for long-term simulation of water balance components. Moreover, the primary purpose of this study was not to differentiate the performances of two alternate cover soils built on the two organic-rich materials. Therefore, the PLHS method was used to randomly sample from the distributions of the two materials grouped together, and the distributions of parameters for these two materials together are used in the illustrative covers for long-term simulation of water balance components.

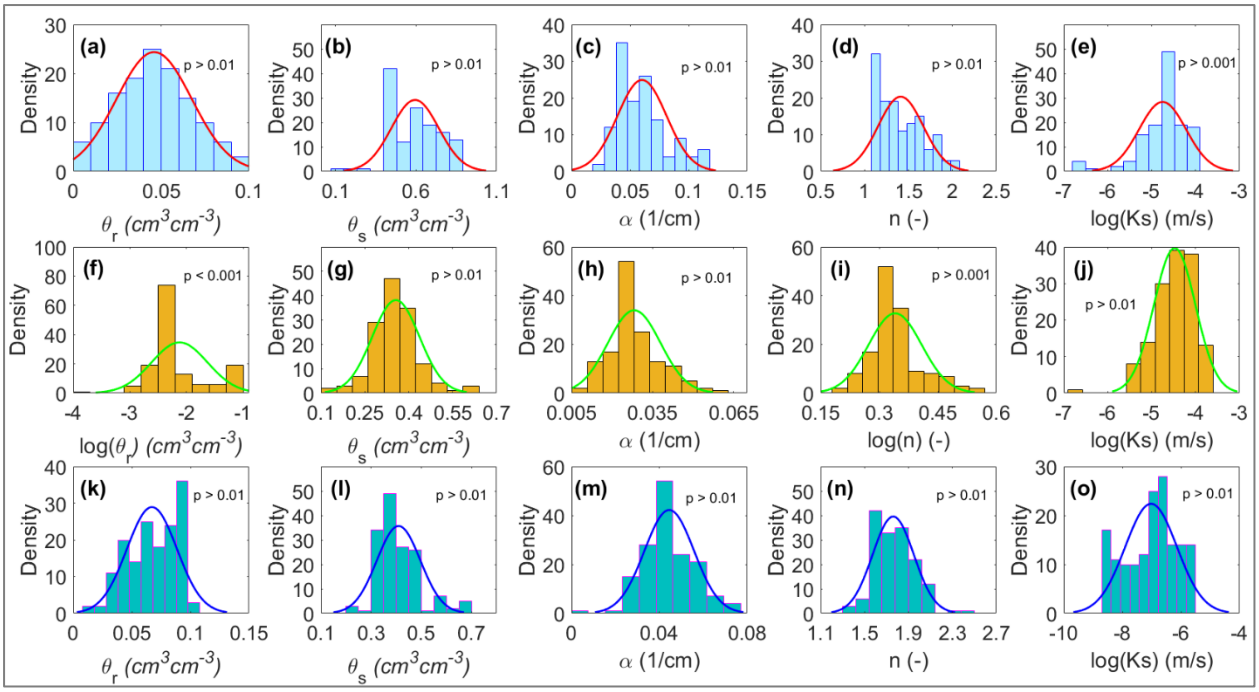

Figure 3-4: Probability density functions (PDFs) fitted to the four VG parameters and Ks obtained from the IM for the three soil types: peat (a-e), subsoil (f-j), and LOS (k-o). The mean and SD of the fitted distributions are shown in Table 3-2.

The variability in the optimized parameter values includes both spatial and temporal variability. The material properties of the treatment covers evolve with time as they vary in space. It seems important to see how these material properties would vary in time, if at all, in addition to the spatial variability. The probability density functions (PDFs) of K_s obtained for all of the cells and all years represent the total variability (spatial plus temporal) in the Ks parameter, while the PDFs for all of the treatment cells with each cell averaged over the 4 monitoring years represent spatial variability alone. Comparison of these PDFs (Fig. 3-5) for K_s (only for K_s as it was the most influential parameter for the treatment covers) shows that the spatial variability contributed more than 90 % (as 90 % of the PDF corresponding to

spatial variability falls within the PDF corresponding to total variability) of the total variability for the three materials. Because temporal variability was not significantly contributing to the total variability, the spatial and temporal variabilities were not separated from the total variability in this study.

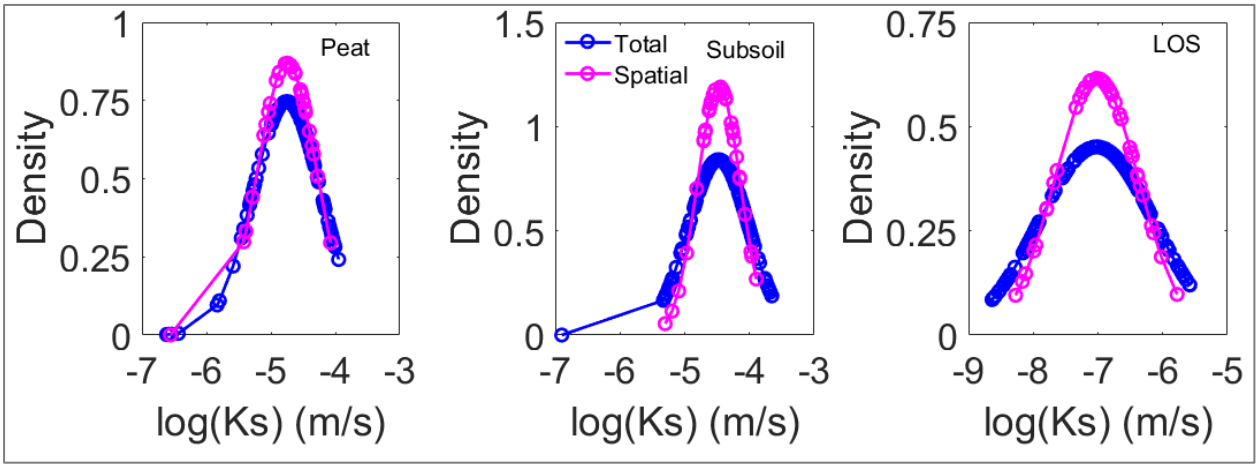

Figure 3-5: PDFs of K_s total variability and spatial variability for the three materials.

A total of 700 parameter sets were randomly sampled from the prescribed probability distributions using the PLHS method. These sampled distributions (Fig. 3-6) accurately captured the IM parameter distributions with the exception of the residual water content (θ_r) for the subsoil layer. In this case, a large number of the IM values were close to zero and the randomly sampled θ_r values consequently underestimate the optimized θ_r values.

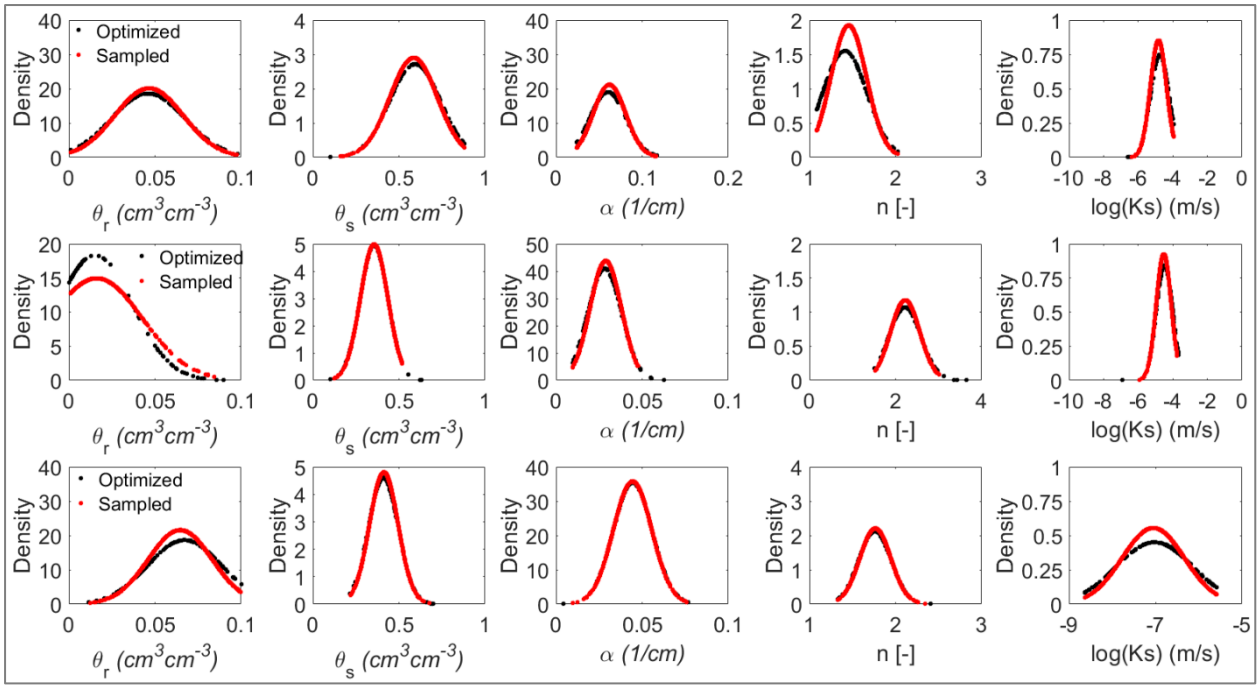

Figure 3-6: PDFs for the optimized and sampled 700 parameter sets for the peat cover soil (top row), subsoil (middle row), and LOS (bottom row).

A further comparison between the optimized and sampled parameter values in terms of their basic statistics (e.g., mean and SD) is shown in Table 3-3. The percentage difference between the mean of the sampled and optimized parameter values varies between 0.01 % and 5.47 %. The average error of 1.64 % includes the larger errors associated with θ_r for the subsoil. The percentage difference between the SD of the sampled and optimized parameter values varies between 0.21 % and 24.72 % with an average error of 8.29 %, including the errors in approximating θ_r for the subsoil and K_s of LOS. The larger error in the approximation of subsoil θ_r and LOS K_s is related to overestimation of the optimized θ_r values and underestimation of the optimized K_s values by PLHS sampling. Overall, the random sampling approach seems to provide a good approximation of soil hydraulic

parameters with regards to their mean and SD values as well as the corresponding PDF patterns.

Table 3-3: Mean and SD values of the optimized and randomly sampled parameters for peat, subsoil, and LOS. The differences between the corresponding mean and SD of the sampled and optimized parameter values are shown as percentages.

Parameter	Peat			Subsoil			LOS		
	Optimized	Sampled	Error (%)	Optimized	Sampled	Error (%)	Optimized	Sampled	Error (%)
θ_r (m^3m^{-3}): Mean	0.0460	0.0470	1.11	0.0150	0.0160	5.47	0.0670	0.0650	3.69
θ_r (m^3m^{-3}): SD	0.0210	0.0200	7.54	0.0217	0.0161	24.7	0.0210	0.0190	13.6
θ_s (m^3m^{-3}): Mean	0.594	0.585	1.47	0.356	0.356	0.0100	0.410	0.412	0.670
θ_s (m^3m^{-3}): SD	0.147	0.137	6.32	0.0810	0.0800	0.950	0.0870	0.0820	4.13
α (m^{-1}): Mean	0.0600	0.0620	2.98	0.0280	0.0290	2.28	0.0450	0.0440	0.160
α (m^{-1}): SD	0.0210	0.0190	10.2	0.0100	0.0100	1.35	0.0110	0.0110	0.790
n [-]: Mean	1.41	1.46	3.22	2.22	2.23	0.230	1.76	1.77	0.280
n [-]: SD	0.257	0.208	19.2	0.0373	0.348	0.820	0.187	0.184	3.47
log(K_s) (ms^{-1}): Mean	-4.75	-4.85	1.53	-4.48	-4.52	0.970	-7.02	-7.05	0.420
log(K_s) (ms^{-1}): SD	0.534	0.468	12.4	0.430	0.431	0.210	0.884	0.719	18.6

3.3.3 Distribution of WRC and Ks parameters

The WRCs for the three cover soils were defined by the four IM-generated VG parameters. These individual parameter distributions were randomly sampled 700 times to generate 700 WRCs. The various VG parameters were considered to be independent parameters with no correlation between them. The choice of 700 samples was selected from sampling tests described below. The 10th percentile, mean, and 90th percentile of the 700 calculated WRCs based on the 700 randomly sampled sets of VG parameters were compared to the corresponding WRCs obtained from the 155 IM-based parameter sets (Fig. 3-7). This comparison is not intended to be a validation of the sampling approach, but more of a visual comparison of the 155 WRCs generated from IM with "virtual" WRCs generated from random sampling of the individual WRC parameters. Despite the correlation between these parameters in the form of a WRC, the PLHS method randomly selected these parameters without considering the correlation between them. However, the PLHS method was able to maintain those correlations when plotted as WRCs as shown in Fig. 3-7 and turns out to be a reliable method that captures the physical relationship between the VG parameters.

The distribution of WRCs is represented by the mean and 90 % confidence intervals (CIs) of WRCs based on the 155 optimized VG parameters (i.e., θ_r, θ_s, α, n) compared to the WRCs generated based on the 700 sampled VG parameters. The randomly sampled VG parameters provide a good representation of the optimized WRCs with a R^2 value of 0.99 for all soil types but with some visually apparent discrepancies in the tails. Generally, the extreme values belong to one of three distributions (Gumbel, Fréchet, or Weibull); however, the PLHS-based sampling was performed using normal distributions of the optimized VG parameters.

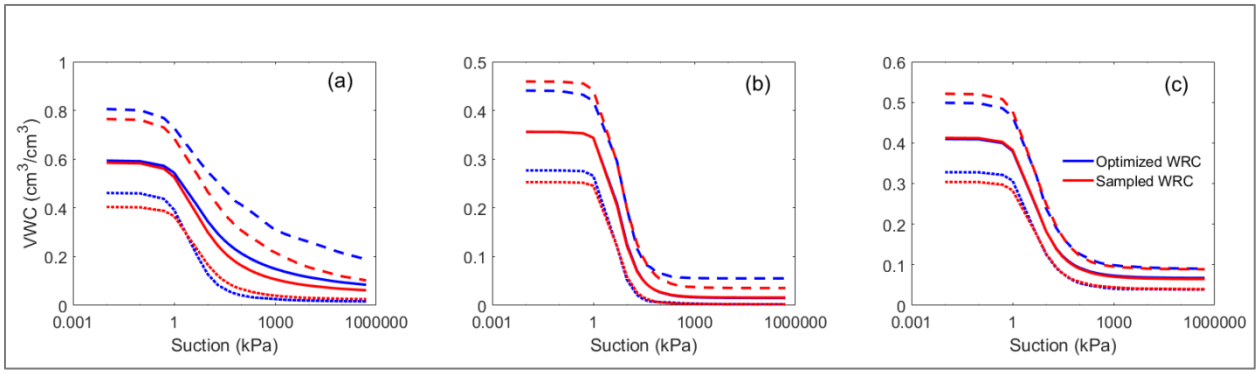

Figure 3-7: Estimated mean (solid lines) with 10^{th} (dotted lines) and 90^{th} (dashed lines) percentiles of the soil water retention curves (WRCs) for (a) peat, (b) subsoil, and (c) LOS obtained from the 155 optimized and 700 randomly sampled parameter values, where VWC denotes volumetric water content.

Huang et al. (2016, 2017) note that the cumulative frequency distributions (CFDs) for K_s values obtained from IM (i.e., optimized K_s values) were similar to those obtained from direct field testing. The field K_s values were measured using air permeameter (AP) and Guelph permeameter (GP) testing. Huang et al. (2016) show that the K_s values from AP and GP testing produced very similar descriptions of variability, although the mean K_s values were slightly offset as might be expected. The sampled Ks values are compared to the optimized Ks values and Ks values obtained from direct field measurements in Fig. 3-8. The CFD of the K_s obtained by random sampling produces a similar distribution to the IM distribution. Similar to the comparisons for the WRC, the random sampling exhibited more "tailing" at the lower values of K_s for the peat and subsoil, while creating a much smoother distribution than those obtained by the optimized K_s values. The discrepancy between the optimized and sampled K_s distributions derives primarily from sampling of the log normal distribution that was fit to the IM distribution. This ensures that the statistical characteristics of the distribution are retained and reflected in the sampled distribution, but may result in specific deviations from the modelled (IM) distribution.

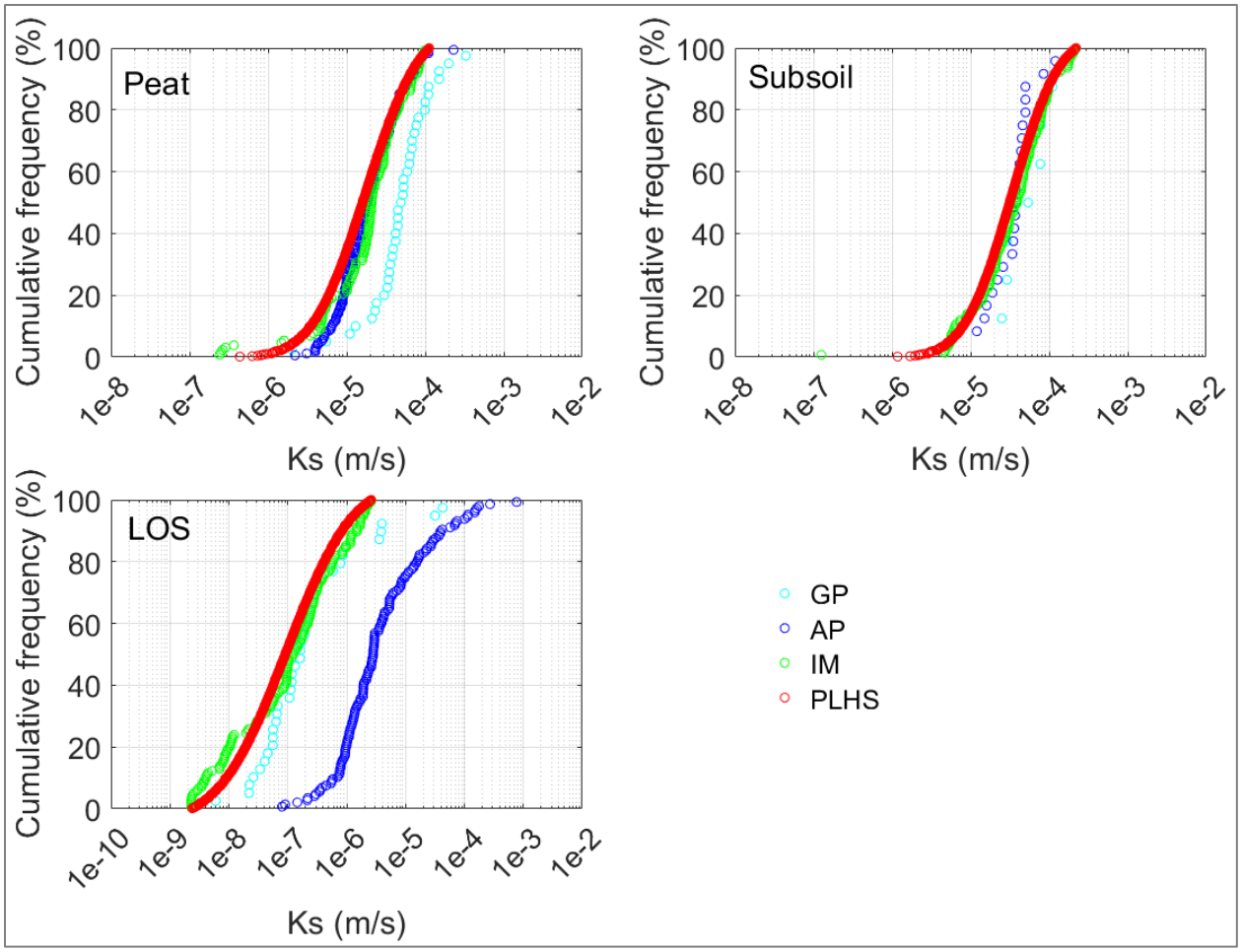

Figure 3-8: Comparison of the cumulative frequency distributions of the field-measured K_s using GP and AP methods, and optimized (IM) K_s values with the randomly sampled (PLHS) 700 Ks values. The results shown are for peat, subsoil, and LOS soil types.

A key parameter of the HYDRUS-1D model for simulating water balance components at the reclaimed land has been the saturated hydraulic conductivity (K_s), which has been measured in the field using a couple of methods. While K_s influences the net percolation rates, the root distribution influences the transpiration rates from the plants on the reclamation covers. The root water uptake model by Feddes et al. (1974) was used in this study, where the root distribution was approximated using exponential equations showing the relationship between relative root density and depth for the treatment covers since exponential root distribution was found to perform better in the near-surface horizons (Li et al., 1998). However, the root distribution is affected by site conditions (Strong and La Roi, 1983). Different root distributions, e.g., exponential, combination of uniform and exponential, and linear, were obtained from previous

studies (Alam et al., 2018a; Huang et al., 2011c, 2015) and evaluated in this study. Finally, the exponential root distributions seem to produce parameter sets where the distributions of K_s match reasonably well with the distributions of measured K_s values.

3.3.4 Selection of an appropriate sample size for PLHS

The probability distributions of the five optimized parameters were sampled using 26 different PLHS sample sizes (ranging from 15 to 2000) and the mean and SD for each sample set were calculated (Fig. 3-9). The mean and SD values clearly converge and remain relatively unchanged when the sample size exceeds 500 in most cases. Comparable sampling sets using the MC method would require more than 5000 samples to reach a similar level of convergence (Figs. A-3 and A-4). To keep the simulation time reasonable, a sample size of 1000 was used to simulate water balance components for the illustrative covers.

a.

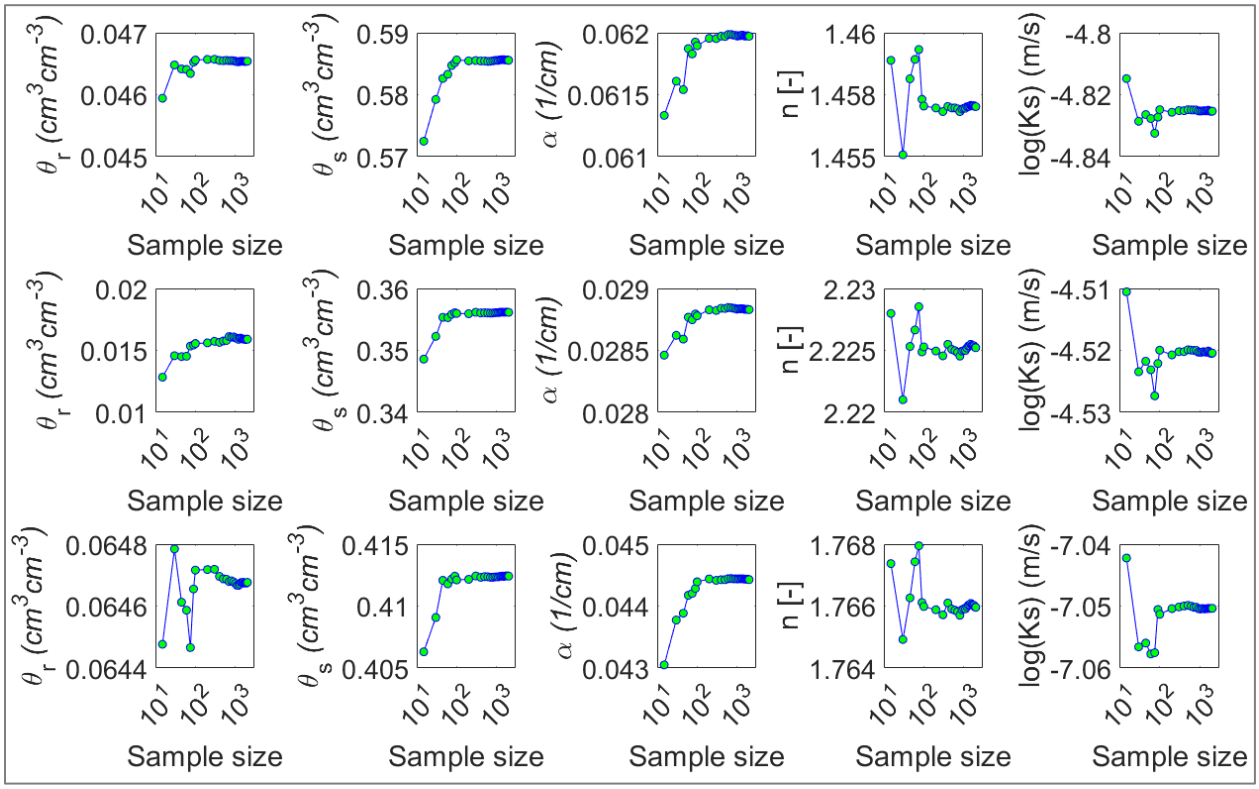
θr (cm3cm-3)
0.047
0.046
0.045
θs (cm3cm-3)
0.59
0.58
0.57
α (1/cm)
0.062
0.0615
0.061
n [-]
1.46
1.458
1.455
log(Ks) (m/s)
-4.8
-4.82
-4.84
0.02
0.015
0.01
0.36
0.35
0.34
0.029
0.0285
0.028
2.23
2.225
2.22
-4.51
-4.52
-4.53
0.0648
0.0646
0.0644
0.415
0.41
0.405
0.045
0.044
0.043
1.768
1.766
1.764
-7.04
-7.05
-7.06
10¹
10²
10³
Sample size

b.

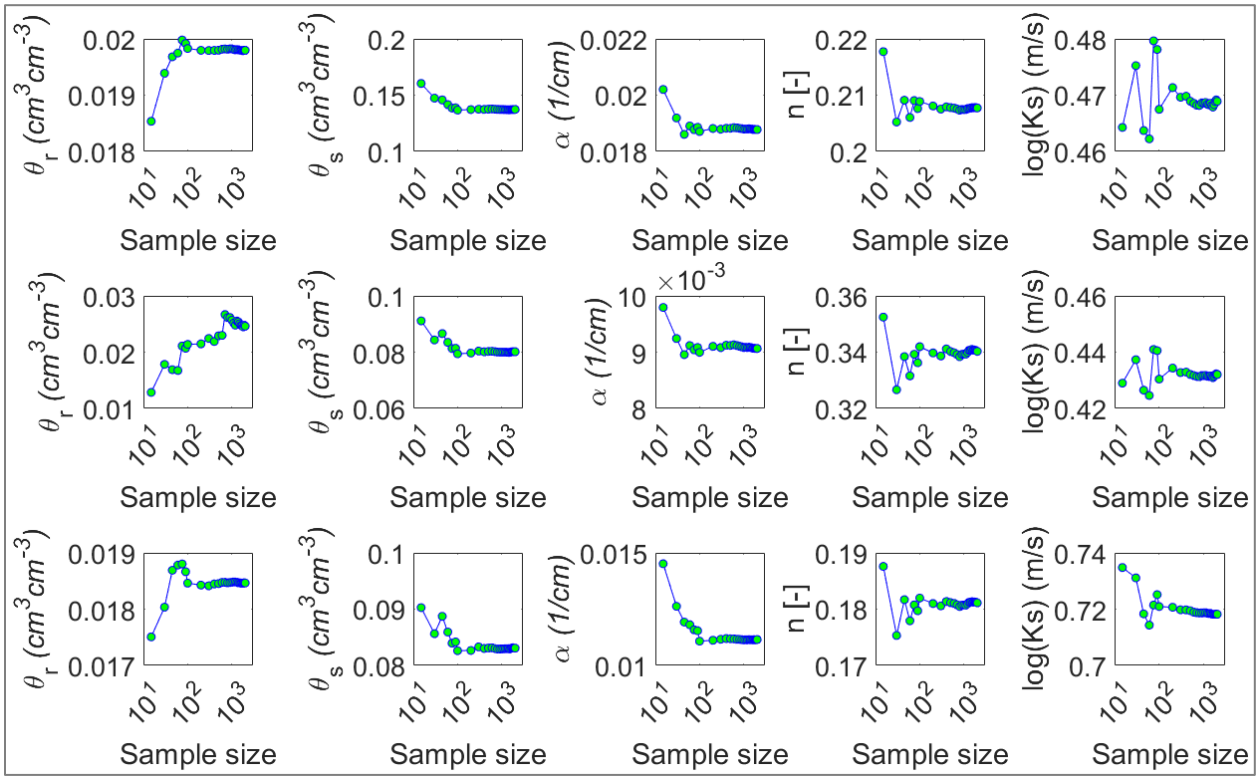

Figure 3-9: (a) Mean and (b) SD of the sampled parameter values corresponding to each sample size. Results are shown for peat (top row), subsoil (middle row), and LOS (bottom row) in both (a) and (b).

The impact of the varying PLHS sample sizes on water balance outcomes (i.e., AET and NP) was also evaluated. A set of 16 different sample sizes (i.e., 15 to 1000) was used to simulate AET and NP (i.e., using a total of 5815 simulations over a 60-year climate cycle) for the A100 illustrative cover (i.e., 0.20 m of peat and 1 m of subsoil placed over 1 m of LOS) with an LAI of 3.0. The results (Fig. A-2) show that the mean and SD of the AET and NP values also converge when the sample size is larger than 500. To be conservative, a PLHS sample size of 700 was used to define the hydraulic parameter distributions for the long-term simulation of the illustrative covers. However, a sample size of several hundred might also have been chosen.

3.3.5 Determination of maximum sustainable LAI using sampled parameter sets

The variability in LAI_max was evaluated using the lower bound (10 %), mean, and upper bound (90 %) of the simulated annual AET values (Fig. 3-10) for a series of simulations in which

the LAI was set to one of six values (i.e., 1.0, 2.0, 3.0, 4.0, 5.0, and 6.0). A literature-based line representing the annual AET required to support a particular LAI value was also plotted on this figure. The intersection points between the simulated and required AET lines were designated as the LAI_max values for each of the five covers. The mean LAI_max values range from 4.12 to 4.50 for the five illustrative covers as shown in Fig. 3-10. The respective lower, mean, and upper LAI_max values for each cover were as follows: A50 (2.73, 4.12, and 5.23); A75 (2.79, 4.25, and 5.36); A100 (2.86, 4.27, and 5.42); A125 (2.94, 4.37, and 5.53); and A150 (3.06, 4.50, and 5.68). These results indicate that all LAI values increase with increasing cover thickness but the difference between the lower and upper LAI_max values also increases with cover thickness.

Huang et al. (2015) showed that the increases in AET are not necessarily proportional to the incremental increases in cover thickness, rather little increment is noticed in the median AET over a climate cycle once a threshold cover thickness is passed. Therefore, it is not a surprise to observe the narrow range of LAI_max values as shown in Fig. 3-10. That said, there is support for decreased NP rates for thicker covers as greater volumes of water can be stored and ultimately released as AET.

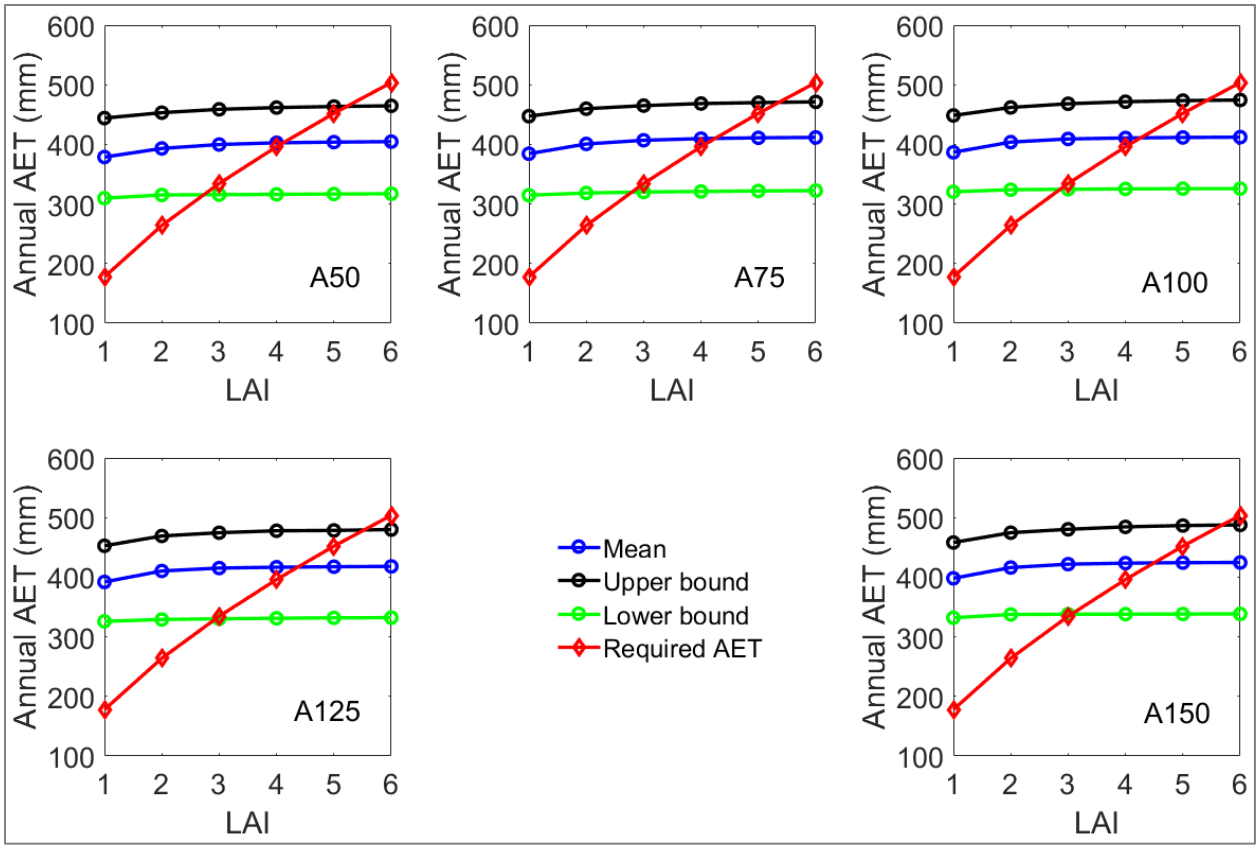

Figure 3-10: Lower (10%), mean, and upper (90%) limits of LAI_max values for the five illustrative covers showing variability in the LAI values based on the simulated annual AET with the 700 parameter sets over a 60-year climate cycle.

3.3.6 Uncertainty in determining the LAI_max values

The LAI_max values (i.e., the mean LAI_max values) from Fig. 3-10 for each illustrative cover were used to simulate the annual AET values for the 60 years of climate data. The results shown in Fig. 3-10 combine the impact of both climate variability and parameter uncertainty (700 parameter sets) on the relationship between LAI_max and the major water balance components of NP and AET. Table 3-4 (last column) shows the mean of LAI_max values as well as the corresponding standard deviations (SD) as calculated from the simulated AET values for the five illustrative covers. The mean and SD of the LAI_max values demonstrate that the parameter variability results in slightly higher LAI_max and slightly lower uncertainty as cover thickness increases. The mean LAI_max values were found to be around 4.12 to 4.50 considering all cases. Overall, the SD of LAI_max values ranges from 3.80 to 4.70 for all five

illustrative covers depending on whether the climate year is drier or wetter. The range is within the measured LAI range for the Canadian boreal forest shown by Barr et al. (2012) to be between 2.0 and 5.20 based on old aspen, old black spruce, and old jack pine.

3.3.7 Uncertainty in estimating water balance components

3.3.7.1 Impact of parameter, climate, and LAI variability on the simulated AET and NP

Three primary sources of uncertainty in the simulated AET are parameter variability, climate variability, and LAI variability. Figure 3-11 shows the distributions of AET resulting from these sources of variability, which were obtained from the simulated AET using 700 parameter sample sets, 60 years of climate data, and three LAI_max values (i.e., min, mean, max). The impact of the three sources of uncertainty was separated as follows: (a) the simulated annual AET values corresponding to the mean LAI_max were averaged over the 60-year climate cycle to demonstrate the parameter variability; (b) the simulated annual AET values corresponding to the mean LAI_max were averaged over the 700 parameter sets to demonstrate the impact of climate variability; and (c) the simulated annual AET values corresponding to the min, mean, and max LAI_max were averaged over the 60-year climate cycle and 700 parameter sets to demonstrate the LAI variability.

The AET distributions are shown as box plots for the five illustrative covers in Fig. 3-11. The results demonstrate that the uncertainty in the simulated AET derived from parameter uncertainty decreases slightly with increasing cover thickness while remaining relatively constant with cover thickness in the case of climate variability. The median annual AET values resulting from the parameter variability and climate variability distributions are similar, particularly for the thinner illustrative covers. Overall, climate variability exerts more impact on the simulated annual AET, followed in turn by parameter variability and then LAI values.

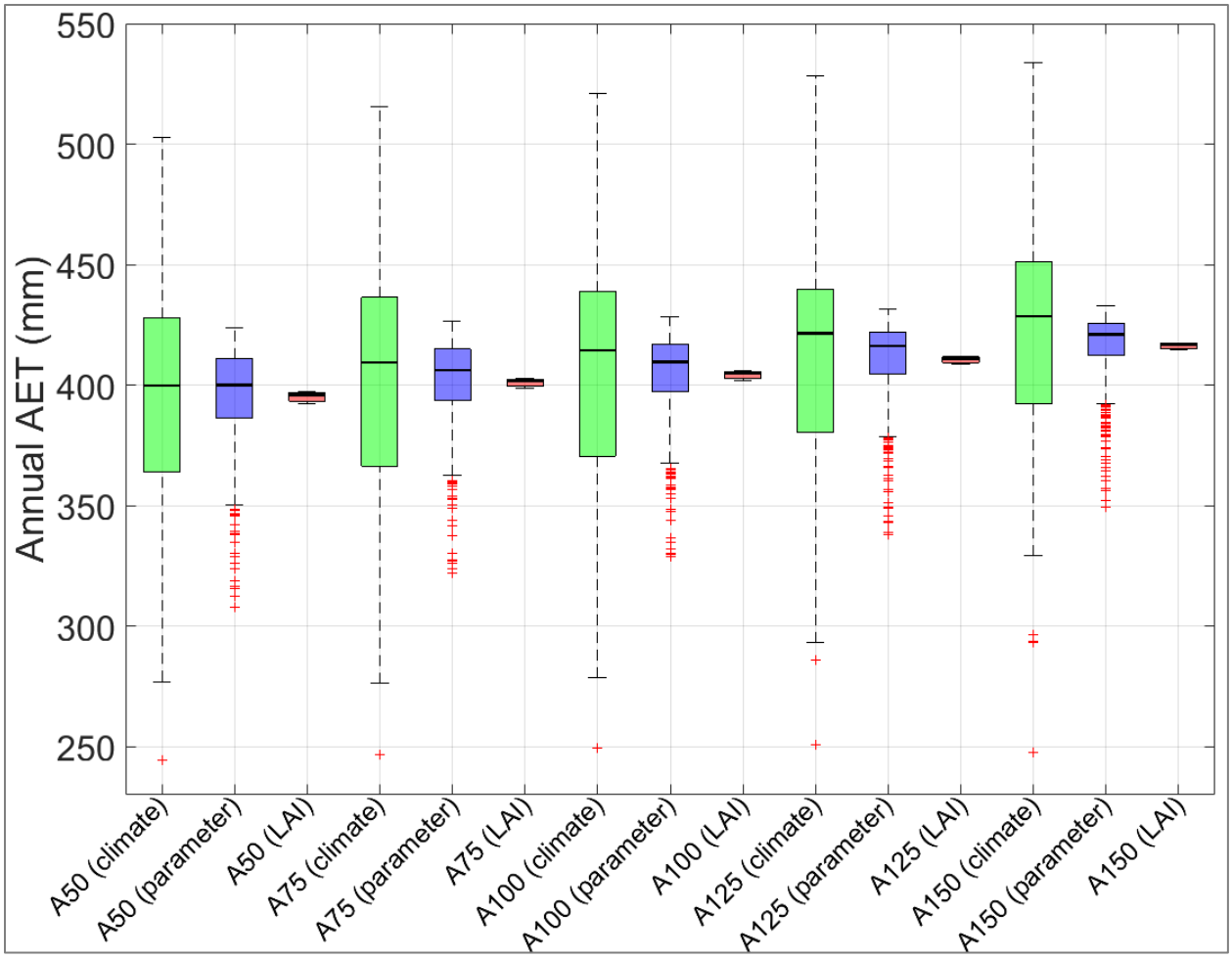

Figure 3-11: Box plots showing the distributions of annual AET obtained from the simulated water balances for the five illustrative covers with 700 parameter sets (blue boxes show parameter variability) over a 60-year climate cycle (green boxes show climate variability) with four LAI values (red boxes show LAI variability). The heavy dark line in each box plot shows the median, the boxes show the first and third quartiles, and the whiskers extend to 1.5 times the inter-quartile range. Outliers are shown as red plus signs.

The impact of the three sources of uncertainty on annual NP is presented in Fig. 3-12. The NP distributions for the five illustrative covers demonstrate that the uncertainty in simulating NP decreases with increasing cover thickness for both the parameter and climate variability cases. In contrast to the AET results, the uncertainty associated with climate variability is similar to that obtained by parameter variability. The distance between the median NP and the first quartile as well as the length of the whiskers seem to decrease with increasing cover thickness, which would mean less extreme annual NP for the thicker covers. The difference between the median annual

NP values obtained from the parameter variability and climate variability appears to decrease with increasing cover thickness. Overall, the parameter variability and climate variability have similar levels of influence on the simulated annual NP, followed by the variability due to the calculated LAI values.

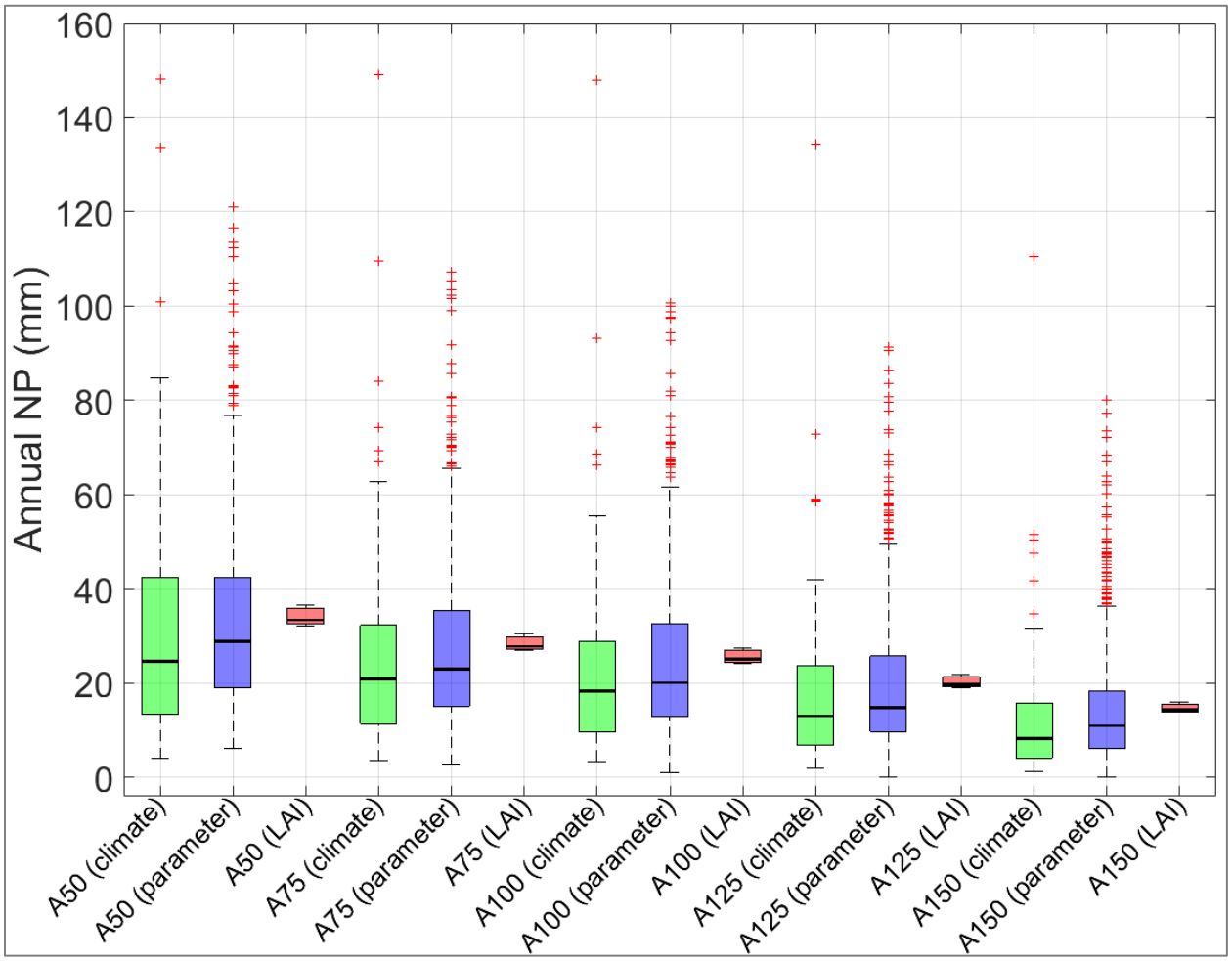

Figure 3-12: Box plots showing the distributions of annual NP obtained from the simulated water balances for the five illustrative covers with 700 parameter sets (blue boxes show parameter variability) over a 60-year climate cycle (green boxes show climate variability) with four LAI values (red boxes show LAI variability). The description of the box plots is the same as for Figure 3-11.

The water balance components for the five illustrative covers are summarized in Table 3-4 based on the corresponding mean LAI_max values for each cover. Among the five illustrative covers, A50 had the lowest annual AET and the highest annual NP. The annual AET increases

with increasing cover thickness, whereas the annual NP decreases with increasing cover depth, similar to previous studies (Huang et al., 2015; Alam et al., 2018a). These trends of annual AET and NP are consistent with the LAI_max values for each soil cover: higher annual AET for the covers with higher LAI_max values and higher annual NP for the covers with lower LAI_max values. The relative AET values reflect the relative productivity of the five illustrative covers, while the relative NP values indicate the thicker covers are capable of storing more water than the thinner covers. Table 3-4 also shows the annual soil moisture deficit (DS) values for the five illustrative covers, where DS increases with increasing cover thickness.

The results showed that climate variability is likely to be a key source of uncertainty for the simulated AET during the historical 60-year period. That said, climate and parameter variabilities appear to might cause similar levels of uncertainty in the simulated NP rates during the same historical period. Our previous studies (Alam et al., 2017; Alam et al., 2018a) showed that the median AET and NP are expected to increase in the future as compared to the historical period irrespective of the climate models (GCM) or scenarios (RCP) used, as well as increased uncertainty in the future AET and NP. The parameter variability combined with climate variabilities due to GCMs and/or RCPs would cause more increased uncertainty in the future period than it appears to cause during the historical period, and it requires further investigation. The elevated water balance components as well as increased uncertainty in the simulated AET and NP rates due to combined impacts of climate and parameter variability would pose increased risks to the management of water migrating through reclaimed mine waste. The risks of increased chemical loading to the downgradient waterbodies due to increased NP rates will require further investigation under changing climate conditions.

Table 3-4: Summary of water balance components for the five illustrative covers obtained using 700 sampled parameter sets with the corresponding LAI_max values (the mean LAI_max value is shown with the corresponding standard deviation)

Illustrative cover	Precipitation	AT	AE	AET	NP	DS	LAI_max ± SD
	(mm)	(mm)	(mm)	(mm)	(mm)	(mm)	[-]
A50	426	297	99.1	397	33.3	-3.41	4.12 ± 0.33
A75	426	303	98.6	402	28.0	-3.47	4.25 ± 0.30
A100	426	305	99.8	405	25.0	-3.53	4.27 ± 0.29
A125	426	310	101	411	20.0	-4.69	4.37 ± 0.27
A150	426	316	101	416	15.0	-5.46	4.50 ± 0.23

3.3.7.2 Impact of Ks of LOS material on the simulated AET and NP

Huang et al. (2017) show that simulated values of AET and NP are most sensitive to the distribution of the K_s of the LOS. To reevaluate this finding in the present study, a specified range of LOS K_s values (i.e., 0.0005, 0.0023, 0.0079, 0.0270, and 0.1916 md^{-1}) was used to simulate AET and NP over the 60-year time period for the A100 illustrative cover. A constant LAI value of 4.0 was used along with the parameter variability for the other hydraulic parameters. The results presented in Fig. 3-13 highlight that the mean annual AET decreases and the mean annual NP increases as K_s increases. In addition, the range of AET and NP is smallest for the lowest values of K_s. A value of K_s lower than 0.005 md^{-1} would represent a restriction to gravity drainage on the order of 5 mmd^{-1}, similar to a maximum rate of daily potential evaporation. As a consequence, these results are not surprising because they highlight a shift in the mechanism for water storage within the covers, specifically from being dominated by the water retention properties of the cover (i.e., high values of K_s) to "perching" of infiltrating waters on the LOS surface (i.e., low values of K_s).

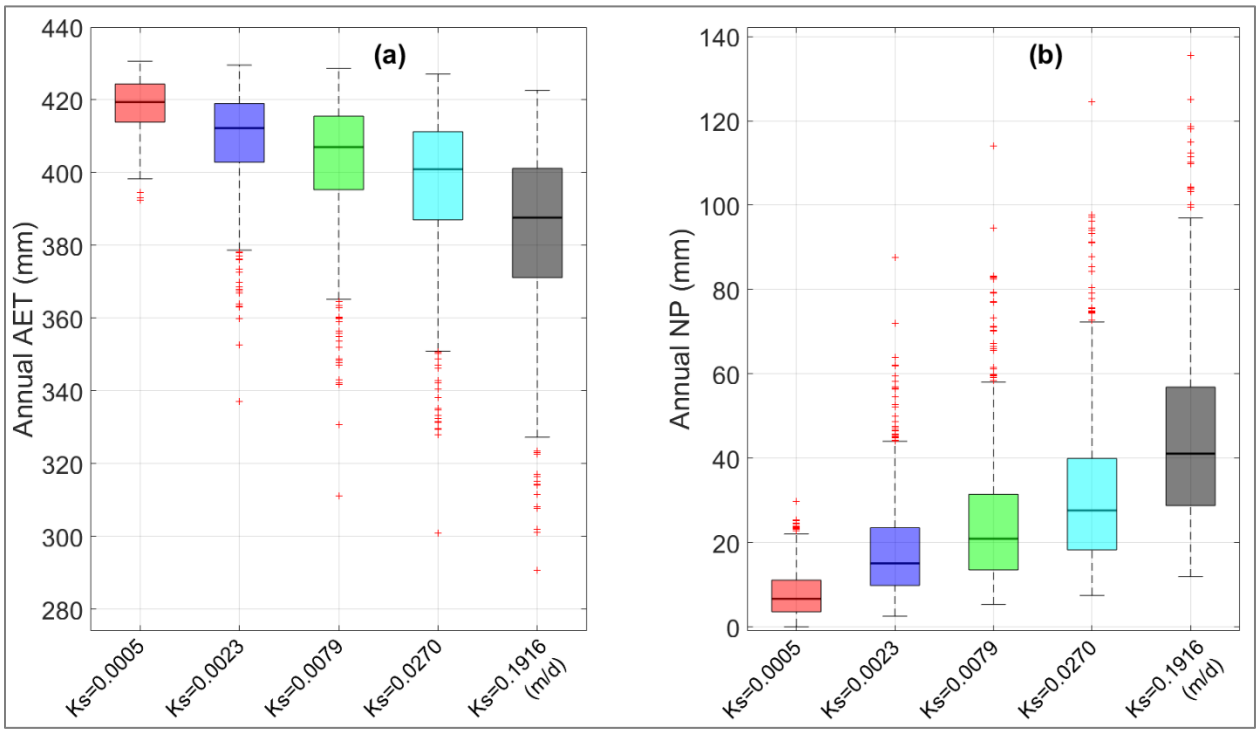

Figure 3-13: Box plots showing the distribution in uncertainty in the simulated water balance components of (a) AET and (b) NP with variation in the soil hydraulic parameters, for instance, K_s of the LOS overburden. Uncertainty of each water balance component is represented for the five illustrative covers. The description of the box plots is the same as for Figure 3-11.

3.4 Conclusions

Long-term cover performance is commonly evaluated without quantification of the uncertainties which may originate from various sources including climate, soil hydraulic parameters, and vegetation index (i.e., leaf area index). The use of a single set of model parameters in the design of reclamation covers precludes our ability to quantify the potential impact of uncertainties in parameters or climate and consequently makes it impossible to quantify the associated risks in performance. While our previous study (Alam et al., 2018a) investigated the impacts of climate in changing climatic conditions on the long-term cover performance, this study investigates the sources of uncertainty associated with the evaluation of long-term cover performances. This study considers a unique way to characterize the spatial and temporal uncertainty in the total parameter uncertainty utilizing field monitoring data from 13 treatment covers (replicated in triplicate and monitored in 4 consecutive years). The field monitoring data include water content, soil temperature, and soil suction values recorded at various depths at each of the treatment covers. There are few instances in the literature where such a large data record is available to quantify uncertainty. It has not been attempted previously in the context of oil sands reclamation covers. While the use of the HYDRUS-1D inverse modelling tool to optimize soil hydraulic parameters (both VG and saturated hydraulic conductivity) is not new, the use of this tool to develop probability distributions for optimized parameter sets from multiple sites and years is novel, particularly when one of the parameters (K_s) can be directly compared to field-measured distributions. Since the risks associated with a cover design would be based on the probability distributions of water balance components, it seems reasonable to use a computationally efficient sampling method (PLHS in this case) to obtain all possible probability distributions of the optimized parameters, which was motivation for the current study.

Inverse modelling (IM) in HYDRUS-1D was used to optimize five soil hydraulic parameters and produced 155 sets of soil hydraulic parameters for 13 treatment covers, replicated in triplicate, over 4 monitoring years. Progressive Latin hypercube sampling (PLHS) was used to sample parameters from the distributions of each of the five hydraulic parameters obtained from the IM approach. The randomly sampled parameters (i.e., 700 realizations) were then used in the simulations of long-term water balance for five illustrative covers. The results from the simulations were used to highlight the coupling that occurs between the parameter variability and the LAI_max values as well as the combined impact of these variabilities on the predicted distributions of AET and NP for the five illustrative covers. Overall, the PLHS method outperforms the widely used MC sampling technique in generating the distributions of five hydraulic parameters by requiring 10 times less sample size in order to achieve similar levels of water balance components for the illustrative covers (Fig. A.3-2).

The study revealed that the peat cover soil reclamation material had the highest variability in the WRC, while the LOS substrate had the greatest variability in K_s. In this study, peat was combined with LFH, which might be the reason for the highest variability in WRC among the materials for three layers of the treatment covers. The results of the long-term simulated water balance highlighted how variability in climate, sampled soil hydraulic parameters, and LAI influenced the uncertainty in both AET and NP. The distributions of the long-term simulated AET showed that climate variability exerted more impact on the uncertainty in annual AET. In the case of NP, the uncertainty derived from climate and parameter variability were similar and much greater than that from LAI variability. The uncertainty in the simulated AET values decreased with increasing cover thickness for parameter variability, while the uncertainty in the simulated NP values decreased with increasing cover thickness for both parameter and climate variability. Median annual AET values resulting from variable parameter sets and climate data seemed to remain approximately equal for the thinner illustrative covers, while median annual NP values remained approximately equal for the thicker covers. The PLHS and MC sampling methods produced a broader range of simulated AET and NP compared to the discrete sampling approach.

Overall, the results of this study help to highlight a wide range of cover performance risks that can occur when parameter variability is combined with climate, LAI, and cover thickness variability. The characterization of the optimized hydraulic parameters as variable, along with the evaluation of the maximum sustainable LAI, improve our ability to characterize the uncertainty associated with the long-term simulation of cover performance beyond what is possible using a single optimized parameter set and presumed value of LAI. This study also enables an examination of how varying cover thickness changes not only cover performance (in terms of AET and NP), but also the uncertainty in cover performance due to both climate and parameter variability. As cover thickness increases, the annual AET increases and the annual NP decreases, as expected; however, the range in these simulated water balance components also decreases predominantly due to parameter variability. A similar insight is also available for the specific case of how variability in the K_s of the LOS affects the magnitude and range of AET and NP. In this case, the shift in cover performance combines the impact of cover thickness (i.e., water storage capacity) and the impact of restricting water flow.

Designs of reclamation covers are typically based on the long-term simulations of AET and NP using a single parameter set that excludes the incorporation of parameter variability in simulating NP rates. This approach is likely to underestimate the possible ranges of NP rates. The elevated NP rates that develop when parameter variability is incorporated is an important finding which will need to be considered by industry in developing their closure designs. The consequences could be elevated volumes of water yield from the reclamation covers to the adjacent surface water bodies as well as associated increases in rates of chemical loading from the underlying mine waste. Given the role that climate change is expected to play in future water balances of reclamation covers and the similar magnitude of impact played by parameter variability in simulating NP, integration of both climate change impacts and parameter variability across the landscapes needs to be adopted in mine reclamation cover design in the future.

In the IM and long-term simulation of water balance components, the rooting depth assumption did not allow direct water uptake from the LOS substrate. A key limitation of this study was the sole use of historical climate data without any consideration of future climate

change and variability. Further research needs to examine the impact of more climate variability due to climate change (based on both global climate models and regional climate models) combined with these sources of variability considered here on long-term cover performance over the next few centuries.

3.5 Acknowledgements

The work was financed by the Natural Sciences and Engineering Research Council of Canada (NSERC) and Syncrude Canada Ltd. (file No. 428588-11). Special thanks are given to Amy Heidman of O'Kane Consultants Inc. for providing uninterrupted access to the Syncrude watershed research database. We appreciate Razi Sheikholeslami and Saman Razavi for sharing the PLHS Toolbox with us. We thank Stephanie Villeneuve for designing Fig. 1a and Larisa Doucette for sharing Fig. 1b.

References

Alam, M. S., Barbour, S. L., Elshorbagy, A., and Huang, M.: The impact of climate change on the water balance of oil sands reclamation covers and natural soil profiles, J. Hydrometeorol., JHM-D-17-0230.1, doi:10.1175/JHM-D-17-0230.1, 2018a.

Alam, M. S., Barbour, S. L., and Huang, M.: An evaluation of soil hydraulic parameter uncertainty on the hydrologic performances of oil sands reclamation covers, 71st Canadian Geotechnical Society Conference, GeoEdmonton 2018, Edmonton, Alberta, 23-26 September, pp. 1–8, 2018b.

Alam, M. S., Barbour, L., Huang, M., and Doucette, L.: An evaluation of parameter uncertainty in the calibration of a soil-vegetation-atmosphere-transfer (SVAT) model for a reclamation cover on LOS, 70th Canadian Geotechnical Society Conference, GeoOttawa 2017, Ottawa, Ontario, 2-4 October, pp. 1–8, 2017.

ASTM: Standard test method for particle-size analysis of soils, method D422-63, American Society for Testing and Materials, Philadelphia, PA, 1998.

Arya, L. M., Leij, F. J., van Genuchten, M. Th., and Shouse, P. J.: Scaling parameter to predict the soil water characteristic from particle-size distribution data. Soil Sci. Soc. Am. J., 63, 510-519, 1999.

Barr, A. G., van der Kamp, G., Black, T. A., McCaughey, J. H., and Nesic, Z.: Energy balance closure at the BERMS flux towers in relation to the water balance of the White Gull Creek watershed 1999-2009, Agric. For. Meteorol., 153, 3–13, doi:10.1016/j.agrformet.2011.05.017, 2012.

Benke, K. K., Lowell, K. E., and Hamilton, A. J.: Parameter uncertainty, sensitivity analysis and prediction error in a water-balance hydrological model, Math. Comput. Model., 47(11–12), 1134–1149, doi:10.1016/j.mcm.2007.05.017, 2008.

Beven, K. and Binley, A.: The future of distributed models: Model calibration and uncertainty prediction, Hydrol. Process., 6(3), 279–298, doi:10.1002/hyp.3360060305, 1992.

Bockstette, S.: Roots in reconstructed soils-how land reclamation practices affect the development of tree root systems, Ph.D. thesis, Department of Renewable Energy, University of Alberta, 108 pp., 2017.

Boese, C. D.: The design and installation of a field instrumentation program for the evaluation of soil-atmosphere water fluxes in a vegetated cover over saline/sodic shale overburden, M.Sc. thesis, Department of Civil and Geological Engineering, University of Saskatchewan, 170 pp., 2003.

Brutsaert, W.: Evaporation into Atmosphere: Theory, History, and Applications, Dordrecht, D. Reidel Publishing Company, 1982.

Carrera-Hernández, J. J., Mendoza, A., Devito, K. J., Petrone, R. M., and Smerdon, B. D.: Effects of aspen harvesting on groundwater recharge and water table dynamics in a subhumid climate, Water Resour. Res., 47(5), 1–18, doi:10.1029/2010WR009684, 2011.

Carman, P. C.: The determination of the specific surface of powders. J. Soc. Chem. Ind. Trans., 57, 225, 1938.

Carman, P. C.: Flow of gases through porous media Butterworths Scientific Publications, London, UK, 1956.

Devito, K., Mendoza, C., and Qualizza, C.: Conceptualizing water movement in the Boreal Plains. Implications for watershed reconstruction, Synthesis report prepared for the Canadian Oil Sands Network for Research and Development, Environmental and Reclamation Group, 164 p. [online] Available from: http://hdl.handle.net/10402/era.30206, last access: 25 October 2018, 2012.

Feddes, R. A., Bresler, E., and Neuman, S. P.: Field test of a modified numerical model for water uptake by root systems, Water Resour. Res., 10(6), 1199–1206, doi:10.1029/WR010i006p01199, 1974.

van Genuchten, M. T.: A closed-form equation for predicting the hydraulic conductivity of unmatured soils, Soil Sci. Soc. Am. J., 44(5), 892–898, 1980.

Gong, W.: An intercomparison of sampling methods for uncertainty quantification of environmental dynamic models, J. Environ. Informatics, 28(1), 11–24, doi:10.3808/jei.201500310, 2015.

Higdon, D., Gattiker, J., Lawrence, E., Jackson, C., Tobis, M., Pratola, M., Habib, S., Heitmann, K., and Price, S.: Computer model calibration using the ensemble kalman filter, Technometrics, 55(4), 488–500, doi:10.1080/00401706.2013.842936, 2013.

Hopmans, J. W., Simunek, J., Romano, N., and Durner, W.: Chapter 3.6.2: Inverse Methods, in: Methods of Soil Analysis: Part 4. Physical methods, edited by J.H. Dane and G.C. Topp, SSSA Book Ser. 5. SSSA, Madison, WI, 2002.

Hossain, F., Anagnostou, E. N., and Bagtzoglou, A. C.: On Latin Hypercube sampling for efficient uncertainty estimation of satellite rainfall observations in flood prediction, Comput. Geosci., 32(6), 776–792, doi:10.1016/J.CAGEO.2005.10.006, 2006.

Huang, M., Barbour, S. L., Elshorbagy, A., Zettl, J. D., and Si, B. C.: Infiltration and drainage processes in multi-layered coarse soils, Can. J. Soil Sci., 91(2), 169–183, doi:10.4141/cjss09118, 2011a.

Huang, M., Elshorbagy, A., Barbour, S. L., Zettl, J., and Si, B. C.: System dynamics modeling of infiltration and drainage in layered coarse soil, Can. J. Soil Sci., 91(2), 185–197, doi:10.4141/cjss10009, 2011b.

Huang, M., Barbour, S. L., Elshorbagy, A., Zettl, J., and Si, B. C.: Water availability and forest growth in coarse-textured soils, Can. J. Soil Sci., 91(2), 199–210, doi:10.4141/cjss10012, 2011c.

Huang, M., Barbour, S. L., and Carey, S. K.: The impact of reclamation cover depth on the performance of reclaimed shale overburden at an oil sands mine in Northern Alberta, Canada, Hydrol. Process., 29(12), 2840–2854, 2015.

Huang, M., Zettl, J. D., Barbour, S. L., and Pratt, D.: Characterizing the spatial variability of the hydraulic conductivity of reclamation soils using air permeability, Geoderma, 262, 285–293, doi:10.1016/j.geoderma.2015.08.014, 2016.

Huang, M., Alam, M.S., Barbour, S.L., and Si, B. C.: Numerical modelling of the impact of cover thickness on the long-term water balance of reclamation soil covers over lean oil sands overburden., Report for Syncrude Canada Ltd., 39pp., 2017.

Iman, R. L. and Conover, W. J.: Small sample sensitivity analysis techniques for computer models.with an application to risk assessment, Commun. Stat. Theor.,, 9(, 1749–1842, doi:10.1080/03610928008827996, 1980.

Iman, R. L. and Helton, J. C.: An investigation of uncertainty and sensitivity analysis techniques for computer models, Risk Anal., 8, 71–90, doi:10.1111/j.1539-6924.1988.tb01155.x, 1988.

Jones, C. E.: Early Vegetation Community Development and Dispersal in Upland Boreal Forest Reclamation, M.Sc. thesis, Department of Renewable Energy, University of Alberta, 92 pp., 2016.

Keshta, N., Elshorbagy, A., and Carey, S.: A generic system dynamics model for simulating and evaluating the hydrological performance of reconstructed watersheds, Hydrol. Earth Syst. Sci., 13(6), 865–881, doi:10.5194/hess-13-865-2009, 2009.

Kosugi, K.: Lognormal distribution model for unsaturated soil hydraulic properties, Water Resour. Res., 32(9), 2697–2703, 1996.

Kozeny, J.: Uber kapillare Leitung des Wassers im Boden. Wien Akad. Wiss. 136, 271, 1927.

Mathan, K. K., Sundaram, A., and Mahendran, P. P.: Application of Kozeni-Carman equation for the estimation of saturated hydraulic conductivity of soils. J. Indian Soc. Soil Sci., 43: 542-544, 1995.

McKay, M. D., Beckman, R. J., and Conover, W. J.: A comparison of three methods for selecting values of input variables in the analysis of output from a computer code, Technometrics, 21(2), 239, doi:10.2307/1268522, 1979.

Meiers, G. P., Barbour, S. L., Qualizza, C. V., and Dobchuk, B. S.: Evolution of the hydraulic conductivity of reclamation covers over sodic/Saline mining overburden, J. Geotech. Geoenvironmental Eng., 137(10), 968–976, doi:10.1061/(ASCE)GT.1943-5606.0000523, 2011.

Metropolis, N., Rosenbluth, A. W., Rosenbluth, M. N., Teller, A. H., and Teller, E.: Equation of state calculations by fast computing machines, J. Chem. Phys., 21(6), 1087–1092, doi:10.1063/1.1699114, 1953.

Mualem, Y.: A New Model for Predicting the Hydraulic Conductivity of Unsaturated Porous Media. Water Resources Research, 12 (3), 513–22. doi:10.1029/WR012i003p00513, 1976.

NorthWind Land Resources Inc.: Summary of work conducted by NorthWind Land Resources Inc. for Syncrude Canada Ltd.'s Aurora Soil Capping Study Project #11-381, Report for Syncrude Canada Ltd., 2013.

O'Kane Consultants Inc. (OKC): PSD reduced data for potential capping study materials., Report for Syncrude Canada Ltd., 2009.

O'Kane Consultants Inc. (OKC): Aurora Soil Capping Study Five Year Performance Monitoring Report November 2012 to September 2017, Report 690/141--001, 2017.

Price, J. S., McLaren, R. G., and Rudolph, D. L.: Landscape restoration after oil sands mining: Conceptual design and hydrological modelling for fen reconstruction, Int. J. Mining,

Reclam. Environ., 24(2), 109–123, doi:10.1080/17480930902955724, 2010.

Qualizza, C., Chapman, D., Barbour, S. L., and Purdy, B.: Reclamation research at Syncrude Canada's mining operation in Alberta's Athabasca oil sands region, Proceedings of the 16th International Conference on Ecological Restoration SER2004, Victoria, B. C. Canada, Society for Ecological Restoration., 2004.

Sheikholeslami, R. and Razavi, S.: Progressive Latin Hypercube Sampling: An efficient approach for robust sampling-based analysis of environmental models, Environ. Model. Softw., 93, 109–126, doi:10.1016/J.ENVSOFT.2017.03.010, 2017.

Simunek, J., Sejna, M., Saito, H., Sakai, M., and van Genuchten, M. T.: The HYDRUS software package for simulating the two- and three- dimensional movement of water, heat, and multiple solutes in variably-saturated media, Univ. California, Riverside, CA, 2013.

Soil Classification Working Group: The Canadian system of soil classification working group. [online] Available at: http://sis.agr.gc.ca/cansis/publications/manuals/1998-cssc-ed3/cssc3_manual.pdf, last access: 31 October 2018, 1998.

Strong, W. L. and La Roi, G. H.: Root-system morphology of common boreal forest trees in Alberta, Canada, Can. J. For. Res., 13, 1164–1173, 1983.

Syncrude Canada Ltd.: Climate and soil monitoring data for the treatment covers at the Aurora North Mine site, Syncrude Water-shed Research Database, available at: https://syncrude.emline.ca, last access: 30 August 2019.

van Genuchten, M. T.: A closed-form equation for predicting the hydraulic conductivity of unmatured soils, Soil Sci. Soc. Am. J., 44, 892–898, 1980.

van Genuchten, M. T., Leij, F. J., and Yates, S. R.: The RETC Code for quantifying the hydraulic functions of unsaturated soils, EPA Report 600/2-91/065, US Salinity Laboratory, USDA, ARS, Riverside, CA, 1991.

CHAPTER 4 - THE IMPACT OF CLIMATE CHANGE ON THE WATER BALANCE OF OIL SANDS RECLAMATION COVERS AND NATURAL SOIL PROFILES (ALAM ET AL. 2018)

Preface

The second objective of this thesis was as follows: "To characterize the impact that future projected climate change will have on the water balance of oil sands reclamation covers". In Chapter 3, climate variabilities are likely to exert more impact on the water balance components (particularly AET), variabilities due to GCMs and/or RCPs are expected to incorporate greater uncertainty in the future water balances compared to the historical values. In this second published paper the long-term performances of oil sands mine reclamation covers under climate change projections was evaluated and compared to the simulated performance of historical climate periods. The climate change projections (e.g. temperature, precipitation, wind speed, net radiation, and relative humidity) were based on the Canadian Global Climate Model (GCM) and the water balance was the physically-based HYDRUS-1D model with parameter sets optimized within previous studies. This study demonstrated how to couple GCM outputs and a physically-based water balance model through the downscaling methods. The downscaling methods used in this study were LARS-WG and Delta Change method, which generated site-specific climate change projections that were originally provided by the GCM at global-scale. This coupling approach was consequently used in Chapter 5 as well for exploring the impacts of climate change using high resolution climate change projections.

I, Md. Shahabul Alam, conceptualized and developed the coupling between the GCM outputs and HYDRUS-1D. Dr. M. Huang developed, calibrated and validated HYDRUS-1D mostly in his previous studies, which I incorporated in this study. I reviewed the literature, conducted numerical simulations, analyzed and discussed the results, and wrote the manuscript. All coauthors, Dr. S. L. Barbour, Dr. A. Elshorbagy, and Dr. M. Huang critically reviewed and edited the manuscript and provided feedbacks on different aspects of the study. The published paper in this chapter is presented with minor changes as suggested by the examining committee. This chapter has been published with the following citation:

Alam, M. S., Barbour, S. L., Elshorbagy, A., and Huang, M. (2018). The Impact of Climate Change on the Water Balance of Oil Sands Reclamation Covers and Natural Soil Profiles. *Journal of Hydrometeorology*, https://doi.org/10.1175/JHM-D-17-0230.1. © American Meteorological Society. Used with permission.

Abstract

The design of reclamation soil covers at oil sands mines in northern Alberta, Canada, has been conventionally based on the calibration of soil–vegetation–atmosphere transfer (SVAT) models against field monitoring observations collected over several years, followed by simulations of long-term performance using historical climate data. This paper evaluates the long-term water balances for reclamation covers on two oil sands landforms and three natural coarse-textured forest soil profiles using both historical climate data and future climate projections. Twenty-first century daily precipitation and temperature data from CanESM2 were downscaled based on three representative concentration pathways (RCPs) employing a stochastic weather generator [Long Ashton Research Station Weather Generator (LARS-WG)]. Relative humidity, wind speed, and net radiation were downscaled using the delta change method. Downscaled precipitation and estimated potential evapotranspiration were used as inputs to simulate soil water dynamics using physically based models. Probability distributions of growing season (April–October) actual evapotranspiration (AET) and net percolation (NP) for the baseline and future periods show that AET and NP at all sites are expected to increase throughout the twenty-first century regardless of RCP, time period, and soil profile. Greater increases in AET and NP are projected toward the end of the twenty-first century. The increases in future NP at the two reclamation covers are larger (as a percentage increase) than at most of the natural sites. Increases in NP will result in greater water yield to surface water and may accelerate the rate at which chemical constituents contained within mine waste are released to downstream receptors, suggesting these potential changes need to be considered in mine closure designs.

4.1 Introduction

Government regulations require that lands disturbed by oil sands mining be reclaimed to an equivalent land capability to what existed prior to mining. The equivalent land capability is based on productivity (e.g., supporting diversified vegetation and wildlife), a Land Capability Classification System (LCCS) rating that quantifies nutrient and water availability regimes and other landscape characteristics necessary for government reclamation certification [Cumulative Environmental Management Association (CEMA); CEMA 2006]. Historically, reclamation cover designs were based on assessments of available water-holding capacity (Elshorbagy and Barbour 2007; Huang et al. 2015). More recent industry designs use physically based water dynamics models calibrated using long-term (up to 10 years) monitoring to predict long-term performance using 60-yr historical climate records (Boese 2003; Huang et al. 2011a,b,c, 2015; Keshta et al. 2009; Price et al. 2010; Qualizza et al. 2004).

The long-term performance of reclaimed land disturbed by oil sands mining will be affected by climate change, driven in part by greenhouse gas emissions. Mining and processing of oil sands are associated with 9.3% of these emissions in Canada and about 0.13% globally, where majority of the emissions caused by the end-users by burning oil and natural gas [Canadian Association of Petroleum Producers (CAPP); CAPP 2016]. Oil sands industry growth since the 1960s has disturbed about 0.02% of Canada's boreal forests, which serve as the largest terrestrial reservoir of emitted carbon and store almost 22% of the global carbon stocks available on land [Intergovernmental Panel on Climate Change (IPCC); IPCC 2000].

Climate change is expected to intensify the global hydrological cycle because of increases in precipitation and potential evapotranspiration (Huntington 2006). The IPCC Fifth Assessment Report (AR5; IPCC 2013) indicated global average temperatures from 2003 to 2012 increased by 0.78^{o}C compared to 1850–1900; this trend is expected to continue throughout the twenty-first century. Global mean surface temperature is projected to be 1^{o}–3.7^{o}C higher in 2081–2100 compared to 1986– 2005, with global mean precipitation likely to increase by 0.5%–4% $^{o}C^{-1}$ under all scenarios [representative concentration pathway (RCP): RCP2.6, RCP4.5, and RCP8.5]. Scenario RCP8.5 considers rises in CO_2 concentrations by the year 2250 to about 2000 ppmv, which is approximately 7 times the preindustrial level. These dramatic changes in climate

and atmospheric composition are expected to cause significant changes in global evapotranspiration by the end of the twenty-first century (Pan et al. 2015). Consequently, their impact on water balances must be understood to assess the future performance of reclaimed land.

Water balances for natural sites and reclaimed waste at oil sands mines in northern Alberta, Canada, have been extensively studied. Huang et al. (2011c) and Zettl et al. (2011) conducted numerical modeling and experimental studies to understand mechanisms controlling infiltration and drainage processes in natural, texturally variable, long-term soil–vegetation (SV) monitoring sites near currently operating mines. Huang et al. (2011b) assessed the impact of soil layering (heterogeneous soil texture), climatic variability (historical climatic record), and various vegetation types on plant-available water at a number of SV sites. Probability distributions, similar to those developed by Elshorbagy and Barbour (2007), highlighted the impact of various factors on the magnitude and variability in actual evapotranspiration. Huang et al. (2015) used a calibrated physically based water dynamics model to examine the impact of cover thickness and climate variability on plant-available water at reclamation covers placed over mine waste (sodic–saline shale overburden) over a 60-yr climate cycle. They found median evapotranspiration did not increase significantly for cover thicknesses greater than 80 cm (all other parameters held constant); however, the frequency of freshwater release from these thicker covers (runoff or interflow) dramatically decreased. This work highlighted the need to optimize reclamation cover designs for long-term climate cycles, taking into consideration both plant-available water and the release of freshwater to adjacent surface water bodies. Several studies used system dynamics models to simulate hydrological (Elshorbagy et al. 2007; Keshta et al. 2009) and infiltration and drainage (Huang et al. 2011a) processes for reclaimed soils at Syncrude's Mildred Lake mine in northern Alberta. However, the potential impact of climate change on oil sands reclamation covers has not been evaluated by linking future climate with physically based simulations of the soil water dynamics at these sites.

Reclamation covers for oil sands mining waste have been conventionally designed so prescribed cover soils and cover depths can provide sufficient plant-available water to support target vegetation over a long-term climate cycle. The climate cycle used in these designs is based on historical monitored climatic conditions (Huang et al. 2015). The purpose here is not to test or

evaluate water balance models as applied to soil cover designs for oil sands mining. Rather, we used water balance models that have already been developed, calibrated, and validated at monitored and characterized study sites. These models were adopted without substantive modification, keeping them as simple as possible to highlight the shifts in water balance that may occur if the historical climatic forcing boundary is replaced by a future climate scenario. Various physically based models [e.g., Soil and Water Assessment Tool (SWAT), HydroGeoSphere (HGS)] have been used to assess the impact of climate change on watershed water balance/streamflow (Githui et al. 2009; Leta et al. 2016; Mango et al. 2011) and water movement and availability in the Boreal Plains of Alberta, Canada (Thompson et al. 2017). Keshta et al. (2012) also used a generic system dynamics water balance model to evaluate the performance of alternate cover designs based on future projections of temperature and precipitation from the Third-Generation Canadian Coupled Global Climate Model (CGCM3) under two Special Report on Emission Scenarios (SRES) emission scenarios (IPCC 2000) but did not incorporate an estimation of uncertainty in the simulations. No previous studies have integrated physically based numerical water balance models (particularly, the widely used HYDRUS-1D in oil sands industry) with future climate projections to assess the impacts of climate change on the water balance of oil sands reclamation covers.

This study utilizes climate change projections based on an archive of forcing scenarios released in September 2013 by phase 5 of the Coupled Model Intercomparison Project (CMIP5) of the IPCC (Taylor et al. 2012). The key question being addressed is how future climate change scenarios, updated in September 2013, will alter key indicators of soil cover water balance performance. The indicators chosen are actual evapotranspiration (AET), because it represents the use of available water by vegetation, and net percolation (NP), because, given the assumption of flat-lying covers without runoff, it captures the total release of water (i.e., water yield) from the covers into the underlying waste and ultimately to downgradient surface water receptors. The study also illustrates a methodology by which field-calibrated physically based water balance models can be coupled with future climate change scenarios; this approach does not appear in the literature to date.

The soil profiles used include reclamation covers over a saline–sodic clay shale overburden [30 dump site (D3)] and a reclaimed sand tailings dyke [Southwest Sand Tailings Storage (SWSS)], as well as three natural profiles of glacial fluvial or dune sand (SV10, SV27, and SV60). Both reclamation sites have extensive long-term-monitoring datasets and physically based soil water dynamics models that were adapted for this study. The natural sites (also extensively characterized and modeled) are included to provide a direct comparison to SWSS. Overall, this study expands our understanding of the potential impact of climate change on the long-term performance of oil sands reclamation covers, an issue with no documented consideration by regulators or industry and relatively limited investigation by scientists (Keshta et al. 2012; Rooney et al. 2015; Schneider 2013).

4.2 Materials and methods

4.2.1 Study sites

All soil profiles are located in the boreal mixed-wood ecoregion (Strong and Leggat 1981) (Fig. 4-1), which has an area of approximately 290×10^3 km^2 and a typical prairie climate with mean annual precipitation of 443 mm, most of which occurs in the summer. Mean winter (December–February) and summer (June–August) temperatures are -16.7 and 15.4 °C, respectively.

4.2.1.1 Natural sites

The coarse-textured SV sites were established by the industry in 2005 (AMEC Earth and Environmental and Paragon Soil and Environmental Consulting Inc. 2005) for long-term soil–vegetation monitoring and feature a range of soil textures and layering. According to the northern Alberta ecological classification system (Beckingham and Archibald 1996), SV10 and SV27 fall in the ‘‘a1’’ ecosite class (xeric/subxeric moisture regime and a poor nutrient regime characterized by rapid drainage and limited volumes of stored plant-available water following precipitation events) and SV60 falls in the ‘‘d2’’ ecosite class (mesic/subhygric moisture regime and a medium nutrient regime with greater volumes of water stored and available for transpiration).

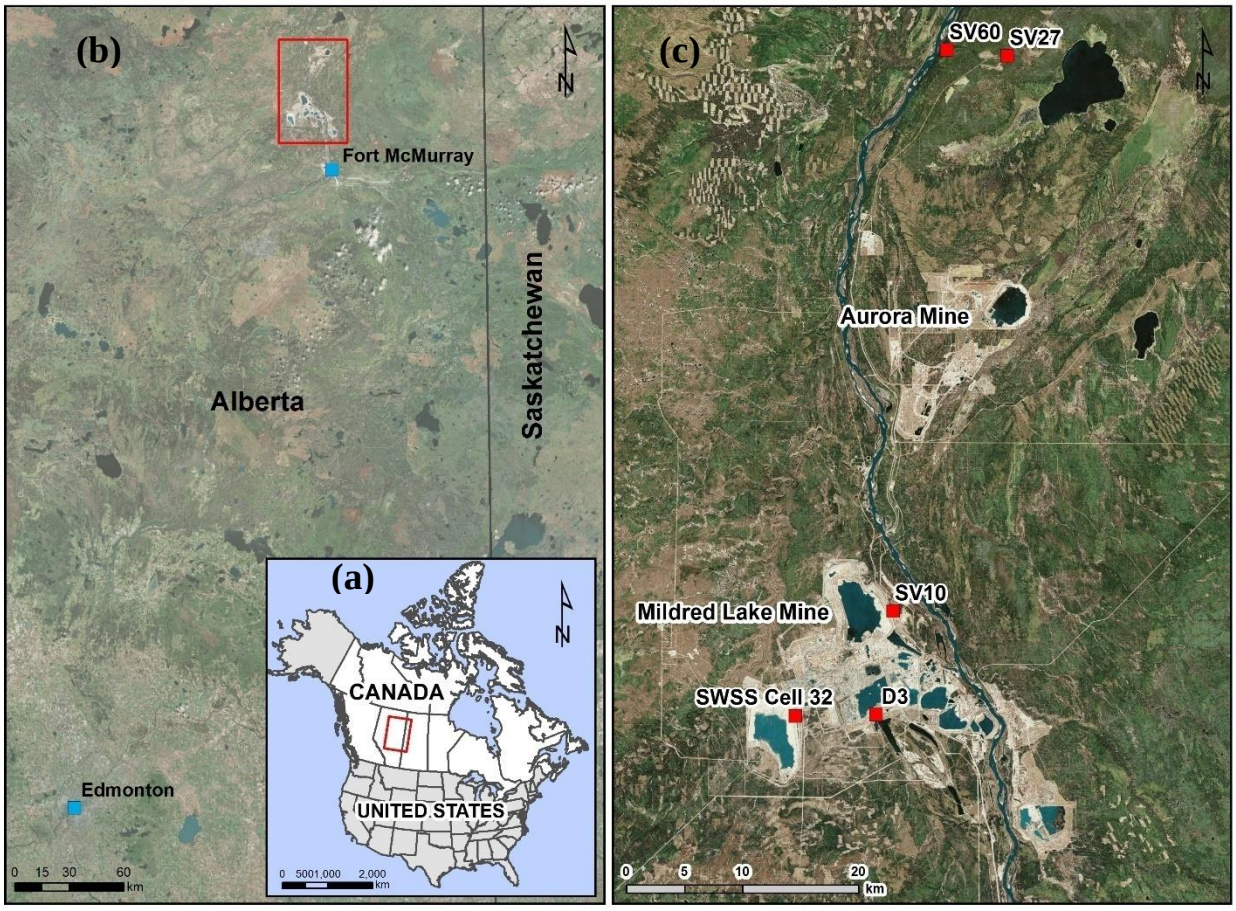

Figure 4-1: (a) Map of Canada with the province of Alberta; (b) map of Alberta with relevant cities and the broad study area identified; (c) map of study area with site locations as red squares where (c) is expanded view of the red box in (b).

Soil type and vegetation coverage of these natural sites are provided by Huang et al. (2011c); details of field experiments, sample collection, particle size distribution, and bulk density measurements are provided by Zettl et al. (2011). The SV10 and SV27 natural sites are texturally homogeneous with fine or medium sands, respectively. The natural SV60 profile is texturally heterogeneous with a fine sand layer (45–84 cm) that is overlain and underlain by coarse sand layers. The dominant vegetation types are jack pine (SV10 and SV27) or white spruce, white aspen, black spruce, and balsam fir (SV60). The average sand, silt, and clay fractions among the three natural sites range from 97.4% to 99.2%, from 0.3% to 1.2%, and from 0.5% to 0.9%, respectively.

4.2.1.2 Reclamation covers

The two reclamation sites are located at the Syncrude Canada Ltd. (SCL) Mildred Lake oil sands mine (Fig. 3-1). The fine-textured D3 reclamation cover has a peat–glacial clay mineral mixture (0–20 cm) overlying a fine-grained glacial soil (20–80 cm) underlain by the overburden clay shale. The SWSS reclamation cover has a very similar peat–mineral mixture (0–45 cm) overlying tailings sand. The dominant vegetation types are trembling aspen and white spruce at D3 and SWSS. The silt and clay size particle fractions in the reclamation covers (e.g., D3) range from 60% to 90% and from 25% to 55%, respectively (Boese 2003).

The reclamation sites have been monitored since 1999 (D3) and 2001 (SWSS). A meteorological tower monitors air temperature, wind speed, radiation, and relative humidity in addition to direct monitoring of the soil cover and underlying mine waste for volumetric water content, suction, and soil temperature. See Barbour et al. (2004), Boese (2003), Huang et al. (2015), and O'Kane Consultants, Inc. (OKC; OKC 2001, 2016) for details of the instrumentation and monitoring program.

4.2.2 Climate change projections and downscaling methods

The observed daily precipitation, minimum/maximum/ mean temperatures, relative humidity, wind speed, and net radiation for the baseline period (1961–90) were obtained from Environment and Climate Change Canada (ECCC) records at the Fort McMurray Airport station (located ~50–100 km south of the study sites). The future climate change projections (i.e., precipitation, temperature, relative humidity, wind speed, and net radiation) for the baseline (1961–90) and future period (2016–2100) were obtained using the Canadian GCM (CanESM2) combined with three RCPs (RCP2.6, RCP4.5, and RCP8.5; Taylor et al. 2012). Climate change projections for CanESM2 were obtained from the Canadian Centre for Climate Modeling and Analysis (http://www.cccma. ec.gc.ca/data). The datasets from CanESM2 for the time periods 1961–90 and 2016–2100 used in this study include precipitation (*pr*), daily minimum near-surface air temperature (*tasmin*), daily maximum near-surface air temperature (*tasmax*), relative humidity (*hur*), near-surface wind speed (*sfcWind*), surface downwelling longwave radiation (*rlds*), surface upwelling longwave radiation (*rlus*), surface downwelling shortwave radiation (*rsds*), and surface upwelling shortwave radiation (*rsus*).

The GCM meteorological outputs, which have a resolution of 200 km, were downscaled to provide climate specific to the local region (Franczyk and Chang 2009; Hashmi et al. 2011). A widely used and statistically based stochastic weather generator, Long Ashton Research Station Weather Generator (LARS-WG; Racsko et al. 1991; Semenov and Barrow 1997), was used to generate the site-scale time series of future daily precipitation and temperature based on the three RCPs of CanESM2, while daily relative humidity, wind speed, and net radiation (where net radiation was estimated from the longwave and shortwave radiation using empirical equations) were downscaled using a ‘‘delta change’’ or ‘‘perturbation’’ method (Prudhomme et al. 2002). Appendix B provides detailed downscaling methods.

4.2.3 Growing season precipitation and potential evapotranspiration (PET)

The daily precipitation from LARS-WG was used to generate accumulated snowpack outside the growing season (November–March), where the growing season starts after a week of frost-free nights in the spring and ends at the first frost in the fall. If the T_{mean} in a day was lower than a specified threshold (i.e., T_{thres}=0 °C), precipitation accumulated within a snowpack. Any accumulated snow depth from November to March was applied as precipitation during an assumed 2-week snowmelt period in the first two weeks of April. If T_{mean} was greater than T_{thres} over the winter period, then snowpack melting was calculated using the degree-day method (Carrera-Hernández et al. 2011), where daily snowmelt s is related to daily mean temperature *Tmean* and a melt factor *M* (mm °C^{-1}day^{-1}) if T_{mean} exceeds a threshold (i.e., T_{thres}=0 °C):

$$s = M\,(T_{mean}-T_{thres}), \tag{3.1}$$

where different factors affecting snowmelt are included in *M*, which varies with time and is estimated using the empirical relationship (Kuusisto 1980):

$$M = 10.4\,\frac{\rho_s}{\rho_w} - 0.7, \tag{3.2}$$

where ρ_s is snow density (kgm^{-3}) and ρ_w is water density (kgm^{-3}).

The calculated melt volume was added to any precipitation that occurred during this winter melt period and to stored water within the soil profile at the start of the April–October simulation period.

Average daily temperature for each of the 100 LARS-WG realizations along with relative humidity, wind speed, and net radiation from the delta change downscaling method were used in the Penman–Monteith equation (Allen et al. 1998; Brutsaert 1982) to calculate the 100 realizations of potential evapotranspiration (PET). The observed daily dewpoint temperature (^{o}C) was from ECCC records at the Fort McMurray Airport station. The 100 realizations of daily PET values during the growing season were used in the model as an input variable.

4.2.4 Water balance model

The physically based soil water dynamics model HYDRUS-1D, version 4.16 (Simunek et al. 2013), was used to simulate the daily water balance for each site as detailed in Huang et al. (2011b,c, 2015). In this approach, Richard's equation for transient unsaturated water flow is coupled to a climate/vegetation water flow boundary that incorporates precipitation (rainfall or snowmelt), actual transpiration from root uptake, and actual surface evaporation. Daily water balance components are then calculated from the simulation results, including infiltration into the ground surface, actual transpiration (AT) from the soil profile over the depth of rooting, actual evaporation (AE) from the soil surface, water release from the active rooting zone into the underlying groundwater system (also referred to as NP), and changes in soil water storage (DS) within the rooting zone.

The D3 site model was based on the model presented by Huang et al. (2015) and was developed by calibrating the model against six years of monitoring data (2006–11) from adjacent site D2 and then validating the model against six years of monitoring data (2006–11) from the D3 site. The calibration and validation phase root-mean-square error (RMSE) were 11.1 and 14.4 mm, respectively. Huang et al. (2011b,c) developed the models for the three natural sites (SV10, SV27, SV60) based on detailed site characterization and field testing. Hydraulic parameters for the SV sites were determined from interpretation of full-scale infiltration and drainage tests conducted by Zettl et al. (2011). The mean and standard deviation (SD) values of van Genuchten– Mualem (VG) parameters (see below) and the saturated hydraulic conductivity were obtained from Huang et al. (2011b). Final validation of the models was undertaken by comparing the predicted AET values for the past 60 years to measured tree growth and forest productivity.

The HYDRUS-1D model for SWSS was developed particularly for this study. Cover soils at SWSS are the same as for D3. Monitoring the climate and reclamation soil profile at SWSS has been ongoing since 2001. The model for SWSS was calibrated against 2010 growing season data using the inverse approach (Simunek et al. 2012) and then validated using 2012 growing season data. The model simulated the soil water content in the cover profile with RMSE and R^2 values of 0.11 mm and 0.89 in calibration and 0.19 mm and 0.69 in validation, respectively. Hydraulic parameters obtained for the two SWSS cover materials and the three D3 cover materials by Huang et al. (2015) are provided for comparison (see Table B-1 in appendix B).

One key difference in these models is that the clay-rich cover soils at the reclamation sites (D3 and SWSS) were characterized using dual-porosity hydraulic functions while the natural profiles (SV sites) were characterized by single-porosity functions. As discussed by Huang et al. (2015), this was due to the presence of a secondary structure of macropore development within the clay-rich cover soils. In both cases, VG equations (van Genuchten 1980) were used to describe these functional relationships for water storage and hydraulic conductivity. These equations and their parameter constants are defined in appendix B (Table B-2 summarizes the parameter values used for the various SV profile simulations).

The modeling domains at each site were as follows: three layers (i.e., peat–mineral soil mixture, secondary clay cover layer, and underlying overburden shale) at the reclaimed D3; two layers (i.e., peat–mineral mixture and tailings sand) at the reclaimed SWSS; and 14, 20, and 18 layers of varying texture and bulk density at SV10, SV27, and SV60, respectively. The large number of layers at the SV sites was recommended by Huang et al. (2011c, 2015) to capture the impact of the observed textural layering on the water balance.

Current industry practice tracks reclamation cover water balances based on monitoring and modeling in one dimension. All previously published models were for flat-lying site profiles, and these conditions were retained here. To make the comparison between the models as simple as possible, we also assumed negligible runoff. This is consistent with the original model development for natural sites that feature well-drained profiles on relatively flat ground. SWSS is also located on similar well-drained sand tailings on flat ground. D3 has both a plateau site with minimal runoff, as well as sloping covers with an average 34 mm of runoff each year (Huang et

al. 2015). Although ‘‘real’’ landscapes are often strongly influenced by the redistribution of water in three dimensions, limiting the models to 1D cases (without runoff) simplified comparison of the performance of a range of cover scenarios under changing climatic conditions. Interpreting all profiles as being on flat-lying sites also eliminates differences resulting from runoff. Excess water (i.e., runoff due to a slope) is largely incorporated in the NP values; all NP eventually reports to downgradient surface water bodies, which can be viewed as parallel to water yield.

All models (as adopted from previous studies) utilized a free drainage (i.e., unit vertical gradient) lower boundary because the water table at all sites is deep and consequently the soil water balance is decoupled from the surface water balance (see Dobchuk et al. 2013). The upper boundary is represented by precipitation (rain or snowmelt) or PET obtained from the Penman–Monteith equation. Rainfall interception was estimated using the Braden (1985) equation. PET is distributed between potential evaporation (PE) and potential transpiration (PT) based on a specified leaf area index (LAI) as per Feddes et al. (1974). PT is distributed across a prescribed root depth based on the prescribed root distribution. AE from the surface is some fraction of PE based on a limiting suction at the ground surface. AT is similarly calculated from PT and some limiting suction over the root depth. The root distributions used in the model are from Huang et al. (2011b, 2015). Simunek et al. (2013) provide a detailed description of this modeling approach.

A set of four different climatic inputs were then used with all models to simulate the long-term hydrological performance of the covers. The climate datasets include historical meteorological monitoring data (1961–90) and three future climate projections.

4.2.5 Coupling of AET and LAI

The assumed seasonal variation in LAI over the growing season was represented as shown in Fig. 4-2. Literature-based relationships describing the minimum required AET to support a particular value of LAI were used to constrain the simulations, similar to Huang et al. (2011b). These relationships link LAI, aboveground net primary production (ANPP), and AET. However, the linear relationship between ANPP, LAI, and AET varies depending on the plant species (see Huang et al. 2011b).

Typical values of LAI at the D3, SWSS, SV10, SV27, and SV60 sites are 4.0, 3.0, 1.5, 1.6, and 2.4, respectively (Barr et al. 2012; Huang et al. 2011b, 2015; OKC 2007). To ensure the LAI was appropriate for future climate, simulations were undertaken using a range of LAI values. The AET values from all simulations were then plotted along with the LAI–AET relationship from the literature (see section 4.3.3) to identify the maximum sustainable LAI at each site using the literature-based LAI–ANPP–AET relationships (i.e., the value at which the simulated AET and literature relationship between LAI and AET intersect).

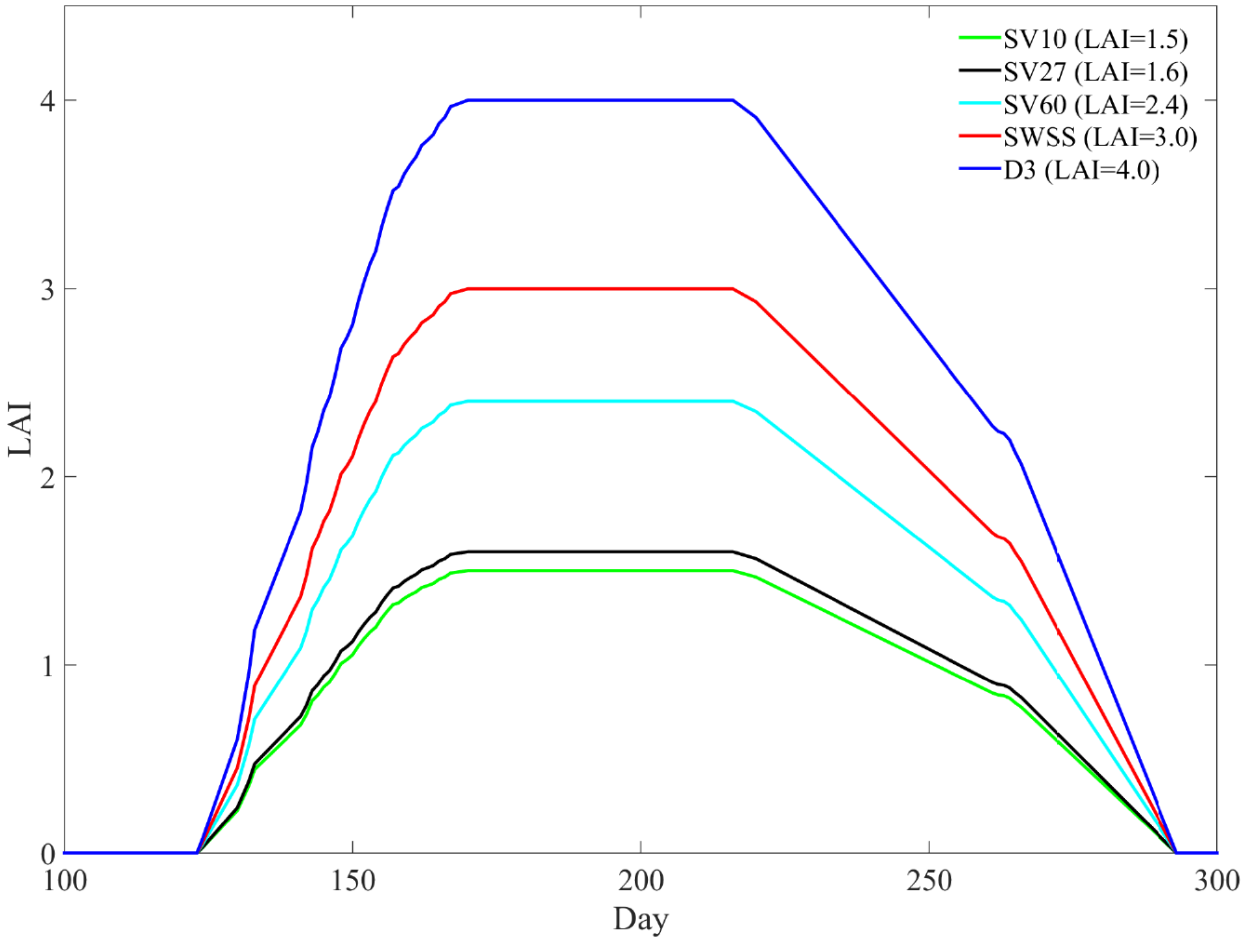

Figure 4-2: Variation in assumed LAI values during the growing season for all five study sites (adapted from Huang et al. 2015).

To compare changes in the water balance components, a single maximum value of LAI, obtained from baseline climatic conditions, was used for each site and climate scenario.

However, potential shifts in LAI were evaluated at each site for each future climate scenario. A more detailed analysis is included in section 4.3.3 (Table 4-2, Figure 4-7).

4.3 Results and discussion

4.3.1 Downscaling performance during the baseline period

The downscaling method (LARS-WG) provided a similar set of climatic observations to the measurements at the ECCC station over the validation period (1991– 2011; Fig. 4-3), and the two were compared. The thick black line dividing the boxplots in Fig. 4-3 represents the median value of the distribution. Each box ranges from the 25^{th} to 75^{th} percentiles of the distribution [e.g., the interquartile range (IQR)]. The whiskers further extend to 1.5 IQR from both ends of the box. The observations used for comparison included mean daily precipitation; mean extreme precipitation; maximum of the extreme precipitation; variance of daily precipitation; proportion of dry days (i.e., with zero precipitation) in each month; and annual, growing season, spring, summer, fall, and winter precipitation.

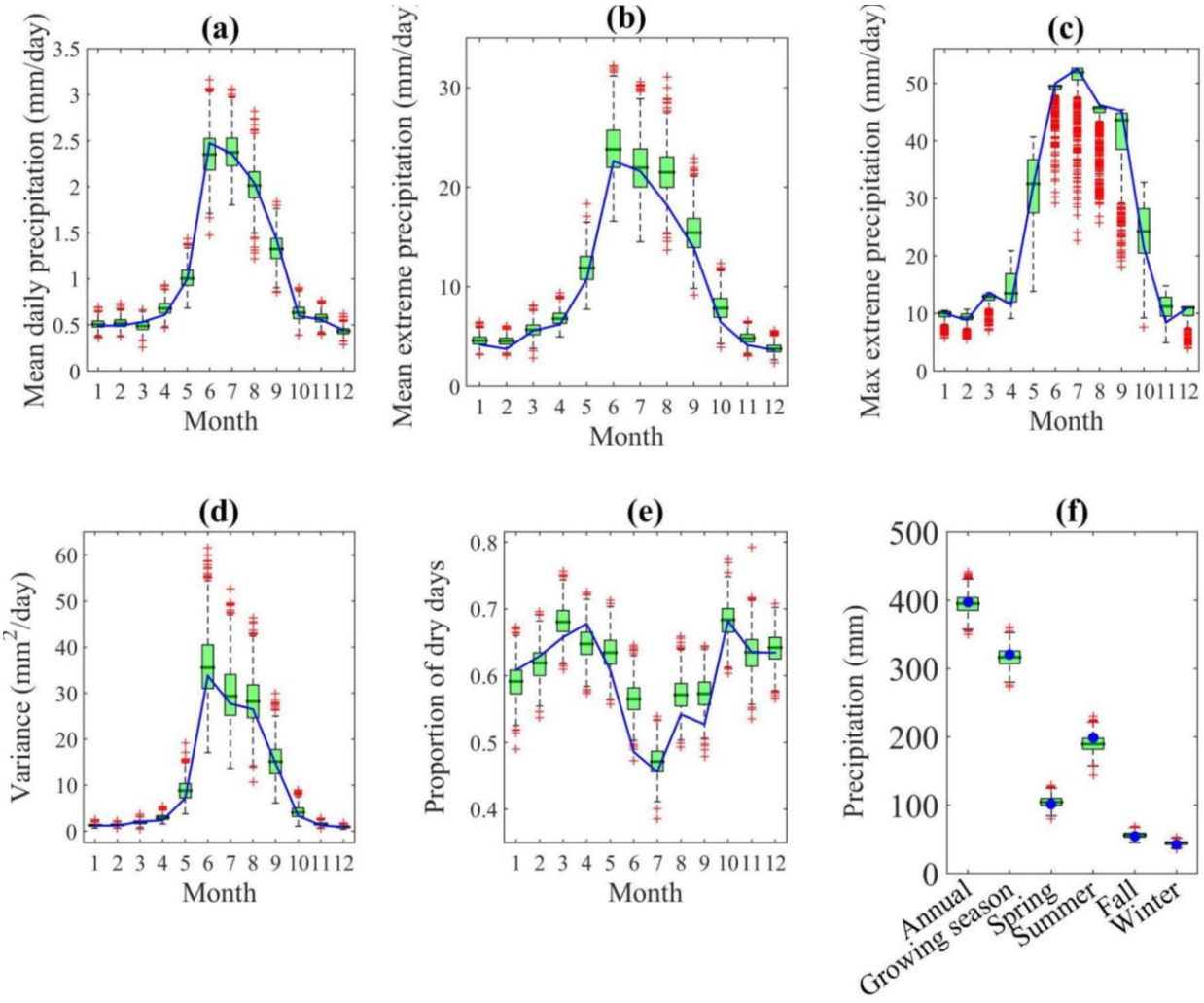

Figure 4-3: Performance of LARS-WG based on the observed monthly (solid lines) and seasonal (circles) properties and 100 realizations of synthetic (box plots) precipitation time series at Fort McMurray Airport station for the validation period (1991-2011). (a) Mean precipitation, (b) mean of extreme precipitation, (c) maximum of the extreme precipitation, (d) variance of daily precipitation, (e) proportion of dry days for each month, and (f) total annual and seasonal precipitation amounts. The box plots depict the range of inter-quartile range (IQR) values (median shown as thick black line) for each scenario with 100 simulations, with whiskers representing values within 1.5 IQR extending from both ends of the boxes and red markers outside the whiskers representing outliers.

The downscaled daily precipitation ranges from 0 (5^{th} percentile) to 16.6 mm (99^{th} percentile) compared to observed values of 0 (5^{th} percentile) and 16.2 mm (99^{th} percentile). The

downscaling method produced minimum daily temperatures ranging from -27.3 (5^{th} percentile) to 14.2 °C (99^{th} percentile), which are comparable to measured values of -30.9 (5^{th} percentile) and 14.6 °C (99^{th} percentile). The downscaled maximum daily temperatures range from -16.4 (5^{th} percentile) to 29.6 °C (99^{th} percentile) compared to observed values of -18.7 (5^{th} percentile) to 30.7 °C (99^{th} percentile). Examination of the downscaled values, calculated by averaging the 100 realizations of precipitation and temperature from LARS-WG, indicates extreme precipitation and temperature values, as well as percentile values of daily mean temperature (Table 4-1) are simulated reasonably well (relative errors <10% in most cases).

4.3.2 Projected changes in temperature, precipitation, and PET

The probability distributions of temperature for the Fort McMurray Airport station during the baseline period (1961-1990) and the three climate change scenarios (CanESM2 with RCP2.6, RCP4.5, and RCP8.5) for 2016-2040, 2041-2070, and 2071-2100 were compared (Figure 4-4). The results indicate summers are projected to be hotter, as extreme maximum temperature (99^{th} percentile) increases in the future (37.2 °C for RCP8.5 during 2071-2100) compared to the baseline case (26.2 °C); winters are also projected to be warmer, with the corresponding extreme minimum temperature (5^{th} percentile) increasing from baseline (-39.4 °C) to 2071-2100 (-24.3 °C) for RCP8.5. All RCPs indicate increasing temperature during the twenty-first century, with RCP8.5 (2071-2100) showing the greatest increase of 138% (median value) and RCP2.6 (2071-2100) and RCP8.5 (2016-2040) showing the least increase of 28% (median value) compared to the baseline period.

Table 4-1: Percentiles of measured and simulated daily precipitation (mm day^{-1}) and temperature (°C) by LARS-WG with relative error (%) at Fort McMurray Airport station during the validation period (1991-2011)

	Percentile					
	5th	***25th***	***50th***	***75th***	***95th***	***99th***
Observed:						
Precipitation	0.0	0.0	0.0	0.6	5.5	16.2
Daily minimum temperature	-30.9	-14.3	-2.4	5.8	12.1	14.6
Daily maximum temperature	-18.7	-3.7	9.3	19.4	26.9	30.7
Daily mean temperature	-24.3	-9.0	3.5	12.6	18.8	21.5
Simulated:						
Precipitation	0.0	0.0	0.0	0.5	5.7	16.6
Daily minimum temperature	-27.3	-14.6	-2.6	5.5	11.5	14.2
Daily maximum temperature	-16.4	-3.7	9.0	19.0	25.9	29.6
Daily mean temperature	-21.5	-9.1	3.2	12.3	18.1	20.5
Relative error (%):						
Precipitation	0.0	0.0	0.0	16.7	3.5	2.5
Daily minimum temperature	11.7	2.1	8.3	5.2	5.0	2.7

Daily maximum temperature	12.3	0.0	3.2	2.1	3.7	3.6
Daily mean temperature	11.5	1.1	8.6	2.4	3.7	4.7

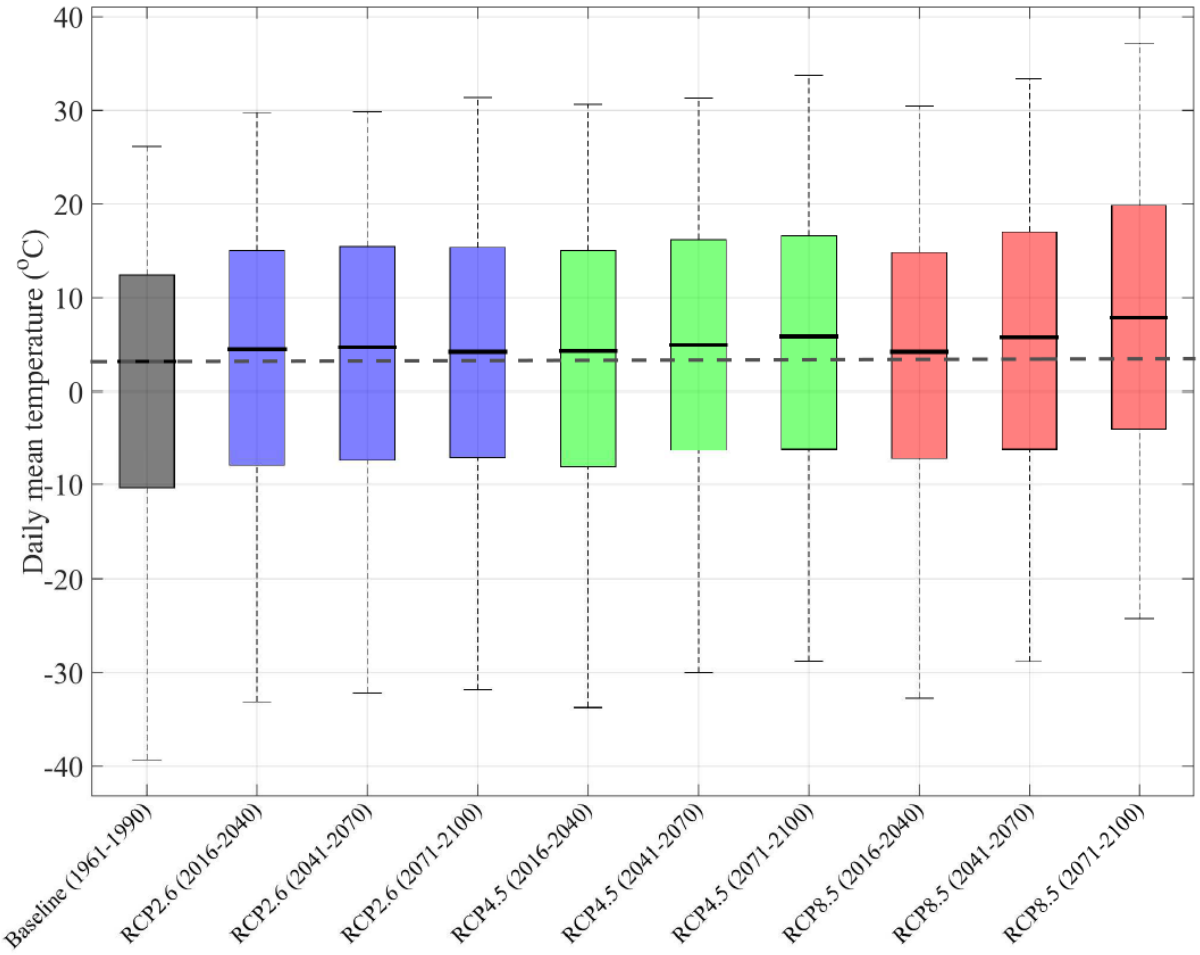

Figure 4-4: Distribution of daily mean temperature based on 100 simulations from LARS-WG during the baseline (1961-1990) and future (2016-2040, 2041-2070, and 2071-2100) periods using three scenarios (RCP2.6, RCP4.5, and RCP8.5) of CanESM2. The horizontal grey dashed line represents baseline daily mean temperature. Description of the box plots is as per Figure 4-3.

The projected growing season (April–October) precipitation [i.e., snow water equivalent (SWE) and rainfall] in each year was also plotted (Fig. 4-5). During the baseline period, the 95% confidence interval (CI) for SWE ranges from 40 to 122 mm and for growing season rainfall ranges from 212 to 483 mm. SWE either shifts upward or downward during the twenty-first century and ranges from 39 to 129mm depending on the RCP and time period. Rainfall shifts upward during the twenty-first century and ranges from 231 to 581mm for all RCPs. RCP8.5 (2071–2100) shows maximum annual increases in median SWE and growing season rainfall of 9.4% and 22.8%, respectively. However, RCP4.5 (2041–70 and 2071–2100) and RCP8.5 (2016–

40) show annual decreases in median SWE, and RCP2.6 (2016–40) shows the minimum increase of 7.4% in growing season median rainfall compared to the baseline period. Some scenarios (e.g., RCP4.5 for 2071–2100) feature a downward shift in median SWE compared to the baseline period but a significant upward shift in growing season median rainfall. These shifts for the same RCP and time period might be due to a warmer winter and extended growing season in the future compared to the baseline period. 100 realizations of precipitation from LARS-WG were used to calculate snowmelt volume using degree-day method (Carrera-Harnandez et al. 2011) when daily mean temperature was below 0 ^{o}C. The calculated snowmelt was added to any precipitation during winter when daily mean temperature exceeded 0 ^{o}C. Thus, as temperature increases in future, winter precipitation was also found to increase in future. So, snowmelt and winter precipitation shown as SWE in Fig. 4-5 increase in future with increasing temperature.

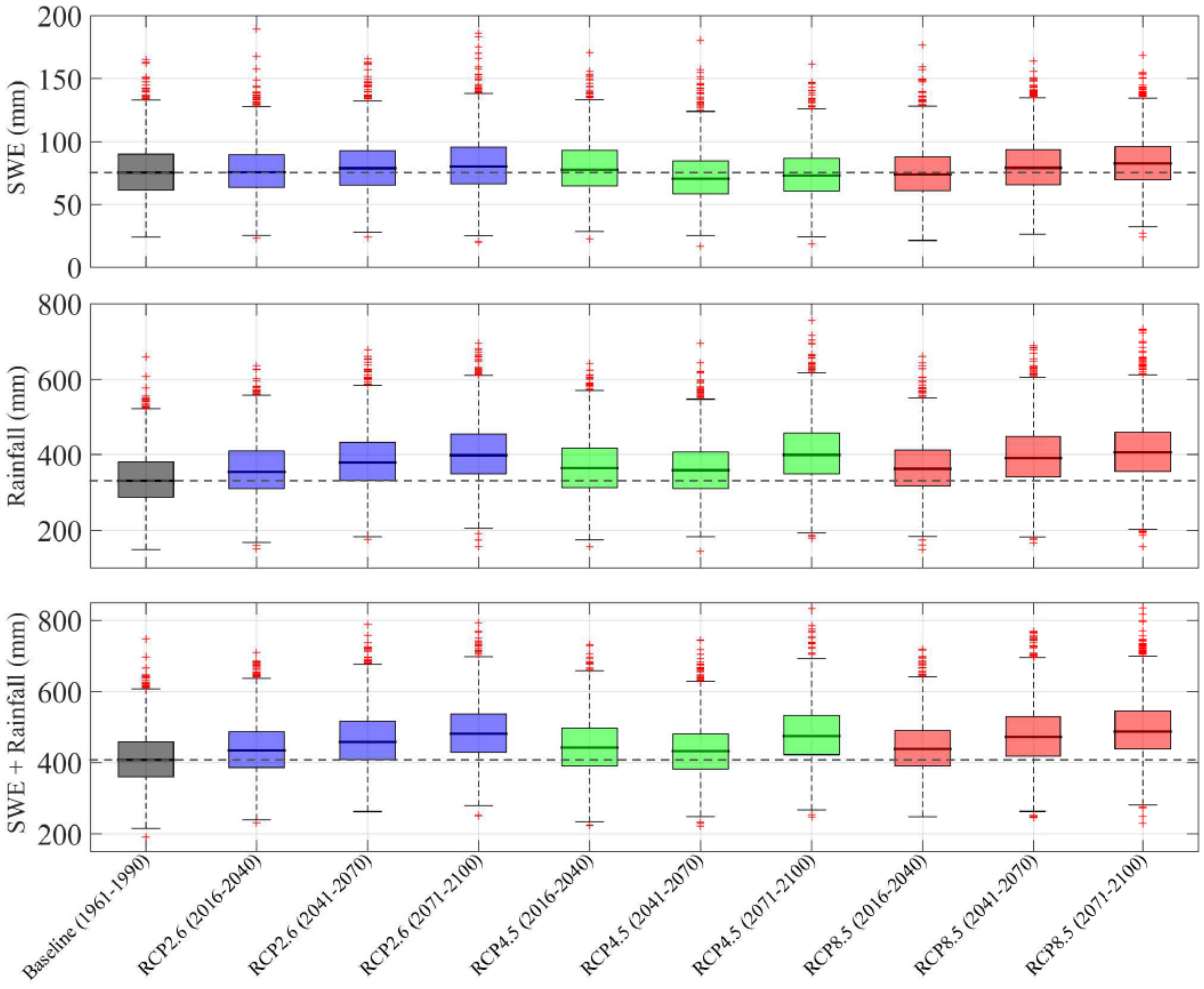

Figure 4-5: Distribution of growing season (April-October) snow water equivalent (SWE), rainfall, and sum of the two based on 100 simulations from LARS-WG during the baseline (1961-1990) and future (2016-2040, 2041-2070, and 2070-2100) periods using three scenarios (RCP2.6, RCP4.5, and RCP8.5) of CanESM2. The horizontal grey dashed lines represent baseline median SWE, Rainfall, and SWE + Rainfall values. Description of the box plots is as per Figure 4-3.

Generally, the future increase in annual precipitation (with the exception of RCP4.5 during 2041–70) is more intensified toward the end of the twenty-first century. Multi-GCM ensembles might be useful to further investigate the irregularity in RCP4.5. A similar behavior (without any exception for RCP4.5) was observed for extreme precipitation intensities in Saskatoon, Saskatchewan, Canada, based on precipitation projections from eight GCMs, three RCPs, and two downscaling methods (Alam and Elshorbagy 2015). Srivastav et al. (2014) also noted increased rainfall intensities during the twenty-first century at four rainfall stations in Canada, while Hassanzadeh et al. (2014) observed increases in short-duration annual maximum precipitation in Saskatoon for all RCPs/emission scenarios. Thompson et al. (2017) showed predicted annual precipitation, based on 13 climate change scenarios, would increase for all scenarios by the end of the twenty-first century at a catchment within the Boreal Plains of northern Alberta. Suncor Energy, Inc. (2007), found annual precipitation would increase in the Fort McMurray region in 2041–69 compared to 1961–90 using Canadian Global Coupled Model, version 2 (CGCM2), and two emission scenarios (A2 and B2); they also used other GCMs, and almost all showed increases in future annual precipitation in the Fort McMurray region.

The distribution of growing season PET is plotted in Fig. 4-6. The 95% CI ranges from 525 to 630mm during the baseline period, increasing to 553–695mm for all RCPs and time periods. Compared to the baseline period, RCP8.5 (2071–2100) had the largest increase (11.9%) in growing season PET, and RCP4.5 (2016–40) had the smallest (3.3%). Growing season PET increases in all future scenarios compared to the baseline period and, generally, intensifies more toward the end of the twenty-first century with the exception of RCP2.6, which is not unexpected as the temperature would peak before the twenty-first century (e.g., 2050) and then decline for RCP2.6 (Rogelj et al. 2012). An increased projection of annual PET rate was also found in other parts of Canada (Kienzle et al. 2012; Schindler and Donahue 2006).

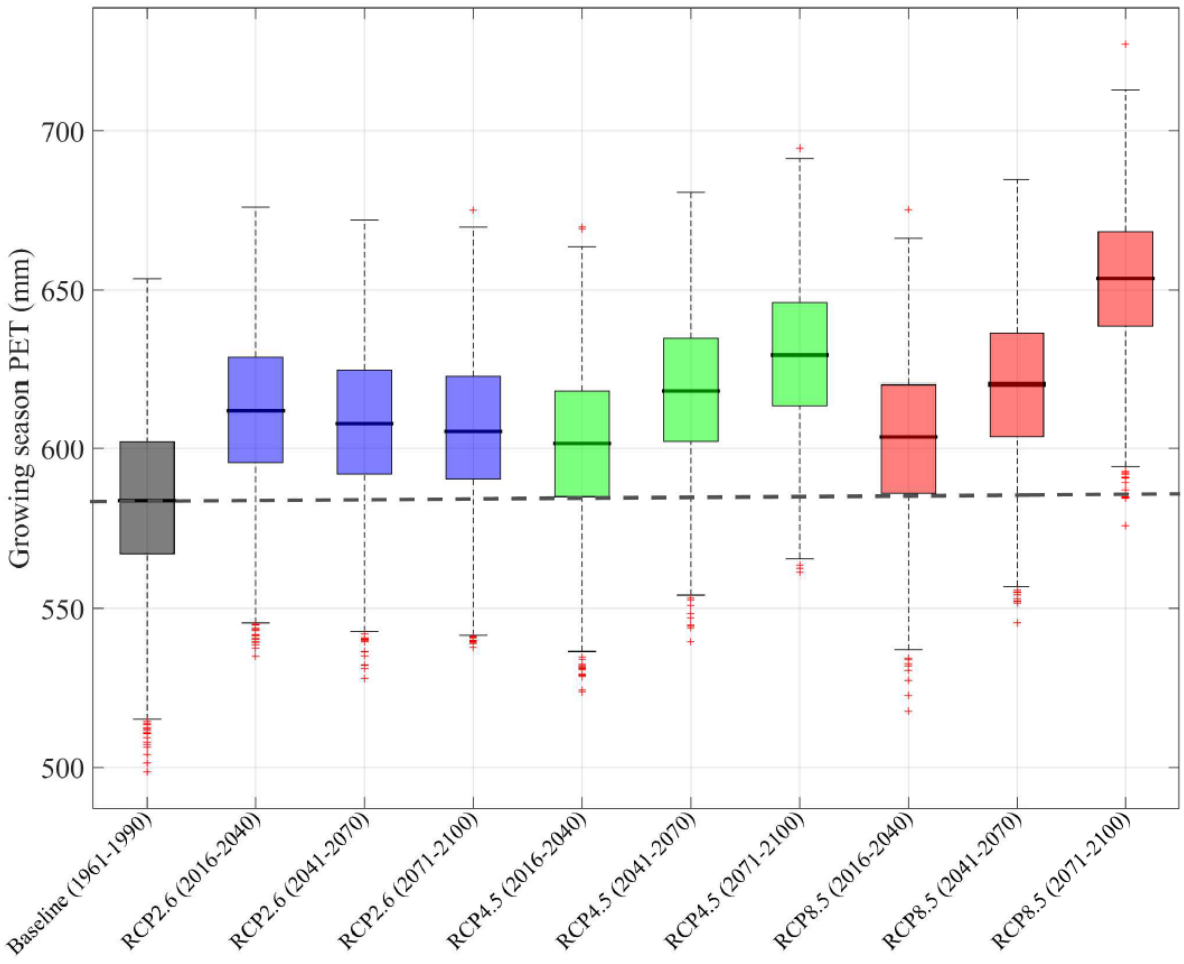

Figure 4-6: Distribution of growing season (April-October) potential evapotranspiration (PET) based on 100 simulations from LARS-WG during the baseline (1961-1990) and future (2016-2040, 2041-2070, and 2070-2100) periods using three scenarios (RCP2.6, RCP4.5, and RCP8.5) of CanESM2. The horizontal grey dashed line represents baseline growing season median PET. Description of the box plots is as per Figure 4-3.

4.3.3 Maximum sustainable LAI and evolution under climate change

The maximum sustainable LAI values (e.g., where simulated AET lines intersect the threshold AET line) at SWSS during the baseline (1961–90) and three future (2016–40, 2041–70, and 2071–2100) periods are 3.8, 4.2, 4.6, and 4.7, respectively. The respective values for SV10 are 1.9, 2.1, 2.2, and 2.3 (see Fig. 4-7). The threshold AET value was obtained from the relationship between the threshold AET and ANPP (Rosenzweig 1968), where the ANPP was calculated based on its linear relationship with LAI using the LAI and ANPP measurements for

all evergreen tree species (Chasmer et al. 2008; Hall et al. 1995; Howard et al. 2004; Lavigne et al. 2005; Vogel and Gower 1998).

The median baseline and future LAI values based on the simulated AET are shown in Table 4-2; values based on RCP8.5 are consistent with those in Fig. 4-7. Notably, the partition of PET into PE and PT is no longer controlled by LAI at LAI values above 2.7 (Huang et al. 2011b), which is also apparent in Fig. 4-7. As a consequence, water balance components for the future climate scenarios presented below are, for consistency, based on the baseline LAI value for each site. However, the estimation of LAI using the simulated AET values results in slightly different LAI values at each site for each time period. The LAI value (Table 4-2, first row) was used for both the baseline and future time periods; using a single LAI value ensured the simulated AET and NP reflect the impact of changes in climate without further coupling to changes in LAI. Overall, all soil profiles could support marginally higher LAI values in the future, with plant physiological changes taking place over time, compared to the baseline period irrespective of the RCP, time period, and soil profile, with more increase evident toward the end of the twenty-first century.

Table 4-2: The simulated median LAI for all scenarios and soil profiles

	Median LAI				
Scenario	***D3***	***SWSS***	***SV10***	***SV27***	***SV60***
Baseline (1961-1990)	3.8	3.8	1.9	2.5	3.6
RCP2.6					
2016-2040	4.1	4.1	2.0	2.7	3.8
2041-2070	4.4	4.5	2.2	2.9	4.1
2071-2100	4.5	4.7	2.2	3.1	4.3
RCP4.5					
2016-2040	4.2	4.2	2.0	2.8	3.9
2041-2070	4.1	4.2	2.1	2.8	3.9
2071-2100	4.6	4.7	2.3	3.1	4.3

RCP8.5					
2016-2040	4.1	4.2	2.1	2.8	3.9
2041-2070	4.5	4.6	2.2	3.0	4.3
2071-2100	4.7	4.7	2.3	3.0	4.3

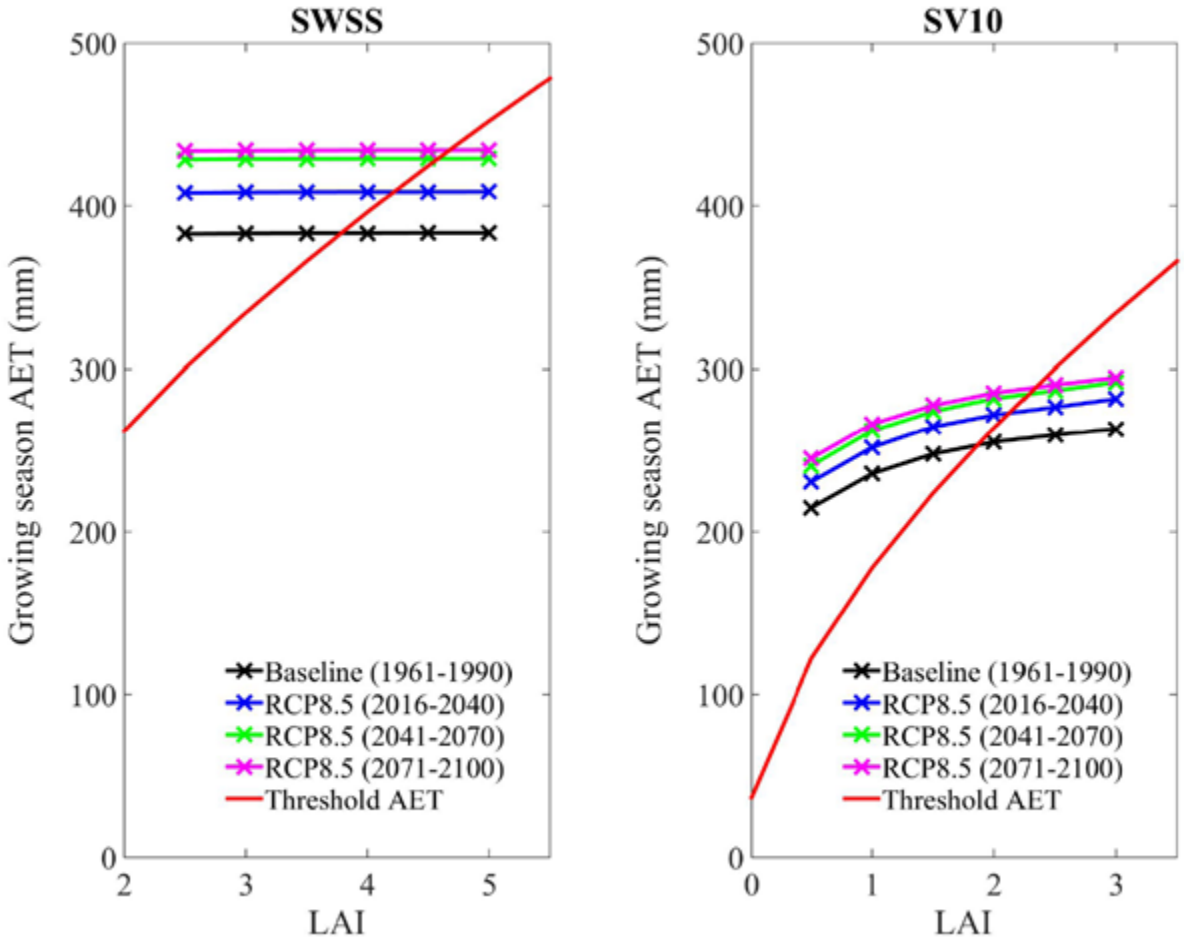

Figure 4-7: Maximum LAI that can be supported by reclamation cover SWSS and natural site SV10 during the baseline (1961-1990) and future (2016-2100 based on RCP8.5) periods.

4.3.4 Baseline water balance components

The long-term (1961–90) growing season (April– October) median water balance components, precipitation (rainfall and SWE), AET (AT and AE), NP (percolation and runoff), and DS, are shown in Table 4-3. The median precipitation at the Fort McMurray Airport station was 407 mm during the growing season with a median rainfall of 331 mm (more than 80% of

total precipitation) and a median SWE of 76 mm (less than 20% of precipitation). The proportion of AET to precipitation at five study sites varies from 62% at SV10 to 94% at SWSS where the proportion of AT to AET varies from 69% to 91%. These two proportions (i.e., AET:precipitation and AT:AET) are higher at the reclamation covers (with higher LAI values) than the natural SV sites. Similarly, the proportion of NP to precipitation varies from 6% at SWSS to 38% at SV10, reflecting the higher NP at the natural SV sites.

4.3.5 Baseline and future water balance

The reclamation covers have higher AET values than natural sites because of higher available water storage. Among all sites, SWSS has the highest AET values (i.e., 383 mm), while SV10 had the lowest (i.e., 253 mm) during the baseline period (Table 4-4). Of the natural sites, AET values for SV60 are the highest (i.e., 370 mm) and closer to values for the reclamation covers than other two natural sites (SV10 and SV27), while AET values for SV10 and SV27 (253 and 302 mm, respectively) are closer to each other. The reclamation cover SWSS is more similar to SV60 than other SV sites with respect to the AET values (383 and 370 mm, respectively).

This pattern of behavior is consistent with the concept of available water-holding capacity (AWHC; volume of water stored between field capacity and wilting point over the depth of the cover, or rooting depth in the case of natural profiles). AWHC is used in the industry to compare natural and reclaimed profiles as part of reclamation cover design. Likewise, AWHC is not used here as a modeling parameter but rather as an index to compare changes in the performance of various sites as a result of climate change and to allow the covers to be grouped based on similar responses to climate change.

AWHC values (for assumed/known cover depth of 100 cm) for SWSS and SV60 are 267 and 146 mm, but for SV10 and SV27 are 74 and 121 mm, respectively (Huang et al. 2011b; Zettl et al. 2011). These values are consistent with the estimated sustainable LAI values for these sites (Table 4-2), with LAI values for SV10 and SV27 being similar and lower (1.9–2.5) and for SWSS and SV60 being similar and much higher (3.6–3.8). The reclamation cover (D3) has an AWHC value of 377 mm and an LAI value of 3.8.

Table 4-3: Median values of the water balance components during baseline period (1961-1990) at five study sites

Study site	Rainfall (mm)	SWE (mm)	AT (mm)	AE (mm)	AET (AT + AE, mm)	NP (Percolation + Runoff, mm)	DS (mm)
D3	331	76	346	36	382	32	-3.23
SWSS	331	76	347	36	383	25	-1.98
SV10	331	76	175	78	253	156	-1.55
SV27	331	76	238	64	302	107	-2.28
SV60	331	76	329	40	369	39	-3.82

The simulated LAI, AET, and NP for the five study sites during the baseline period were compared to those for a range of boreal forest sites determined by Barr et al. (2012; Table 4-4 herein) to place the simulated water balances for the study sites within the context of sites in the same region. Despite the differences in site vegetation and soil texture, some clear similarities between the boreal forest sites and the simulations are evident.

Of the five sites, D3 and SWSS (reclamation covers) and SV60 (d2 ecosite) most resemble the Old Aspen site from Barr et al. (2012) with respect to ET, NP, and LAI values, while SV10 and SV27 (a1 ecosites) resemble the Old Jack Pine and Old Black Spruce sites.

The reclamation covers have the lowest NP values during the baseline period compared to the SV sites (Table 4-4), consistent with their higher AET values and consequently less water released to NP (Straker et al. 2014). The SV sites produce greater NP because they are unable to store and utilize the available water for growing season AET. Among the natural sites, SV60 has the lowest NP during the baseline period, while SV10 has the highest. NP rates for reclamation covers D3 and SWSS are closer to each other than to the natural sites. Of the natural sites, the NP rates for SV60 are closer to the rates of the reclamation covers than the other two natural sites (SV10 and SV27), while the NP rates of SV10 and SV27 are closer to each other.

Table 4-4: Mean*/median (standard deviation) of the annual*/growing season precipitation (mm), evapotranspiration (mm), NP (mm), and LAI at all study sites compared to other work conducted on the southern boreal forests of Western Canada

Site (Ecosite)	Period	Mean*/median Prec. (SD)	Mean*/median ET (SD)	Mean*/median NP (SD)	LAI
D3	1961-1990	407 (73)	382 (47)	32 (18)	3.8
SWSS	1961-1990	407 (73)	383 (46)	25 (21)	3.8
SV60 (d2)	1961-1990	407 (73)	370 (51)	39 (34)	3.6
Old Aspen*	1999-2009	458 (148)	427 (74)	30 (35)	3.9-5.2
SV10 (a1)	1961-1990	407 (73)	253 (31)	156 (54)	1.9
SV27 (a1)	1961-1990	407 (73)	302 (41)	107 (45)	2.5
Old Black Spruce*	1999-2009	491 (115)	382 (26)	108 (85)	3.0
Old Jack Pine*	2002-2009	527 (145)	306 (21)	187 (55)	2.0

*Barr et al. (2012)

Median growing season precipitation and AET and NP values for all sites and simulation time periods are summarized in Table 4-5, respectively. The growing season median precipitation, AET, and NP increase (shown in parentheses) for all RCPs and future time periods compared to the baseline period; these changes are more pronounced toward the end of the twenty-first century. Considering all RCPs, the maximum increase in precipitation and AET for all sites is approximately 20%–25% and 12%–14%, respectively. All study sites show greater increases in precipitation and AET toward the end of the twenty-first century regardless of RCP.

However, because of the relatively low NP rates from sites with the highest water storage (i.e., reclamation covers), their relative changes in NP rates are actually greater (195% for SWSS, 149% for SV60, 138% for D3, 62% for SV27, and 46% for SV10 for 2071–2100) than most of the SV sites, taking all three RCPs into account.

The simulated AET and NP values for the five study sites in the 2041–70 climate period for the three RCPs are compared to the baseline period in Figs. 4-8 and 4-9, respectively. The variability in AET and NP during the future periods is similar to the baseline period, as illustrated by the parallel probability distributions. The magnitude of the growing season AET and NP and corresponding shifts in future AET and NP compared to the baseline period are dependent on the selection of RCP and future time period at each of the study sites. The multiple (100) realizations of LARS-WG, as input to the soil–vegetation–atmosphere transfer (SVAT) model, encompass the uncertainty in the water balance components because of natural climate variability. Overall, the study sites are expected to have increased AET and NP rates (see Table 4-5 and Figs. 4-8, 4-9) regardless of which RCP and time period are considered from the Canadian GCM (CanESM2).

Table 4-5: Growing season median precipitation, AET, NP, and DS in mm for all scenarios and soil profiles. Percentage increase/decrease in future median precipitation, AET, NP, and DS compared to the respective baseline median precipitation, AET, NP, and DS is shown in parentheses.

	Precipitation in mm (% change)	**Actual evapotranspiration (AET) in mm (% change)**					**Net percolation (NP) in mm (% change)**					**Change in soil water storage (DS) in mm (% change)**				
Scenario	***Fort McMurray Airport station***	***D3***	***SWSS***	***SV10***	***SV27***	***SV60***	***D3***	***SWSS***	***SV10***	***SV27***	***SV60***	***D3***	***SWSS***	***SV10***	***SV27***	***SV60***
Baseline (1961-1990)	407	382	383	253	302	369	32	25	156	107	39	-3.23	-1.98	-1.55	-2.28	-3.82
RCP2.6																
2016-2040	438 (8%)	400 (5%)	403 (5%)	263 (4%)	314 (4%)	384 (4%)	41 (28%)	31 (25%)	173(11%)	122 (14%)	54 (38%)	-3.13 (3%)	-2.89 (46%)	-2.25 (46%)	-3.27 (44%)	-5.15 (35%)
2041-2070	466 (14%)	418 (9%)	422 (10%)	278 (10%)	330 (9%)	404 (9%)	48 (50%)	37 (51%)	187 (20%)	134 (26%)	63 (60%)	-2.49 (23%)	-2.99 (51%)	-2.50 (62%)	-3.50 (54%)	-5.59 (46%)
2071-2100	489 (20%)	427 (12%)	434 (13%)	282 (12%)	339 (12%)	415 (12%)	57 (78%)	49 (98%)	204 (31%)	148 (39%)	73 (87%)	-1.04 (68%)	-2.13 (8%)	-2.27 (47%)	-3.14 (38%)	-5.03 (32%)
RCP4.5																
2016-2040	450 (11%)	405 (6%)	408 (6%)	267 (6%)	320 (6%)	391 (6%)	44 (38%)	33 (34%)	178 (14%)	126 (18%)	57 (45%)	-2.85 (12%)	-2.85 (44%)	-2.20 (42%)	-3.14 (38%)	-5.31 (39%)
2041-2070	439 (8%)	404 (6%)	406 (6%)	270 (7%)	321 (6%)	390 (5%)	37 (16%)	27 (11%)	166 (6%)	116 (9%)	47 (21%)	-3.37 (4%)	-2.71 (37%)	-2.11 (37%)	-3.04 (33%)	-4.71 (23%)
2071-2100	487 (20%)	430 (13%)	434 (13%)	284 (12%)	340 (13%)	416 (13%)	54 (69%)	46 (88%)	200 (28%)	145 (36%)	70 (80%)	-1.86 (42%)	-2.72 (37%)	-2.38 (54%)	-3.33 (46%)	-5.23 (37%)
RCP8.5																
2016-2040	443 (9%)	405 (6%)	409 (7%)	269 (7%)	321 (7%)	392 (6%)	39 (22%)	28 (15%)	171 (10%)	120 (13%)	49 (24%)	-3.12 (3%)	-2.74 (38%)	-2.12 (37%)	-3.07 (35%)	-5.12 (34%)
2041-2070	479 (18%)	423 (11%)	429 (12%)	279 (11%)	334 (11%)	411 (11%)	53 (66%)	46 (87%)	198 (27%)	144 (35%)	70 (78%)	-1.77 (45%)	-2.91 (47%)	-2.56 (65%)	-3.58 (57%)	-5.76 (51%)
2071-2100	510 (25%)	434 (14%)	434 (13%)	283 (12%)	337 (12%)	416 (13%)	76 (138%)	73 (195%)	228 (46%)	173 (62%)	97 (149%)	-1.38 (57%)	-3.60 (81%)	-3.00 (94%)	-4.17 (83%)	-6.37 (67%)

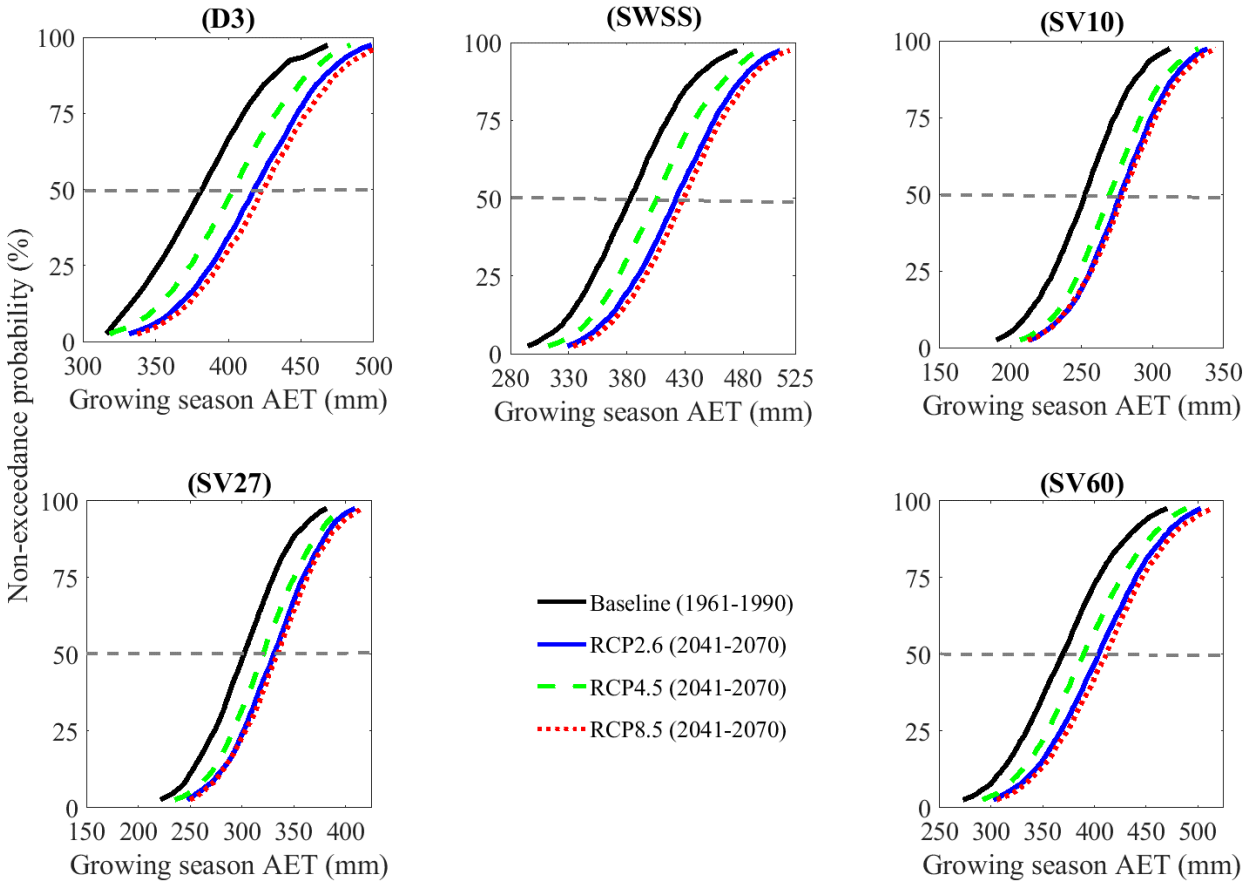

Figure 4-8: Probability distribution of growing season (April-October) actual evapotranspiration (AET) in each soil profile based on 100 simulations from HYDRUS-1D during the baseline (1961-1990) and future (2041-2070) periods using three scenarios (RCP2.6, RCP4.5, and RCP8.5) of CanESM2. Future time period 2041-2070 is only shown as an example. The horizontal grey dashed line represents the growing season median AET for all cases.

It is clear from Figs. 4-8 and 4-9 that the probability of exceeding the baseline median AET and NP at each of the five study sites will increase from 50% to approximately 80% for RCP8.5 in 2041–70. This higher frequency of elevated AET is expected to be reflected in more rapid vegetation growth and possibly a shift in dominant species at each site. The increase in NP could have both a positive and negative impact. It would increase the water yield from these landforms, which might support receiving wetlands. However, it could also lead to more rapid flushing and release of chemical constituents of concern from the underlying mine waste.

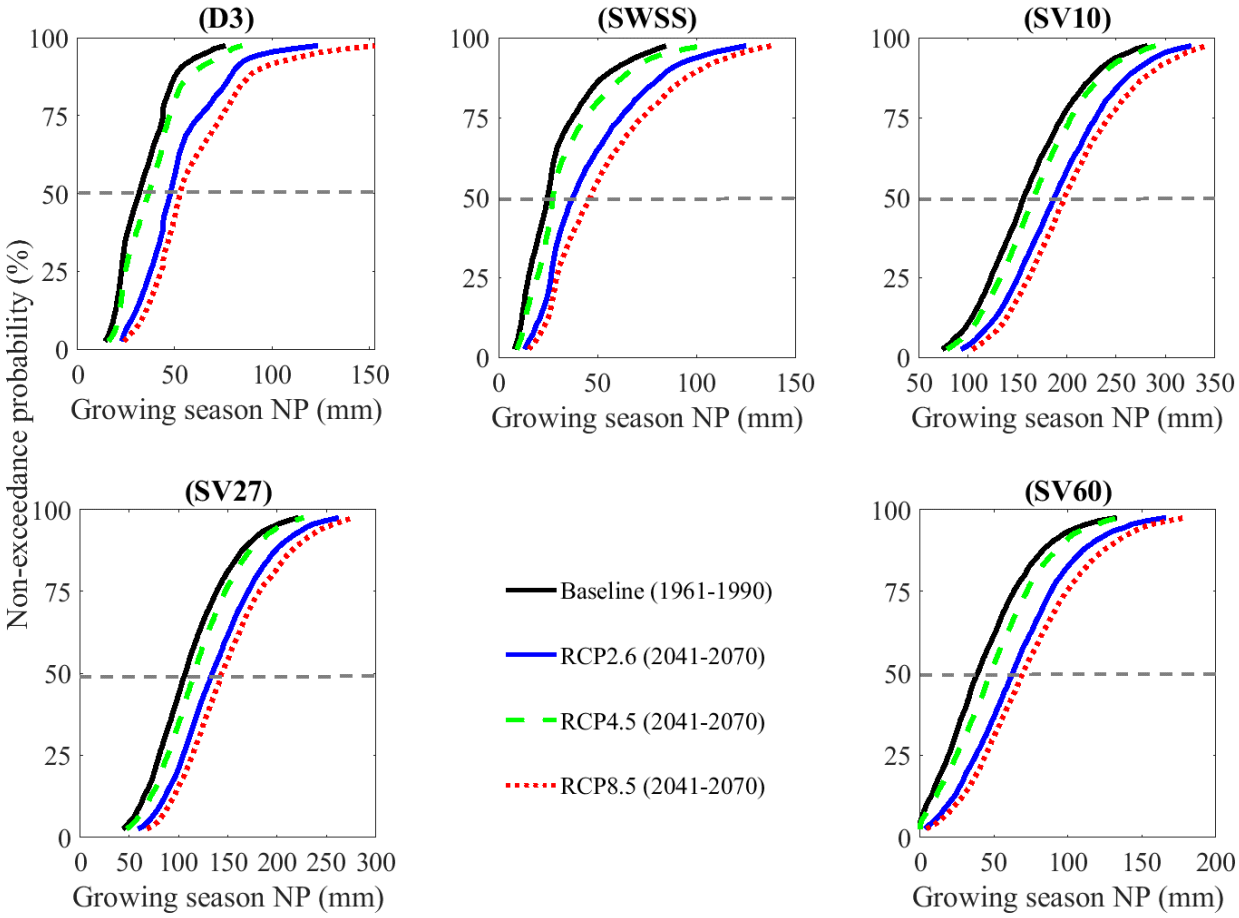

Figure 4-9: Probability distribution of growing season (April-October) NP based on 100 simulations from HYDRUS-1D during the baseline (1961-1990) and future (2041-2070) periods using three scenarios (RCP2.6, RCP4.5, and RCP8.5) of CanESM2. Future time period 2041-2070 is only shown as an example. The horizontal grey dashed line represents the growing season median A for all cases.

4.3.6 Seasonal water balance

The long-term median seasonal cycle of water balance components (i.e., precipitation, AET, and NP) over the growing season is shown in Fig. 4-10. The median monthly precipitation at the Fort McMurray Airport station peaks in April (as snowmelt starts at the beginning of the spring season) and also in July (coinciding with the summer rainfall). This pattern is the same for the future period (2041–70) as it was for the baseline. Although all RCPs show higher precipitation in April than the baseline case, RCP8.5 shows lower precipitation in July than the baseline case.

This could be due to increased precipitation in the winter and decreased precipitation in the summer for RCP8.5. May, September, and October seem to be the months with lower precipitation compared to other months. In general, the long-term median monthly AET is higher in May, June, and July than other months for both the baseline, as well as the RCPs, consistent with the seasonal variation of LAI (shown in Fig. 4-2). Although Fig. 4-8 shows increased AET rates for all RCPs compared to the baseline case, the monthly AET might be lower than the baseline case for some RCPs as shown in Fig. 4-10. In general, the long-term median monthly NP is the highest in April for both the baseline and the RCPs. According to the probability distribution of NP in Fig. 4-9, all RCPs show increased NP in the future compared to the baseline NP rates; however, the median monthly NP might be lower in the future than the baseline NP in some months.

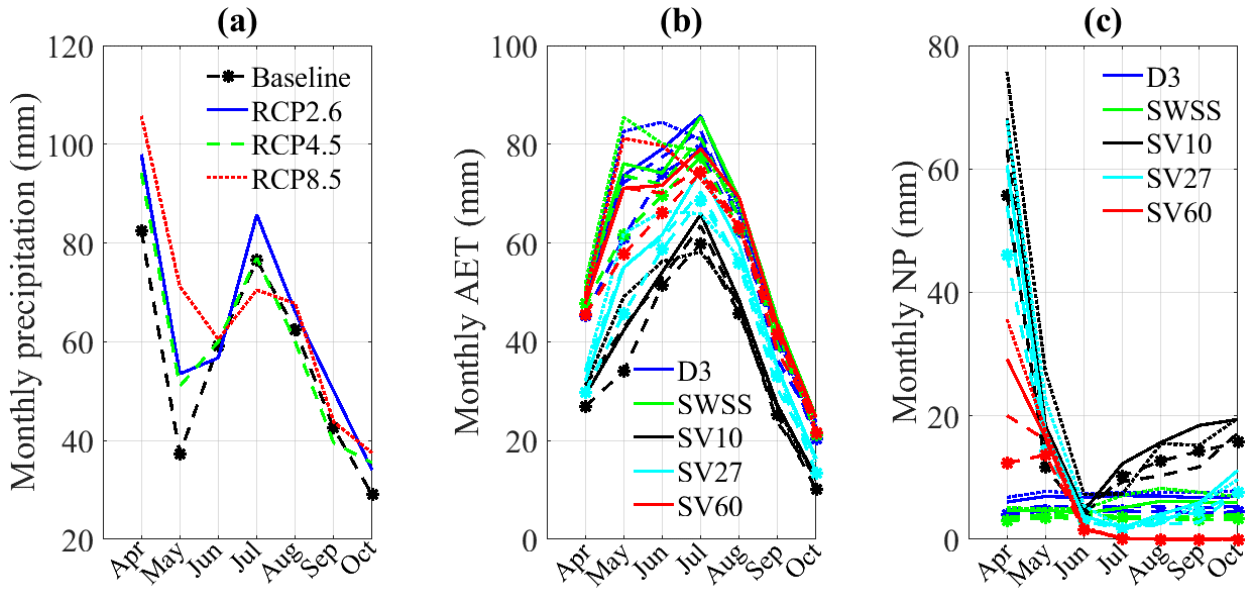

Figure 4-10: Seasonal variation in the water balance components (a) monthly precipitation at the Fort McMurray Airport station, (b) monthly actual evapotranspiration at five study sites, and (c) monthly net percolation at five study sites. All the above plots show water balance components for baseline (1961-1990) as well as three RCPs (during 2041-2070) at the five study sites. The line styles for the baseline and three RCPs in (b) and (c) follow the corresponding line styles in (a).

4.3.7 Uncertainty in the simulated water balance components

The simulated 100 realizations of water balance components (AET and NP) were used to demonstrate uncertainty in the simulated median AET and NP due to natural variability. This is represented by the coefficient of variation (CV) values for the corresponding baseline period and future time periods and RCPs for each of the study sites (Table 4-6). The calculated CV values show that variability in the simulated AET and NP due to natural climate variability may not change significantly in the future compared to the baseline case, where the uncertainty due to natural variability is not attributable to climate change (Alam and Elshorbagy 2015). Moreover, uncertainties due to GCMs are most important in future projections of climate variables (Najafi et al. 2011). Therefore, more focus was given here to uncertainty in future water balance components due to GCMs and associated RCPs and future time periods.

Table 4-6: Coefficient of variation (CV) of the simulated 100 realizations of growing season median AET and NP for the baseline period as well as future periods and RCPs at each study site.

	CV (%) of the simulated AET					**CV (%) of the simulated NP**				
Scenario	***D3***	***SWSS***	***SV10***	***SV27***	***SV60***	***D3***	***SWSS***	***SV10***	***SV27***	***SV60***
Baseline (1961-1990)	12.3	11.5	11.9	13.2	13.3	50.4	64.3	32.2	38.5	73.4
RCP2.6										
2016-2040	10.3	11.1	11.9	12.9	12.7	38.9	60.1	30.1	35.6	60.9
2041-2070	10.0	11.0	11.2	12.3	12.7	40.9	59.6	29.8	34.8	58.6
2071-2100	9.7	10.4	11.0	12.0	12.3	47.0	56.2	28.9	33.8	53.4
RCP4.5										
2016-2040	10.5	11.0	12.1	13.1	12.9	42.2	60.2	30.9	36.2	66.1
2041-2070	10.3	11.3	11.4	12.8	12.9	40.4	63.4	30.6	36.2	62.1
2071-2100	10.2	10.1	11.6	12.7	12.8	41.5	56.5	28.9	33.7	54.1
RCP8.5										
2016-2040	10.4	11.1	11.6	12.7	12.9	37.6	61.2	30.5	36.1	65.1
2041-2070	10.1	10.9	11.7	12.6	12.7	43.8	58.3	28.6	33.7	55.6
2071-2100	10.1	11.1	11.4	12.8	13.1	41.7	47.4	26.1	29.2	42.7

4.3.8 Changes in the soil water storage

Importantly, net changes in annual water storage will be small relative to other aspects of the water balance over a long climate cycle, for which, ‘‘on average,’’ the change in water storage tends to zero. However, when the climate is more variable and nonstationary, determining if changes in water storage dynamics are reflected in the various climate change scenarios is of value. Mean changes in soil water storage of the five study sites were calculated over a 30-yr climate cycle for the baseline and future time periods based on three RCPs and three future time periods (Table 4-5). DS would decrease in the future for the D3 reclamation cover but increase for the remaining soil covers (i.e., SWSS, SV10, SV27, and SV60). These results are not unexpected as, different from D3, the SWSS reclamation cover and three SV sites have low storage capabilities. Overall, the values of DS (typically 1–6 mm) are relatively small compared to other water balance components AET (on the order of hundreds of millimeters) and NP (on the order of from tens to hundreds of millimeters). Therefore, DS dynamics were not used here to compare the performance of reclamation covers with natural soil profiles.

4.3.9 Water balance components as proportion of precipitation and PET

The proportions of AET and NP expressed as a percentage of precipitation (PPT) and PET are shown in Fig. 4-11 for the baseline and future periods. NP proportions for the sites with lower LAI values (e.g., SV10) are higher, and vice versa; these trends are reversed for the AET proportions. Little to no increase in future AET/PPT or AET/PET ratios compared to the baseline is evident, suggesting a linear response of AET to increases in either PPT or PET. In contrast, the increase in NP/PPT and NP/PET becomes larger particularly toward the end of the twenty-first century and for the higher-water-storage sites (e.g., reclamation covers).

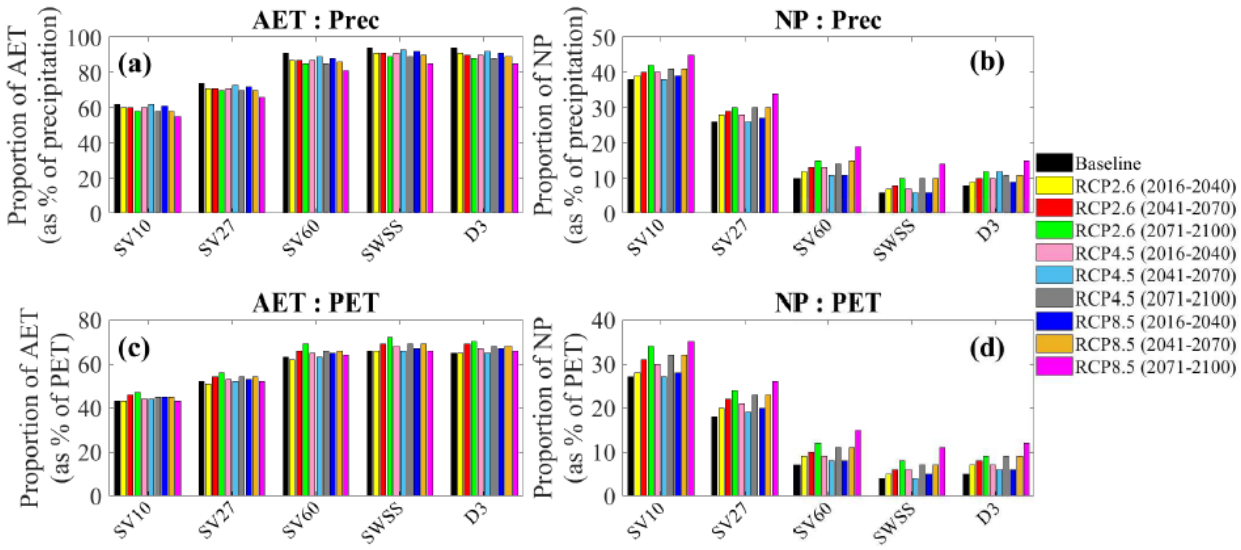

Figure 4-11: The proportions of growing season (a) AET to precipitation; (b) NP to precipitation; (c) AET to PET; and (d) NP to PET during the baseline (1961-1990) and future (2016-2040, 2041-2070, and 2071-2100) periods based on RCP2.6, RCP4.5, and RCP8.5 of CanESM2 for all five study sites.

The increase in future AET relative to the baseline is approximately the same as the increase in PET (results not shown) and, obviously, not the same as the increase in precipitation. The future precipitation increases faster than AET (shown in the probability distributions in Fig. 4-12 for precipitation and AET at all study sites). Consequently, the increase in future precipitation from the baseline results in increasing NP rates during the twenty-first century.

The NP rates for a cover system can be classified as ‘‘very low,’’ ‘‘low,’’ and ‘‘moderate’’ when the proportion of NP for a given year is between 1% and 5%, between 5% and 15%, and between 10% and 40% of precipitation for a given year, respectively (Ayres and O’Kane 2013). Based on this classification, the D3, SWSS, and SV60 sites have low rates, while SV10 and SV27 have moderate NP rates during the baseline period. With climate change, D3, SWSS, and SV60 might begin to shift from low to slightly moderate NP rates, while SV10 and SV27 remain in the moderate range (see Fig. 4-11b).

Although NP increases at all sites, the relative shifts in NP are greater at sites with more water storage. The higher rates of NP will lead to more water moving through the reclamation cover and into the underlying waste, ultimately passing through this waste to be released to

downgradient surface water and groundwater. An increase in NP with time would result in more rapid flushing of mobile contaminants from the waste but at the cost of great chemical loading to the downgradient receptors. Increasing NP may also change the water content within the underlying waste, leading to changes in rates of weathering (e.g., oxidation).

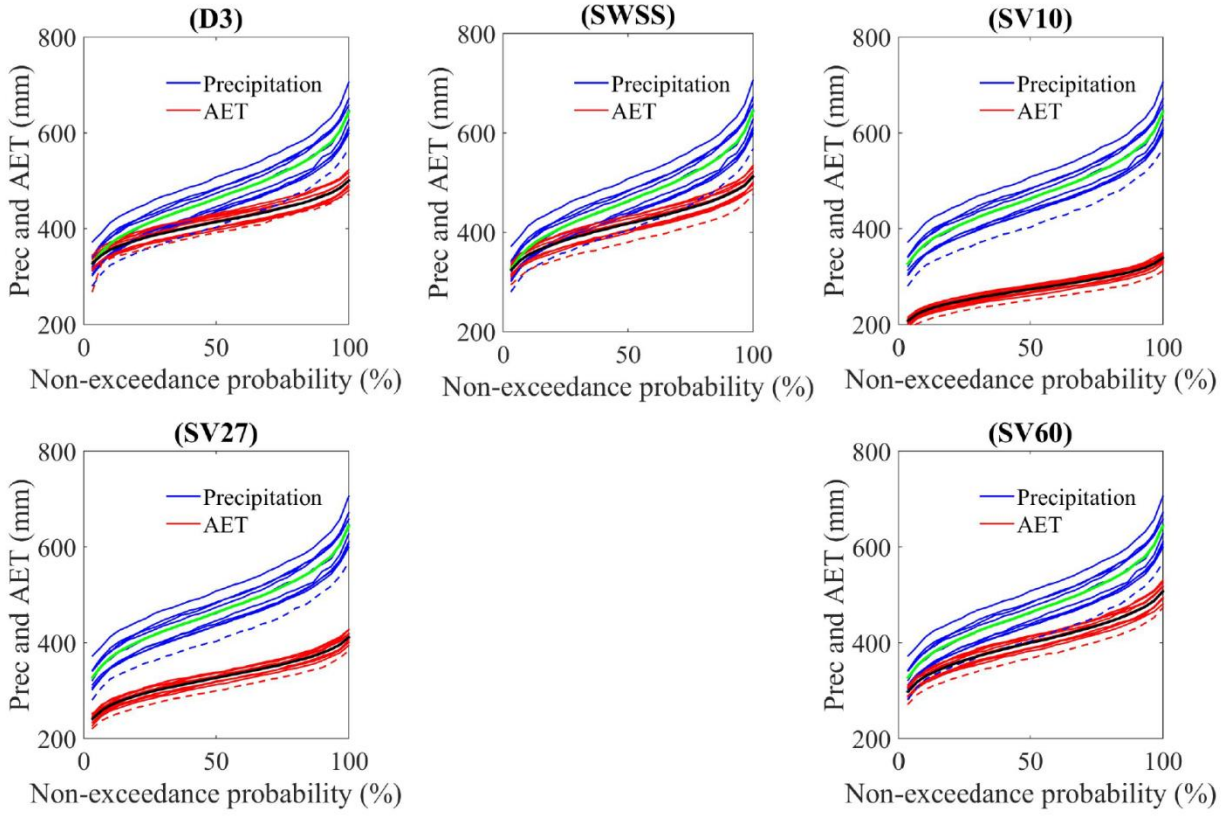

Figure 4-12: Rate of change in the probability distributions of growing season precipitation and AET during the baseline (dashed lines) and future periods (solid lines) based on three RCPs at each of the study sites. Green and black lines show the average probability distributions of all the future time periods and RCPs for precipitation and AET, respectively, reflecting the relative slopes at which future precipitation and AET are expected to change.

4.4 Conclusion

This study utilized future climate change projections based on the most recent GCM outputs as input for physically based SVAT models of water balance for reclamation soil covers and natural soil profiles near Fort McMurray, Alberta, Canada. The downscaled temperature

indicates increases for all RCPs during the twenty-first century, with a maximum increase of 138% and minimum increase of 28% (median values) compared to the baseline period. Overall, the growing season precipitation and PET are projected to increase irrespective of RCP and time period during the twenty-first century according to the Canadian GCM (CanESM2). Maximum increases in projected growing season precipitation and PET for RCP8.5 in 2071–2100 are 25.5% and 11.9%, respectively.

During the historical baseline period (1961–90), reclamation covers show higher AET and lower NP than natural sites. Overall, the important water balance components (i.e., AET and NP) of the reclamation covers and natural sites are expected to increase throughout the twenty-first century, regardless of the RCP, time period, or soil profile considered. However, the magnitude of the shifts in projected AET and NP are subject to the selection of RCP, time period, and study site. Greater increases in AET and NP are expected toward the end of the twenty-first century in response to increases in growing season PET and precipitation. When compared to shifts in future AET, changes in NP between baseline and future values for the sites with higher water storage (i.e., the two reclamation covers) are more dramatic. As a consequence, increases in NP for these sites will likely have a greater impact on adjacent water bodies because of proportionally greater water release and the concomitant release of constituents flushed from the mine waste (e.g., overburden or tailings).

The implications for higher future rates of NP are wide ranging. Increased rates of NP may lead to increases in base flow in surface water courses that feed wetlands or lakes. They also might lead to more rapid flushing of mobile chemical constituents present within the mine waste, with a resultant increase in chemical loading to these surface water receptors in the short term. Increases in NP could also result in elevated degrees of saturation, a rise in water pressure, and a concomitant rising water table within the mine waste. This may reduce weathering processes tied to oxygen availability but also result in an increased risk of geotechnical instability of the waste dumps and containment structures. Future studies should be undertaken in which this modeling approach is applied to an entire site-specific oil sands mine waste landform to evaluate some of these potential changes in landform performance.

The fine-textured reclamation covers placed over fine-textured mine waste (e.g., South Bison Hill) are designed to maximize the storage of plant-available water and consequently have relatively low rates of NP. However, the fine-textured mine waste also contains large concentrations of readily soluble salts (e.g., Appels et al. 2017) that will be released to adjacent surface waters because of flushing by water ingress into, and subsequently out of, the dump. The salts are introduced to the covers by evaporation from underlying shallow shale in which the pyrite is oxidized and generate sulphate (Appels et al. 2017). The SWSS reclamation cover is designed in a similar manner with fine-textured cover soils placed over relatively free-draining sand tailings to maximize plant-available water for re-vegetation efforts. However, in this case, large increases in NP might have a positive influence on mine closure by flushing mobile salts from the sand tailings more rapidly, thereby reducing long-term loading from the reclaimed site to surface waters (Booterbaugh et al. 2015).

Multiple (100) realizations of LARS-WG were integrated into HYDRUS-1D to encompass the uncertainty in the water balance components due to natural climate variability, with the estimation of uncertainty due to the use of three RCPs and three future time periods. Overall, the uncertainty ranges (95th minus 5th percentile value) of both AET and NP increase in the future relative to the baseline but vary depending on the RCP and time period. The increases in future growing season median AET and NP relative to baseline values are also subject to uncertainty because of the selection of RCP and time period. Further research is in progress to include multiple GCMs with the RCPs to incorporate uncertainties in the simulations of water balance components at the reclamation covers and natural sites with spatial and temporal variability in vegetation, soil properties, and topographical settings.

4.5 Acknowledgements

We acknowledge funding provided by Syncrude Canada, Ltd., the Natural Sciences and Engineering Research Council (NSERC) of Canada (File 428588-11), and the Department of Civil, Geological and Environmental Engineering, University of Saskatchewan, Canada. The first author also acknowledges financial support from the Government of Saskatchewan in the form of an SK Innovation and Opportunity Scholarship. The first author thanks Dr. Willemijn

Appels for her assistance in creating a batch controller for HYDRUS-1D using MATLAB. We thank Stephanie Villeneuve for designing Fig. 4-1.

References

Alam, M. S., and A. Elshorbagy, 2015: Quantification of the climate change-induced variations in intensity-duration-frequency curves in the Canadian prairies. J. Hydrol., 527, 990–1005, https://doi.org/10.1016/j.jhydrol.2015.05.059.

Allen, R. G., L. S. Pereira, D. Raes, and M. Smith, 1998: Crop evapotranspiration—Guidelines for computing crop water requirements. FAO Irrigation and Drainage Paper 56, 300 pp.

AMEC Earth and Environmental and Paragon Soil and Environ-mental Consulting, Inc., 2005: Results from long term vege-tation plots established in the oil sands region. Cumulative Environmental Management Association Oil Sands Soil and Vegetation Working Group Rep., 65 pp.

Appels, W. M., S. N. Wall, S. L. Barbour, M. J. Hendry, C. F. Nichol, and S. R. Chowdhury, 2017: Pyrite weathering in re-claimed shale overburden at an oil sands mine near Fort McMurray, Canada. Mine Water Environ., 36, 479–494, https:// doi.org/10.1007/s10230-017-0454-4.

Ayres, B., and M. O'Kane, 2013: Design, construction, and perfor-mance of closure cover systems for spent heap leach piles—A state-of-the-art review. Proc. Int. Heap Leach Conf., Vancou-ver, BC, Canada, The University of British Columbia, 240–251.

Barbour, S. L., and Coauthors, 2004: Tracking the evolution of reclaimed landscapes through the use of instrumented water-sheds—A brief history of the Syncrude Southwest 30 Overburden Reclamation Research Program. Proc. Int. Instrumented Watershed Symp., Edmonton, AB, Canada, Syncrude Canada Limited and Natural Sciences and Engineering Research Council of Canada.

Barr, A. G., G. van der Kamp, T. A. Black, J. H. McCaughey, and Z. Nesic, 2012: Energy balance closure at the BERMS flux towers in relation to the water balance of the White Gull Creek watershed 1999–2009. Agric. Meteor., 153, 3–13,https:// doi.org/10.1016/j.agrformet.2011.05.017.

Beckingham, J. D., and J. H. Archibald, 1996: Field guide to eco-sites of northern Alberta. Natural Resources Canada Special Rep. 5, 516 pp.

Boese, C. D., 2003: The design and installation of a field in-strumentation program for the evaluation of soil–atmosphere water fluxes in a vegetated cover over saline/sodic shale overburden. M.S. thesis, Dept. of Civil Engineering, Uni-versity of Saskatchewan, 170 pp., http://hdl.handle.net/10388/ etd-12172012-083151.

Booterbaugh, A. P., R. B. Laurence, and C. A. Mendoza, 2015: Geophysical characterization of an undrained dyke containing an oil sands tailings pond, Alberta, Canada. J. Environ. Eng. Geophys., 20, 303–317, https://doi.org/10.2113/JEEG20.4.303.

Braden, H., 1985: Ein Energiehaushalts- und Verdunstungsmodell for Wasser und

Stoffhaushaltsuntersuchungen landwirtschaftlich genutzer Einzugsgebiete. Mittelungen Dtsch. Bodenkd. Geselschaft, 42, 294–299.

Brutsaert, W., 1982: Evaporation into Atmosphere: Theory, His-tory, and Applications. D. Reidel, 302 pp.

CAPP, 2016: Canada's oil sands. CAPP Rep., 31 pp., http:// www.oscaalberta.ca/wp-content/uploads/2017/06/CAPP-Oil-Sands-Fact-Booklet.pdf.

Carrera-Hernández, J. J., C. A. Mendoza, K. J. Devito, R. M. Petrone, and B. D. Smerdon, 2011: Effects of aspen harvesting on groundwater recharge and water table dynamics in a sub-humid climate. Water Resour. Res., 47, 1–18, https://doi.org/ 10.1029/2010WR009684.

CEMA, 2006: Field Manual for Land Capability Determination. Vol. 1, Land Capability Classification System for Forest Eco-systems in the Oil Sands, 3rd ed., Alberta Environment, 148 pp., http://www.assembly.ab.ca/lao/library/egovdocs/2006/alen/158348.pdf.

Chasmer, L., H. McCaughey, A. Barr, A. Black, A. Shashkov, P. Treitz, and T. Zha, 2008: Investigating light-use efficiency across a jack pine chronosequence during dry and wet years. Tree Physiol., 28, 1395–1406, https://doi.org/10.1093/treephys/ 28.9.1395.

Dobchuk, B. S., R. E. Shurniak, S. L. Barbour, M. A. O'Kane, and Q. Song, 2013: Long-term monitoring and modelling of a reclaimed watershed cover on oil sands tailings. Int. J. Min. Reclam. Environ., 27, 180–201, https://doi.org/10.1080/ 17480930.2012.679477.

Elshorbagy, A., and S. L. Barbour, 2007: Probabilistic approach for design and hydrologic performance assessment of re-constructed watersheds. J. Geotech. Geoenviron. Eng., 133, 1110–1118, https://doi.org/10.1061/(ASCE)1090-0241(2007) 133:9(1110).

——, A. Jutla, and J. Kells, 2007: Simulation of the hydrological processes on reconstructed watersheds using system dynamics. Hydrol. Sci. J., 52, 538–562, https://doi.org/10.1623/hysj.52.3.538.

——, A. Nazemi, and M. S. Alam, 2015: Analyzing the variations in intensity-duration-frequency (IDF) curves in the city of Sas-katoon under climate change. University of Saskatchewan Centre for Advanced Numerical Simulation Series Rep. CAN-15-01, 167 pp.

Feddes, R. A., E. Bresler, and S. P. Neuman, 1974: Field test of a modified numerical model for water uptake by root systems. Water Resour. Res., 10, 1199–1206, https://doi.org/10.1029/WR010i006p01199.

Franczyk, J., and H. Chang, 2009: The effects of climate change and urbanization on the runoff of the Rock Creek basin in the Portland metropolitan area, Oregon, USA. Hydrol. Processes, 23, 805–815, https://doi.org/10.1002/hyp.7176.

Gerke, H. H., and M. T. van Genuchten, 1993: Evaluation of a first-order water transfer term for variably saturated dual-porosity flow models. Water Resour. Res., 29, 1225–1238, https://doi.org/10.1029/92WR02467.

Githui, F., W. Gitau, F. Mutua, and W. Bauwens, 2009: Climate change impact on SWAT simulated streamflow in western Kenya. Int. J. Climatol., 29, 1823–1834,

https://doi.org/10.1002/ joc.1828.

Hall, F. G., Y. E. Shimabukuro, and K. F. Huemmrich, 1995: Re-mote sensing of forest biophysical structure using mixture decomposition and geometric reflectance models. Ecol. Appl., 5, 993–1013, https://doi.org/10.2307/2269350.

Hashmi, M. Z., A. Y. Shamseldin, and B. W. Melville, 2011: Comparison of LARS-WG and SDSM for simulation and downscaling of extreme precipitation events in a watershed. Stochastic Environ. Res. Risk Assess., 25, 475–484, https:// doi.org/10.1007/s00477-010-0416-x.

Hassanzadeh, E., A. Nazemi, and A. Elshorbagy, 2014: Quantile-based downscaling of precipitation using genetic programming: Application to IDF curves in Saskatoon. J. Hydrol. Eng., 19, 943– 955, https://doi.org/10.1061/(ASCE)HE.1943-5584.0000854.

Howard, E. A., S. T. Gower, J. A. Foley, and C. J. Kucharik, 2004: Effects of logging on carbon dynamics of a jack pine forest in Saskatchewan, Canada. Global Change Biol., 10, 1267–1284, https://doi.org/10.1111/j.1529-8817.2003.00804.x.

Huang, M., A. Elshorbagy, S. L. Barbour, J. Zettl, and B. C. Si, 2011a: System dynamics modeling of infiltration and drainage in layered coarse soil. Can. J. Soil Sci., 91, 185–197, https://doi.org/ 10.4141/cjss10009.

——, S. L. Barbour, A. Elshorbagy, J. Zettl, and B. C. Si, 2011b: Water availability and forest growth in coarse-textured soils. Can. J. Soil Sci., 91, 199–210, https://doi.org/10.4141/cjss10012.

——, ——, ——, ——, and ——, 2011c: Infiltration and drainage processes in multi-layered coarse soils. Can. J. Soil Sci., 91, 169–183, https://doi.org/10.4141/cjss09118.

——, ——, and S. K. Carey, 2015: The impact of reclamation cover depth on the performance of reclaimed shale overburden at an oil sands mine in northern Alberta, Canada. Hydrol. Pro-cesses, 29, 2840–2854, https://doi.org/10.1002/hyp.10229.

Huntington, T. G., 2006: Evidence for intensification of the global water cycle: Review and synthesis. J. Hydrol., 319, 83–95, https://doi.org/10.1016/j.jhydrol.2005.07.003.

IPCC, 2000: Land Use, Land-Use Change and Forestry: A Special Report of the IPCC. R. Watson et al., Eds., Cambridge Uni-versity Press, 30 pp.

——, 2013: Climate Change 2013: The Physical Science Basis. Cambridge University Press, 1535 pp., https://doi.org/10.1017/ CBO9781107415324.

Keshta, N., A. Elshorbagy, and S. Carey, 2009: A generic system dynamics model for simulating and evaluating the hydrological performance of reconstructed watersheds. Hydrol. Earth Syst. Sci., 13, 865–881, https://doi.org/10.5194/hess-13-865-2009.

——, ——, and ——, 2012: Impacts of climate change on soil moisture and evapotranspiration in reconstructed watersheds in northern Alberta, Canada. Hydrol. Processes, 26, 1321–1331, https://doi.org/10.1002/hyp.8215.

Kienzle, S. W., M. W. Nemeth, J. M. Byrne, and R. J. MacDonald, 2012: Simulating the hydrological impacts of climate change in the upper North Saskatchewan River basin,

Alberta, Canada. J. Hydrol., 412–413, 76–89, https:// doi.org/10.1016/j.jhydrol.2011.01.058.

Kuusisto, E., 1980: On the values and variability of degree-day melting factor in Finland. Nord. Hydrol., 11, 235–242, https:// doi.org/10.2166/nh.1980.0011.

Lavigne, M. B., R. J. Foster, G. Goodine, P. Y. Bernier, and C. H. Ung, 2005: Alternative method for estimating aboveground net pri-mary productivity applied to balsam fir stands in eastern Canada. Can. J. For. Res., 35, 1193–1201, https://doi.org/10.1139/x05-052.

Leta, O. T., A. I. El-Kadi, H. Dulai, and K. A. Ghazal, 2016: As-sessment of climate change impacts on water balance com-ponents of Heeia watershed in Hawaii. J. Hydrol. Reg. Stud., 8, 182–197, https://doi.org/10.1016/j.ejrh.2016.09.006.

Mango, L. M., A. M. Melesse, M. E. McClain, D. Gann, and S. G. Setegn, 2011: Land use and climate change impacts on the hydrology of the upper Mara River basin, Kenya: Results of a modeling study to support better resource management. Hy-drol. Earth Syst. Sci., 15, 2245–2258, https://doi.org/10.5194/ hess-15-2245-2011.

Najafi, M. R., H. Moradkhani, and I. W. Jung, 2011: Assessing the uncertainties of hydrologic model selection in climate change impact studies. Hydrol. Processes, 25, 2814–2826, https:// doi.org/10.1002/hyp.8043.

OKC, 2001: Southwest sand storage and 30-dump automated water balance monitoring systems at Syncrude Canada Ltd. OKC Rep. 653-2, 19 pp.

——, 2007: Soil-atmosphere field response modelling of Southwest Sand Storage facility cell 32. OKC Rep. 690/14-01, 16 pp.

——, 2016: Instrumented watershed monitoring program at the Southwest Sand Storage facility: Performance monitoring re-port for the period January 2015 to December 2015. OKC Rep. 690/01-72, 26 pp.

Pan, S., and Coauthors, 2015: Responses of global terrestrial evapotranspiration to climate change and increasing atmo-spheric CO2 in the 21st century. Earth's Future, 3, 15–35, https://doi.org/10.1002/2014EF000263.

Price, J. S., R. G. McLaren, and D. L. Rudolph, 2010: Landscape restoration after oil sands mining: Conceptual design and hydrological modelling for fen reconstruction. Int. J. Min. Reclam. Environ., 24, 109–123, https://doi.org/10.1080/17480930902955724.

Prudhomme, C., N. Reynard, and S. Crooks, 2002: Downscaling of global climate models for flood frequency analysis: Where are we now? Hydrol. Processes, 16, 1137–1150, https://doi.org/ 10.1002/hyp.1054.

Qualizza, C., D. Chapman, S. L. Barbour, and B. Purdy, 2004: Reclamation research at Syncrude Canada's mining operation in Alberta's Athabasca oil sands region. Proc. 16th Int. Conf. on Ecological Restoration, Victoria, BC, Canada, Society for Ecological Restoration.

Racsko, P., L. Szeidl, and M. Semenov, 1991: A serial approach to local stochastic weather models. Ecol. Modell., 57, 27–41, https://doi.org/10.1016/0304-3800(91)90053-4.

Rogelj, J., M. Meinshausen, and R. Knutti, 2012: Global warming under old and new scenarios

using IPCC climate sensitivity range estimates. Nat. Climate Change, 2, 248–253, https://doi.org/10.1038/nclimate1385.

Rooney, R. C., D. T. Robinson, and R. Petrone, 2015: Megaproject reclamation and climate change. Nat. Climate Change, 5, 963– 966, https://doi.org/10.1038/nclimate2719.

Rosenzweig, M. L., 1968: Net primary productivity of terrestrial communities: Prediction from climatological data. Amer. Nat., 102, 67–74, https://doi.org/10.1086/282523.

Schindler, D. W., and W. F. Donahue, 2006: An impending water crisis in Canada's western prairie provinces. Proc. Natl. Acad. Sci. USA, 103, 7210–7216, https://doi.org/10.1073/pnas.0601568103.

Schneider, R. R., 2013: Alberta's natural subregions under a changing climate: Past, present, and future. Alberta Bio-diversity Monitoring Institute Rep., 80 pp.

Semenov, M. A., and E. M. Barrow, 1997: Use of a stochastic weather generator in the development of climate change sce-narios. Climatic Change, 35, 397–414, https://doi.org/10.1023/ A:1005342632279.

——, and ——, 2002: LARS-WG: A stochastic weather generator for use in climate impact studies. Rothamsted Research Rep., 28 pp., http://resources.rothamsted.ac.uk/sites/default/files/groups/ mas-models/download/LARS-WG-Manual.pdf.

Simunek, J., N. J. Jarvis, M. T. van Genuchten, and A. Gardenas, 2003: Review and comparison of models for describing nonequilibrium and preferential flow and transport in the vadose zone. J. Hydrol., 272, 14–35, https://doi.org/10.1016/ S0022-1694(02)00252-4.

——, M. T. van Genuchten, and M. Sejna, 2012: The HYDRUS software package for simulating the two- and three-dimensional movement of water, heat, and multiple solutes in variably-saturated porous media. University of California, Riverside, Rep., 230 pp.

——, M. Sejna, H. Saito, M. Sakai, and M. T. van Genuchten, 2013: The HYDRUS-1D software package for simulating the one-dimensional movement of water, heat, and multiple solutes in variably-saturated media. University of California, Riverside, Rep., 305 pp.

Srivastav, R. K., A. Schardong, and S. P. Simonovic, 2014: Equi-distance quantile matching method for updating IDF curves under climate change. Water Resour. Manage., 28, 2539–2562, https://doi.org/10.1007/s11269-014-0626-y.

Straker, J., M. O'Kane, S. Carey, T. E. Baker, D. Charest, and R. Shurniak, 2014: Towards an ecohydrologic classification of reclaimed watersheds: Methods for estimating soil water regime on reclaimed mine waste materials; and relationships between reclamation and surface water balances in Teck's reclaimed coal-mining watersheds. 38th Annual British Columbia Mine Reclamation Symp., Prince George, BC, Canada, British Columbia Technical and Research Commit-tee on Reclamation, https://doi.org/10.14288/1.0042684.

Strong, W. L., and K. R. Leggat, 1981: Ecoregions of Alberta.

Alberta Energy and Natural Resources Tech. Rep. T/4, 64 pp.

Suncor Energy, Inc., 2007: Climate change in the oil sands region. Voyager South Project

Environmental Impact Rep., 134 pp.

Taylor, K. E., R. J. Stouffer, and G. A. Meehl, 2012: An overview of CMIP5 and the experiment design. Bull. Amer. Meteor. Soc., 93, 485–498, https://doi.org/10.1175/BAMS-D-11-00094.1.

Thompson, C., C. A. Mendoza, and K. J. Devito, 2017: Potential influence of climate change on ecosystems within the Boreal Plains of Alberta. Hydrol. Processes, 31, 2110–2124, https://doi.org/10.1002/hyp.11183.

van Genuchten, M. T., 1980: A closed-form equation for pre-dicting the hydraulic conductivity of unmatured soils. Soil. Sci. Soc. Amer. J., 44, 892–898, https://doi.org/10.2136/sssaj1980.03615995004400050002x.

Vogel, J. G., and S. T. Gower, 1998: Carbon and nitrogen dynamics of boreal jack pine stands with and without a green alder understory. Ecosystems, 1, 386–400, https://doi.org/10.1007/s100219900032.

Zettl, J., S. L. Barbour, M. Huang, B. Si, and L. A. Leskiw, 2011: Influence of textural layering on field capacity of coarse soils. Can. J. Soil Sci., 91, 133–147, https://doi.org/10.4141/cjss09117.

CHAPTER 5 - USING STATISTICAL AND DYNAMICAL DOWNSCALING TO ASSESS CLIMATE CHANGE IMPACTS ON MINE RECLAMATION COVER WATER BALANCES (ALAM ET AL. 2020)

Preface

This final paper, which has been published in the *Journal of Mine Water and the Environment*, is focused on the last objective of the thesis: "To evaluate methods of downscaling global climate change projections to regional (local) scales to evaluate changes in future water balances." The published paper in this chapter is presented with minor changes as suggested by the examining committee.

In the previous chapters, the impacts of climate and parameter variability on the long-term cover performances were explored using observed meteorological records, climate change projections from the global climate model, and parameter variability obtained from inverse modelling approach. This chapter extends that analysis to explore the impacts of climate change projections obtained from a high-resolution regional climate model (RCM), with an aim to compare the relative impacts between the statistical and dynamical downscaling methods in characterizing future water balance components of the reclamation covers. This chapter is therefore a logical and methodological continuation of the findings from Chapter 3, and the framework for coupling GCM and water balance model through the statistical downscaling methods in Chapter 4. In this chapter, the high-resolution climate change projections from weather research and forecasting (WRF) model are used to characterize convective rainfall which are usually not represented by the GCMs.

Dr. S. L. Barbour initially proposed the idea of comparison between the statistical and dynamical downscaling results in terms of reclamation cover performances under climate change, while Dr. Y. Li provided the dynamical downscaling results using Weather Research and Forecasting model. I as a PhD candidate significantly extended this idea and developed a novel approach to characterize climate change impacts on mine reclamation covers and natural soil profiles. The candidate reviewed the literature, conducted numerical simulations, analyzed and

discussed the results, and wrote the manuscript. All coauthors critically reviewed and edited the manuscript and provided feedbacks on different aspects of the study. This chapter has been accepted for publication with the following citation:

Alam, M. S., Barbour, S. L., Huang, M., and Li, Y. (2020). Using Statistical and Dynamical Downscaling to Assess Climate Change Impacts on Mine Reclamation Cover Water Balances, *Mine Water and the Environment*, MWEN-D-20-00039.

Abstract

The oil sands industry in Canada uses soil-vegetation-atmosphere-transfer (SVAT) water balance models, calibrated against short-term (<≈10 years) field monitoring data, to evaluate long-term (≈60 years) reclamation cover design performance. These evaluations use long-term historical climate data; however, the effects of climate change should also be incorporated in these analyses. Although statistical downscaling of global climate change projections is commonly used to obtain local, site-specific climate, high resolution dynamical downscaling can also be used. The value of this latter approach to obtain local site-specific projections for mine reclamation covers has not been evaluated previously. This study explored the differences in key water balance components of three reclamation covers and three natural sites in northern Alberta, Canada, under future, site-specific, statistical, and dynamical climate change projections. Historical meteorological records were used to establish baseline periods. Temperature datasets were used to calculate potential evapotranspiration (PET) using the Hargreaves-Samani method. Statistical downscaling uses the Long Ashton Research Station Weather Generator (LARS-WG) and global circulation model (GCM) projections of temperature and precipitation. Dynamical climate change projections were generated on a 4 km grid using the weather research and forecasting (WRF) model. These climate projections were applied to a physically-based water balance model (i.e. Hydrus-1D) to simulate actual evapotranspiration (AET) and net percolation (NP) for the baseline and future periods. The key findings were: (a) LARS-WG outperformed WRF in simulating baseline temperatures and precipitation; (b) both downscaling methods showed similar directional shifts in the future temperatures and precipitation; (c) this, in turn, created similar directional shifts in future growing season median AET and NP, although the increase in future NP for LARS-WG was higher than that for WRF. The relative increases in

future NP were much higher than the relative increases in future AET, particularly for the reclamation covers.

5.1 Introduction

Oil sands represent 98% of Canada's proven oil reserves and the extraction and mining of oil sands in northern Alberta plays an important role in Canada's economy. Total oil production in 2018 was 4.59 million barrels per day and is expected to reach 5.86 million barrels per day by the end of 2035 (CAPP 2019). The oil sands underlie ≈ 140,000 km^2 in northern Alberta, Canada, where shallow (up to 75 m depth) mineable reserves comprise an area of ≈ 4800 km^2, of which more than 895 km^2 (18% of the total shallow mineable area) has been disturbed or cleared in association with surface mining activities (Government of Alberta 2017). The oil sands industries are obliged by law to reclaim the land to an equivalent land capability after oil sands have been extracted (CEMA 2006).

The design of reclamation covers is currently based on the use of soil-vegetation-atmosphere-transfer (SVAT) water balance models calibrated against relatively short-term (<≈10 years) monitoring undertaken on prototype covers. These calibrated models are then used along with long-term (≈60 years) historical climate records to simulate future cover performance (Boese 2003; Huang et al., 2015a, 2011a, b, c; Keshta et al. 2009; Price et al. 2010; Qualizza et al. 2004). There is a growing appreciation by industry that this design approach must begin to incorporate the potential impacts of climate change.

Historical climate records have indicated that temperature and precipitation are increasing globally (e.g. Alexander et al. 2006; IPCC 2013; Zhang et al. 2000) with more frequent extreme weather (e.g. drought, flooding, and heatwaves; Chen 2013; Held and Soden 2006; Karl et al. 1995; Li et al. 2017; Liu et al. 2017; Sun 2014; Wood et al. 1997). In Canada, there has been a 0.3 ºC increase in annual mean temperature and a 5-35% increase in annual precipitation from 1950 to 1998 (Zhang et al. 2000). The 21st century climate change projections indicate precipitation increases across Canada including the Canadian prairies (e.g. Alam and Elshorbagy 2015; Hassanzadeh et al. 2014; Srivastav et al. 2014; Suncor Energy Inc. 2007; Thompson et al. 2017).

The primary tool for future climate projections has been the general circulation models (GCMs; Meehl et al. 2007). These projections play a vital role in studying the impacts of climate change and variability (Fowler et al. 2007). The GCM projections have been coordinated and distributed by the coupled model intercomparison project (CMIP) with support from the world climate research programme's (WCRP) working group on coupled modelling (WGCM). Since program inception, five different phases of multi-model research activity (Meehl et al. 2004, 2007; Taylor et al. 2012) have been published; these form the central basis of national and international studies of climate change (IPCC 2013).

GCMs have coarse spatial resolutions (typically 100-300 km), which limit their value in predicting local (site specific) and regional (typically 25-50 km) climate change characteristics since convective cloud processes (a primary producer of precipitation) are not represented adequately at these scales (Joubert and Hewitson 1997). The most commonly used methods of downscaling GCMs to local and regional scales has been through statistical or dynamical downscaling techniques (Fowler et al. 2007; Wilby and Wigley 1997). Both approaches have certain advantages and disadvantages. For example, while statistical downscaling is computationally efficient, dynamic downscaling is able to produce high resolution climate variables based on physical processes (Fowler et al. 2007; Wilby and Dawson 2004). Since northern Alberta is located in the Canadian Prairies, the precipitation in this region is mostly contributed by summer convection; consequently, any downscaling method must capture these convection-driven effects.

Statistical downscaling is based on the statistical relationships between the local-scale climate variables (the predictands) and the global-scale climate variables (the predictors) to generate site-specific climate change projections (Wilby et al. 1998). Statistical downscaling approaches developed over the past 20-30 years include both simple methods (e.g. delta change) and more sophisticated methods (e.g. regression models, stochastic weather generators, weather typing schemes). Each of these methods are based on a range of theories; however, all of them rely on the fundamental relationship established between large-scale atmospheric condition and local-scale features (Fowler et al. 2007). In practice, two or more approaches can be combined and therefore, many approaches are a hybrid of the basic methods (Wilby and Wigley 1997).

A potential improvement in downscaling has been the use of dynamical downscaling by parameterizing physical atmospheric processes. In a dynamical downscaling approach, finer resolution information from GCM-based outputs is generated by embedding a high-resolution regional climate model (RCM) within a GCM (Fowler et al. 2007; Wilby and Dawson 2007). The high resolution projections explicitly account for underlying surface and local circulation patterns to represent several small-scale characteristics and atmospheric processes that cannot be captured using GCMs (Castro et al. 2005; Gao et al. 2012; May 2008).

RCMs can provide more resolution of small-scale processes than the GCMs; however, RCMs are still at a relatively coarse resolution where convection-dominated precipitation is poorly represented. A high-resolution weather forecasting model with convection-permitting scheme known as weather research and forecasting (WRF; Skamarock et al. 2008) model incorporates horizontal grid spacing of less than 4 km. At this grid spacing, WRF begins to reflect the impact of convective processes, as influenced by underlying surface topography (Li et al. 2019). Despite its higher computational costs, high resolution WRF has demonstrated benefits when used in dynamical downscaling (Done et al. 2004; Fosser et al. 2015; Prein et al. 2017; Weisman et al. 2008). WRF simulations also add value to the study of climate change impacts in regions such as western Canada where small-scale atmospheric processes (e.g. summer convections) are important (Li et al. 2017, 2019). However, the outputs of WRF (as well as the outputs of any RCM) are impacted by a series of procedures connected to climate model uncertainties due to nested modelling. The series of uncertainties (termed as cascade of uncertainty by Mitchell and Hulme, 1999) has impact on the outcomes of the subsequent levels. For example, GCMs outputs are impacted by the uncertainties in the assumption of emission scenarios, while the WRF outputs are impacted by the uncertainties in the simulations of the driving GCMs. These uncertainties are propagated from emission scenarios to GCMs toward WRF outputs with increasing magnitude. It is important to note that these uncertainties are accounted for in the end projections of climate change, where these uncertainties are recognized as inevitable in the process of climate modelling (Foley 2010).

The key components of the water balance for the design of reclamation soil covers are the actual evapotranspiration (AET), reflective of vegetative growth, and net percolation (NP),

reflective of the contribution to groundwater flow through the underlying mining waste, which may transport chemical constituents from these deposits. Previous studies have shown that increases in future temperature will result in increases in both AET and NP. Alam et al. (2017) incorporated climate change projections from three GCMs (e.g. CanESM2, BCC-CSM1.1, and IPSL-CM5A-LR) based on three representative concentration pathways (RCP2.6, RCP4.5, and RCP8.5) into a physically-based water balance model (i.e. Hydrus-1D) to quantify uncertainties in the projected AET and NP of an oil sands reclamation cover and a natural soil profile. Alam et al. (2018) used a similar framework to quantify uncertainties in the projected AET and NP of two reclamation covers and three natural soil profiles using the fourth generation Canadian GCM (CanESM2), based on the three RCPs.

Keshta et al. (2012) studied reclamation cover water balances using a generic system dynamics water balance model in which they incorporated climate change projections. The projections were taken from the third generation Canadian GCM (i.e. CGCM3) based on two scenarios from the special report on emission scenarios (SRES); emission scenarios (A2 and B1, IPCC 2000). Their study showed that decreases in soil moisture deficit and increases in AET are associated with the projected increases in precipitation. They did not evaluate potential changes in NP.

High-resolution WRFs or RCMs have not been previously used to evaluate the future water balance performance of mine reclamation soil covers. The overall objective of this study was to evaluate the relative impact of using statistically and dynamically downscaled climate change projections from the GCMs on predictions of the future water balance performance of three reclamation soil covers and three natural vegetation sites in northern Alberta, Canada. These predictions were undertaken in a manner to also quantify the uncertainties in the projected AET and NP of the oil sands reclamation covers and natural soil profiles for each of the downscaling methods.

5.2 Materials and methods

5.2.1 Study sites, reclamation covers, and natural sites

The study area is situated within the boreal mixed-wood ecoregion (Strong and Leggat 1981), ≈ 40-80 km north of Fort McMurray, Alberta, Canada. The climate is a typical prairie climate with an average annual precipitation of 427 mm (1944-2018), approximately two-thirds of which occurs in the summer months. The mean spring (March-May), summer (June-August), fall (September-November), and winter (December-February) temperatures are 2.0, 15.5, 5.7, and -15.2 ºC, respectively. The average annual potential evapotranspiration (PET) in Fort McMurray is 670 mm, based on the Hargreaves-Samani method and meteorological observations from the Fort McMurray Airport station over a 75-year period (1944-2018).

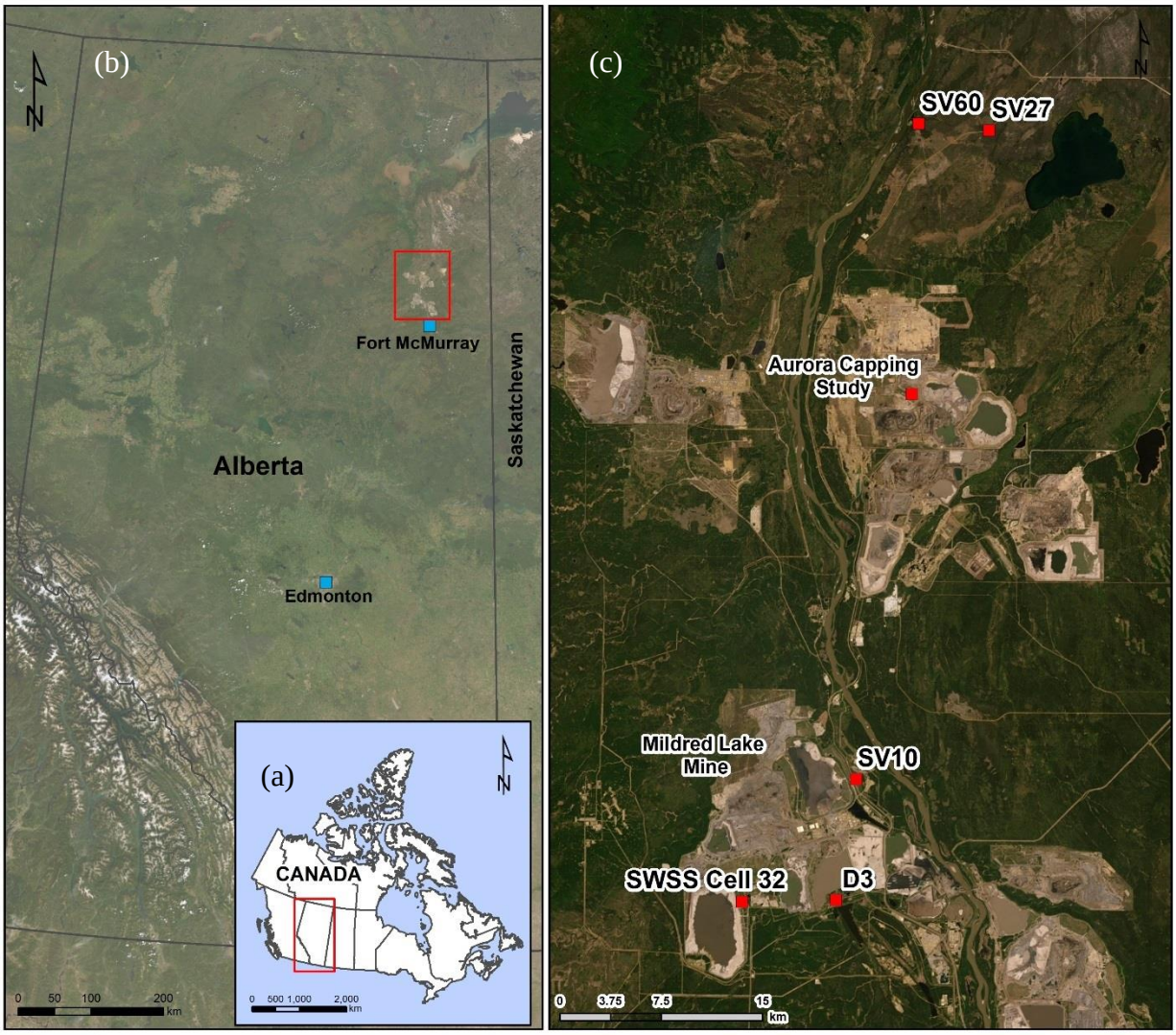

Figure 5-1: (a) Map of Canada showing the province of Alberta, (b) map of Alberta showing the relevant cities and general study area, and (c) map of the study area showing the site locations with red squares where (c) is the zoom out view of the red rectangle in (b) [Map sources: Esri, DigitalGlobe, GeoEye, Earthstar, Geographics, CNES/Airbus DS, USDA, USGS, Aerogrid, IGN, and the GIS User Community].

This study focuses on three reclamation soil cover sites [South Bison Hill (D3), Southwest Sand Tailings Storage (SWSS), Aurora Capping Study (ACS)] as well as three monitored natural soil profiles (soil vegetation sites SV10, SV27, and SV60) located at undisturbed reference sites (Fig. 5-1). Two of the reclamation covers (D3 and SWSS) are located at Syncrude Canada Ltd's (SCL) Mildred Lake mine site, while the ACS reclamation cover is located at the SCL Aurora

North mine, ≈ 20 km to the north of the Mildred Lake Mine. The D3 and ACS prototype covers are ≈ 1 hectare in size but sit within much larger areas (several hundred hectares) of reclaimed mine waste.

The reclamation soil profiles at each site are:

- D3 site: 20 cm of a salvaged peat-glacial clay mineral mixture overlying 80 cm of a glacial clay soil overlying shale overburden;
- SWSS: 45 cm of peat-glacial clay mineral mixture overlying tailings sand;
- ACS: 20 cm of cover soil (either salvaged peat or upland surface litter layer) overlying 100 cm of salvaged sandy subsoil placed over lean oil sands (LOS) overburden.

The reclamation covers have been monitored since 1999 (D3), 2001 (SWSS), and 2012 (ACS). The monitoring includes meteorology (precipitation, air temperature, wind speed, net radiation, and relative humidity), as well as soil monitoring (volumetric water content, suction, and soil temperature) across the cover profile and into the underlying mine waste. Details of the instrumentation and monitoring program can be found in Barbour et al. (2004), Boese (2003), Huang et al. (2015a), O'Kane Consultants Inc. (OKC 2001, 2016).

The monitored natural soil profile locations follow: SV10 is at the Mildred Lake Mine site and SV27 and SV60 are ≈ 20 km north of the ACS reclamation cover site. The SV10 and SV27 sites are texturally homogeneous with fine or medium sands, respectively. SV60 is texturally heterogeneous with a fine sand layer (45-84 cm) overlain and underlain by coarse sand layers. The details of these sites, including field experiments and measurements of soil properties, can be found in Huang et al. (2011b) and Zettl et al. (2011).

5.2.2 Data collection

The reference historical data set for the region was a 60 year (1956-2015) daily climate monitoring record obtained from Environment and Climate Change Canada (ECCC) records at the Fort McMurray Airport station (syncrude.emline.ca/Syncrude/Pages/default.aspx). The global scale future climate change projections (i.e. precipitation and temperature) for the historical period (1976-2005) and future period (2086-2100) were obtained from the CMIP5

GCMs (see the list in Table C-1), based on the representative concentration pathways (RCP8.5). The climate change projections were obtained from the CMIP5 data archive (https://esgf-node.llnl.gov/search/cmip5/). The WRF-simulated climate change projections (i.e. hourly precipitation and temperature) for the baseline (2001-2015) and future (2086-2100) periods were obtained through dynamical downscaling from Li et al. (2017, 2019). All the climate change projections were obtained for the Fort McMurray Airport station (56.6488° N, 111.2305° W).

5.2.3 Downscaling methods

Two approaches to downscaling were used in this study. The first was statistical downscaling of GCM projections using the Long Ashton Research Station Weather Generator (LARS-WG) and the second was dynamical downscaling based on WRF simulations.

The high computational demands of the WRF model (≈ 2 years run time using Compute Canada's resources) required that this study rely on currently available simulation time periods. This included 15 years of simulation results for the 2001-2015 historical period and the 2086-2100 future period. This was further constrained by the long-term historical and future time horizons for the GCMs used for the LARS-WG downscaling. These time horizons were 1976-2005 and 2086-2100, respectively. These differing historical and future time periods for the two downscaling methods were unavoidable and complicate the inter-comparisons. As a result, the inter-comparisons between the LARS-WG and WRF models was only possible for the shorter period of overlap (2001-2005).

5.2.3.1 Statistical downscaling

The statistical downscaling method in this study was the latest version of LARS-WG 5.5 (Racsko et al. 1991; Semenov 2007; Semenov and Barrow 1997). The stochastic weather generator LARS-WG can generate synthetic weather time-series (e.g. daily precipitation, and daily minimum and maximum temperatures) for any duration. LARS-WG computes a set of parameters for the distributions of observed climate variables as well as correlations between different observed daily climate variables. Synthetic time series of climate variables are generated using the set of parameters by randomly selecting values from the appropriate distributions. These selected parameter distributions for a given site are then perturbed by the

relative changes as projected by the GCMs (i.e. climate scenario) to generate a future climate scenario for the site.

Future climate scenarios were calculated using the synthetic monthly distributions from historic GCM projections, adjusted to align with historical distributions of these variables, and then perturbed based on the GCM projections of future climate change. In this study, the climate scenarios for LARS-WG simulations were derived from the CMIP5 multi-model ensemble based on the mean of 17 member GCMs for RCP8.5 scenario during the future period 2086-2100 relative to the historical period 1976-2005. The list of the member GCMs from CMIP5 used in LARS-WG simulations are shown in Table C-1 of Appendix C.

5.2.3.2 Dynamical downscaling

The WRF model was used to simulate the regional climate for the historical baseline and future climate with reanalysis and climate change forcing based on the ensembles of CMIP5 GCMs (RCP8.5), respectively. The dynamical downscaling technique relied on simulations undertaken by Li et al. (2017, 2019) using the WRF version 3.6.1 model (Skamarock et al. 2008). This WRF model simulated historical (2001-2015) climate and dynamically downscaled projected climate for a future period (2086-2100) over a domain covering western Canada from British Columbia to the Yukon. The WRF model domain was composed of 700×640 grid points with a horizontal resolution of 4 km.

The WRF simulations included an initial simulation [control experiment (CTL)] of the historical baseline climate by directly forcing 6 hour 0.7º ERA-Interim reanalysis data (Dee et al. 2011). A second simulation, based on a climate perturbation of sensitivity experiment [pseudo-global warming (PGW); Rasmussen et al. 2011, 2014)], was used to simulate future climate change projections using the PGW forcing derived from climate change signals from a 19-member ensemble mean of CMIP5 GCMs, as recommended by Liu et al. (2017). The PGW simulation for a 15 year period (2086-2100) was forced with the same ERA-interim reanalysis as in CTL, plus a climate perturbation based on ensemble of CMIP5 RCP8.5 projections:

$$\text{PGW-forcing} = \text{ERA-Interim} + \Delta_{CMIP5\_RCP8.5} \tag{5.1}$$

Where $\Delta_{CMIP5\_RCP8.5}$ is the climate change signals derived from the CMIP5 multi-model ensemble based on the mean of 19 member GCMs for RCP8.5 scenario during the future period 2071-2100 relative to the historical period 1976-2005. For more details on WRF simulations, please refer to Li et al. (2017, 2019). The list of these member GCMs from CMIP5 used in WRF simulations are shown in Table C-1 of Appendix C.

5.2.4 Water balance modelling

The physically-based soil water dynamics model, Hydrus-1D (Simunek et al. 2013), was used to simulate key water balance components (AET and NP) for each of the study sites. This modelling approach has been used extensively to study long-term water balance, soil water dynamics, and alternative reclamation cover designs for oil sands reclamation covers (e.g. Huang et al. 2011 a, b, c, 2015a, b; Sigouin et al. 2016; Zettl et al. 2011).

The model is based on the solution of Richard's equation for transient water flow through unsaturated soil including soil-atmosphere transfers (i.e. evaporation and transpiration) using the method proposed by Feddes et al. (1974). In this method, actual evaporation and actual transpiration are calculated based on prescribed vegetation characteristics, such as leaf area index (LAI) and root length density. Details of the models including the material properties, the vegetation (i.e. LAI), and root densities were presented in previous papers (Alam et al. 2017, 2018; Huang et al. 2011b, c, 2015a). Typical particle size distributions, water retention curves (WRCs), and distributions of saturated hydraulic conductivity (Ks) are shown in the Appendix C (Figs. C-1, C-2, and C-3).

The Hydrus-1D model was previously calibrated and validated against field monitoring data at the study sites including: D3 (Huang et al. 2015a), SWSS (Alam et al. 2018), ACS (Alam et al. 2020), and three natural sites (SV10, SV27, and SV60; Huang et al. 2011b, c). The model domains used for each site were:

- D3: three layers (i.e., peat-mineral soil mixture, secondary clay layer, and underlying overburden shale);
- SWSS: two layers (i.e., peat-mineral mixture and tailings sand);

- ACS: three layers (i.e., peat cover soil, coarse-textured subsoil, and lean oil sand substrate);
- Natural Profiles: the texturally variable natural sand profiles required 14, 20, and 18 layers of varying texture and bulk density at SV10, SV27, and SV60, respectively.

A lower free drainage (i.e. unit vertical gradient) boundary condition was used in all of the models, consistent with the deep water table at all sites. This allows the surface soil water balance to be decoupled from the deeper hydrogeologic system (Dobchuk et al. 2013).

The simulated growing season precipitation and the calculated PET using Hargreaves-Samani method were used to represent the upper boundary condition in Hydrus-1D model. The Hargreaves equation (Hargreaves and Samani 1985) was used to calculate PET (mm day^{-1}), based on the daily temperature values:

$$PET = 0.0023\, R_a\, (T_{mean} + 17.8)(T_{max} - T_{min})^{0.5} \quad (5.2)$$

where Ra = water equivalent of extraterrestrial radiation ($mmday^{-1}$); T_{mean} = mean daily air temperature (^oC); T_{max} = mean daily maximum air temperature (^oC); T_{min}= mean daily minimum air temperature (^oC). The calculated daily PET during the growing season was applied as input in the water balance model.

The daily precipitation during the winter (typically November-March) from both WRF and LARS-WG were accumulated within a snowpack if the mean temperature in a day was less than 0 ºC. The accumulated snowpack was then released into the soil domain over an assumed two-week snowmelt period (typically in the first two weeks of April). The volume of snowpack melt over the winter period was calculated when the mean temperature in a day exceeded 0 ºC using the degree-day method as outlined by Carrera-Hernandez et al. (2011). A similar approach was used by Alam et al. (2018). The details are not repeated here for brevity. In brief, the calculated volume of melted snowpack was added to the precipitation amounts that occurred during the winter melt period and to any stored profile water within the soil profile at the beginning of the growing season.

The near surface hydraulic conductivity at all the sites was higher than that of the underlying soil layers (i.e. > 1×10^{-06} m/s or 86 mm/d). The cover soils typically have a hydraulic

conductivity >$1x10^{-06}$ m/s, while the underlying soils have a typical hydraulic conductivity of <$1x10^{-06}$ m/s (Huang et al. 2016, 2015, 2011a,c; Meiers et al. 2011). The reclamation covers were constructed with an average slope less than 10%, while the natural soil vegetation sites were flat. The higher surface hydraulic conductivity and the flat-lying topography (Alam et al. 2018; Bockstette 2018; Huang et al. 2011b; Meiers et al. 2011) enabled us to simplify the models by assuming there was no runoff. Infiltrated water in excess of available storage reports as net percolation which now defines the total water release (i.e. water yield) from the reclamation covers.

5.3 Results and discussion

The simulated climate change projections from the two downscaling methods (WRF and LARS-WG) are compared with historic observational data as well as for future time periods. The climate projections from both downscaling methods are also applied to the physically-based model to simulate both historic and future key water balance components (i.e. AET and NP) for three reclamation covers and three natural soil profiles.

5.3.1 Downscaled climate change projections

5.3.1.1 Comparison of WRF and LARS-WG Models with Historical Observations

The range of daily temperatures (Tmin, Tmax, and Tmean) and total precipitation each month from the LARS-WG and WRF-CTL simulations are compared with observations from the Fort McMurray Airport Station.in Fig. 5-2.

The LARS-WG reproduces the overall seasonal variations in precipitation and temperature (i.e. Tmin, Tmax, and Tmean) reasonably well with relatively small over- or under-estimates of precipitation and temperature in some months. In this study, the overall performance of LARS-WG was acceptable with relative errors of less than 10% between the observed and simulated median precipitation and temperature values in most months. Similar results were obtained in previous studies (e.g. Alam and Elshorbagy 2015; Alam et al. 2018; Chun et al. 2013; Nazemi et al. 2011).

WRF is able to reproduce the mid-summer through fall monthly temperature variability with similar peak values of temperature and precipitation occurring in July, consistent with the observed dataset. The simulated temperatures were lower in all months, while the WRF-simulated precipitation was higher in most months than the observed dataset. The overall relative error was 69.5% between the observed and simulated median precipitation and temperature values, considering all months.

Both downscaling models were better able to replicate the observed variability of precipitation than that of temperature in most months. The WRF-simulated temperature and precipitation were systematically under- and over-estimated, respectively, for most months, while LARS-WG outperformed WRF (Fig. 5-2). The underestimated temperature was due to the cold biases (particularly between March and July), while the overestimated precipitation was due to the wet biases for all seasons and more pronounced biases in the extreme precipitation amounts, as explained by Li et al. (2019). The July simulated values from WRF, as compared to the observations, are illustrative of the cold and wet biases of the WRF model. The simulated Tmin, Tmax, and Tmean in July were 8.43, 22.3, and 15.4 ºC, respectively, while the observations were 10.5, 24.3, and 17.3 ºC, respectively, and the median monthly precipitation in July was 115 mm for WRF, compared to the observed value of 61.5 mm.

These biases in temperature and precipitation would result in biases in the calculated PET and simulated water balance components, which are described in the following sections. Results with biases relative to the historical observed values will be used in the subsequent interpretations; therefore, the directions of change in the future water balance components relative to the baseline values from WRF simulations will be the basis of comparison with the LARS-WG simulations.

The observed annual median daily Tmin, Tmax, Tmean, and total precipitation are -2.2, 9.1, and 3.6 ºC, and 421.1 mm, respectively, during the 1976-2005 time period and -2.3, 9.0, and 3.2 ºC, and 374.2 mm, respectively, during the 2001-2015 time period. The statistics associated with these two different historical time periods are not significantly different and consequently provide a valid comparison to the downscaled model projections. The median daily Tmin, Tmax, Tmean, and total precipitation from the LARS-WG projections were -2.3, 9.0, and 3.4 ºC, and

424.2 mm, respectively for 1976-2005. The WRF projections were -4.7, 1.3, and -1.4 ºC, and 584.5 mm, respectively, for 2001-2015.

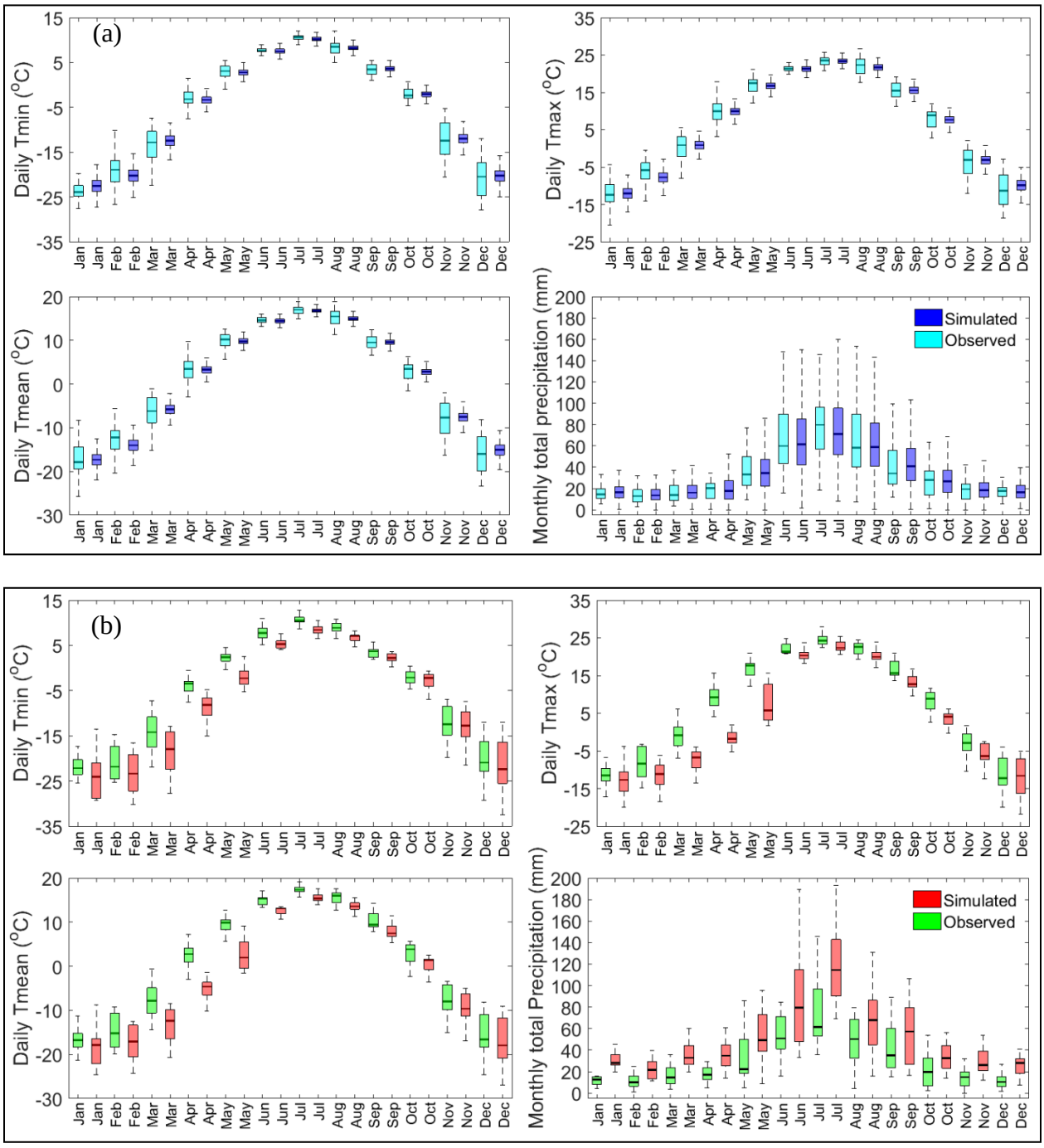

Figure 5-2: Comparison between the month-wise temperature and precipitation for the observed ECCC time series, and the time series generated by (a) LARS-WG during the historical baseline period 1976-2005 and (b) WRF-CTL during the historical baseline period 2001-2015 at Fort

McMurray Airport station. The boxplots represent the inter quartile range (IQR) values with median shown as black thick line, with whiskers showing values within 1.5 IQR extending from both ends of the boxes.

5.3.1.2 Comparison of LARS-WG and WRF in Future Periods

Changes in the monthly median temperature and precipitation from the baseline to future period predictions for the two downscaling methods are shown in Table 5-1. Overall, both models show increases in temperature and precipitation in nearly all months (the exceptions being June and September precipitation changes for WRF and the August changes in precipitation for LARS). The maximum temperature and precipitation for both models occur in July with the minimum temperature and precipitation in February for both the baseline and future periods. Both models show a similar shift in all monthly temperatures from baseline to future time periods of ≈ 3.2-8.9 ºC (average monthly change of 5.0 ºC for LARS and 5.5 ºC for WRF). They also show a consistent shift in monthly precipitation of ≈ 8.0 mm decrease to 22.9 mm increase (average monthly change of 3.4 mm for LARS and 5.8 mm for WRF). The increases in temperature in both the spring and fall highlight a potential increased growing season and a shorter winter period during which the snowpack might accumulate.

In general, the baseline and future temperature from WRF shows higher variability than those from LARS-WG. The average CV values for LARS-WG during baseline and future periods were 13.8% and 18.8%, respectively, while the corresponding CV values for WRF were 93.2% and 58.9%. In contrast, the baseline and future precipitation from LARS-WG shows greater variability than that predicted by WRF. The average CV values for LARS-WG during baseline and future periods were 52.3% and 53.6%, respectively, while the corresponding CV values for WRF were 42.3% and 40.8%. Table C-2 (Appendix C) shows the monthly CV values from the baseline to future period predictions for the two downscaling methods.

Since the LARS-WG predictions are based on adjusting the predicted precipitation probability distributions to the local scale observations, the impact of local scale convective precipitation events is implicitly reflected within these adjustments. Generally, GCMs are unable to represent the convective processes and are expected to show less variability than WRF, while both raw GCMs and WRF simulations are expected to show less variability than the site-specific

LARS-WG simulations. In this way, extreme convective events are more realistically captured by LARS-WG or WRF than GCMs simulations. The calculated CV values for the future daily precipitation for raw GCMs, WRF, and LARS-WG were 213, 219, and 242%, respectively, while the maximum daily precipitation amounts simulated by the GCMs, WRF, and LARS-WG were 61, 101, and 101 mm, respectively. However, it should be kept in mind that the WRF results are affected by the inherited biases from the driving GCMs.

Table 5-1: The median daily future Tmean and total precipitation during the baseline and future periods, and changes in median daily future Tmean and total precipitation relative to the corresponding baseline periods during each month for two downscaling methods.

	LARS-WG						WRF					
	Tmean (°C)			Precipitation (mm)			Tmean (°C)			Precipitation (mm)		
Month	Baseline	Future	Change	Baseline	Future	Change	Baseline	Future	Change	Baseline	Future	Change
Jan	-17.3	-10.2	7.1	16.5	19.5	3.0	-17.9	-12.1	5.8	28.2	38.3	10.1
Feb	-14.0	-7.7	6.3	13.8	17.2	3.4	-17.0	-11.7	5.3	21.7	26.1	4.4
Mar	-5.8	-1.1	4.7	16.4	19.9	3.5	-12.4	-5.8	6.6	32.8	48.1	15.3
Apr	3.3	6.5	3.2	18.1	21.5	3.5	-4.6	1.3	5.9	34.9	39.7	4.8
May	9.8	14.0	4.2	34.7	41.2	6.5	2.0	9.5	7.5	49.2	72.1	22.9
Jun	14.4	18.9	4.5	61.8	67.1	5.3	13.1	16.5	3.4	79.4	72.8	-6.6
Jul	16.8	21.8	5.0	71.8	78.7	6.9	15.4	19.0	3.6	114.5	114.9	0.4
Aug	15.0	20.4	5.4	59.6	55.1	-4.5	13.6	17.6	4.0	68.0	73.4	5.4
Sep	9.6	14.6	5.0	41.5	44.4	2.9	7.5	11.5	4.0	57.3	49.3	-8.0
Oct	2.8	6.4	3.6	26.9	31.7	4.8	1.4	5.6	4.2	32.7	37.2	4.5
Nov	-7.5	-3.0	4.5	18.7	21.8	3.1	-9.6	-2.5	7.1	26.3	31.8	5.5
Dec	-15.1	-8.3	6.8	16.8	19.4	2.6	-17.9	-9.0	8.9	28.2	39.3	11.1
Overall	1.0	6.0	5.0	33.1	36.5	3.4	-2.2	3.3	5.5	47.8	53.6	5.8

Both downscaling methods predict increased growing season precipitation and PET in the future (2086-2100), relative to their baseline (1976-2005 for LARS-WG and 2001-2015 for WRF), as shown in Fig. 5-3. The median growing season precipitation measured at the Fort McMurray Airport station was 387 and 362 mm during 1976-2005 and 2001-2015, respectively. These values were well estimated by LARS-WG (387 mm) but overestimated by WRF (523 mm) due to a wet bias in the WRF model inherited from the driving GCMs. The median growing season PET values estimated using the Hargreaves-Samani method for 1976-2005 and 2001-2015 were 638 and 653 mm, respectively. The LARS-WG simulation was able to replicate this PET value for the corresponding baseline period (638 mm); however, WRF (541 mm) underestimated the PET value due to a cold bias.

Despite these differences, the overall relative shift (magnitude and direction) from the baseline to the future period for both growing season precipitation and PET were similar for both models. For example, the increase in median growing season precipitation for LARS-WG was 22.7%, while WRF predicted an increase of 11.5%. The increase in median growing season PET was 19.6% for LARS-WG and 19.4% increase for WRF. The uncertainty associated with growing season precipitation was larger for LARS-WG than WRF, while the same associated with PET was larger for WRF than LARS-WG, as evident in the distribution of the corresponding boxplots (Fig. 5-3) and CV values (not shown).

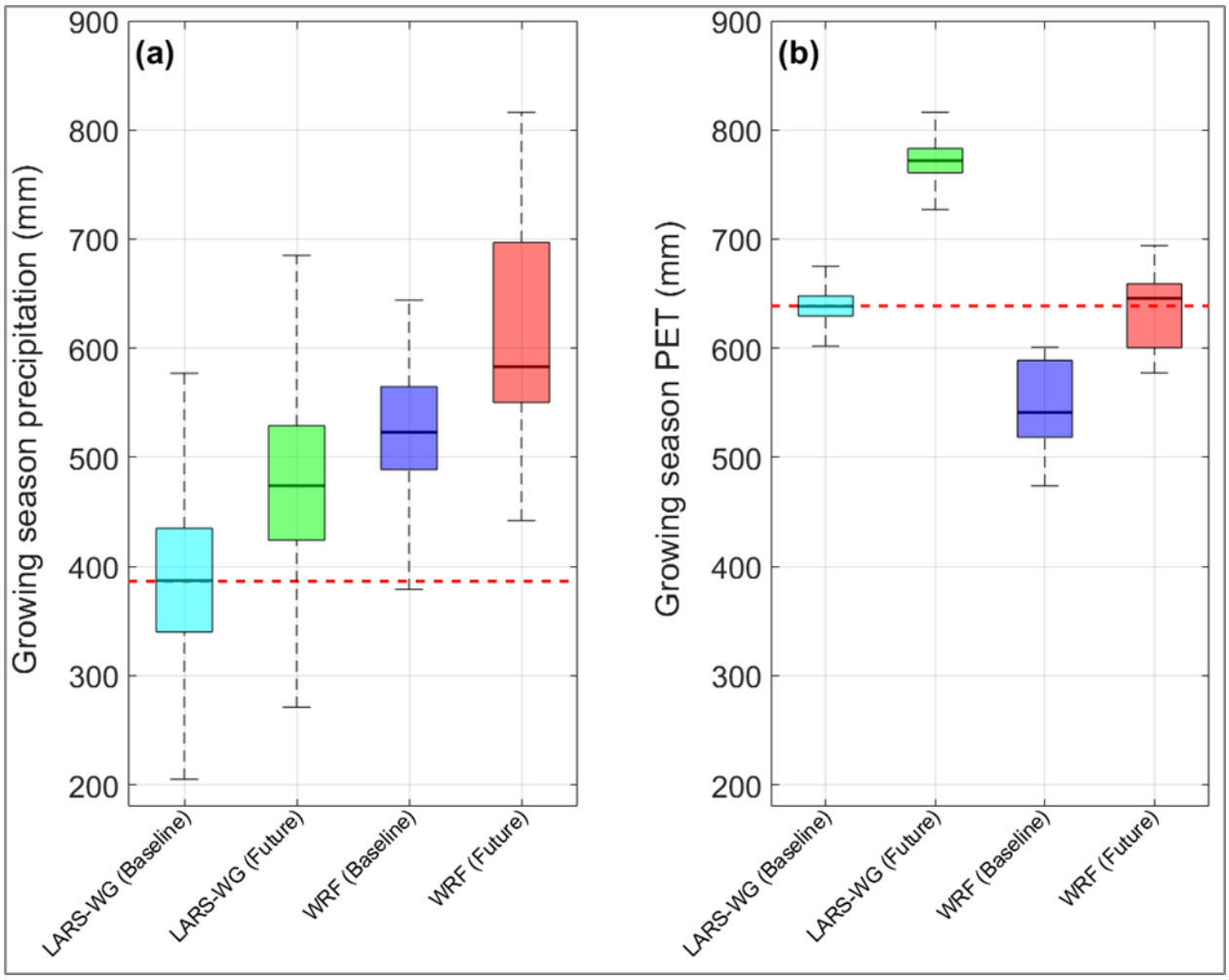

Figure 5-3: Distributions of (a) growing season precipitation and (b) growing season PET based on 100 realizations from LARS-WG during baseline (1976-2005) and future (2086-2100) periods as well as based on WRF simulations for baseline (2001-2015) and future (2086-2100) periods at Fort McMurray Airport station. The horizonal dashed lines show median growing season precipitation and PET based on the observed monitoring data at Fort McMurray Airport station during 1976-2005. Description of boxplots is given in Figure 5-2.

A probability density function (PDF) of growing season daily precipitation events can be used to compare the individual models and associated observations in a manner that highlights extreme precipitation events (Fig. 5-4). The comparison periods are 1976-2005 for LARS-WG, and 2001-2015 for WRF. It is apparent that the WRF simulations overestimate the magnitude of precipitation events at all frequencies but increasingly so for high precipitation events. The LARS-WG simulations are consistent with the observed distribution, with the exception of the most extreme event.

Fig. 5-4 also includes the distribution of daily growing season precipitation events for future periods: 2086-2100 for LARS-WG (Fig. 5-4a), and 2086-2100 for WRF (Fig. 5-4b). It is expected that an increase in extreme daily precipitation events would lead to increases in runoff. The differences in the shift of the PDF from the baseline to future predictions for the two models is quite striking. LARS-WG predicts a modest increase in daily precipitation at nearly all frequencies, while the WRF predictions show similar magnitudes of precipitation events for both baseline and future predictions at frequencies greater than 0.5% but nearly double the magnitude of events in the future from the baseline at frequencies smaller than 0.05%. These more pronounced extreme events by WRF might be due to the overestimated distribution of baseline daily extreme precipitation relative to the historical observed amounts in the case of WRF. The shifted distribution of future daily extreme precipitation amounts relative to the baseline amounts demonstrates that these extreme precipitation events could be more prevalent in a changing climate condition.

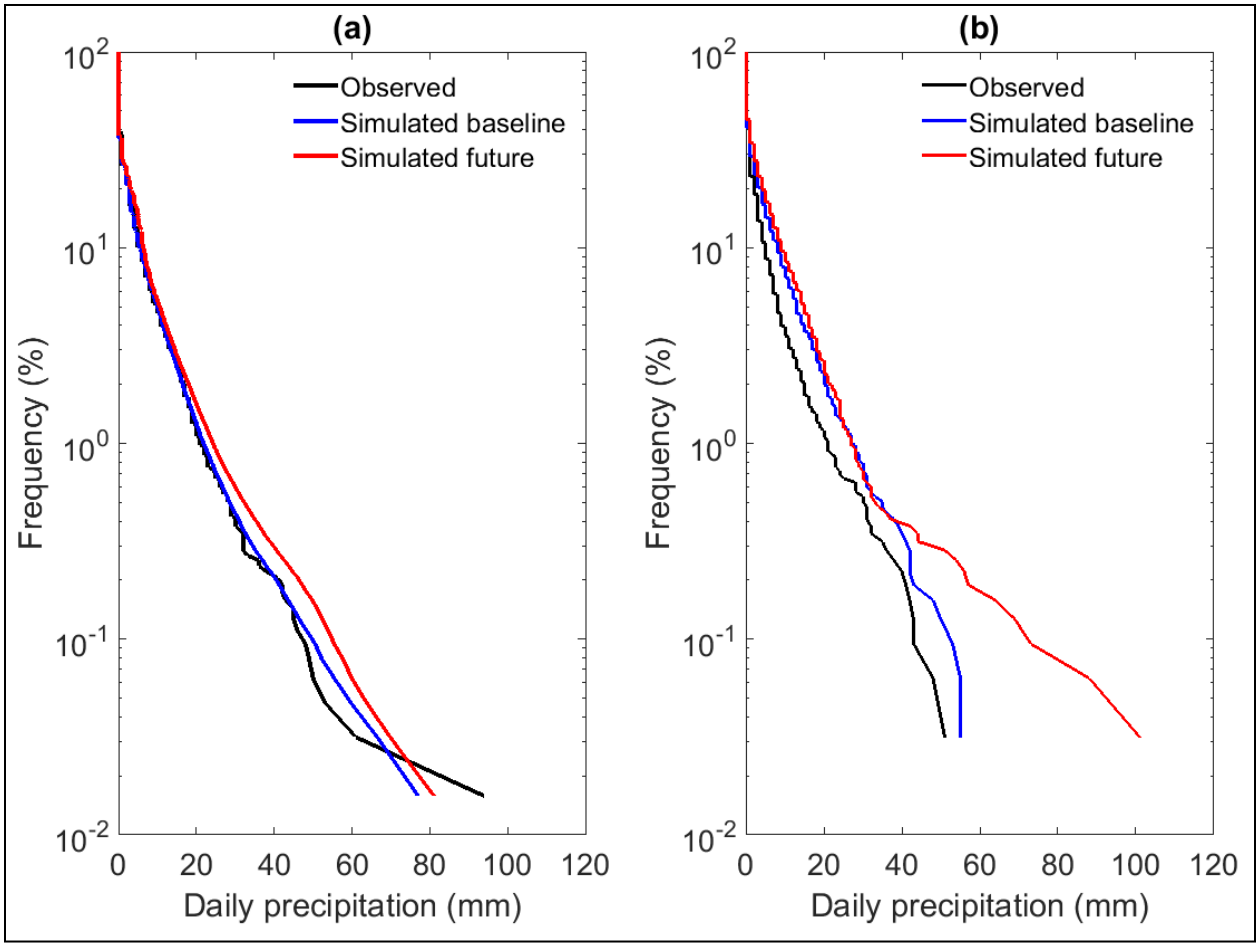

Figure 5-4: Probability density function of daily precipitation during the growing season (i.e. April to October) at Fort McMurray Airport Station as (a) observed during 1976-2005, statistically downscaled by LARS-WG for the baseline (1976-2005) and future (2086-2100) periods and (b) observed during 2001-2015, dynamically downscaled by WRF for the baseline (2001-2015) and future (2086-2100) periods.

5.3.2 Simulated water balance components

The baseline historical climate projections for LARS-WG (1976-2005) and WRF (2001-2015) as well as the future projections (2086-2100) for both models were used as climatic inputs to the Hydrus water balance modeling of each of the three reclamation cover sites (D3, SWSS, and ACS) and the three natural soil profile sites (SV10, SV27, and SV60).

Figure 5-5 presents the simulated AET for the three reclamation covers and natural soil profiles. The AET for the reclamation covers are higher than for the natural soil profiles in all cases due to the finer texture of the reclamation covers (Alam et al. 2018). The magnitude and

direction of change in the future median growing season AET, relative to the corresponding baseline AET using the two downscaling methods are similar for all of the study sites.

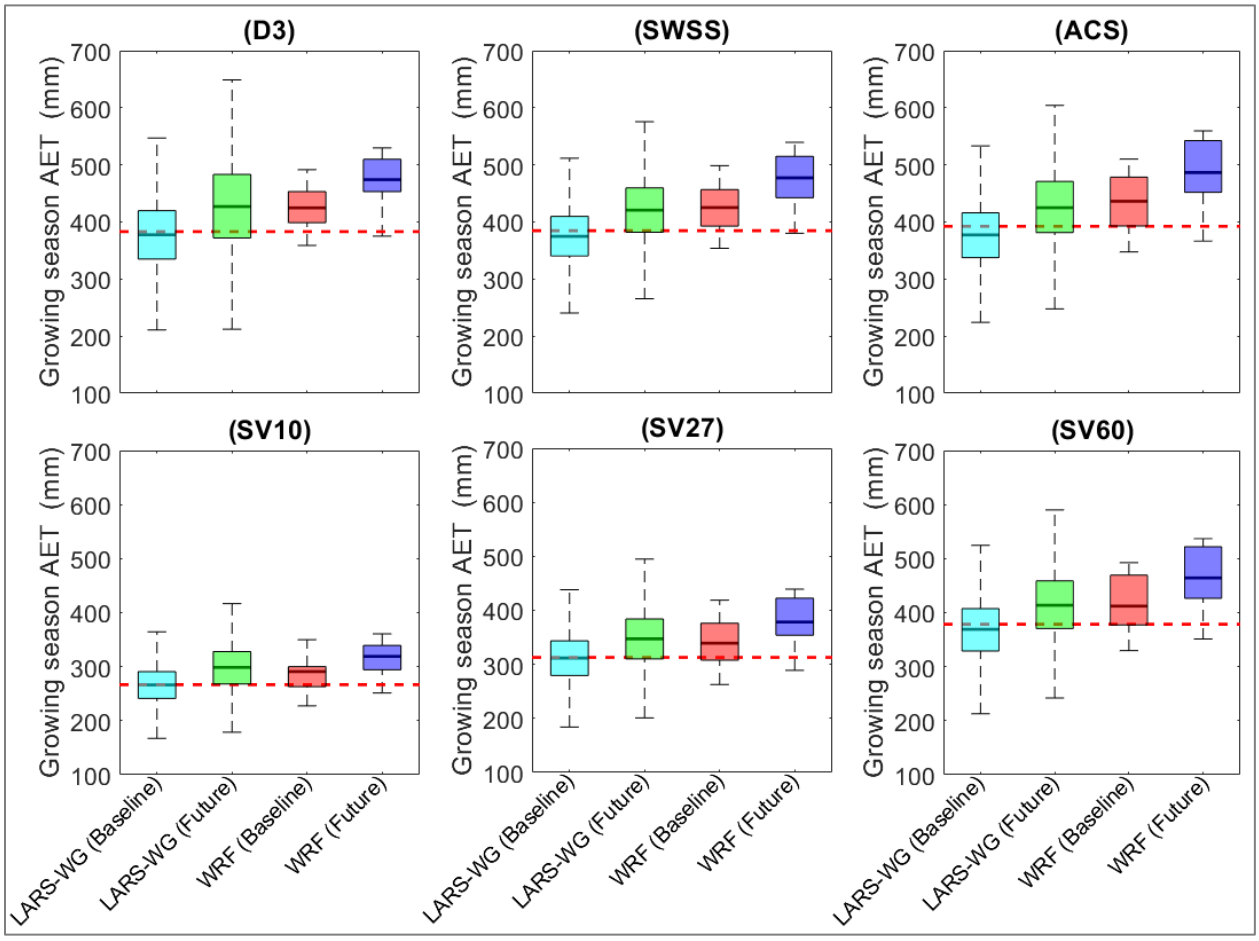

Figure 5-5: Distributions of growing season AET for 100 realizations of climate change projections from LARS-WG during 1976-2005 (i.e. Baseline) and climate change projections from WRF during 2001-2015 (i.e. Baseline) as well as during 2086-2100 (i.e. Future). The results are shown for three reclamation covers (D3, SWSS, and ACS) and three natural soil profiles (SV10, SV27, and SV60). The horizonal dashed lines show median growing season AET based on the observed monitoring data at Fort McMurray Airport station during 1976-2005. Description of boxplots is given in Figure 5-2.

Figure 5-6 presents the simulated NP using the LARS-WG and WRF projections. All simulations show that NP is higher for the three natural soil profiles than the reclamation covers, as expected given their coarser texture (Alam et al. 2018). The direction of change in future NP, relative to the corresponding baseline NP are similar for both downscaling methods with similar

directions of change in the future growing season NP for all of the study sites, although the shifts in future NP are greater for WRF than for LARS-WG.

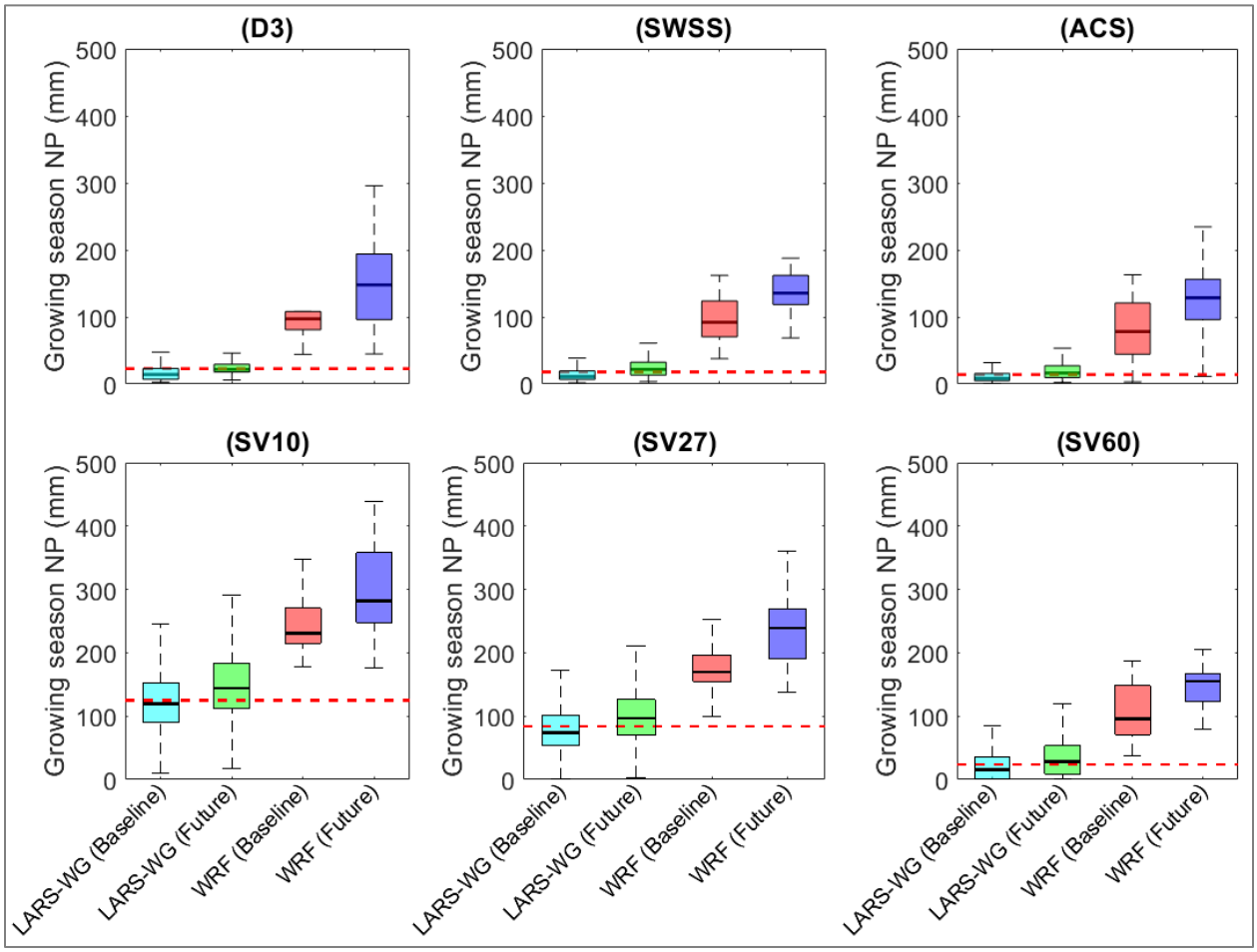

Figure 5-6: Distributions of growing season NP for 100 realizations of climate change projections from LARS-WG during 1976-2005 (i.e. Baseline) and climate change projections from WRF during 2001-2015 (i.e. Baseline) as well as during 2086-2100 (i.e. Future). The results are shown for three reclamation covers (D3, SWSS, and ACS) and three natural soil profiles (SV10, SV27, and SV60). The horizonal dashed lines show median growing season NP based on the observed monitoring data at Fort McMurray Airport station during 1976-2005. Description of boxplots is given in Figure 5-2.

The relative change in the simulated future AET relative to the baseline periods for the LARS-WG and WRF simulations are presented in Fig. 5-7. The median change in the future AET for both the WRF simulations and LARS-WG simulations are similar (boxes overlap in Fig. 5-7) to each other and similar for all cover types to the end of the 21st century. However,

Fig. 5-7 also highlights that LARS-WG based simulations have a greater degree of variability in the projected changes in AET than the WRF simulations. WRF climate projections capture more variability in monthly temperatures, while LARS-WG capture more variability in monthly precipitation. The variability in future AET and corresponding % changes appear to be controlled by variability in future precipitation rather than variability in future PET, with the result that higher variability in future precipitation leads to higher variability in future AET.

This is also true for the occurrence of extreme high and low AET values. The prevalence of extreme AET events, in the case of LARS-WG, reflects more extremely wet or dry years toward the end of the 21st century compared to the WRF simulations. This would suggest a potential shift in optimal vegetation/tree selection for reclamation covers to adapt to more variability in AET if LARS-WG simulations are used for reclamation cover design.

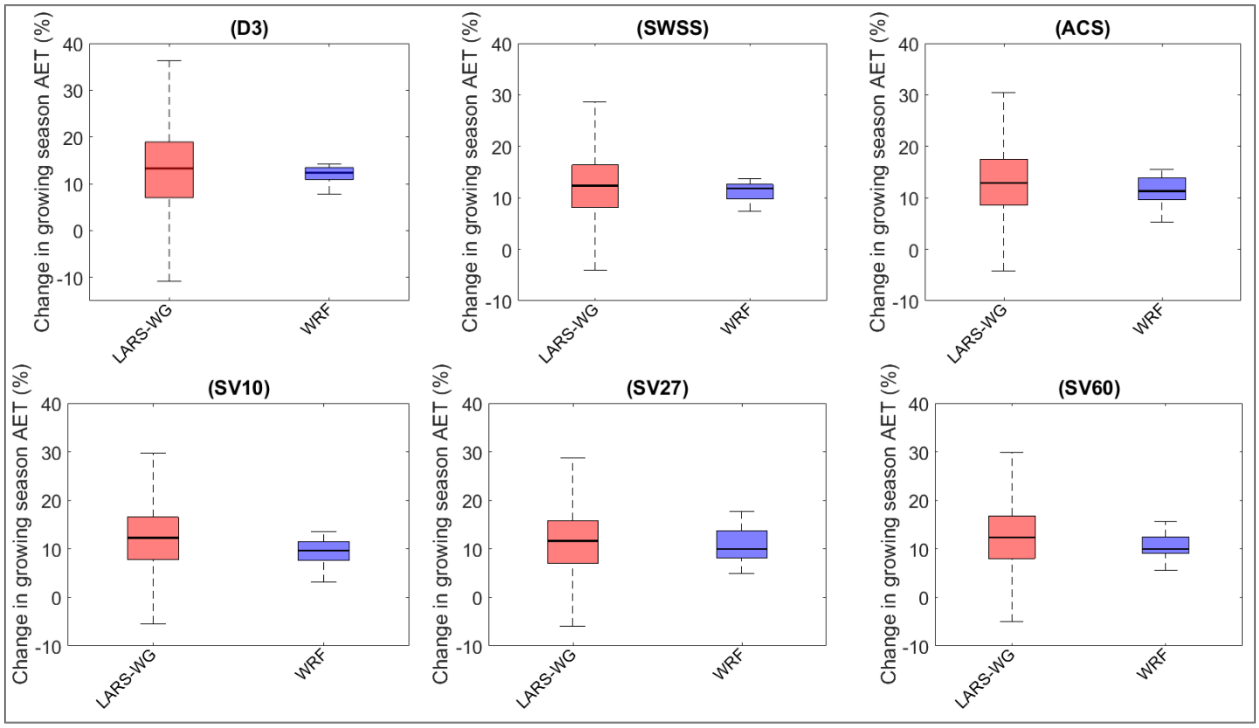

Figure 5-7: Distributions of growing season AET based on an ensemble of 17 GCMs based on RCP8.5 from CMIP5 and downscaled by LARS-WG (red boxes) and based on the climate change projections downscaled by WRF (blue boxes) during the end of the 21st century. The results are shown for three reclamation covers (D3, SWSS, and ACS) and three natural soil profiles (SV10, SV27, and SV60). Description of boxplots is given in Figure 5-2.

Figures 5-8 shows the percent change in the simulated future NP. The median % change in NP for both downscaling methods are once again similar (boxes overlap in Fig. 5-8); however, both LARS-WG and WRF show higher % changes in future NP for the reclamation covers (48-95%) than the three natural soil profiles (21-89%). Once again, the percentage change in NP exhibits more variability for the LARS-WG based simulations than for WRF, including a greater change in the percentage of extreme annual NP values.

Similar to the % changes in future AET, the variability in future NP appears to be controlled by the variability in future precipitation. The prevalence of extreme NP events, in the case of LARS-WG, reflects either more extreme wet or dry years toward the end of the 21st century compared to the WRF simulations. This might suggest that water yield from the reclaimed mine waste may be more variable if LARS-WG simulations are considered for the design of mine closure landscapes.

The relative magnitudes of the simulated precipitation for LARS-WG and WRF models seems to be reflected in the simulated water balance components (AET and NP) during the end of the 21st century. In particular, precipitation is the dominant climate variable in the predictions of the two key water balance components.

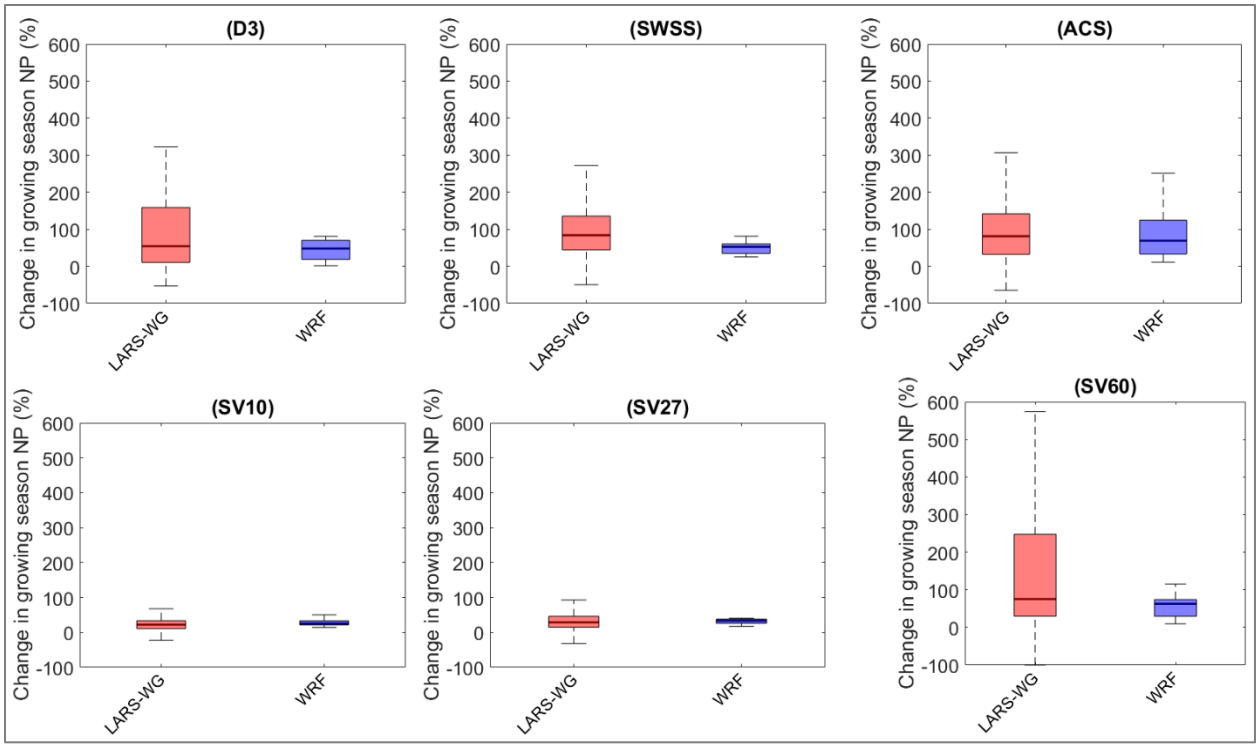

Figure 5-8: Distributions of growing season NP based on an ensemble of 17 GCMs based on RCP8.5 from CMIP5 and downscaled by LARS-WG (red boxes) and based on the climate change projections downscaled by WRF (blue boxes) during the end of the 21st century. The results are shown for three reclamation covers (D3, SWSS, and ACS) and three natural soil profiles (SV10, SV27, and SV60). Description of boxplots is given in Figure 5-2.

The range of the predicted changes in the future growing season AET and NP relative to the baseline periods is higher for LARS-WG than WRF, even though WRF predictions might be expected to capture more variability due to regional scale convective precipitation events. We mentioned earlier that LARS-WG showed higher variability in future precipitation than that shown by WRF and precipitation is the dominant variable in simulating AET and NP. It is important to note, however, that convective events generally last for only an hour in most cases. As a result, daily water balance modelling, as undertaken in this study, does not capture the potential impact of these events in triggering runoff events. The impact of these convective events is further diminished when the results are accumulated into monthly and/or growing season amounts.

The key growing season water balance components (i.e. AET and NP) for all sites are summarized in Table 5-2. The median growing season AET values from LARS-WG for the baseline period were comparable to the values reported by Alam et al. (2018) for all sites, except ACS. This was despite the baseline periods being different (1976-2005 in this study and 1961-1990 in Alam et al. 2018). The baseline period AET of the ACS site was less (377 mm) than in the previous study (402 mm; Alam et al. 2020), due to the difference in the median growing season precipitation used in the model simulations for the two baseline periods (387 mm from 1976-2005 in this study; 407 mm from 1961-1990 for Alam et al. 2018), while Alam et al. (2020) used a value of 426 mm for the baseline period 1954-2013. Zhang et al. (2018) showed that the selection of baseline period is a likely source of uncertainty in studying the impacts of climate change.

The simulated growing season NP in this study are also different from those in the previous studies because of the differences in growing season precipitation from the different baseline periods, which in turn directly affect the growing season AET and NP values, as shown by LARS-WG simulations. Considering all sites, the increases in AET are ≈ 11.4-13.1% for LARS-WG and 9.6-12.6% for WRF, while the increases in NP are ≈ 20.8-95.0% for LARS-WG and 21.9-64.5% for WRF. In particular, reclamation covers and natural soil sites show a similar range of increase in AET; however, the percentage increases in NP are more pronounced for the reclamation covers than the natural sites. The increased future AET might be expected to produce a change in overall productivity of these sites but may also result in a shift in the vegetative regime that is established. The increased future NP could lead to increased water release from these reclaimed mine waste landforms with a concomitant increase in chemical loading due to flushing of these deposits by recharge waters.

Table 5-2: Growing season median precipitation, AET, and NP for the baseline and future periods based on the LARS-WG and WRF simulations. The percentage increase in the future median precipitation, AET and NP relative to the baseline median precipitation, AET and NP is shown in the parentheses.

	Precipitation (mm)				AET (mm)				NP (mm)			
	LARS-WG		WRF		LARS-WG		WRF		LARS-WG		WRF	
Site	Baseline (1976-2005)	Future (2086-2100)	Baseline (2001-2015)	Future (2086-2100)	Baseline (1976-2005)	Future (2086-2100)	Baseline (2001-2015)	Future (2086-2100)	Baseline (1976-2005)	Future (2086-2100)	Baseline (2001-2015)	Future (2086-2100)
D3	387	474 (22.7%)	523	583 (11.5%)	377	427 (13.1%)	425	474 (11.6%)	14.2	21.9 (53.9%)	97.3	148 (52.0%)
SWSS	387	474 (22.7%)	523	583 (11.5%)	375	421 (12.2%)	425	477 (12.2%)	11.2	21.9 (94.7%)	92.2	136 (47.2%)
ACS	387	474 (22.7%)	523	583 (11.5%)	377	425 (12.6%)	436	487 (11.5%)	8.5	16.5 (95.0%)	78.2	129 (64.5%)
SV10	387	474 (22.7%)	523	583 (11.5%)	266	299 (12.2%)	291	319 (9.6%)	119	144 (20.8%)	231	282 (21.9%)
SV27	387	474 (22.7%)	523	583 (11.5%)	312	347 (11.4%)	339	378 (11.6%)	74.3	96.6 (30.1%)	170	239 (40.7%)
SV60	387	474 (22.7%)	523	583 (11.5%)	369	414 (12.1%)	412	464 (12.6%)	15.1	28.5 (88.9%)	95.3	155 (62.8%)

5.4 Conclusions

The impact of climate change projections on the long-term water balances of reclamation covers, as well as natural soil profiles, was evaluated using a physically-based water balance model and future climate change predictions from different downscaling methods. The use of both dynamical (WRF) and statistical (LARS-WG) downscaling methods provides a novel approach for comparing the long-term future performances of reclamation covers compared to those of natural soil profiles.

When comparing the simulated temperature and precipitation from the downscaling models to the observational data, it is clear that the statistical downscaling method (LARS-WG) outperformed the dynamical downscaling method (WRF). In most months, WRF predictions systematically underestimated temperature and overestimated precipitation. In addition, the computational demand for WRF simulations was much higher than that for LARS-WG. The directional shifts in the monthly future temperature and precipitation from the baseline periods were, however, similar for both downscaling methods. Both downscaling methods also showed similar directional shifts in the future median growing season AET and NP from the baseline periods.

The magnitude of increase in growing season median AET and NP using the WRF climate predictions were not significantly different from those using the LARS-WG climate predictions, although LARS-WG showed more variability in these water balance components. Overall, the increases (%) in future NP were significantly higher than increases (%) in future AET, particularly for the reclamation covers. LARS-WG based projections had more extreme (high and low) AET and NP values than the WRF model. Although the two downscaling methods are based on different approaches, both methods indicate similar relative changes in the growing season water balance components (i.e. AET and NP) by the end of the 21st century. Overall, the changes in the future key water balance components for LARS-WG show greater variability than those of the WRF model.

The systematic under- and over-estimation of temperature and precipitation, respectively, during the baseline period (2001-2015) by WRF was explained by Li et al. (2019) as being due to cold and wet biases, respectively. These biases are expected to carry into the future projections

and the resulting future growing season water balance components. This allows the relative changes in the water balance components arising due to climate change to be evaluated, but not the absolute values. The WRF model would require bias correction to generate realistic absolute water balance components.

Both downscaling methods have advantages and limitations, although further comparisons for aligned modelling time frames will be required to guide policy makers and industry on how to best make reliable decisions on cover performance. It is likely that a multi-model approach (multiple GCM, RCPs, and downscaling methods) will be required to fully explore the potential impact of future climate changes on reclamation cover performance and ultimately on mine closure strategies.

Since the LARS-WG and WRF showed similar directions of shifts in the future water balance components from the baseline periods using an ensemble of GCMs from CMIP5, future extensions of this study will re-evaluate the shifts in future water balance components from LARS-WG and WRF using the newly released ensemble of GCMs from CMIP6. The CMIP6 includes more GCMs and newly developed socio-economic emission scenarios (Eyring et al. 2016). Further evaluation will be expanded to the full range of reclamation covers and mine waste types currently being used by the oil sands industry (e.g. reclamation covers over overburden, lean oil sands, coke, treated fine tailings). The relative contributions of spatial and temporal variability in the soil hydraulic properties and future climate variability to the total variability in the water balance components will be investigated using the full range of reclamation covers being monitored over many years and climate change projections from the downscaling methods.

5.5 Acknowledgements

The work was financed by the Natural Sciences and Engineering Research Council of Canada (NSERC) and Syncrude Canada Ltd. (File No. IRCPJ 428588-11; IRCSA 428587-11). Special thanks to (a) Dr. Zhenhua Li for sharing the WRF model outputs, and (b) Amy Heidman of O'Kane Consultants Inc. for providing uninterrupted access to the Syncrude watershed research database. We thank Stephanie Villeneuve for preparing Fig. 5-1.

References

Alam MS, Barbour SL, Huang M (2020) Characterizing uncertainty in the hydraulic parameters of oil sands mine reclamation covers and its influence on water balance predictions. Hydrol Earth Syst Sci 24: 735-759. https://doi.org/10.5194/hess-24-735-2020

Alam MS, Barbour SL, Elshorbagy A, Huang M (2018) The impact of climate change on the water balance of oil sands reclamation covers and natural soil profiles. J Hydrometeorol 19: 1731-1752. https://doi.org/10.1175/JHM-D-17-0230.1

Alam MS, Barbour SL, Elshorbagy A, Huang M (2017) The impact of climate change on the performance of oil sands reclamation covers: a comparison of multiple general circulation models and representative concentration pathways. Proc, 70th Canadian Geotechnical Soc Conf, Ottawa, pp 8

Alam MS, Elshorbagy A (2015) Quantification of the climate change-induced variations in intensity-duration-frequency curves in the Canadian prairies. J Hydrol 527: 990–1005. https://doi.org/10.1016/j.jhydrol.2015.05.059

Alexander LV, Zhang X, Peterson TC, Caesar J, Gleason B, Klein Tank AMG, Haylock M, Collins D, Trewin B, Rahimzadeh F, Tagipour A, Rupa Kumar K, Revadekar J, Griffiths G, Vincent L, Stephenson DB, Burn J, Aguilar E, Brunet M, Taylor M, New M, Zhai P, Rusticucci M, Vazquez-Aguirre JL (2006) Global observed changes in daily climate extremes of temperature and precipitation. J Geophys Res 111: 1-22. https://doi.org/10.1029/2005JD006290

Barbour SL, Chapman D, Qualizza C, Kessler S, Boese C, Shurniak R, Meiers M, O'Kane M, Wall S (2004) Tracking the evolution of reclaimed landscapes through the use of instrumented watersheds – A brief history of the Syncrude southwest 30 overburden reclamation research program. Proc, International Instrumented Watershed Symposium, Edmonton, pp 8

Bockstette J (2018) The role of soil reconstruction and soil amendments in forest reclamation. MSc thesis, Department of Rnewable Resources, Univ of Alberta

Boese CD (2003) The design and installation of a field instrumentation program for the evaluation of soil-atmosphere water fluxes in a vegetated cover over saline/sodic shale

overburden. MSc thesis, Univ of Saskatchewan.

CAPP (Canadian Assoc of Petroleum Producers) (2019) Crude oil forecast, markets and transportation [online]. Available at https://www.capp.ca/resources/reports/. Accessed: Jan. 10, 2020.

Carrera-Hernandez JJ, Mendoza CA, Devito KJ, Petrone RM, Smerdon BD (2011) Effects of aspen harvesting on groundwater recharge and water table dynamics in a subhumid climate. Water Resources Research 47(5): 1-18. https://doi.org/10.1029/2010WR009684

Castro CL, Pielke RA, Leoncini G. (2005) Dynamic downscaling: Assessment of value retained and added using the regional atmospheric modeling system (RAMS). J Geophys Res 110: 1-21. https://doi.org/10.1029/2004JD004721

Chen H (2013) Projected change in extreme rainfall events in China by the end of the 21st century using CMIP5 models. Chinese Sci Bull 58(12): 1462–1472. https://doi.org/10.1007/s11434-012-5612-2

Chun KP, Wheater HS, Nazemi A, Khaliq MN (2013) Precipitation downscaling in Canadian prairie provinces using the LARS-WG and GLM approaches. Can Water Resour J 38(4): 311–332. https://doi.org/10.1080/07011784.2013.830368

CEMA (Cumulative Environmental Management Assoc) (2006) Land capability classification system for forest ecosystems in the oil sands, 3rd edition, volume 1: Field manual for land capability determination. Alberta Environment.

Dee DP, Uppala SM, Simmons AJ, Berrisford P, Poli P, Kobayashi S, Andrae U, Balmaseda MA, Balsamo G, Bauer P, Bechtold P, Beljaars ACM, van de Berg L, Bidlot J, Bormann N, Delsol C, Dragani R, Fuentes M, Geer AJ, Haimberger L, Healy SB, Hersbach H, Holm EV, Isaksen L, Kallberg P, Kohler M, Matricardi M, McNally AP, Monge-Sanz BM, Morcrette JJ, Park BK, Peubey C, de Rosnay P, Tavolato C, Thepaut JN, Vitart F (2011) The ERA-Interim reanalysis: configuration and performance of the data assimilation system. Q J R Meteorol Soc 137(656): 553–597. https://doi.org/ 10.1002/qj.828

Dobchuk BS, Shurniak RE, Barbour SL, O'Kane MA, Song Q (2013) Long-term monitoring and modelling of a reclaimed watershed cover on oil sands tailings. Int J Min Reclam Env 27(3): 180–201. https://doi.org/ 10.1080/17480930.2012.679477

Done J, Davis CA, Weisman M (2004) The next generation of NWP: explicit forecasts of convection using the weather research and forecasting (WRF) model. Atmos Sci Lett 5(6): 110–117. https://doi.org/10.1002/asl.72

Eyring V, Bony S, Meehl GA, Senior CA, Stevens B, Stouffer RJ, Taylor KE (2016) Overview of the coupled model intercomparison project phase 6 (CMIP6) experimental design and organization. Geosci Model Dev 9: 1937–1958. https://doi.org/ 10.5194/gmd-9-1937-2016

Feddes RA, Bresler E, Neuman SP (1974) Field test of a modified numerical model for water uptake by root systems. Water Resour Res 10: 1199–1206. https://doi.org/10.1029/WR010i006p01199

Foley AM (2010) Uncertainty in regional climate modelling: A review. Prog Phys Geogr 34: 647–670. https://doi.org/10.1177/0309133310375654

Fosser G, Khodayar S, Berg P (2015) Benefit of convection permitting climate model simulations in the representation of convective precipitation. Clim Dyn 44(1-2): 45–60. https://doi.org/10.1007/s00382-014-2242-1

Fowler HJ, Blenkinsop S, Tebaldi C (2007) Linking climate change modelling to impacts studies : recent advances in downscaling techniques for hydrological. Int J Climatol 27: 1547–1578. https://doi.org/10.1002/joc

Gao Y, Fu JS, Drake JB, Liu Y, Lamarque JF (2012) Projected changes of extreme weather events in the eastern United States based on a high resolution climate modeling system. Environ Res Lett 7(4): 1-12. https://doi.org/10.1088/1748-9326/7/4/044025

Government of Alberta (2017) Oil sands: Facts and stats. In: Government of Alberta. open.alberta.ca/publications/oil-sands-facts-and-stats Accessed 2020-01-06

Hargreaves GH, Samani ZA (1985) Reference crop evapotranspiration from temperature. Appl Eng Agric 1(2): 96–99.

Hassanzadeh E, Nazemi A, Elshorbagy A (2014) Quantile-based downscaling of precipitation using genetic programming: Application to IDF curves in Saskatoon. J Hydrol Eng 19(5): 943–955. https://doi.org/10.1061/(ASCE)HE.1943-5584.0000854

Held IM, Soden BJ (2006) Robust responses of the hydrological cycle to global warming. J

Climate 19(21): 5686–5699. https://doi.org/10.1175/JCLI3990.1

Huang M, Barbour SL, Carey SK (2015a) The impact of reclamation cover depth on the performance of reclaimed shale overburden at an oil sands mine in Northern Alberta, Canada. Hydrol Process 29(12): 2840–2854. https://doi.org/10.1002/hyp.10229

Huang M, Hilderman JN, Barbour SL (2015b) Transport of stable isotopes of water and sulphate within reclaimed oil sands saline-sodic mine overburden. J Hydrol 529: 1550–1561. https://doi.org/10.1016/j.jhydrol.2015.08.028

Huang M, Elshorbagy A, Lee Barbour S, Zettl J, Si BC (2011a) System dynamics modeling of infiltration and drainage in layered coarse soil. Can J Soil Sci 91(2): 185–197. https://doi.org/10.4141/cjss10009

Huang M, Lee Barbour S, Elshorbagy A, Zettl J, Si BC (2011b) Water availability and forest growth in coarse-textured soils. Can J Soil Sci 91(2): 199–210. https://doi.org/10.4141/cjss10012

Huang M, Lee Barbour S, Elshorbagy A, Zettl JD, Si BC (2011c) Infiltration and drainage processes in multi-layered coarse soils. Can J Soil Sci 91(2): 169–183. https://doi.org/10.4141/cjss09118

IPCC (Intergovernmental Panel on Climate Change) (2013) Climate change 2013: the physical science basis. In: Stocker, et al. (Eds.), Contribution of Working Group I to the Fifth Assessment Report of the Intergovernmental Panel on Climate Change. Cambridge University Press, Cambridge, United Kingdom and New York.

IPCC (Intergovernmental Panel on Climate Change) (2000) Land Use, Land-Use Change and Forestry: A Special Report of the IPCC. Watson, R., Noble I., Bolin, B., Ravindranath, N. H., Verardo, D., & Andrasko, K. (eds)

Joubert AM, Hewitson BC (1997) Simulating present and future climates of southern Africa using general circulation models. Prog Phys Geogr 21(1): 51–78. doi/pdf/10.1177/030913339702100104

Karl TR, Knight RW, Plummer N (1995) Trends in high-frequency climate variability in the twentieth century. Nature,377(6546): 217–220. https://doi.org/10.1038/377217a0

Keshta N, Elshorbagy A, Carey S (2012) Impacts of climate change on soil moisture and evapotranspiration in reconstructed watersheds in northern Alberta, Canada. Hydrol Process 26(9): 1321–1331. https://doi.org/10.1002/hyp.8215

Keshta N, Elshorbagy A, Carey S (2009) A generic system dynamics model for simulating and evaluating the hydrological performance of reconstructed watersheds. Hydrol Earth Syst Sci 13(6), 865–881, https://doi.org/10.5194/hess-13-865-2009

Li Y, Li Z, Zhang Z, Chen L, Kurkute S, Scaff L, Pan X (2019) High-resolution regional climate modeling and projection over western Canada using a weather research forecasting model with a pseudo-global warming approach. Hydrol Earth Syst Sci 23(11): 4635–4659. https://doi.org/10.5194/hess-23-4635-2019

Li Y, Szeto K, Stewart RE, Thériault JM, Chen L, Kochtubajda B, Liu A, Boodoo S, Goodson R, Mooney C, Kurkute S (2017) A numerical study of the June 2013 flood-producing extreme rainstorm over southern Alberta. J Hydrometeorol 18(8): 2057–2078. https://doi.org/10.1175/JHM-D-15-0176.1

Liu C, Ikeda K, Rasmussen R, Barlage M, Newman AJ, Prein AF, Chen F, Chen L, Clark M, Dai A, Dudhia J, Eidhammer T, Gochis D, Gutmann E, Kurkute S, Li Y, Thompson G, Yates D (2017) Continental-scale convection-permitting modeling of the current and future climate of North America. Clim Dyn 49(1-2): 71–95. https://doi.org/10.1007/s00382-016-3327-9

May W (2008) Potential future changes in the characteristics of daily precipitation in Europe simulated by the HIRHAM regional climate model. Clim Dyn 30(6): 581–603. https://doi.org/10.1007/s00382-007-0309-y

Meehl GA, Covey C, Delworth T, Latif M, McAvaney B, Mitchell JFB, Stouffer RJ, Taylor KE (2007) The WCRP CMIP3 multimodel dataset: A new era in climate change research. Bull Am Meteorol Soc 88(9): 1383–1394. https://doi.org/10.1175/BAMS-88-9-1383

Meehl GA, Covey C, Mcavaney B, Latif M, Stouffer RJ (2004) Overview of the Coupled Model Intercomparison Project. Bull Am Meteorol Soc 86(1): 89-96. https://doi.org/10.1175/BAMS-86-1-89

Meiers GP, Barbour SL, Qualizza C V, Dobchuk BS (2011) Evolution of the Hydraulic Conductivity of Reclamation Covers over Sodic/Saline Mining Overburden. J Geotech and

Geoenviron 137(10): 968–976. https://doi.org/10.1061/(ASCE)GT.1943-5606.0000523

Mitchell TD, Hulme M (1999) Predicting regional climate change: Living with uncertainty. Prog Phys Geogr 23: 57–78. https://doi.org/10.1191/030913399672023346

Nazemi A, Elshorbagy A, Pingale S (2011) Uncertainties in the estimation of future annual extreme daily rainfall for the city of Saskatoon under climate change effects. Proc, 20th Canadian Hydrotechnical Conf, Ottawa, pp 10

OKC (O'Kane Consultants Inc.) (2016) Instrumented watershed monitoring program at the southwest sands storage facility: Performance monitoring report for the period January 2015 to December 2015. OKC Report 690-01-72, pp 26

OKC (O'Kane Consultants Inc.) (2001) Southwest sand storage and 30-dump automated water balance monitoring systems at Syncrude Canada Ltd. OKC Report 653-2, pp 19

Prein AF, Rasmussen RM, Ikeda K, Liu C, Clark MP, Holland GJ (2017) The future intensification of hourly precipitation extremes. Nat Clim Chang 7(1): 48–52. https://doi.org/10.1038/nclimate3168

Price JS, McLaren RG, Rudolph DL (2010) Landscape restoration after oil sands mining: conceptual design and hydrological modelling for fen reconstruction. Int J Min Reclam Env 24(2): 109–123. https://doi.org/: 10.1080/17480930902955724

Qualizza C, Chapman D, Barbour SL, Purdy B (2004) Reclamation research at Syncrude Canada's mining operation in Alberta's Athabasca oil sands region. Proc, 16th International Conf on Ecological Restoration SER2004, Victoria.

Racsko P, Szeidl L, Semenov M (1991) A serial approach to local stochastic weather models. Ecol Model 57(1-2): 27–41. https://doi.org/10.1016/0304-3800(91)90053-4

Rasmussen R, Ikeda K, Liu C, Gochis D, Clark M, Dai A, Gutmann E, Dudhia J, Chen F, Barlage M, Yates D, Zhang G (2014) Climate Change Impacts on the Water Balance of the Colorado Headwaters: High-Resolution Regional Climate Model Simulations. J Hydrometeorol 15(3): 1091–1116. https://doi.org/10.1175/JHM-D-13-0118.1

Rasmussen R, Liu C, Ikeda K, Gochis D, Yates D, Chen F, Tewari M, Barlage M, Dudhia J, Yu W, Miller K, Arsenault K, Grubisic V, Thompson G, Gutmann E (2011) High-Resolution

Coupled Climate Runoff Simulations of Seasonal Snowfall over Colorado: A Process Study of Current and Warmer Climate. J Climate 24(12): 3015–3048. https://doi.org/10.1175/2010JCLI3985.1

Semenov MA (2007) Development of high-resolution UKCIP02-based climate change scenarios in the UK. Agric For Meteorol 144(1-2): 127–138. https://doi.org/10.1016/j.agrformet.2007.02.003

Semenov MA, Barrow EM (1997) Use of a stochastic weather generator in the development of climate change scenarios. Clim Change 35(4): 397–414. https://doi.org/10.1023/A:1005342632279

Sigouin, M.J.P., Dyck, M., Si, B.C., Hu W (2016) Monitoring soil water content at a heterogeneous oil sand reclamation site using a cosmic-ray soil moisture probe. J Hydrol 543(Part B): 510–522. https://doi.org/10.1016/j.jhydrol.2016.10.026

Simunek J, Sejna M, Saito H, Sakai M, van Genuchten MT (2013) The HYDRUS software package for simulating the two- and three- dimensional movement of water, heat, and multiple solutes in variably-saturated media, Technical manual version 2.0. University of California, Riverside, CA.

Skamarock C, Klemp B, Dudhia J, Gill O, Barker D, Duda G, Huang X, Wang W, Powers G (2008) A description of the advanced research WRF version 3. NCAR Technical Note NCAR/TN-475+STR (2008). https://doi.org/10.5065/D68S4MVH

Srivastav RK, Schardong A, Simonovic SP (2014) Equidistance quantile matching method for updating IDF curves under climate change. Water Resour Manag 28(9): 2539–2562. https://doi.org/10.1007/s11269-014-0626-y

Strong WL, Leggat KR (1981) Ecoregions of Alberta. Alberta Energy and Natural Resources Tech. Report T/4, pp 64

Sun J (2014) Record-breaking SST over mid-North Atlantic and extreme high temperature over the Jianghuai–Jiangnan region of China in 2013. Chinese Sci Bullet 59(27): 3465–3470. https://doi.org/10.1007/s11434-014-0425-0

Suncor Energy Inc. (2007) Climate change in the oil sands region. Voyager South Project Environmental Impact Reprot, Appendix 3, pp 134. In: Government of Alberta.

open.alberta.ca/publications/4070009 Accesed 2020-01-06

Taylor KE, Stouffer RJ, Meehl GA (2012) An overview of CMIP5 and the experiment design. Bull Am Meteorol Soc 93(4): 485–498. https://doi.org/10.1175/BAMS-D-11-00094.1

Thompson C, Mendoza CA, Devito KJ (2017) Potential influence of climate change on ecosystems within the Boreal Plains of Alberta. Hydrol Process 31(11): 2110–2124. https://doi.org/10.1002/hyp.11183

Weisman ML, Davis C, Wang W, Manning KW, Klemp JB, Weisman ML, Davis C, Wang W, Manning KW, Klemp JB (2008) Experiences with 0–36-h explicit convective forecasts with the WRF-ARW model. Weather Forecast 23(3): 407–437. https://doi.org/10.1175/2007WAF2007005.1

Wilby RL, Dawson CW (2007) SDSM 4.2 – A decision support tool for the assessment of regional climate change impacts: Version 4.2, User Manual, Lancaster University, UK.

Wilby RL, Wigley TML, Conway D, Jones PD, Hewitson BC, Main J, Wilks DS (1998) Statistical downscaling of general circulation model output: A comparison of methods. Water Resour Res, 34: 2995–3008. https://doi.org/10.1029/98WR02577

Wilby RL, Wigley TML (1997) Downscaling general circulation model output: a review of methods and limitations. Prog Phys Geogr 21(4): 530–548. https://doi.org/ 10.1177/030913339702100403

Wood AW, Lettenmaier DP, Palmer RN (1997) Assessing climate change implications for water resources planning. Clim Change 37: 203–228. https://doi.org/10.1007/978-94-017-1051-0_12

Zettl J, Lee Barbour S, Huang M, Si BC, Leskiw LA (2011) Influence of textural layering on field capacity of coarse soils. Can J Soil Sci 91(2): 133–147. https://doi.org/10.4141/cjss09117

Zhang L, Nan Z, Yu W, Zhao Y, Xu Y (2018) Comparison of baseline period choices for separating climate and land use/land cover change impacts on watershed hydrology using distributed hydrological models. Sci Total Environ 622–623: 1016–1028. https://doi.org/10.1016/j.scitotenv.2017.12.055

Zhang X, Vincent LA, Hogg W, Niitsoo A (2000) Temperature and precipitation trends in Canada during the 20th century. Atmos Ocean 38(3): 395–429. https://doi.org/10.1080/07055900.2000.9649654

CHAPTER 6 - CONCLUSIONS AND RECOMMENDATIONS

6.1 General conclusions

Spatial and temporal variability (i.e. variability in model parameters and climate including climate change) has not previously utilized within SVAT models used to evaluate long-term hydrologic performance of mine reclamation covers, particularly those associated with oil sands mining. The global objective of the research presented in this thesis was to develop methods for evaluating spatial and temporal variability in the interpretation of the hydrologic performance of oil sands reclamation covers and to incorporate this variability in SVAT models to evaluate the performance of these covers over the long-term.

Three specific objectives were set out to address in this work:

(1) To quantify parameter variability in the modelling of water balance for oil sands reclamation covers by obtaining optimized parameter sets for the cover materials based on independent soil monitoring locations (spatial variability) and for different time series (temporal variability), using the combination of the SVAT modelling packages and inverse modelling techniques;

(2) To characterize the impact that future projected climate change will have on the water balance of oil sands reclamation covers; and

(3) To evaluate methods of downscaling global climate change projections to regional (local) scales to evaluate changes in future water balances.

The key findings from this research in regard to each of these objectives will be summarized in the following subsections.

6.1.1 Impact of parameter variability on water balance predictions

Five soil hydraulic parameters were optimized using inverse modelling (IM) to produce 155 sets of soil hydraulic parameters for 13 treatment covers, replicated in triplicate, over four monitoring years (Chapter 3, Manuscript #1). Progressive Latin Hypercube Sampling (PLHS) was used to sample parameters from the distributions of each of the five hydraulic parameters obtained from the IM approach. The results from the simulations were used to highlight the coupling that occurs between the parameter variability and the maximum sustainable leaf area

index (LAI_max) values as well as the combined impact of the variability in these parameters on the simulated long-term distributions of AET and NP for the five illustrative covers.

The study demonstrated that in the case of the ACS site, the highest variability in the WRC and Ks was associated with the peat cover layer and the LOS substrate, respectively. Combining peat with LFH might have produced additional variability in the WRC among the three soil types used in the reclamation covers. In the long-term simulations, climate variability was the primary source of variability in annual AET while both climate and parameter variability exerted the greatest influence on variability in NP. The variability in the simulated AET values decreased with an increasing cover thickness for parameter variability, while the variability in the simulated NP values decreased with an increasing cover thickness for both parameter and climate variability. The median annual AET of thinner covers, while the median annual NP of thicker covers seemed insensitive to the variability derived from variable parameter sets and climate data. The PLHS and MC sampling methods produced a wider range of simulated AET and NP compared to the percentile-based sampling approach.

6.1.2 Impact of climate change on water balance components

Future climate change projections from the most recent GCM outputs were used along with a physically based SVAT water balance model to evaluate changes in the future water balances of reclamation soil covers and natural soil profiles near Fort McMurray, Alberta, Canada (Chapter 4, Manuscript #2).

During the historical baseline period (1961-1990), reclamation covers show higher AET and lower NP than the natural sites. Overall, the important water balance components (i.e., AET and NP) of the reclamation covers and natural sites are expected to increase throughout the 21st century for all the RCPs, time periods, and soil profiles considered. The median growing season AET and NP showed greater increase toward the end of the 21st century in response to increases in growing season PET and precipitation. The shifts in future NP relative to the baseline period were more dramatic when compared to shifts in future AET for the sites with higher water storage (i.e., the two reclamation covers).

6.1.3 Impact of downscaling methods on water balance predictions

The impact of climate change projections on the long-term water balances of reclamation covers as well natural soil profiles was evaluated using the changes in future water balance relative to the baseline values as projected by an ensemble of multiple GCMs from CMIP5 and downscaled by LARS-WG and WRF (Chapter 5, Manuscript #3). The use of both statistical (LARS-WG) and dynamical (WRF) downscaling methods provides a novel approach to evaluate changes in the water balance of reclamation covers and natural soil profiles into the future.

Key findings of the study show that the magnitude of the increase in growing season median AET and NP from WRF is not significantly different from that simulated by LARS-WG, although LARS-WG shows more variability in future precipitation. In addition, the magnitude of the increase in future NP is significantly higher than the increases in future AET, particularly for the reclamation covers. Although the two downscaling methods are based on different approaches, both methods indicate similar relative changes in the growing season key water balance components (i.e. AET and NP) by the end of the 21st century. Overall, the changes in the future key water balance components for LARS-WG show greater variability than those for the WRF model.

6.2 Implications of the study

The first objective helped to characterize the cover performance risks associated with parameter variability combined with climate, LAI, and cover thickness variability. Characterization of parameter variability presents a novel analysis tool to characterize uncertainty associated with the long-term cover performance which is not possible using conventional analysis approach using a single set of optimized model parameters. This may prove to be a valuable tool for industry to help quantify the risk associated with mine closure performance. Risk assessments cannot be carried out without a 'probability of occurrence'. In conventional SVAT modelling this probability could only be expressed in terms of climate variability.

This study enabled the evaluation of cover performance in terms of the two key water balance components (AET and NP) with the change of maximum sustainable LAI and cover thickness along with the variability in soil hydraulic parameters and long-term historical climate.

As expected, increasing cover thickness is associated with an increase in AET, a decrease in NP, and a decrease in the range of the simulated water balance components due to parameter variability. In the specific case of the variability of LOS Ks, it was demonstrated that variability in LOS Ks values could result in a shift in the mechanism controlling NP. For example, at higher values of Ks, the control on NP was primarily the water storage capacity of the covers; while at lower values of Ks, the NP was controlled primarily by perching of infiltrating water on LOS surface.

The second objective was to determine the impacts of climate change projections on the long-term cover performances of reclamation covers and natural soil profiles. Higher NP rates in future as revealed by this study might have broader range of implications. The increased NP rates will potentially pose greater threats on adjacent water bodies as a consequence of proportionally increasing water release through underlying mine waste and the concomitant release of chemical constituents. The elevated NP rates could also lead to higher degrees of saturation, in response to an elevated water pressure, and associated rising water table within the reclaimed mine waste. As a consequence, weathering processes linked to oxygen availability might be reduced although the risk of geotechnical instability of the waste dumps and containment structures might be increased. Another implication of the increasing NP rates is that it might promote rapid flushing of mobile salts from the reclaimed fine-textured mine waste to the adjacent surface waters, thereby reducing long-term salt flushing to the surface waters out of the reclaimed sites.

The third objective was to evaluate the long-term cover performances in terms of water balance components using two different downscaling methods, one being statistical (LARS-WG) and another being dynamical (WRF). Although two downscaling methods are based on different approaches, both methods indicate similar directional shifts (increases) in key components of the water balance (i.e. AET and NP) towards the end of the 21st century at all study sites, while greater increases in the future NP rates than the AET are shown by both methods.

6.3 Recommendations for future research

The research included in this thesis was focused on selected oil sands mine reclamation sites from a variety of reclamation covers. The following recommendations for future research are expected to advance the ongoing research program for SCL mine sites. The further research can include covers with different hydraulic properties such as fine-textured covers placed over fine-

and coarse-textured mine waste. This extension could easily be incorporated using the framework developed in the research of this thesis, which would aid to better characterize the parameter variability (spatial and temporal) of the common reclamation cover system designs.

The second manuscript includes integration of climate change projections into a physically based water balance model to characterize uncertainty in the simulated water balance components due to natural climate variability as well as uncertainty due to RCPs, time periods, and type of soil profiles. The uncertainty in the simulated water balance components due to the choice of downscaling methods was also evaluated in this study. Future research may include selection of the GCMs from multiple available options from the archives (e.g. CMIP5) based on the skills of the GCMs using some skill scores (as explained by Taylor, 2001).

The future design of reclamation covers needs to be seen through the lens of climate change adaptation plan since the typical design of reclamation covers is based on the long-term simulation of AET and NP using a single set of optimized parameters with historical climate data. This approach is likely to underestimate the possible ranges of the simulated NP rates. The combined impacts of parameter and future climate variability are expected to generate elevated NP rates which the mine industry will need to consider in developing the long-term mine closure designs.

This study demonstrates that the absolute values of the future water balance components obtained from the two different downscaling methods could be difficult to compare given all the biases demonstrated by the WRF model. Besides these differences between the two downscaling methods, both methods indicate similar directions of relative change in the growing season key water balance components (i.e. AET and NP) by the end of the 21st century. Results indicate that the WRF model would require further a bias correction to generate realistic absolute water balance components; however, LARS-WG doesn't seem to require any further post-processing. Both downscaling methods demonstrate their advantages and limitations, although their comparison would help policy makers and reclamation cover designers to make reliable decisions if multi-model approach (multiple GCM, RCPs, RCMs, and statistical downscaling methods) is adopted to reveal the complete picture of climate change implications in the context of reclamation cover design.

Future extensions of this study could investigate the impact of climate change on the long-term performances of all the available reclamation covers in northern Alberta, Canada using an ensemble of high-resolution RCMs (along with WRF) and GCMs because use of a single RCM and/or GCM may not be recommended due to the associated uncertainties (Najafi et al. 2011; Schardong and Simonovic 2019; Semenov and Stratonovitch 2010; Wilby et al. 2004). The potential impact of climate change on the extreme water balance components of the reclamation covers will possibly be repeated using the newly released ensemble of GCMs from the sixth phase of CMIP (CMIP6) which includes more number of GCMs and newly developed socio-economic emission scenarios (which incorporate a wide range of adaptation and mitigation challenges) as described by Eyring et al. (2016).

APPENDIX A

Latin hypercube sampling (LHS) and progressive Latin hypercube sampling (PLHS)

LHS is based on the concept of a "Latin square", which forms an n-by-n matrix filled with n different objects (i.e., parameter values in this study) such that each parameter value occurs exactly once in each row and exactly once in each column. Briefly, a unit hypercube [0;1] in a multi-dimensional space (dimension is equal to the number of parameters in this study) is divided into n intervals (*n* is the sample size) with an equal length of 1/*n*. This division generates *n* equally probable intervals for each dimension. Sample points are then selected from each of the equally probable intervals such that the distribution of the sample points follows a uniform distribution and the sample represents a Latin hypercube. This sampling strategy ensures that sampling is representative of each equally probable interval in the total sample size. In the case of PLHS, the total sample is sliced into *s* slices, where the sample size of each slice is m (*m* = *n/s*). Sample points are selected for each slice that follows a uniform distribution, and the sample points from previous slices (each of which is a Latin hypercube) are added sequentially such that the resulting *n*-point sample is a Latin hypercube. The employment of PLHS as a sampling technique ensures that the sample size from each slice is not discarded even if it fails to be an appropriate sample size. Finally, the uniformly distributed samples are transformed to the desired distributions (e.g., normal, log-normal) by the associated transformation functions. For more details, interested readers are referred to the development of PLHS by Sheikholeslami and Razavi (2017).

Grouping of soil materials based on optimized parameters

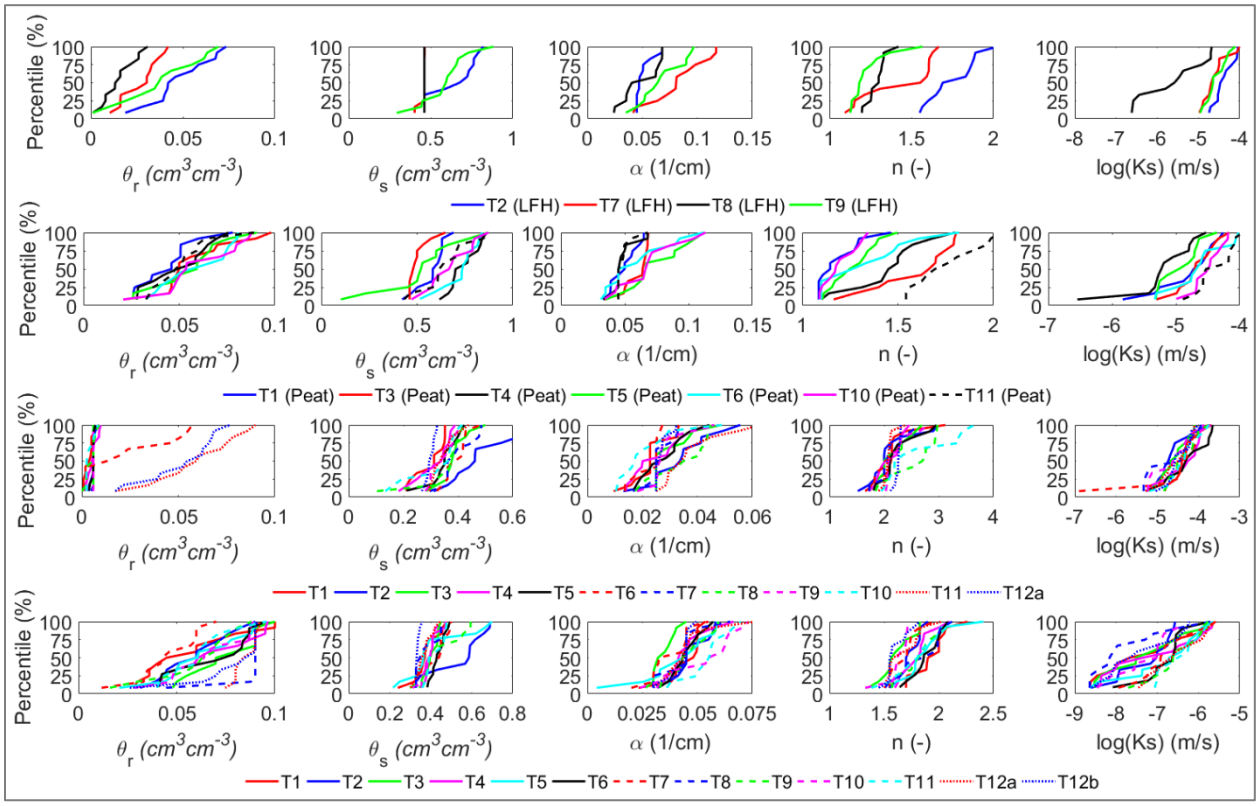

Figure A-1: Frequency distributions of the optimized parameters for LFH (top row), peat (second row) subsoil (third row), and LOS (bottom row) materials.

Selection of an appropriate sample size for PLHS

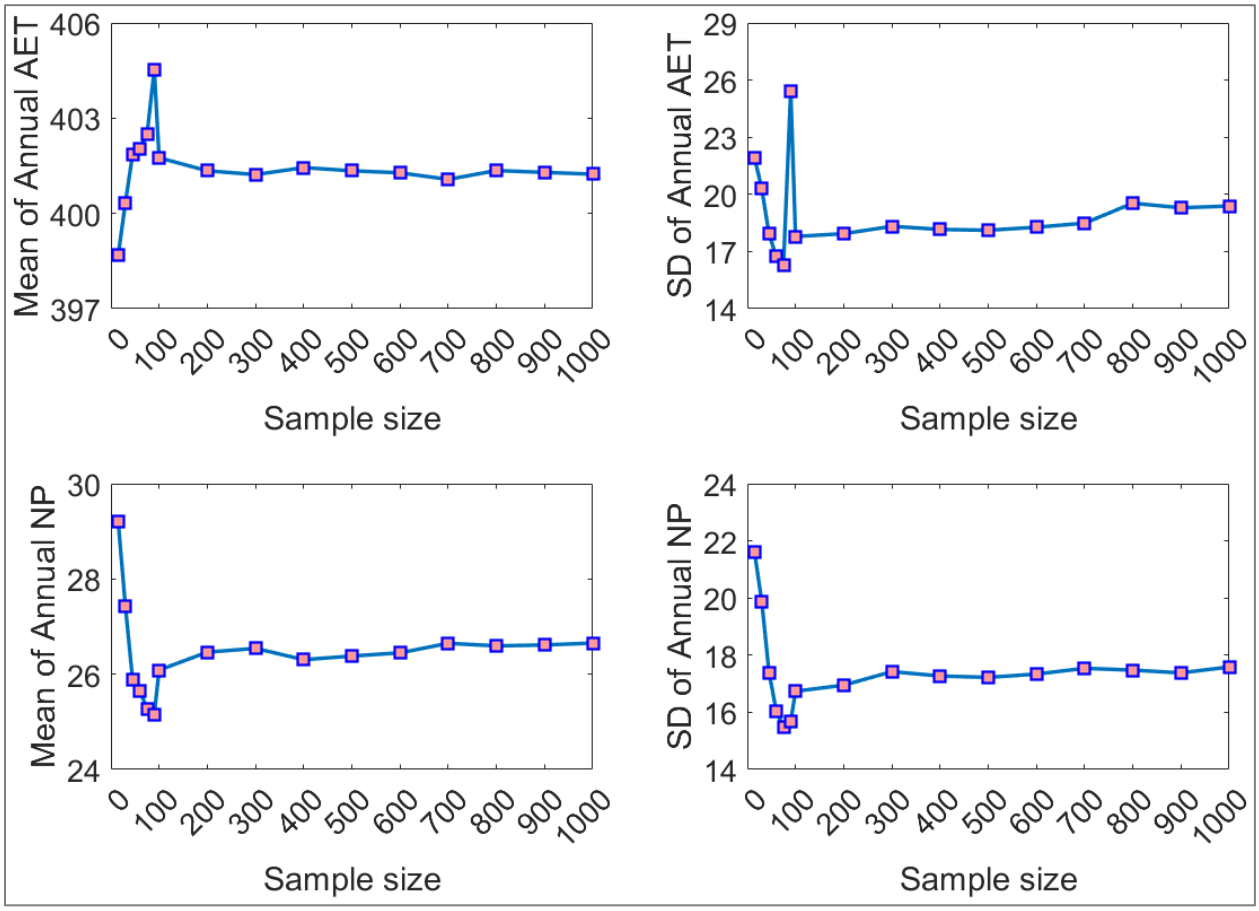

Figure A-2: Mean and SD values of the annual AET and NP corresponding to each sample size.

Selection of an appropriate sample size for MC

a.

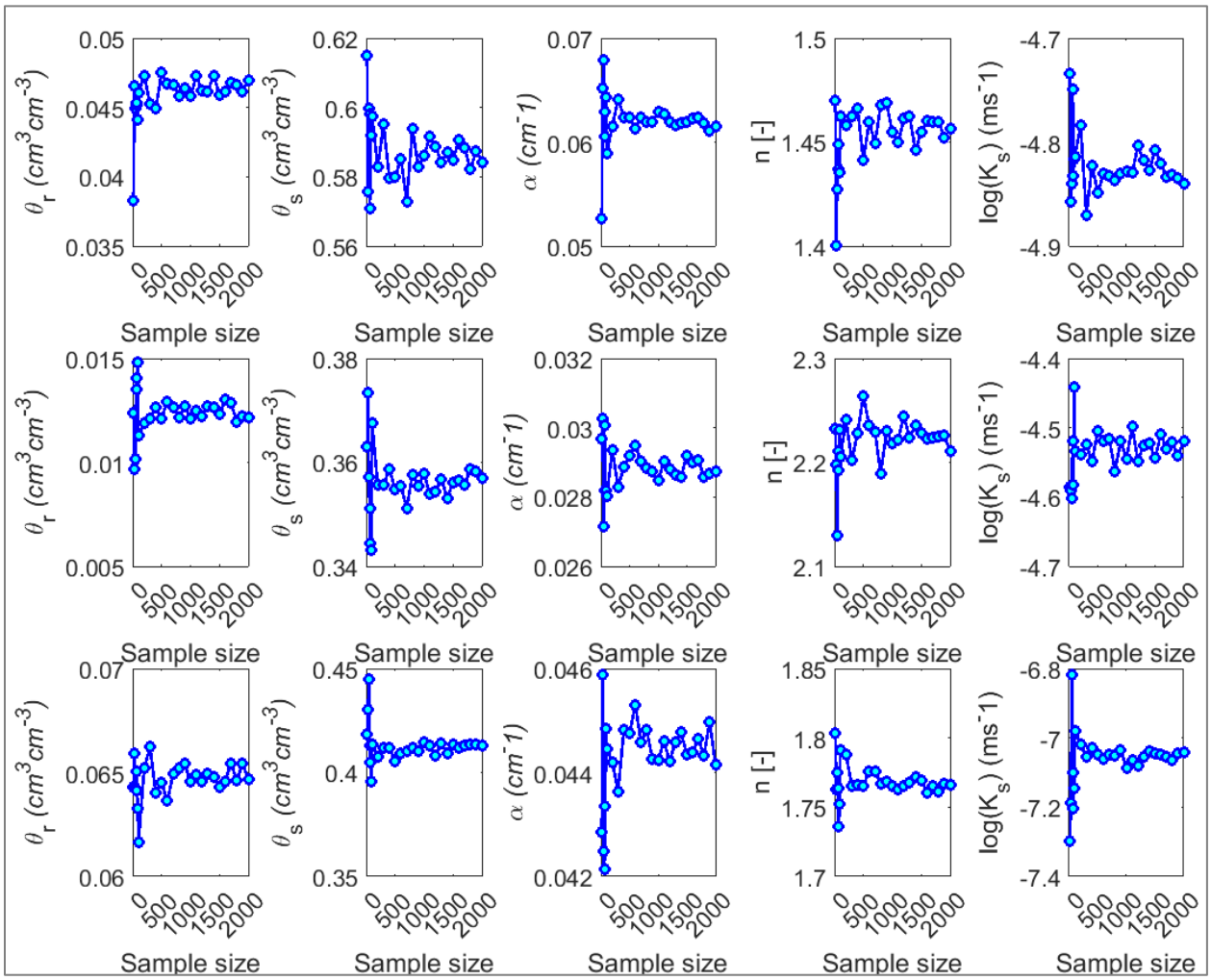

b.

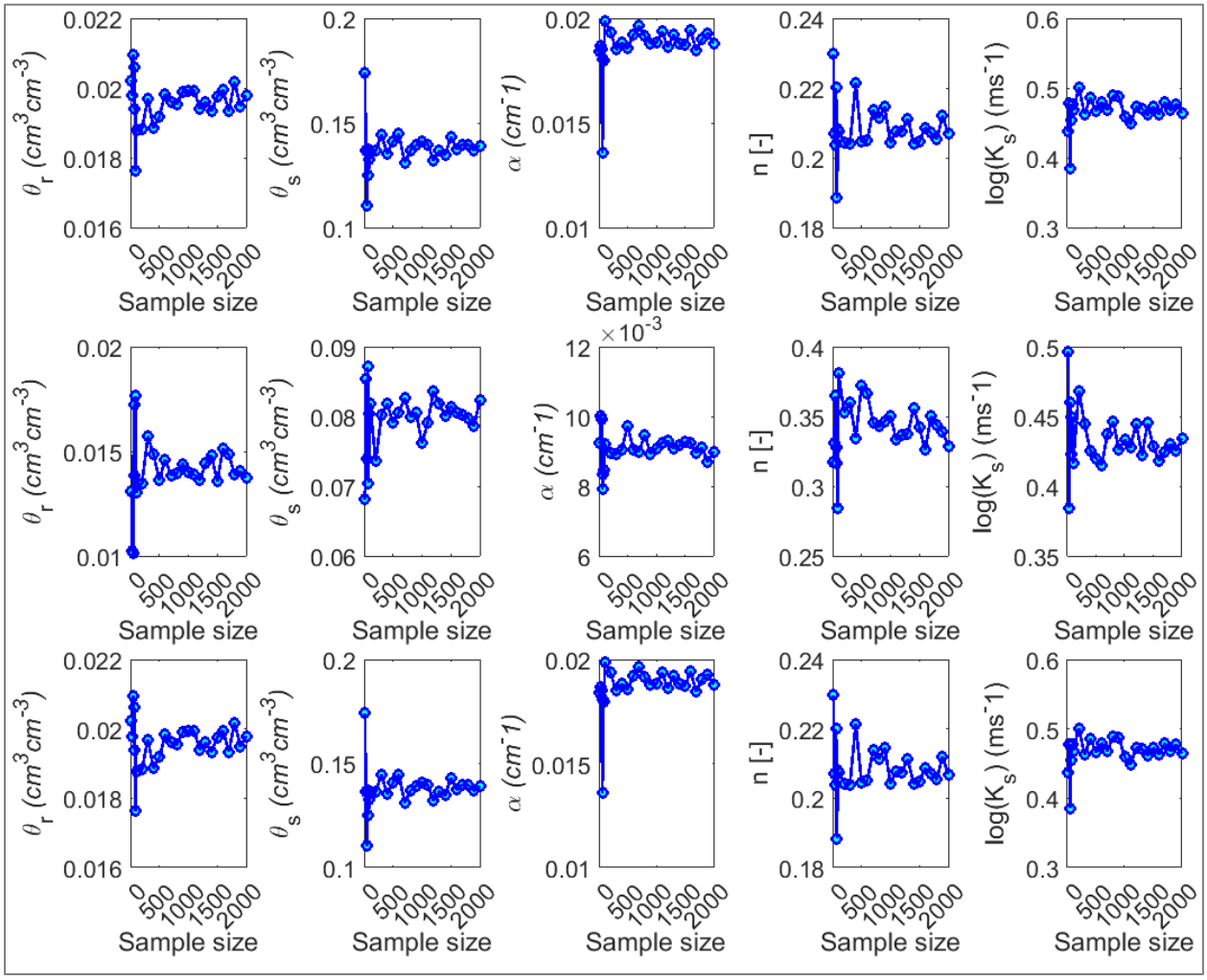

Figure A-3: (a) Mean and (b) SD of the sampled parameter values corresponding to each sample size from the MC sampling method. Results are shown for peat (top row), subsoil (middle row), and LOS (bottom row) in both (a) and (b).

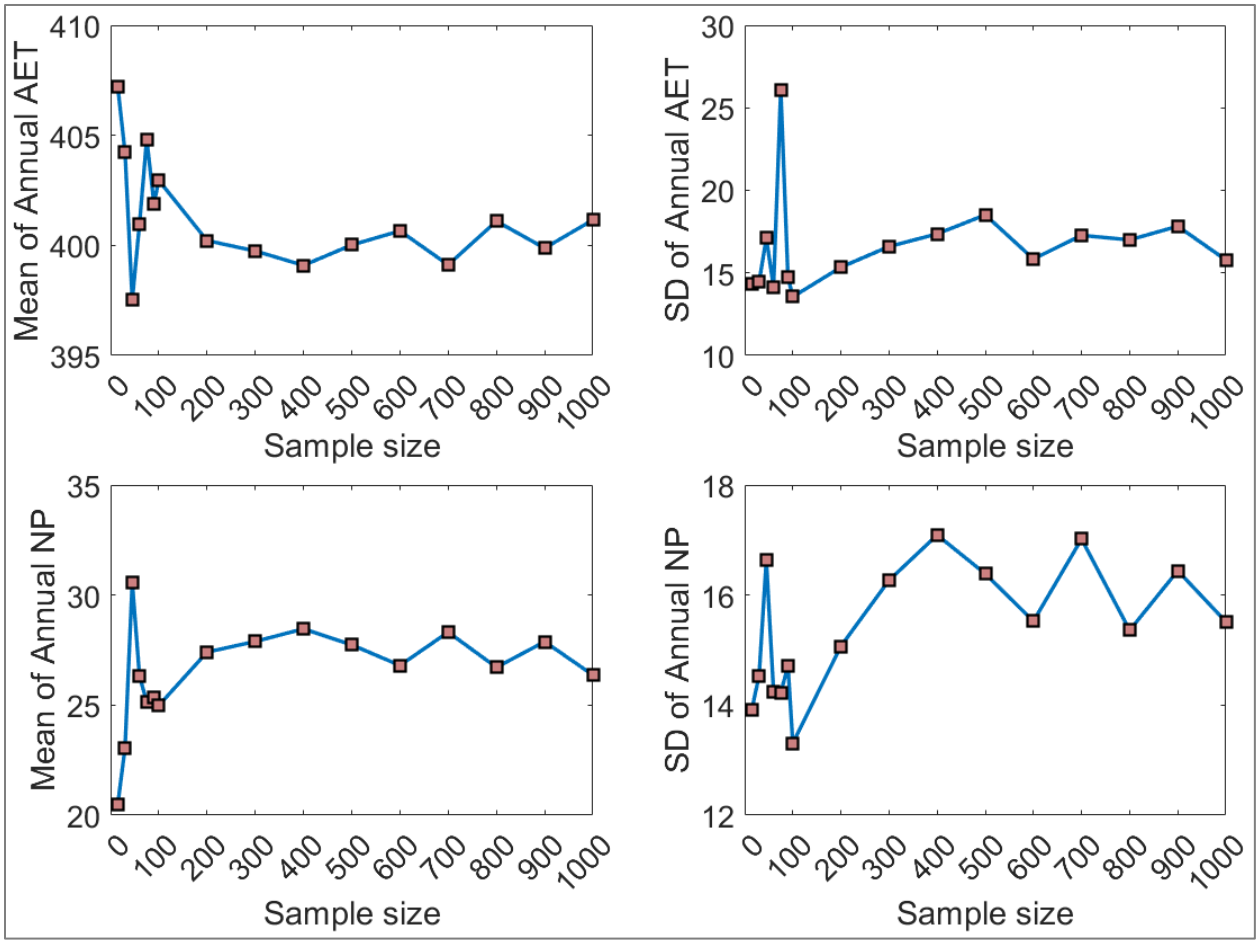

Figure A-4: Mean and SD values of the annual AET and NP corresponding to each sample size for MC sampling method.

Partition of water balance components with LAI

This section evaluated how AET might be portioned into AT and AE as shown in Fig. A-5. The results showed that almost 75 % of AET was used as AT and approximately 25 % was used as AE for the five illustrative covers. However, the share of AE vs. AT was higher at lower LAI; the share of AT monotonically increased, while the share of AE monotonically decreased once the LAI was higher than 1.5.

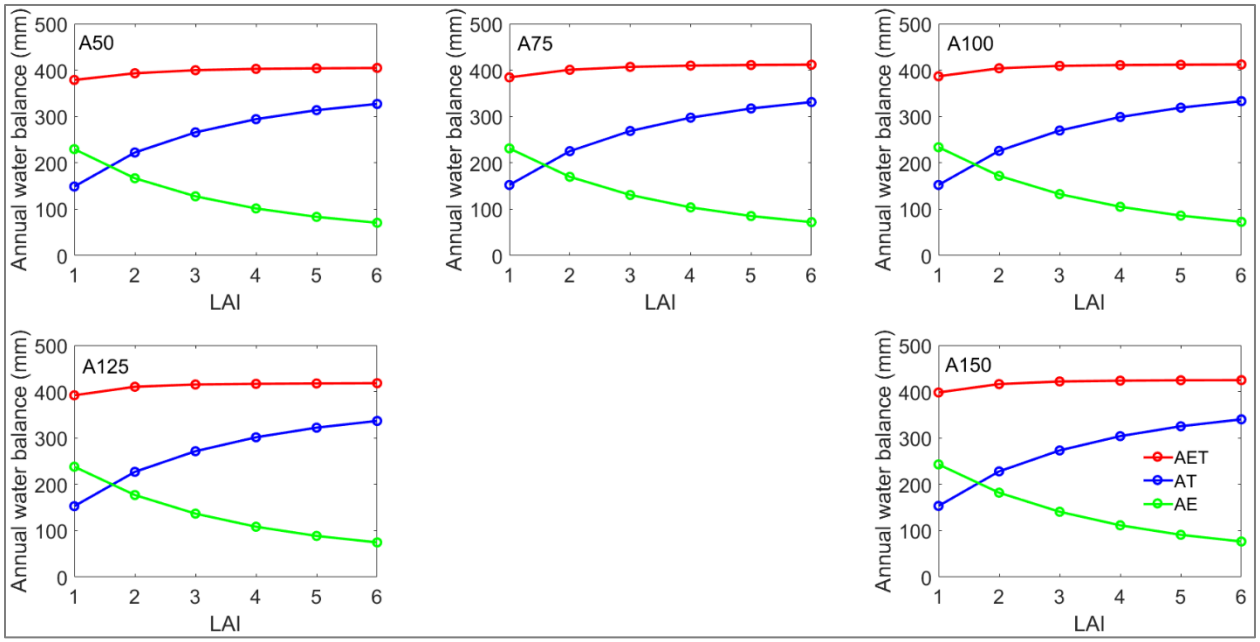

Figure A-5: Partition of AET into AT and AE with the variation of LAI for the five illustrative covers

Uncertainty in the simulated AET and NP due to sampling methods

Figure A-6 compares the distributions of the simulated water balance components (i.e., annual AET and NP) of the A100 illustrative cover obtained from PLHS, discrete, and MC sampling methods based on a constant LAI of 4.0. Over-all, the PLHS and MC methods show a wider inter-quartile range compared to the discrete approach in the case of AET and NP. In addition, PLHS and MC result in slightly higher annual AET and slightly lower NP than the discrete method; however, PLHS and MC sampling methods seem to capture similar variability as well as approximately equal median water balance components. However, the computational effort required for MC sampling and simulation is approximately 10 times greater than for the PLHS method.

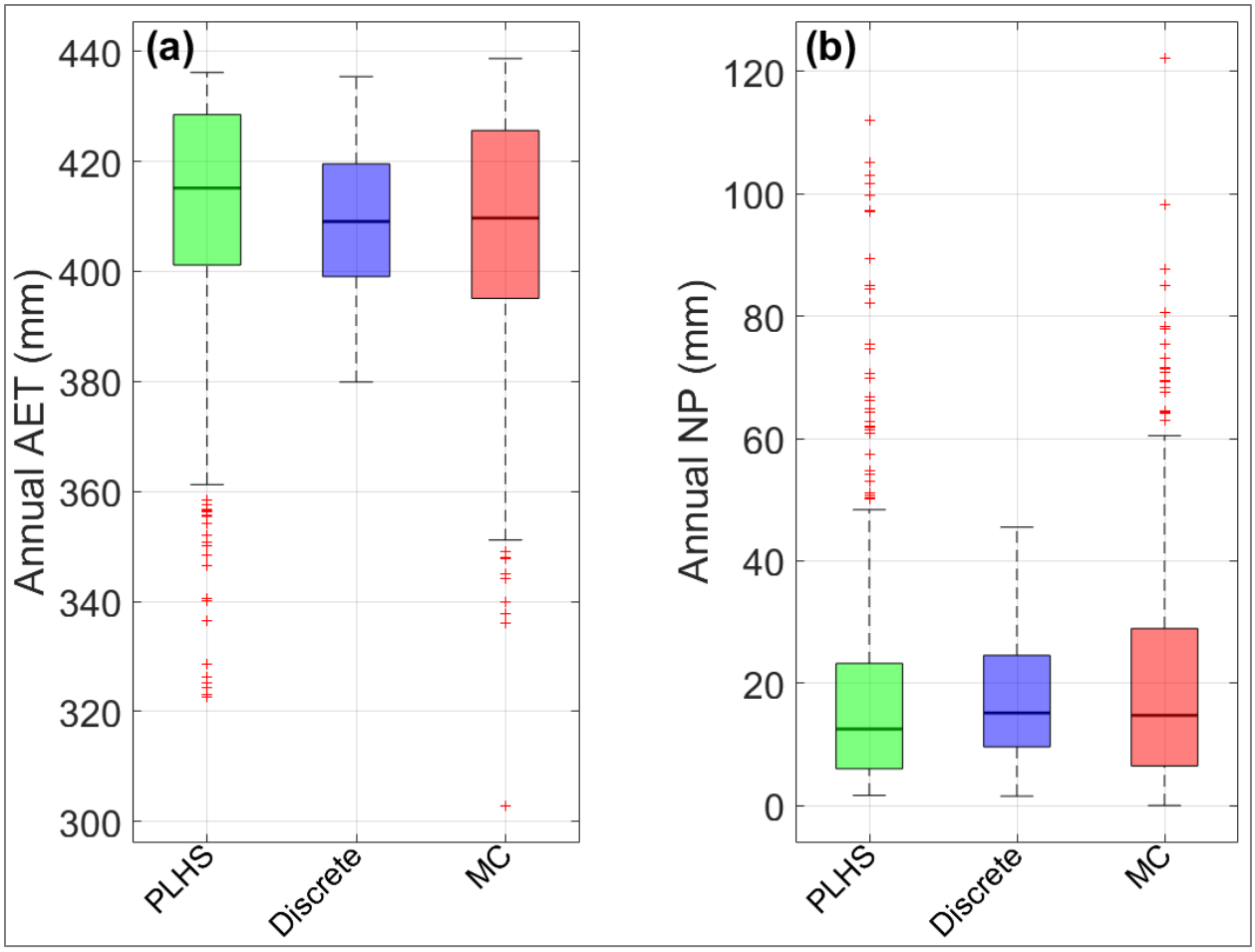

Figure A-6: Box plots showing the distributions of (a) annual AET and (b) annual NP obtained from the simulated water balances for A100 illustrative cover with 700 parameter sets for PLHS (green boxes), 135 parameter sets for discrete sampling (blue boxes), and 1000 parameter sets for MC (red boxes) over a 60-year climate cycle. The description of the box plots is the same as for Figure 3-11.

APPENDIX B

Downscaling methods

LARS-WG

The calibration and validation were undertaken in a similar manner to Elshorbagy et al. (2015) and Hashmi et al. (2011). Daily precipitation and temperature data from the Environment Canada station at the Fort McMurray Airport for the baseline period (1961-1990) were used to obtain probability distributions for local precipitation and temperature. This set of parameters was used to generate 100 simulations of the precipitation and temperature series, which were then validated against the observed daily precipitation and temperature for the period 1991-2011. Projected changes in future daily precipitation and temperature are incorporated in LARS-WG using relative change factors (RCF) (Semenov and Barrow 2002; Alam and Elshorbagy 2015) for each month. The RCF for each month is calculated using

$$RCF_{i,j}^{k} = \frac{S_{i,j}^{k,f}}{S_{i,j}^{k,b}}, \tag{B.1}$$

$$RCF_{i,j}^{k,T} = \bar{T}_{i,j}^{k,f} - \bar{T}_{i,j}^{k,b} , \tag{B.2}$$

where S is either the monthly mean precipitation, wet (i.e., a day with precipitation >0) or dry (i.e., a day with no precipitation) spell lengths, or standard deviation of daily mean temperature; $\bar{T}$ is the monthly mean of max/min temperature, respectively; k represents the corresponding month; f represents future period; b represents baseline period; i is the GCM; and j is the RCP.

The monthly mean of precipitation, monthly mean of wet and dry spell lengths, standard deviation of daily mean temperature, and monthly mean of max and min temperature for the RCPs are perturbed as follows:

$$S_{RCP}^{k} = S_{Obs}^{k} \times \frac{S_{i,j}^{k,f}}{S_{i,j}^{k,b}} , \tag{B.3}$$

$$\bar{T}_{RCP}^{k} = \bar{T}_{Obs}^{k} + (\bar{T}_{i,j}^{k,f} - \bar{T}_{i,j}^{k,b}). \tag{B.4}$$

The statistics ‘S’ and monthly mean of max and min temperature for RCPs during the future periods are perturbed using the observed monthly statistics (S_{Obs}^{k}) and observed mean monthly

temperatures ($\bar{T}_{Obs}^{k}$) in Equations B.3 and B.4, where the subscripts are defined as above. An example of the calculated RCFs for CanESM2 based on RCP2.6 during 2071-2100 is included in Table B-1. The perturbed monthly statistics calculated from the daily outputs (i.e., precipitation and temperature) of the GCMs at the coarse scale are used to simulate multiple realizations of the output time series for the RCPs of any length at the local scale using LARS-WG.

Table B-1: Relative change factors for CanESM2 based on RCP2.6 during 2071-2100 used in LARS-WG

Month	Mean monthly prec.	Wet spell length	Dry spell length	Mean monthly min temp.	Mean monthly max temp.	[1]SD of daily mean temp.
Jan	1.23	1.00	0.93	5.69	4.48	0.89
Feb	1.07	1.09	0.88	4.87	3.56	0.94
Mar	1.15	1.11	0.81	4.03	2.02	0.92
Apr	1.39	1.20	0.88	0.29	0.13	0.98
May	1.47	1.29	0.93	2.59	2.48	0.96
Jun	1.16	1.13	0.81	3.12	3.51	0.93
Jul	1.12	1.23	1.16	3.42	3.68	1.18
Aug	1.15	0.98	0.83	3.25	3.54	0.97
Sep	1.13	1.21	0.95	2.74	2.58	1.02
Oct	1.28	1.45	0.82	0.72	1.41	0.95
Nov	1.14	1.13	1.06	3.61	1.04	0.84
Dec	1.41	1.08	0.88	5.52	4.36	0.81

[1]SD is the standard deviation

Delta change method

This method involves calculation of the change factor (CF) in a similar manner as the RCFs based on the outputs from CanESM2 during the future and baseline periods; however, the daily variables in a month are obtained by multiplying the CF of the corresponding month with the observed daily variables in the same month. The daily values are perturbed here instead of perturbing the statistics as done in a weather generator. The approach can be described as follows:

$$X_{RCP,F}^{d/m} = X_{Obs}^{d} x \frac{\bar{X}_{RCP,F}^{m}}{\bar{X}_{Baseline}^{m}}, \tag{B.5}$$

where *X* represents daily relative humidity, wind speed, or net radiation; *d/m* and *m* represent day in a given month and month, respectively; and *F* represents a future period.

van Genuchten-Mualem (VG) equations

Single-porosity model

The unsaturated hydraulic properties for the mobile and immobile zones of water flow were described using van Genuchten-Mualem (VG) equations (van Genuchten 1980):

$$\theta(h) = \begin{cases} \theta_r + \frac{\theta_s - \theta_r}{[1+|\alpha h|^n]^m} & h < 0 \\ \theta_s & h \geq 0 \end{cases}, \tag{B.6}$$

$$K(h) = \begin{cases} K_s S_e^{1/2} \left[1 - \left(1 - S_e^{1/m}\right)^m\right]^2 & h < 0 \\ K_s h \geq 0 \end{cases}, \tag{B.7}$$

$$S_e = \frac{\theta - \theta_r}{\theta_s - \theta_r}, \tag{B.8}$$

where S_e is the effective saturation; h is the pressure head [L]; θ is the volumetric water content [L^3/L^3]; subscripts r and s refer to residual and saturated volumetric water contents, respectively; α [L^{-1}], n, and m are VG equation parameters where m=1-1/n; and K_s is the saturated hydraulic conductivity [LT^{-1}].

Dual-porosity model

In a dual-porosity model, water flow in the fractures (or macropores) is assumed as the dominant form of flow under saturated condition, while the matrix (intra-aggregate pores) contains relatively immobile water. Therefore, the liquid phase is portioned into mobile, θ_m, and immobile, θ_{im}, regions.

$$\theta = \theta_m + \theta_{im}, \tag{B.9}$$

The water exchange between the mobile and immobile regions is calculated using a first-order process described by Gerke and van Genuchten (1993). A mixed formulation of the Richards equation and a mass balance equation are used as follows to describe water flow in the fractures and water dynamics in the matrix, respectively, for the dual-porosity modelling (Simunek et al. 2003):

$$\frac{\partial \theta_m}{\partial t} = \frac{\partial}{\partial z}\left[K(h_m)\left(\frac{\partial h_m}{\partial z} + 1\right)\right] - S_m - \Gamma_w, \tag{B.10}$$

$$\frac{\partial \theta_{im}}{\partial t} = -S_{im} + \Gamma_w, \tag{B.11}$$

where t is time (T), K (h_m) is the unsaturated hydraulic conductivity function (L/T) in mobile region, hm is pressure head in mobile region (L), z is the vertical coordinate (positive upwards; L), S_m and S_{im} are the sink terms for both regions, and Γ_w is water transfer rate from the fractures to the matrix pores, which is calculated as follows (Gerke and van Genuchten 1993):

$$\Gamma_w = \omega_w(h)(h_m - h_{im}), \tag{B.12}$$

where Γ_w is taken as proportional to the difference in pressure heads between the two pore regions, ω_w is the first-order mass transfer coefficient (1/LT), and h_{im} is pressure head in the intra-aggregate pores. More details are available in Simunek et al. (2003).

Parameters of HYDRUS-1D

The van Genuchten (VG) parameters for the mobile region (i.e. θ_{rm}, θ_{sm}, α_m, n_m) and for the immobile region (i.e. θ_{rim}, θ_{sim}, α_{im}, n_{im}) in Table B-2 or for the single region (i.e. θ_r, θ_s, α, n) in Table B-3 are used to characterize the soil water retention curve (WRC) for the respective region, while Ks is used to define the hydraulic conductivity function, K(h) of the soil profile in HYDRUS-1D. Tables B-2 and B-3 shows the calibrated and validated parameters used to simulate long-term water balance of the respective oil sands mine reclamation covers.

Table B-2: van Genuchten (VG) parameters and saturated hydraulic conductivity for the two SWSS cover materials and three D3 cover materials

	SWSS		**D3**		
VG parameters	**Peat-mineral mix**	**Tailings sand**	**Peat-mineral mix**	**Glacial soil**	**Shale**
Mobile					
θ_{rm} ($cm^3\ cm^{-3}$)	0	0	0	0	0
θ_{sm} ($cm^3\ cm^{-3}$)	0.060	0.390	0.106	0.098	0.125
α_m (cm^{-1})	0.005	0.114	0.021	0.021	0.021
n_m	1.410	1.570	2.030	2.080	2.600
Immobile					
θ_{rim} ($cm^3\ cm^{-3}$)	0.105	0.062	0.105	0.062	0.120
θ_{sim} ($cm^3\ cm^{-3}$)	0.500	0.344	0.454	0.344	0.310
ω_w ($cm^{-1}\ d^{-1}$)	3.99e-3	0	$9.70e^{-4}$	$2.46e^{-2}$	$7.03e^{-3}$
K_s ($cm\ d^{-1}$)	10.100	78.900	432	8.640	0.260

Table B-3: Statistics of the estimated and optimized VG parameters and saturated hydraulic conductivity for the three SV sites (adapted from Huang et al. 2011b)

Parameters	**SV10 (14 materials)**		**SV27 (20 materials)**		**SV60 (18 materials)**	
	Mean	***SD***	***Mean***	***SD***	***Mean***	***SD***
θ_r (cm^3 cm^{-3})	0.008	0.011	0	0	0.002	0.004
θ_s (cm^3 cm^{-3})	0.433	0.045	0.405	0.043	0.390	0.078
α (cm^{-1})	0.058	0.021	0.023	0.011	0.067	0.025
n	3.360	0.377	2.680	0.412	2.260	0.319
K_s (cm d^{-1})	2.54e3	3.45e2	4.20e2	79.200	7.27e2	3.77e2

APPENDIX C

Table C-1: A list of GCMs from CMIP5 used for deriving climate scenarios for LARS-WG and climate perturbations for the WRF simulations of future climate variables.

Model name	Grid resolution (Lat × Lon degrees)	Used in LARS-WG	Used in WRF
ACCESS1-3	1.25 × 1.875	√	√
CanESM2	2.79 × 2.81	√	√
CCSM4	0.94 × 1.25	×	√
CESM1-CAM5	0.94 × 1.25	×	√
CMCC-CM	0.75 × 0.75	√	√
CNRM-CM5	1.40 × 1.41	√	√
CSIRO-Mk3-6-0	1.87 × 1.88	√	√
GFDL-CM3	2.0 × 2.5	√	√
GFDL-ESM2M	1.52 × 2.5	√	√
GISS-E2-H	2.0 × 2.5	√	√
HadGEM2-CC	1.2 × 1.875	√	√
HadGEM2-ES	1.25 × 1.875	√	√
INM-CM4	1.50 × 2.00	√	√
IPSL-CM5A-MR	1.27 × 2.50	√	√
MIROC5	1.40 × 1.41	√	√
MIROC-ESM	2.79 × 2.81	√	√
MPI-ESM-LR	1.87 × 1.88	√	√
MPR-ESM-MR	1.87 × 1.88	√	√
MRI-CGCM3	1.12 × 1.12	√	√

Table C-2: The coefficient of variation [CV (%)] of the median daily future Tmean and total precipitation projections during the baseline and future periods for each month and two downscaling methods.

	LARS-WG				WRF			
	Tmean		Precipitation		Tmean		Precipitation	
Month	Baseline	Future	Baseline	Future	Baseline	Future	Baseline	Future
Jan	10.0	13.0	45.5	45.4	24.1	32.9	24.6	29.0
Feb	12.4	17.5	50.4	52.1	22.9	32.0	38.6	42.8
Mar	23.8	100.2	54.6	56.5	29.1	52.2	33.1	34.7
Apr	31.4	13.4	64.2	67.6	47.3	366.1	37.0	34.7
May	8.0	5.2	54.3	55.9	123.2	20.1	48.6	51.4
Jun	4.2	3.1	48.4	48.4	10.2	5.7	54.3	54.1
Jul	3.1	2.4	44.1	45.2	7.3	6.6	29.3	39.2
Aug	4.5	3.4	52.1	58.2	8.4	5.2	46.8	38.6
Sep	7.7	4.9	53.6	56.2	20.6	12.0	57.0	44.9
Oct	32.1	12.9	57.5	57.5	748.2	30.6	40.9	33.9
Nov	17.6	34.0	55.3	51.9	42.3	95.5	51.9	50.4
Dec	11.3	15.4	47.4	48.0	34.4	47.6	45.5	35.6
Overall	13.8	18.8	52.3	53.6	93.2	58.9	42.3	40.8

Particle size distributions, WRCs, and distributions of hydraulic conductivity

Typical particle size distributions, water retention curves (WRCs), and saturated hydraulic conductivity values for the three distinct soil layers (i.e., peat, subsoil, and overburden) in the are shown in Figures C-1, C-2, and C-3, respectively.

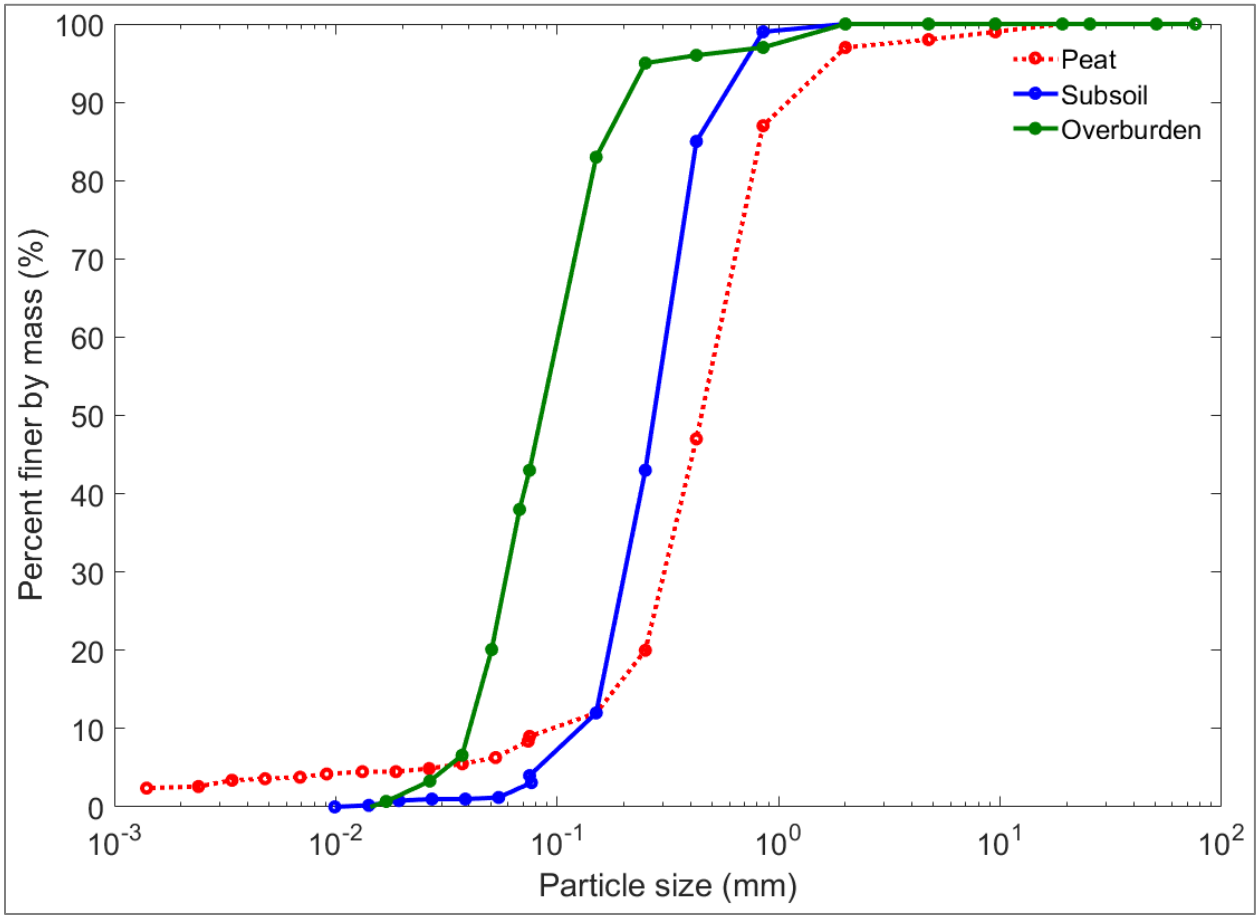

Figure C-1: Typical particle size distribution of soil layers (i.e. peat, subsoil, and overburden) used in oil sands mine reclamation covers in northern Alberta, Canada.

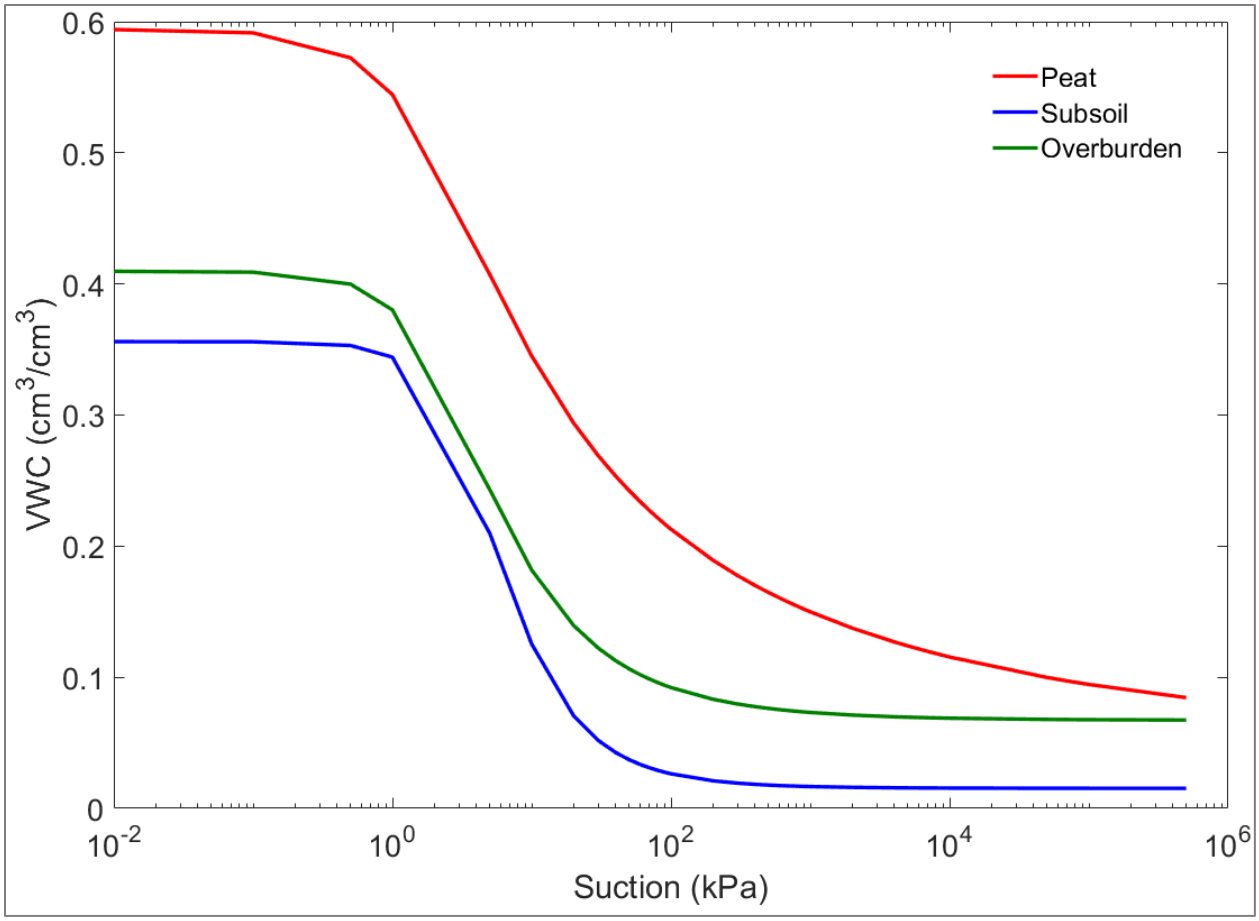

Figure C-2: Typical water retention curves (WRCs) of soil layers (i.e. peat, subsoil, and overburden) used in oil sands mine reclamation covers in northern Alberta, Canada.

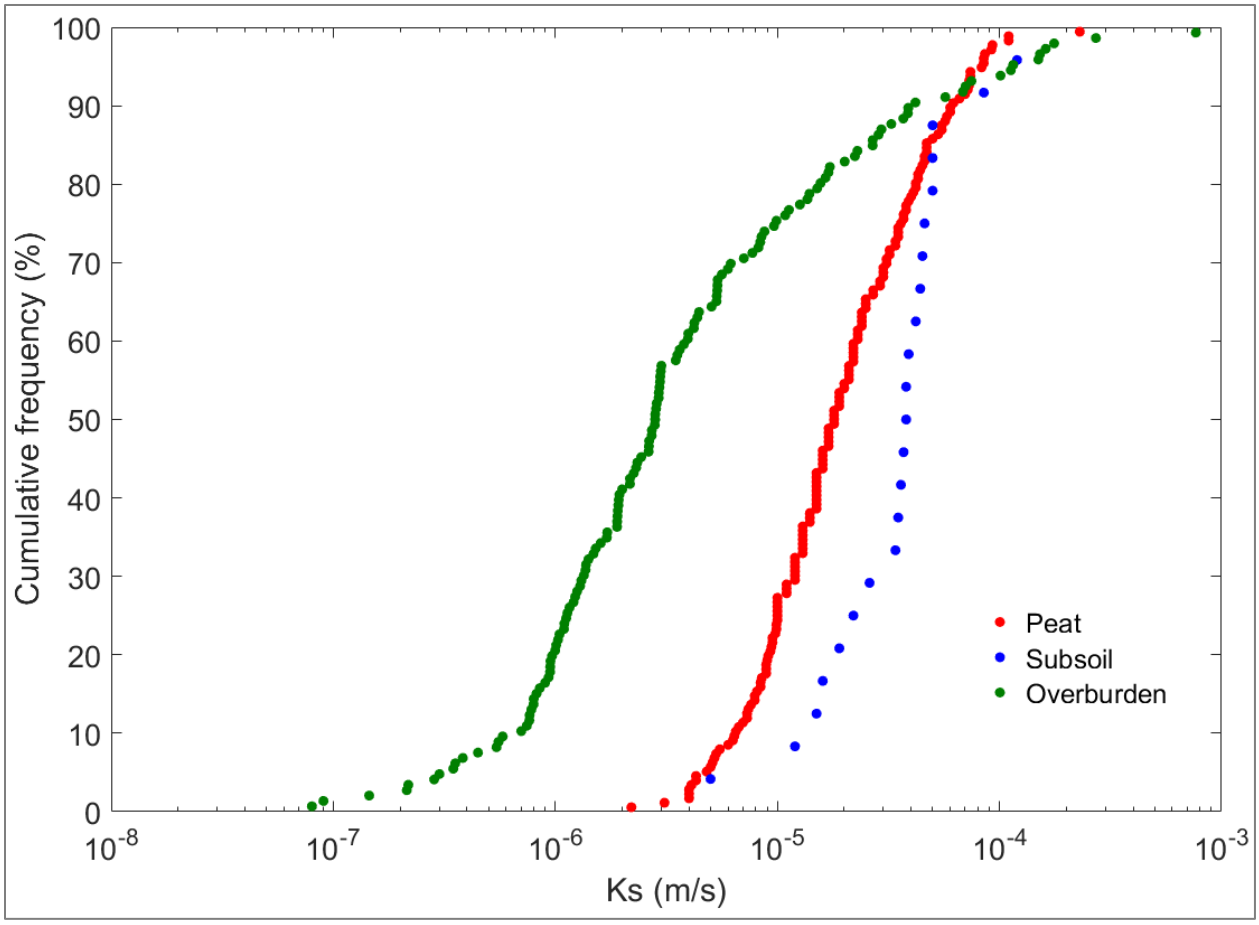

Figure C-3: Typical distribution of saturated hydraulic conductivity (Ks) values of soil layers (i.e., peat, subsoil, and overburden) at the oil sands mine reclamation covers in northern Alberta, Canada.